



Discrimination in the solid state during crystallization : application to phenanthrene ultrapurification

Antoine Burel

► To cite this version:

Antoine Burel. Discrimination in the solid state during crystallization : application to phenanthrene ultrapurification. Other [cond-mat.other]. Normandie Université, 2017. English. NNT : 2017NORMR102 . tel-01739265

HAL Id: tel-01739265

<https://theses.hal.science/tel-01739265>

Submitted on 20 Mar 2018

HAL is a multi-disciplinary open access archive for the deposit and dissemination of scientific research documents, whether they are published or not. The documents may come from teaching and research institutions in France or abroad, or from public or private research centers.

L'archive ouverte pluridisciplinaire **HAL**, est destinée au dépôt et à la diffusion de documents scientifiques de niveau recherche, publiés ou non, émanant des établissements d'enseignement et de recherche français ou étrangers, des laboratoires publics ou privés.



Normandie Université

THÈSE

Pour obtenir le diplôme de doctorat

Spécialité Physique

Préparée au sein de l'Université de Rouen-Normandie

Discrimination à l'état solide durant la cristallisation : application à l'ultrapurification du Phénanthrène

**Présentée et soutenue par
Antoine BUREL**

**Thèse soutenue publiquement le 20 octobre 2017
devant le jury composé de**

Mme. Sylvie MALO	Professeur des universités, ENSICAEN	Présidente du jury
M. Jérôme RANDON	Professeur des universités, Université Claude Bernard Lyon I	Rapporteur
M. Tom LEYSSENS	Professeur des universités, Université Catholique de Louvain	Rapporteur
M. Joop TER HORST	Professeur des universités, University of Strathclyde, Glasgow	Rapporteur
M. Pascal CARDINAËL	Professeur des universités, Université de Rouen-Normandie	Examineur
M. Gérard COQUEREL	Professeur des universités, Université de Rouen-Normandie	Directeur de thèse

Thèse dirigée par M. Gérard COQUEREL, professeur des universités au laboratoire Sciences et Méthodes Séparatives (EA 3233 SMS)



Normandie Université

Ph. D. thesis

Physics

Université de Rouen-Normandie

Discrimination in the solid state during crystallization: application to Phenanthrene ultrapurification

Defended by
Antoine BUREL

Public defense in october 2017

Jury composed of:

Mrs. Sylvie MALO	Professor ENSICAEN	<i>Chairwoman</i>
Mr. Jérôme RANDON	Professor Université Claude Bernard Lyon I	<i>Reviewer</i>
Mr. Tom LEYSSENS	Professor Université Catholique de Louvain	<i>Reviewer</i>
Mr. Joop TER HORST	Professor University of Strathclyde	<i>Reviewer</i>
Mr. Pascal CARDINAËL	Professor Université de Rouen-Normandie	<i>Examiner</i>
Ph. D. thesis directed by	Prof. Gérard COQUEREL Lab. SMS (EA 3233) Université de Rouen-Normandie	
Co-supervisors	Dr. Yohann CARTIGNY and Dr. Séverine TISSE Lab. SMS (EA 3233) Université de Rouen-Normandie	

Laboratory: *Sciences et Méthodes Séparatives* (EA 3233)

Doctoral school: *Physique, Sciences de l'Ingénieur, Matériaux, Énergie PSIME* (ED 591)

à mon grand-père, Georges.

REMERCIEMENTS

ACKNOWLEDGMENTS

The present manuscript marks the end of three years of Ph. D. thesis spent at the « Sciences et Méthodes Séparatives » laboratory of the University of Rouen-Normandy. I would like to thank Prof. Gérard COQUEREL for the supervision of this thesis, and Drs. Yohann CARTIGNY and Séverine TISSE for their mentoring. Région Normandie is also gratefully acknowledged for its financial support on this research project.

I am grateful to Profs. Sylvie MALO, Jérôme RANDON, Tom LEYSSENS and Joop TER HORST for having accepted to judge this work and for giving me the opportunity to defend my work.

Je passe désormais au français, pour remercier Pascal CARDINAËL et Nicolas COUV RAT pour leurs supports respectifs et les nombreux échanges constructifs que nous avons pu avoir durant ces trois années. Merci à tous les deux de m'avoir mis le pied à l'étrier il y a désormais six ans !

Je ne saurais résumer cette thèse sans aborder la très motivante ambiance qui règne au laboratoire. J'adresse donc ma reconnaissance à l'ensemble de ses membres : doctorants, ATER et post-doctorants (Méla, Ben, Quentin, Emeline, Emilie, FX, DSJ, les deux Lina, Manon, Simon, Ryusei, Bienvenu, Grace et Aliou), enseignants et/ou chercheurs (Morgane, Clément, Gabin, Samuel, les deux Valérie, Ivo et les autres), sans oublier nos trois indispensables techniciennes : Framboise, Marie et Céline. J'espère que les futures générations qui se côtoieront sauront faire perdurer cet esprit.

Je n'oublie pas non plus Sander et James, que j'ai eu le privilège d'encadrer durant mes travaux. Merci à tous les deux pour votre travail rigoureux et source d'opportunités !

Pour terminer, je tiens à remercier Pierre pour son soutien quotidien, ainsi que ma famille et mes amis pour leurs encouragements durant cette période. Votre présence me fut précieuse.

Table of contents

Introduction.....	13
Chapter I: Basic notions on phase equilibria, material purification and characterization.....	23
Chapter II: The Phenanthrene system.....	83
Chapter III: Development of an analytical method to assess Phenanthrene purity.....	105
Chapter IV: Ultrapurification of Phenanthrene by crystallization.....	171
Conclusion.....	285

Introduction

INTRODUCTION

TABLE OF CONTENTS

INTRODUCTION.....	16
REFERENCES.....	21

INTRODUCTION

The chemical purification of solid materials is a procedure of major importance that intervenes during various processes:

- the development of medicinal drugs: biological activities of Active Pharmaceutical Ingredients (APIs) and all their impurities have to be assessed separately [1,2], which requires their prior separation and purification.
- the elaboration of materials dedicated to electronics, which requires impurity levels to be extremely low, to minimize the formation of defects and maximize electron mobility.
- the manufacturing of analytical standards.
- etc.

During drug development, crystallization procedures are often employed to design solids (particle size, crystal shape, crystalline phase, etc). The nature of the solid phase (*i. e.*, the polymorph) obtained during this process has to be controlled, as it directly impacts the physical properties of the product (solubility, bioavailability, rate of dissolution, physical stability, etc). Up to now, many studies revealed that the presence of impurities in the product can influence the crystallization process, and several cases were reported in the literature.

During crystallization of 4-aminoquinoline from solution, Braun *et al.* showed that traces of Chloro-4-aminoquinoline and Carboxaldehyde-4-aminoquinoline enhanced the formation of a new form, previously unknown, of compound monohydrate [3]. This phase was found to be more stable than the other monohydrate discovered previously by Tai *et al.* using a purer starting material [4]. Similar case was encountered by Martins *et al.* during crystallization of API BN83495 (from IPSEN company) in Dimethylsulfoxide: presence or absence of impurity Letovicite led to crystallization of different polymorphs of compound solvate [5]. In addition, Viel *et al.* highlighted that the levels of impurity Theophylline in API Diprophylline influenced the nature of the polymorph obtained during crystallization of the compound from the amorphous state [6]. Another similar case was reported by Prasad *et al.* during crystallization from solution of a TADDOL analogue in presence or absence of a chiral impurity [7].

Other purity-related issues during crystallization were reported by several researchers: modification of crystal growth mechanisms (Prasad *et al.* on Paracetamol [8], Davis *et al.* on Calcite [9]), formation of fluid inclusions and modification of crystal shapes (Keith and Padden on melt crystallization [10,11]).

Besides, the presence of impurities can also impact the properties of materials dedicated to electronics: Pizzini *et al.* showed that impurities in Silicone can substantially decrease the efficiency of solar cells [12–14]; Rep *et al.* evidenced the effect of impurities on the stability in time of current-voltage characteristics of organic semiconductors [15]; MgB₂ superconductivity was also found to be influenced by impurities (Xu *et al.* [16] and Jiang *et al.* [17]); etc.

Consequently, during the development of solid products, a rigorous attention must be paid to chemical purity. Indeed, the properties of the final product depend on it. However, we will see that definitions and specifications on purity and purity grades are not that obvious. These two points require clarification, which is attempted thereafter.

Let us try to define chemical purity. Basically, this notion is related to the number and proportions of chemical species in a system – in other words, to the composition of this system. Consequently, the purity of a substance corresponds to the fraction of the most abundant species. However, a particular attention must be paid to the units in which are expressed chemical purities, as species fractions can be expressed in mass or mole %.

To illustrate the importance of that point, let us consider a binary system made of a component of interest and its impurity. Mass and molar proportions of these two components can drastically deviate when the difference in molecular weights of the two species increases (see fig. 1). For example, a 99 mole % purity compound is pure at 49.7 % in mass if the impurity molecular weight is 100 times higher than that of the interest component. Consequently, this highlights that expressing purities with solely percentage values is not sufficient, and that the nature of the percentage (mass or mole) **must** be indicated.

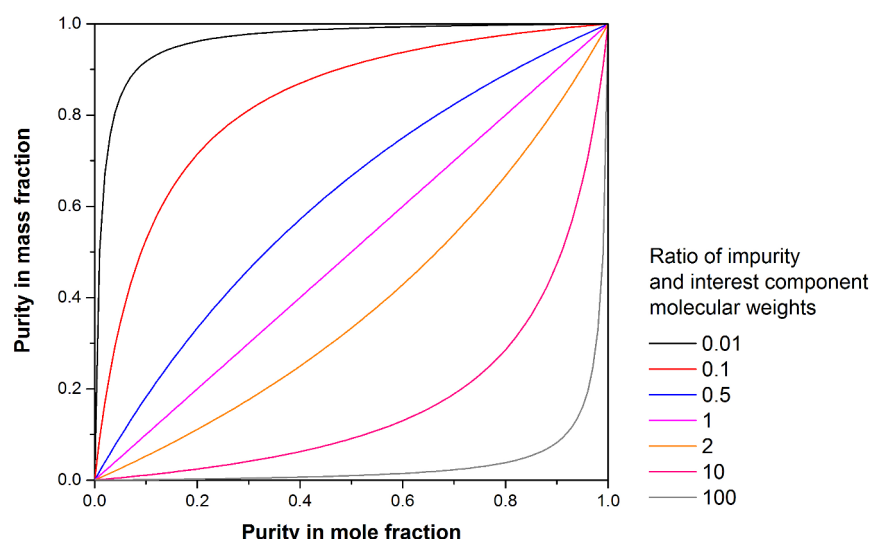


FIG. 1: **Conversion of interest component mass and molar purities in binary systems**

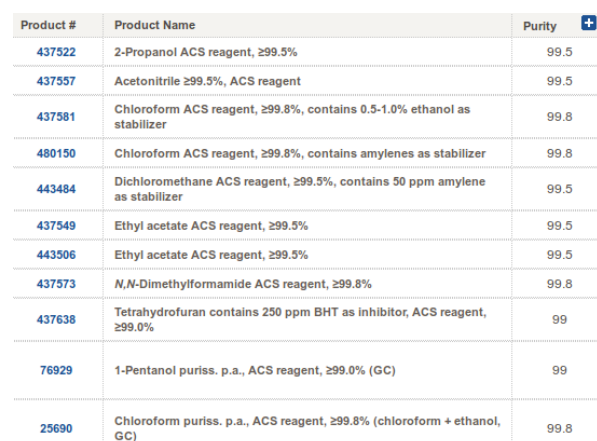
Along with the definition of chemical purity, another point has to be clarified: that of purity grades. Indeed, chemicals available for purchasing are generally marked with grades by the manufacturers. However, there is no international standardization of them, even if some normalization organizations (US pharmacopoeia, European pharmacopoeia, American Chemical Society, etc) attempted to established some specifications associated with different grades (USP grade [18], EP grade [19], ACS reagent [20], ...). However, USP and EP grade specifications are not applicable to every substance, and are generally established for specific chemicals (APIs, excipients, solvents, ...).

Besides, several suppliers proposed similar grade denominations, with commonly agreed specifications (see tab. 1). However, in many cases, no indication on the unity of purity (mass

or mole %) is given (see asterisks in tab. 1). This consequently shows that purity grades have no sense when the corresponding purity criteria are not correctly expressed. As revealed by fig. 2, industrial practices do not comply with this requirement, which justifies a systematic re-evaluation of chemical purity of purchased materials before their use for critical applications. The major problem that arises from these considerations is the feasibility of ultrapure, solar and semiconductor grades purity assessment. Indeed, appropriate analytical methods must be developed and combined, if appropriate, to measure such purities.

TAB. 1: Purity grades commonly agreed

Purity grade	Chemical purity	Applications
Technical	> 90 %* [21]	Non critical tasks (vessel rinsing, starting materials for industrial production processes...). Not appropriate for laboratory use.
Reagent (or synthesis)	> 95 %* [21]	Synthesis
Ultrapure	> 99.9 mole % [22]	Analysis, calibration, ...
Solar (or 5N)	> 99.999 %* [23]	Photovoltaics
Semiconductor (or 9N)	> 99.999999 %* [23]	Advanced electronics



Product #	Product Name	Purity
437522	2-Propanol ACS reagent, ≥99.5%	99.5
437557	Acetonitrile ≥99.5%, ACS reagent	99.5
437581	Chloroform ACS reagent, ≥99.8%, contains 0.5-1.0% ethanol as stabilizer	99.8
480150	Chloroform ACS reagent, ≥99.8%, contains amylenes as stabilizer	99.8
443484	Dichloromethane ACS reagent, ≥99.5%, contains 50 ppm amylene as stabilizer	99.5
437549	Ethyl acetate ACS reagent, ≥99.5%	99.5
443506	Ethyl acetate ACS reagent, ≥99.5%	99.5
437573	N,N-Dimethylformamide ACS reagent, ≥99.8%	99.8
437638	Tetrahydrofuran contains 250 ppm BHT as inhibitor, ACS reagent, ≥99.0%	99
76929	1-Pentanol puriss. p.a., ACS reagent, ≥99.0% (GC)	99
25690	Chloroform puriss. p.a., ACS reagent, ≥99.8% (chloroform + ethanol, GC)	99.8

FIG. 2: Screenshot of a part of Sigma-Aldrich online catalog, highlighting that chemical purity values are not correctly expressed – from [24].

For all the reasons developed in this introduction, the purity of commercial materials has sometimes to be increased before further use. In this view, many methods can be employed and combined if appropriate. Among them, crystallization [25], that serves for solid state design, can also be used for purification purposes. During this process, molecules of the recrystallized substance self assembly from the mother phase thanks to some kind of self recognition system. Thanks to this mechanism, discrimination in the solid state between the interest component and its impurities can occur. In case of sufficient discrimination, the impurities do not assembly with the molecules of the target compound and remain in the mother phase. Eventually, a phase separation procedure permits the recovery of the purified product.

Of course, such discrimination is governed by phase equilibria between all the species involved in the considered system. Indeed, several studies performed on chiral systems highlighted the relation between the structural similarity of several components and their

ability at assembling together during crystallization [26–28]. During recrystallization in solution, the molecule of interest generally does not include impurities when their respective molecular structures are different enough (fig. 3a). Conversely, when the target compound and its impurity exhibit structural similarities, impurities are generally included in the crystals (fig. 3b).

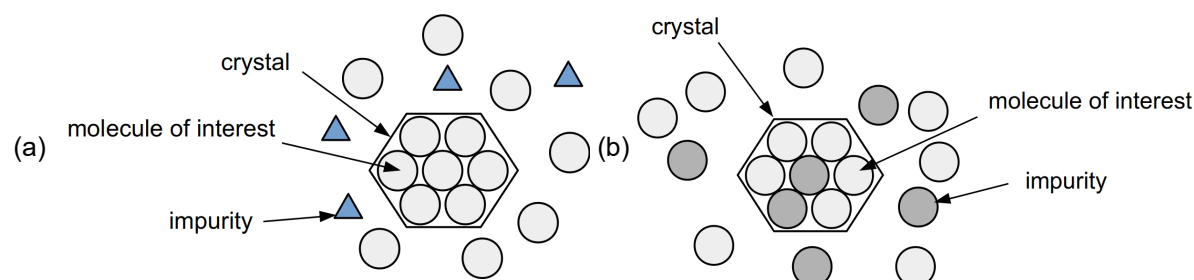


FIG. 3: **Illustration of the concept of discrimination in the solid state during crystallization –**
(a) large discrimination, (b) poor discrimination

The thesis developed in this manuscript is that the purifying effect of a crystallization method is closely related to this mechanism of discrimination in the solid state between the compound of interest and its impurities. In particular, the following points are demonstrated: in case of poor discrimination, limited purifying effects are observed during crystallization, and several pathways can be envisaged to bypass such unfavorable phenomena: (i) increasing the order of the system by adding a third component leading to the crystallization of another solid phase. In favorable cases, the new phase is more selective and offers larger purifying effects, (ii) and/or modifying the chemical identity of the system by selective chemical modification of undesirable impurities to make them unable at assembling with the target molecule during crystallization.

To demonstrate that, Phenanthrene molecule was chosen as model compound. Indeed, for structural study purposes, ultrapurification of this product (*e. g.*, an increase of its molar purity above 99.9 mole %) was required. The pathways mentioned above were investigated on this molecule in order to answer two intrinsically related questions that arose from this challenge: (i) is it possible to measure ultrapurity on Phenanthrene samples? (ii) is it possible to access to ultrapure grade by means of crystallization?

To answer these questions, the manuscript is divided into 4 different chapters:

- In chapter I, an introduction to thermodynamics and phase equilibria is made to present the different basic concepts associated with crystallization procedures and solid state chemistry. Moreover, a few elements on material purification and characterization are provided.
- In chapter II, the Phenanthrene system is introduced. A presentation of the problematics related to the solid state of this molecule is made. State of the art on the characterization and purification of this product are also provided, in order to highlight the need for a critical re-investigation of this system. In particular, the two following points are evidenced: the need for an analytical method able at measuring Phenanthrene purity

values above 99.9 mole %; the necessity of developing and optimizing purification processes to reach the target purity for this compound.

- Chapter III aims at presenting works performed to develop an analytical method for Phenanthrene purity assessment meeting with the requirements mentioned above. Basic notions on Gas Chromatography (GC), an analytical technique that was selected for Phenanthrene analysis, are provided, before reporting the original procedures attempted to reach analytical requirements.
- In chapter IV, reports on Phenanthrene purification by means of various crystallization methods (solvent assisted recrystallization, Zone Melting, vacuum sublimation and co-crystallization in solution) are provided. All these methods were tested separately on the molecule, before attempting to combine them on commercial samples, or products treated to modify their impurities. In this chapter, a particular attention was paid to the relation between crystallization method purifying effect and discrimination between Phenanthrene and its impurities.

Eventually, the general conclusion of this manuscript attempts to validate the thesis described above by answering the questions raised above. Moreover, a procedure for non-polar polycyclic aromatic hydrocarbons is proposed, thanks to the key learnings highlighted during this work.

REFERENCES

- [1] S. (Sut) Ahuja, Assuring quality of drugs by monitoring impurities, *Adv. Drug Deliv. Rev.* 59 (2007) 3–11. doi:10.1016/j.addr.2006.10.003.
- [2] L. Müller, R.J. Mauthe, C.M. Riley, M.M. Andino, D.D. Antonis, C. Beels, J. DeGeorge, A.G.M. De Knaep, D. Ellison, J.A. Fagerland, R. Frank, B. Fritschel, S. Galloway, E. Harpur, C.D.N. Humfrey, A.S. Jacks, N. Jagota, J. Mackinnon, G. Mohan, D.K. Ness, M.R. O'Donovan, M.D. Smith, G. Vudathala, L. Yotti, A rationale for determining, testing, and controlling specific impurities in pharmaceuticals that possess potential for genotoxicity, *Regul. Toxicol. Pharmacol.* 44 (2006) 198–211. doi:10.1016/j.yrtph.2005.12.001.
- [3] D.E. Braun, H. Oberacher, K. Arnhard, M. Orlova, U.J. Griesser, 4-Aminoquinoline monohydrate polymorphism: prediction and impurity aided discovery of a difficult to access stable form, *CrystEngComm*. 18 (2016) 4053–4067. doi:10.1039/C5CE01758K.
- [4] X.-S. Tai, J. Xu, Y.-M. Feng, Z.-P. Liang, 4-Amino-2-methylquinoline monohydrate, *Acta Crystallogr. Sect. E Struct. Rep. Online*. 64 (2008) o1026–o1026. doi:10.1107/S1600536808013093.
- [5] D. Martins, M. Sanselme, O. Houssin, V. Dupray, M.N. Petit, D. Pasquier, C. Diolez, G. Coquerel, Physical transformations of the active pharmaceutical ingredient BN83495: enantiotropic and monotropic relationships. Access to several polymorphic forms by using various solvation–desolvation processes, *CrystEngComm*. 14 (2012) 2507–2519. doi:10.1039/C2CE06537A.
- [6] Q. Viel, C. Brandel, Y. Cartigny, M.E.S. Eusébio, J. Canotilho, V. Dupray, E. Dargent, G. Coquerel, S. Petit, Crystallization from the Amorphous State of a Pharmaceutical Compound: Impact of Chirality and Chemical Purity, *Cryst. Growth Des.* 17 (2017) 337–346. doi:10.1021/acs.cgd.6b01566.
- [7] K.R. Prasad, A. Chandrakumar, A.G. Dikundwar, T.N.G. Row, Polymorphism in a TADDOL analogue induced by the presence of a chiral impurity, *CrystEngComm*. 12 (2010) 3452–3454. doi:10.1039/C0CE00103A.
- [8] K.V.R. Prasad, R.I. Ristic, D.B. Sheen, J.N. Sherwood, Crystallization of paracetamol from solution in the presence and absence of impurity, *Int. J. Pharm.* 215 (2001) 29–44. doi:10.1016/S0378-5173(00)00653-0.
- [9] K.J. Davis, P.M. Dove, J.J. De Yoreo, The Role of Mg^{2+} as an Impurity in Calcite Growth, *Science*. 290 (2000) 1134–1137. doi:10.1126/science.290.5494.1134.
- [10] H.D. Keith, F.J. Padden, Spherulitic Crystallization from the Melt. I. Fractionation and Impurity Segregation and Their Influence on Crystalline Morphology, *J. Appl. Phys.* 35 (1964) 1270–1285. doi:10.1063/1.1713606.
- [11] H.D. Keith, F.J. Padden, Spherulitic Crystallization from the Melt. II. Influence of Fractionation and Impurity Segregation on the Kinetics of Crystallization, *J. Appl. Phys.* 35 (1964) 1286–1296. doi:10.1063/1.1713607.
- [12] S. Pizzini, C. Calligaris, On the Effect of Impurities on the Photovoltaic Behavior of Solar-Grade Silicon I. The Role of Boron and Phosphorous Primary Impurities in p-type Single-Crystal Silicon, *J. Electrochem. Soc.* 131 (1984) 2128–2132. doi:10.1149/1.2116033.
- [13] S. Pizzini, L. Bigoni, M. Beghi, C. Chemelli, On the Effect of Impurities on the Photovoltaic Behavior of Solar Grade Silicon II. Influence of Titanium, Vanadium, Chromium, Iron, and Zirconium on Photovoltaic Behavior of Polycrystalline Solar Cells, *J. Electrochem. Soc.* 133 (1986) 2363–2373. doi:10.1149/1.2108409.
- [14] S. Pizzini, Towards solar grade silicon: Challenges and benefits for low cost photovoltaics, *Sol. Energy Mater. Sol. Cells*. 94 (2010) 1528–1533. doi:10.1016/j.solmat.2010.01.016.
- [15] D.B.A. Rep, A.F. Morpurgo, W.G. Sloof, T.M. Klapwijk, Mobile ionic impurities in organic semiconductors, *J. Appl. Phys.* 93 (2003) 2082–2090. doi:10.1063/1.1538338.
- [16] X. Xu, M.J. Qin, K. Konstantinov, D.I. dos Santos, W.K. Yeoh, J.H. Kim, S.X. Dou, Effect of boron powder purity on superconducting properties of MgB_2 , *Supercond. Sci. Technol.* 19 (2006) 466–469. doi:10.1088/0953-2048/19/6/009.
- [17] J. Jiang, B.J. Senkowitz, D.C. Larbalestier, E.E. Hellstrom, Influence of boron powder purification on the connectivity of bulk MgB_2 , *Supercond. Sci. Technol.* 19 (2006) L33–L36. doi:10.1088/0953-2048/19/8/L02.
- [18] USP–NF, (n.d.). <http://www.usp.org/usp-nf> (accessed February 16, 2017).
- [19] European Pharmacopoeia Reference Standards - Purpose and Use | EDQM - European Directorate for the Quality of Medicines & HealthCare, (n.d.). <https://www.edqm.eu/en/ph-eur-reference-standards-purpose-and-use> (accessed February 16, 2017).
- [20] American Chemical Society Publications: Reagent Chemicals, 10th Edition, (n.d.). <http://pubs.acs.org/reagents/> (accessed February 16, 2017).
- [21] Brands and Grades, Sigma-Aldrich. (n.d.). <http://www.sigmaaldrich.com/united-kingdom/technical-services/brands-and-grades.html> (accessed February 16, 2017).

- [22] A. König, M. Stepanski, A. Kuszlik, P. Keil, C. Weller, Ultra-purification of ionic liquids by melt crystallization, *Chem. Eng. Res. Des.* 86 (2008) 775–780. doi:10.1016/j.cherd.2008.04.002.
- [23] B.R. Bathey, M.C. Cretella, Solar-grade silicon, *J. Mater. Sci.* 17 (1982) 3077–3096. doi:10.1007/BF01203469.
- [24] ACS Grade Solvents - ACS and Reagent Grade Solvents | Sigma-Aldrich, (n.d). <http://www.sigmaaldrich.com/chemistry/solvents/products.html?TablePage=14577688> (accessed July 27, 2017).
- [25] G. Coquerel, Crystallization of molecular systems from solution: phase diagrams, supersaturation and other basic concepts, *Chem. Soc. Rev.* 43 (2014) 2286–2300. doi:10.1039/C3CS60359H.
- [26] G. Coquerel, Chiral Discrimination in the Solid State: Applications to Resolution and Deracemization, in: *Adv. Org. Cryst. Chem.*, Springer, Tokyo, 2015: pp. 393–420. doi:10.1007/978-4-431-55555-1_20.
- [27] L. Renou, T. Morelli, S. Coste, M.-N. Petit, B. Berton, J.-J. Malandain, G. Coquerel, Chiral Discrimination at the Solid State of Methyl 2-(Diphenylmethylsulfinyl)acetate, *Cryst. Growth Des.* 7 (2007) 1599–1607. doi:10.1021/cg070075f.
- [28] Y. Amharar, S. Petit, M. Sanselme, Y. Cartigny, M.-N. Petit, G. Coquerel, Crystal Structures, Dehydration Mechanism, and Chiral Discrimination in the Solid State of a Hydantoin Derivative, *Cryst. Growth Des.* 11 (2011) 2453–2462. doi:10.1021/cg200243y.

Chapter I

**Basic notions on phase equilibria,
material purification
and characterization**

Chapter I

BASIC NOTIONS ON PHASE EQUILIBRIA, MATERIAL PURIFICATION AND CHARACTERIZATION

TABLE OF CONTENTS

NOMENCLATURE.....	27
I. INTRODUCTION.....	29
II. BASIC NOTIONS ON PHASE EQUILIBRIA.....	29
1) Thermodynamic phase, free energy, state of equilibrium, variance.....	29
a) Concept of thermodynamic phase.....	29
b) Thermodynamic quantities.....	29
c) State of equilibrium.....	30
d) Variance.....	31
2) Unary systems.....	32
a) Factors of equilibrium.....	32
b) Variance.....	32
c) Phase free energy and representation of phase stability domains.....	32
i. Topological representation of phase equilibria.....	32
ii. Free energy surfaces, one- and two-phase equilibria.....	33
iii. Three-phase equilibria.....	33
d) Polymorphism.....	34
i. Enantiotropy.....	35
ii. Monotropy – monotropic behavior.....	36
iii. Polymorphism at constant pressure.....	36
iv. Metastable systems.....	38
v. Phase transitions in unary systems.....	38
3) Binary systems at constant pressure.....	39
a) Variables of the system and representation.....	39
b) Variance.....	39
c) Lever rule.....	40
d) Phase Gibbs free energy.....	41
i. Notion of solution.....	41
ii. Free energy of binary solutions.....	41
iii. Tangent rule.....	43
iv. A first illustration of the tangent rule: case of miscibility gaps.....	43
v. Two-phase equilibria.....	44
vi. Invariant equilibria.....	45
e) Examples of binary phase diagrams.....	47
i. Complete miscibility in the solid and liquid states.....	47
ii. Binary invariant transformations.....	48
iii. Intermediate phases.....	49
iv. Calorimetry of invariant transformations.....	50
4) Ternary systems at constant pressure and temperature.....	51
a) Variance.....	51
b) Variables of composition.....	51
c) Topological representation.....	52
d) Phase free energy.....	53
i. Generalities.....	53
ii. Two-phase domains.....	53
iii. Three-phase domains.....	54

e) From binary to ternary phase diagrams.....	56
III. EXPERIMENTAL TECHNIQUES FOR MATERIAL AND PHASE EQUILIBRIA CHARACTERIZATION.....	
1) Differential Scanning Calorimetry	60
a) Principle of HF-DSC.....	60
b) Signal delay.....	61
c) Characterization of binary phase equilibria.....	62
i. Binary systems with complete miscibility in the solid and liquid states.....	62
ii. Binary system involving invariant transformations.....	62
2) X-Ray Powder Diffraction	63
a) Solid phase crystal structure.....	63
b) Principle of PXRD.....	63
i. Description of the measurement procedure, Bragg's condition.....	63
c) Application to phase identification.....	64
3) Analysis of chemical composition	65
4) The problem of sample preparation	66
IV. TECHNIQUES FOR MATERIAL CHEMICAL PURIFICATION AND PURITY ASSESSMENT.....	
1) Methods for chemical purification	67
2) Methods for chemical composition assessment	68
V. CONCLUSION.....	70
VI. APPENDICES.....	71
1) Phase transitions in unary systems	71
a) Displacive and reconstructive phase transitions.....	71
b) Order-disorder transitions.....	71
c) Ehrenfest classification of phase transitions.....	73
2) Calorimetry of the eutectic transformation	76
VII. REFERENCES.....	78

NOMENCLATURE

Variables

c	[-]	Number of components
C_p	[J·mol ⁻¹ ·K ⁻¹]	Molar heat capacity
d	[m]	Inter-reticular plane distance
f	[-]	Phase fraction
G	[J·mol ⁻¹]	Gibbs molar free energy
H	[J·mol ⁻¹]	Molar enthalpy
I	[arbitrary unit]	Intensity
k	[-]	Number of external constraints
k	[-]	Segregation coefficient
m	[kg]	Mass
n	[mol]	Amount of matter
N	[-]	Number of equilibrium factors
p	[Pa]	Pressure
Q	[J·mol ⁻¹]	Amount of molar heat
r	[-]	Number of chemical relationships
S	[J·mol ⁻¹ ·K ⁻¹]	Molar entropy
T	[K]	Temperature
T_{fus}	[K]	Melting point
U	[J·mol ⁻¹]	Molar internal energy
V	[m ³ ·mol ⁻¹]	Molar volume
v	[-]	Variance
X	[-]	System or sub-system composition
$\Delta_{mix} G$	[J·mol ⁻¹]	Free energy of mixing
$\Delta_{mix} H$	[J·mol ⁻¹]	Heat/enthalpy of mixing
$\Delta_{fus} H$	[J·mol ⁻¹]	Latent heat of fusion
$\Delta_T H$	[J·mol ⁻¹]	Latent heat of solid-solid phase transition
$\Delta_{mix} S$	[J·mol ⁻¹ ·K ⁻¹]	Entropy of mixing
λ	[m]	Wavelength
φ	[-]	Number of phases
ϕ	[W·kg ⁻¹]	Specific heat flux
θ	[°]	Diffraction angle

Abbreviations

DSC	Differential Scanning Calorimetry
G	Gas phase
L	Liquid phase
S	Solid phase
ss	Solid solution
XRPD	X-Ray Powder Diffraction

Operators

Δ	Difference between two thermodynamic states
∂	Operator for partial derivative
Σ	Sum

Constants

$R = 8,314 \text{ J}\cdot\text{mol}^{-1}\cdot\text{K}^{-1}$	The gas constant
---	------------------

I. INTRODUCTION

In the field of material purification, phase separation processes are the most employed methods to separate target species from their impurities. These methods simply consist in taking advantage of phase equilibria between the chemical species involved in the corresponding process. Consequently, in the first part, this chapter aims at introducing some basic notions related to phase equilibria and phase diagrams, from unary to ternary systems.

As the assessment of phase equilibria requires specific devices and procedures, a second part presents the main material characterization tools employed to establish phase diagrams.

Then, a third part introduces the main purification process based on phase separation, with the support of phase diagrams to help at understanding the relationships between phase equilibria and chemical species separation. As developing purification methods requires to monitor their purifying effect, a few elements on analytical chemistry are presented to close this chapter.

II. BASIC NOTIONS ON PHASE EQUILIBRIA

1) Thermodynamic phase, free energy, state of equilibrium, variance

a) Concept of thermodynamic phase

In the field of thermodynamics, a phase is a part of a system whose properties (*e. g.*, density, chemical composition, ...) are uniform in space. In other terms, a phase is a part of space which is homogeneous in the macroscopic scale. Three main types of phases exist: solid phases, in which the components exhibit a long-range order; liquid phases, which are associated with a short-range order, and gases which are disordered.

b) Thermodynamic quantities

To describe the energetic state of a system, Gibbs molar free energy (G , in $\text{J}\cdot\text{mol}^{-1}$) is a state function commonly employed in case of transformations induced by pressure (p , in Pa) and temperature (T , in K). Its expression is given by the following relationship [1]:

$$G = U + pV - TS \quad (1)$$

U being the molar internal energy of the system (in $\text{J}\cdot\text{mol}^{-1}$), V the molar volume (in $\text{m}^3\cdot\text{mol}^{-1}$), and S the molar entropy (in $\text{J}\cdot\text{mol}^{-1}\cdot\text{K}^{-1}$). These three quantities are state functions, too. Internal energy corresponds to the sum of kinetic and potential energies of the atoms/molecules that constitute the system. Entropy is a state function introduced by Clausius [2], which was associated with the disorder of the system (*e. g.*, the number of configurations that the system can take in given conditions, which is a positive quantity) by Boltzmann [3].

Note that, when a system is made of several phases, its molar free energy is the weight mean of every phase energy, as indicated by eq. 2, in which f_{phase} is the molar fraction of the considered phase in the system:

$$G = \sum_{phase} f_{phase} G_{phase} \quad (2)$$

Since it is a function of p and T , G varies with respect to both quantities according to its partial derivatives that can be deduced from Maxwell's identities [4]. For chemically pure systems:

$$dG = \left(\frac{\partial G}{\partial p} \right)_T dp + \left(\frac{\partial G}{\partial T} \right)_p dT = V dp - S dT \quad (3)$$

When pressure is maintained constant (which is the case for all the transformations carried out under atmospheric pressure, for example), the molar free energy of a system becomes:

$$G = H - TS \quad (4)$$

H being the enthalpy of the system, often defined as its total amount of heat (in $\text{J} \cdot \text{mol}^{-1}$).

A system can also be described using its heat capacity (C_p , in $\text{J} \cdot \text{mol}^{-1} \cdot \text{K}^{-1}$, eq. 5), which corresponds to the amount of heat required to elevate by an infinitesimal value its temperature, at constant pressure – thus, it is a positive quantity. C_p is not a state function, but a macroscopic property of matter.

$$C_p = \left(\frac{\partial H}{\partial T} \right)_p \quad (5)$$

Additionally, C_p is also related to the variation of entropy with respect to temperature:

$$\left(\frac{\partial S}{\partial T} \right)_p = \frac{C_p}{T} \quad (6)$$

It can be deduced that H and S are both increased when temperature raises. Nevertheless, at constant pressure, $dG = -S dT$ (eq. 3). Therefore, as S is a positive quantity, G decreases as temperature increases.

Two important properties associated with free energy should be reminded [1,5,6]:

- A single transformation of a system is made spontaneous when the free energy of the final state (G_f) is lower than that of the initial one (G_i), which yields: $\Delta G = G_f - G_i$ (**Theorem 1**)
- The most stable state of a thermodynamic system is attained when its molar free energy is at its lowest possible value (**Theorem 2**).

c) State of equilibrium

A system is in the state of equilibrium when no motion of any kind (*e. g.*, matter or energy) occurs inside it, which yields [1]:

$$\frac{dG}{dt} = 0 \quad (7)$$

t being time.

Nevertheless, one has to distinguish two types of equilibrium states: **stable** and **metastable** equilibria (fig. 1). A stable equilibrium is always associated with the lowest possible value of

G (here, G_2). Metastable equilibria correspond to local minimum values of G (here, G_1). The transformation of the system from a metastable state to a stable one is always possible as $\Delta G = G_f - G_i < 0$. Nevertheless, such transformation can occur only when the sufficient activation energy is provided, so that the system could “jump” the energy barrier (ΔG_a).

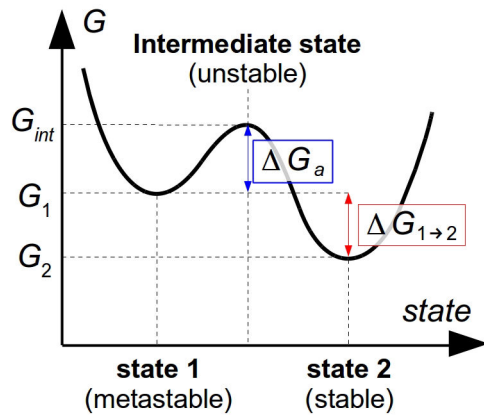


FIG. 1: Relationship between stability, metastability and Gibbs free energy

Generally, a metastable material undergoing transformations transits between intermediate metastable states before reaching the most stable one [7,8]. This empirical observation has been formalized by Ostwald rule of stages [9–11]. However, a few exceptions are known [12–14].

d) Variance

In the state of equilibrium, the variance of a system, v , is given by the following relationship (Gibbs' phase rule [15]):

$$v = c - r - k + N - \varphi \quad (8)$$

c being the number of chemical species in the system, r the number of chemical reactions between the different species, k the number of external constraints (for example, when pressure is maintained constant, $k = 1$), N the number of equilibrium factors (*e. g.*, p and T , so $N = 2$), and φ the number of phases.

Physically, the variance corresponds to the largest number of thermodynamic variables that can be changed simultaneously without altering the equilibrium (*e. g.*, without changing the number and the nature of the phases in the system).

Equilibria complying with $v = 0$ are called “invariant”.

2) Unary systems

The study of phase equilibria in unary systems deals with chemically pure components, which means that:

- Compounds containing impurities fall outside of this framework,
- Chemically pure compounds which undergo irreversible chemical transformations during heating or during an increase of pressure cannot behave as unary systems in the range of physical conditions in which the transformations occur.

a) Factors of equilibrium

In unary systems, the stability of every phase depends on pressure and temperature, that are the two thermodynamic parameters that impact phase equilibria.

b) Variance

In unary systems, $c = 1$. Assuming that:

- no external constraint is applied to the system ($k = 0$),
- no chemical transformation occurs inside the system ($r = 0$);
- phase equilibria are only governed by two intensive variables: p and T ($N = 2$).

Then, $\nu = 3 - \phi$ (9)

Consequently, the variance of the system in one-phase (p, T) domains equals 2, which means that pressure and temperature can be changed without altering the nature of the phase. For two-phase equilibria, $\nu = 1$. Therefore, a modification of one of the parameters (p or T) without changing the nature of phases in equilibrium implies that the other parameter is imposed by the equilibrium. Eventually, in three-phase equilibria, $\nu = 0$, which means that the conditions of occurrence of such equilibria are unique – there is no degree of freedom.

c) Phase free energy and representation of phase stability domains

i. Topological representation of phase equilibria

The most convenient way to represent the stable states of a unary system is a 2-axis plot, in which pressure and temperature are used as variables. Such plot completed with legends denoting the domains of stability of the different phases is the topological phase diagram of the system.

According to Gibbs' phase rule, the different phase domains can be represented according to tab. 1 entries [5].

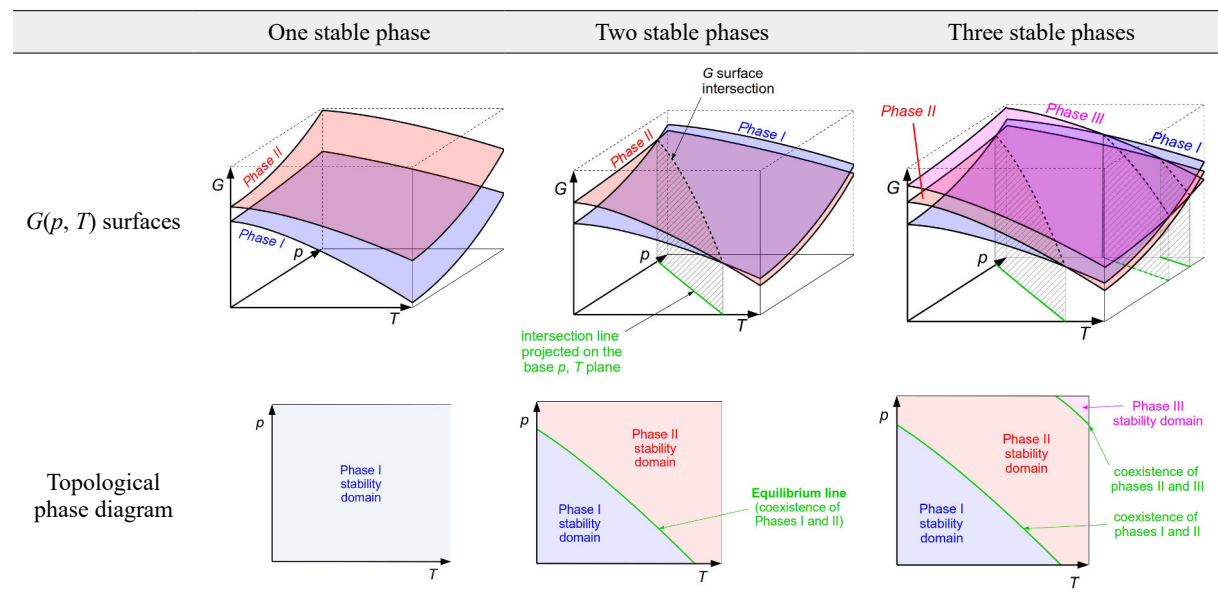
TAB. 1: Representation of phase equilibria on topological phase diagrams

Type of equilibrium	Variance	Representation on a (p, T) chart
one-phase	2	surface
two-phase	1	line
three-phase	0	point

ii. Free energy surfaces, one- and two-phase equilibria

In unary systems, the stability of the different phases is governed by their Gibbs free energy (eq. 1). In given p , T conditions, the most stable phase is the one that has the lowest $G(p, T)$ value (theorem 2). Stability domains of one-phase equilibria are represented by surfaces. When two phases have the same $G(p, T)$ values, the corresponding p , T coordinates denote the coexistence of these phases. These coordinates correspond to two-phase equilibrium lines. Illustrations of these notions are provided in tab. 2, in which several cases involving one- and two-phase equilibria are represented.

TAB. 2: Examples of unary system Gibbs free energy and phase diagrams plots with one- and two-phase equilibria



iii. Three-phase equilibria

In unary systems, it is possible to observe that $G(p, T)$ surfaces of three different phases intercept each other at one discrete (p, T) point. In this case, the three phases are coexisting at these coordinates, which denotes the existence of a triple point, the latter being invariant.

According to the rules applicable to phase relative stability ($G(p, T)$ surfaces relative values), it is possible to show that the triple point corresponds to the intersection of three different two-phase equilibrium lines, as shown in fig. 2. Nevertheless, the latter should obey to Schreinemaker's rule [16] which states that the prolongation of a given two-phase equilibrium line beyond the triple point should lie in the one-phase domain of the third phase involved in the invariant equilibrium (see fig. 2b).

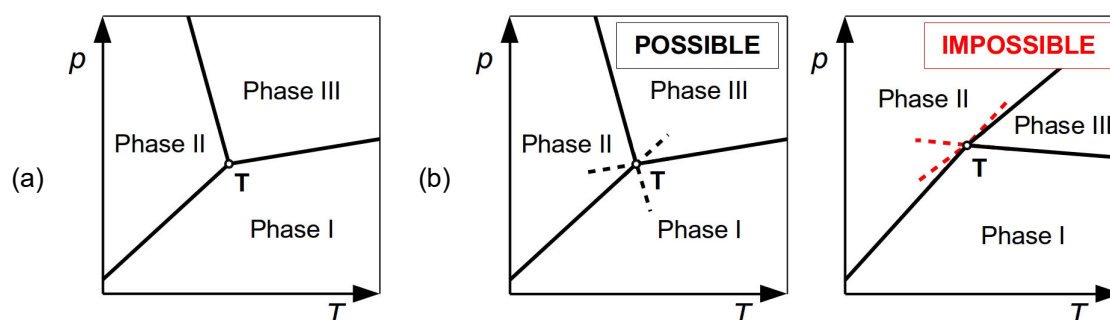


FIG. 2: **Unary phase diagrams with existence of triple point (T)** – (a) ordinary example; (b) illustration of Schreinemaker's rule

The most simple unary systems generally present three different phases: solid (S), liquid (L) and gas (G). This implies the existence of a triple point T at which they coexist. In addition, increasing pressure and temperature leads to the decrease of the difference between liquid and gas phase properties (refraction index, density...) up to a single critical point (C) beyond which there is no difference anymore. In that region, the system behaves as a supercritical fluid (SCF). An example of ordinary unary phase diagram exhibiting triple and critical points is shown in fig. 3.

Two-phase equilibrium lines denote the possible occurrence of phase transformations inside the system when changing p and T . These transformations are named according to tab. 3 entries.

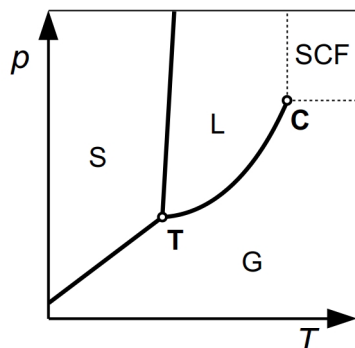


FIG. 3: **Ordinary unary phase diagrams with existence of triple (T) and critical (C) points**

TAB. 3: **Names of phase transformations**

Starting phase	Final phase	Name of the phase transformation
S	L	melting
L	S	solidification
S	G	sublimation
G	S	condensation
L	G	vaporization
G	L	liquefaction

d) Polymorphism

Many chemical species can present different solid phases (*e. g.*, crystalline phases in which the packing of atoms or molecules are different). This phenomenon is known as “*allotropism*” (for simple bodies) or “*polymorphism*” (for chemical compounds). To illustrate this notion, 8 allotropes of Carbon are shown in fig. 4, as well as the phase diagram of this system (stable equilibria only).

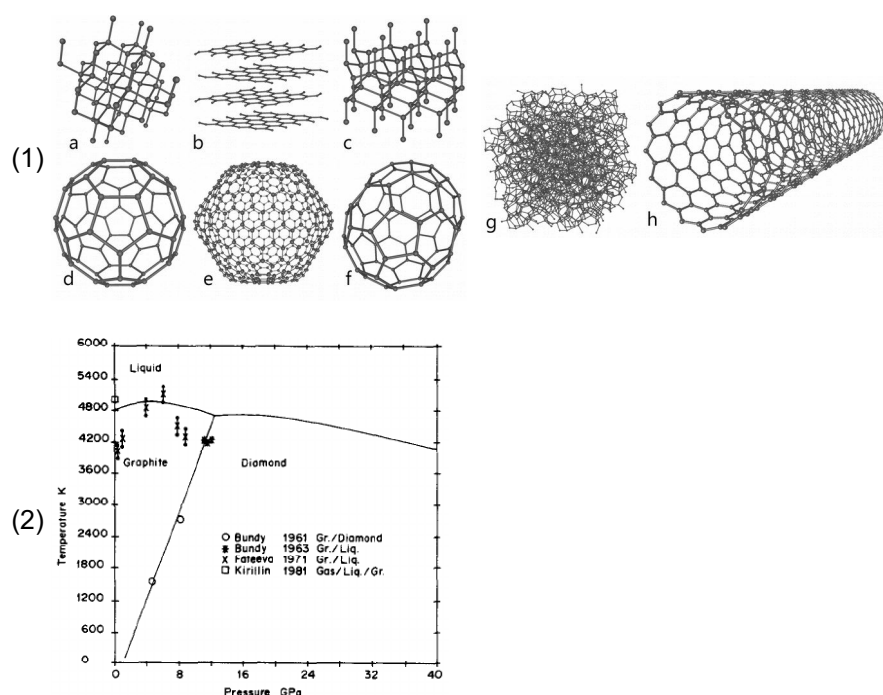


FIG. 4: **The Carbon system** – (1) *Different allotropes of Carbon*: a. diamond; b. graphite; c. lonsdaleite; d. fullerene C60; e. fullerene C540; f. fullerene C70; g. amorphous Carbon¹; h. nanotube. From Wikimedia [17]; (2) *Stable equilibrium phase diagram of Carbon*, from [18].

Every phase has its own molar free energy that changes with pressure and temperature. According to the rules governing phase stability, two- and three-phase equilibria between the different solid phases and another one (liquid or gas, for example) are possible. Nevertheless, two distinct cases can be envisaged. Indeed, the two solid phases can exhibit enantiotropic relationships or monotropic behaviors.

i. Enantiotropy

Two solid phases are enantiotropically related when, by changing pressure and temperature, reversible reversal of their stability occurs [19,20]. In such case, the unary phase diagram of the corresponding system lets appear two concomitant stability domains of these two solids (fig. 5a). By considering the existence of the two liquid and gas phases, such case implies the existence of at least three different stable triple points. However, the prolongation of two-phase equilibrium lines in their domain of metastability evidences the existence of a fourth triple point that is metastable (fig. 5b).

Beside that of Carbon [18], many species present enantiotropically related solid phases. Among them, benfluorex hydrochloride [21] or flurbiprofen [22] can be mentioned (non-exhaustive list).

1. Amorphous Carbon is not, in fact, a crystalline species – so it is not an allotrope, and no metastable equilibria involving an amorphous phase can occur. Amorphous phases are rather defined as being liquids exhibiting viscosity of solids. They are out of equilibrium and can turn into crystalline phase(s) if the required activation energy is provided.

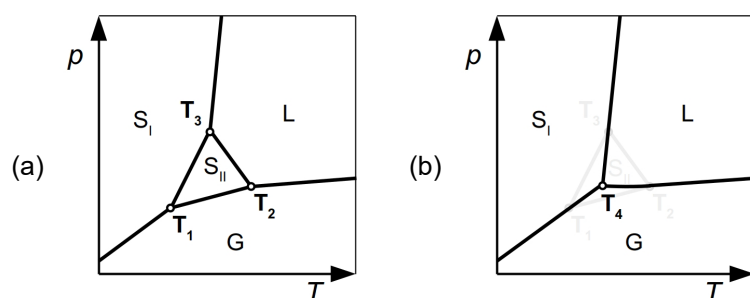


FIG. 5: **Unary phase diagram with existence of two solid phases (S_I and S_{II}) enantiotropically related** – (a) stable equilibria; (b) metastable equilibria (stable equilibrium lines are shown in gray)

ii. Monotropy – monotropic behavior

Two phases are said monotropically related if one of them is more stable than the other, whatever p and T [19,20]. In fact, it is not possible to compare the stability of two solid phases complying with this behavior in conditions in which another phase (liquid or gas) is stable. This is why “*monotropic behavior*” is preferred to describe such cases, instead of “*monotropy*”.

Such case implies the existence of one stable triple point and another metastable one (fig. 6).

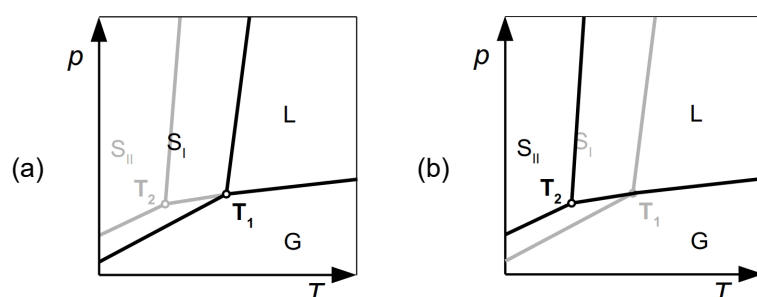


FIG. 6: **Unary phase diagram with existence of two solid phases (S_I and S_{II}) exhibiting monotropic behaviors with respect to each other** – (a) stable equilibria; (b) metastable equilibria

Biclotymol [23], Rimonabant [24] and Cimetidine [25] are a few examples (among many others) of molecules whose solid phases show monotropic behaviors.

iii. Polymorphism at constant pressure

At constant pressure, the free energy ($G = H - TS$) associated with one considered phase is only a function of temperature. Representation of phase H and G functions in energy vs. temperature charts were introduced by Burger and Ramberger [19,20] in order to assess the stability of different crystalline forms associated with one pure compound. Many rules were stated by these two researchers to deduce, of two crystalline phases, which one has the highest stability.

Here, these rules will not be enunciated, but energy vs. temperature plots will be discussed in order to explain the occurrence of phase transitions in chemically pure systems.

Enthalpy and entropy are two state functions that exhibit a strong temperature dependence. Moreover, both increase when temperature raises (the reciprocal statement is true, too), due to their properties:

$$H(T) = H(T_0) + \int_{T_0}^T C_p dT$$

$$S(T) = S(T_0) + \int_{T_0}^T C_p \frac{dT}{T}$$
(10)

For every phase, the $-TS$ contribution to G is more important than that of H , which means that G decreases as temperature is increased (eq. 3: $dG = -SdT$). Nevertheless, according to the properties associated with every phase ($H(T_0)$, $S(T_0)$, $C_p(T)$, ...), the $G(T)$ functions of the solid phases can describe enantiotropic or monotropic behaviors.

One way to describe enantiotropic and monotropic systems is the representation of Burger plots (fig. 7). In these plots, the $H(T)$ and $G(T)$ functions of solid and liquid phases are represented (here, the case of a dimorphic system is approached).

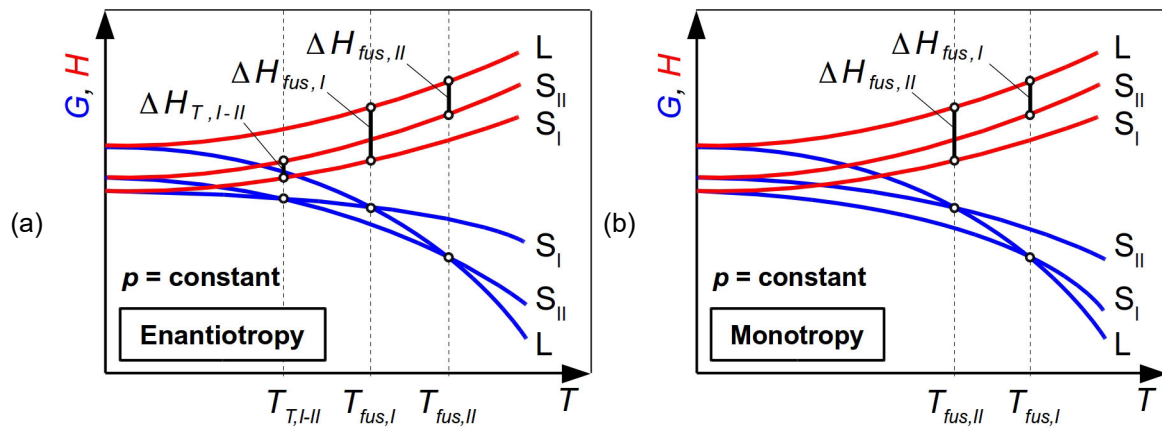


FIG. 7: **Burger diagrams of an ordinary unary system** – (a) case of enantiotropy; (b) case of monotropy

In the case of enantiotropy (fig. 7a), the stability of S_I and S_{II} solid phases is reversed at $T_{T,I-II}$, the temperature of reversible transition between the two crystalline forms. Here, S_I is stable below $T_{T,I-II}$, S_{II} is stable between $T_{T,I-II}$ and $T_{fus,II}$, and the liquid phase is stable above $T_{fus,II}$. Such case also implies the existence of a metastable melting point of S_I at $T_{fus,I}$. Note that the reversible transitions go hand in hand with a change of enthalpy that can be deduced from $H(T)$ curves. Therefore, these transitions are associated with certain latent heat values (ΔH).

In the case of monotropic behavior (fig. 7b), S_I is always stable below its melting point ($T_{fus,I}$), whereas S_{II} is metastable. This case implies the existence of a metastable melting point of S_{II} at $T_{fus,II}$. It is worth noting that the metastable solid can always turn into the stable one if the sufficient activation energy is provided. Such phenomenon goes hand in hand with the release of the corresponding latent heat. However, such transformation is irreversible because $G_{II} > G_I$.

iv. Metastable systems

Due to many reasons, metastable forms can be obtained during the crystallization of a pure compound (whatever the technique employed to reach the solid state). Many factors can influence such processes: the undercooling [6] (in case of crystallization from the melt), the presence of surfaces enhancing the heterogeneous nucleation of one specific form [26–31], the presence of impurities [32,33], the nature of the solvent (in case of crystallization from solution) [34,35], ...

These factors explain why a pure compound can be obtained as a metastable phase instead of the stable one. Consequently, these factors engender experimental difficulties to detect and master polymorphism in molecules, which can be matter of troubles in several applications such as active pharmaceutical ingredient development [36–38].

v. Phase transitions in unary systems

Pure components can undergo reversible phase transitions. The latter can be classified into several categories, but several classifications were previously proposed. Among them, Ehrenfest's one is widely agreed by the scientific community. A few elements on phase transitions and their classification are provided in appendix 1 (p. 71).

3) Binary systems at constant pressure

The study of binary systems is related to thermodynamic systems that contain two independent components ($c = 2$).

a) Variables of the system and representation

In addition to the pressure and temperature values they are submitted to, binary systems should be described using a third variable related to their composition. In a system containing two A and B independent components, the molar fractions (X) of the two components are:

$$X_A = \frac{n_A}{n_A + n_B} \quad (11)$$

$$X_B = \frac{n_B}{n_A + n_B} \quad (12)$$

n being the number of moles. Moreover, one has:

$$X_A + X_B = 1 \quad (13)$$

which means that the molar fractions of the two components are intrinsically related, and, therefore, only one of them is independent. **Hereafter, the composition of A/B binary systems will be designated by $X = X_B$.**

Note that the compositions can also be expressed as mass fractions.

Generally, binary equilibria are studied by maintaining pressure constant. Therefore, only temperature influences equilibria. Consequently, at constant pressure, phase equilibria in binary systems are governed by two variables: the temperature of the system (T) and its composition (X). Binary phase diagrams are thus represented on temperature vs. composition charts.

b) Variance

In a binary system of given composition, when:

- no chemical transformation occurs inside the system ($r = 0$);
- pressure is maintained constant ($k = 1$);

then the variance of the system is:

$$v = 3 - \varphi \quad (14)$$

Then it follows that the different types of possible equilibria are represented on $T(X)$ charts according to tab. 4 entries.

TAB. 4: **Representation of binary phase equilibria at constant pressure**

Equilibria	Variance	Representation on $T(X)$ chart
one-phase	2	surface
two-phase	1	line (one per phase)
three-phase	0	point

c) Lever rule

In binary systems in two-phase equilibrium at a certain temperature (T_{eq}), the respective proportions of the two phases can be calculated from the global composition of the system and those of the two phases.

An ordinary case of binary system in a two-phase equilibrium is represented in fig. 8, on which the coordinates of the system and its two phases in equilibrium are shown. The two phases (e. g., phases I and II) in equilibrium are represented by points **N** and **O**, respectively, and the system by point **M**. X_0 , X_I and X_{II} are the compositions of the system and its two phases ($X_I < X_0 < X_{II}$). The respective proportions of phases I and II can be calculated from a matter balance.

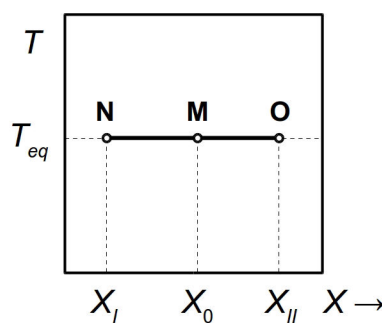


FIG. 8: **Illustration of the lever rule** – representation of the coordinates of the global mixture (**M**), and those of phase I (**N**) and phase II (**O**) in equilibrium, on a T vs. X chart

A balance applied to the system leads to the following system of equations:

$$\begin{aligned} n &= n_I + n_{II} \\ n X_0 &= n_I X_I + n_{II} X_{II} \end{aligned} \quad (15)$$

n being the number of moles in the system, and n_I and n_{II} the number of moles in the two phases in the state of equilibrium. Therefore, the respective molar fractions of the two phases (f) are:

$$f_I = \frac{n_I}{n} = \frac{X_0 - X_{II}}{X_I - X_{II}} \quad (16)$$

$$f_{II} = \frac{n_{II}}{n} = \frac{X_I - X_0}{X_I - X_{II}} \quad (17)$$

These fractions can also be calculated using the algebraic distances between points **M**, **N** and **O** shown in fig. 8:

$$f_I = \frac{\overline{MO}}{\overline{NO}} \quad (18)$$

$$f_{II} = \frac{\overline{NM}}{\overline{NO}} \quad (19)$$

Note that, as two phases coexist, $f_I + f_{II} = 1$.

d) Phase Gibbs free energy

Binary phase energy depends on X and T , the two variables that govern phase stability in binary systems. In this part, basic energetic models are presented in order to help at understanding phase formation and separation in such systems.

i. Notion of solution

Solutions are condensed binary phases in which the A and B components are mixed in the same phase. Two types of solutions exist: liquid and solid solutions. If the concept of liquid solution is clearly understood, that of solid solutions implies two cases: the formation of substitution or insertion solid solutions. Substitution solid solutions correspond to solid phases in which A and B components randomly occupy the different positions of the same crystal lattice. Insertion solid solutions correspond to solid phases in which the B component randomly occupies the different sites of A crystal lattice (see fig. 9).

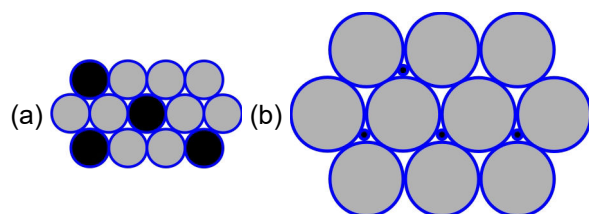


FIG. 9: **Illustration of the concept of solid solution** – (a) Substitution solid solution, (b) Insertion solid solution

The solubility of one component in a considered solid solution (*e. g.*, the ability of the two components at coexisting in the same single phase) depends on the interactions between atoms or molecules in the solid state and on the mechanical constraints engendered by the mixing (Hume-Rothery rules [39]). For example, Nickel and Copper have the same crystal structure and exhibit similar atomic radius values, and they are miscible in the solid state whatever their proportions. Oppositely, Lead and Tin have different crystal structures and atomic radii, their respective solubility values in the phase of the other are low.

In some papers related to organic molecules, the “*mixed crystals*” expression is used to designate solid solutions.

To approach the notion of miscibility of two components in the solid and liquid states, basic models of mixture free energy are helpful.

ii. Free energy of binary solutions

Let us consider a A/B binary system of composition X at constant temperature. Two states of this system are distinguished: the physical mixture (state #1) and the solution between the two components (state #2, see fig. 10 for the schematic representation).

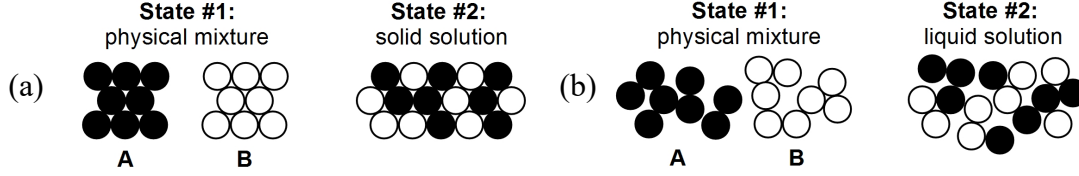


FIG. 10: **Schematic illustration of solution formation from physical mixtures**

In state #1, the free energy of the system is given by the following relationship:

$$G_1 = (1-X)G_A + XG_B \quad (20)$$

G_A and G_B being the molar free energies of pure A and B in the considered (liquid or solid) phase.

In state #2, the free energy is:

$$G_2 = G_1 + \Delta_{mix}G \quad (21)$$

$\Delta_{mix}G$ being the change of free energy associated with the mixing of both components. Starting from the first principle of thermodynamics, one has:

$$\Delta_{mix}G = \Delta_{mix}H - T\Delta_{mix}S, \text{ with } \Delta_{mix}H = H_2 - H_1 \text{ and } \Delta_{mix}S = S_2 - S_1 \quad (22)$$

On the one hand, in ideals systems, statistical physics permits to express $\Delta_{mix}S$ as follows [6]:

$$\Delta_{mix}S = -R[(1-X)\ln X + X\ln X] \quad (23)$$

which means that the increase of entropy engendered by the formation of the solution is positive.

On the other hand, $\Delta_{mix}H$ depends on the interactions between the A and B species, and their respective proportions in the system.

In the case of interactions between A and B, $\Delta_{mix}H < 0$ and, consequently, $\Delta_{mix}G < 0$. In other words, the formation of the solution is possible and favored from an energetic point of view, as $G_2 < G_1$. In case of repulsion between A and B, $\Delta_{mix}H > 0$. Therefore, if $T\Delta_{mix}S < \Delta_{mix}H$, then $\Delta_{mix}G > 0$, which means that the formation of the solution is not possible as $G_2 > G_1$. These two cases are represented in fig. 11.

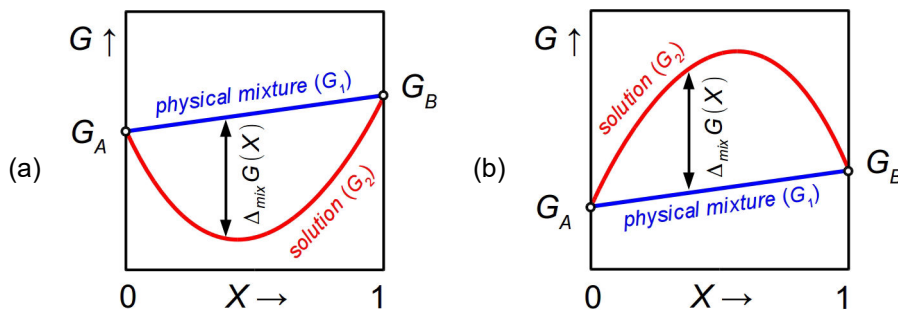


FIG. 11: **Free energy curves of binary physical mixtures and solutions** – (a) case favorable to the formation of the solution, (b) unfavorable case

iii. *Tangent rule*

When, at a certain temperature:

- the $G(X)$ curve of a phase present two inflection points ($d^2G/dX^2 = 0$) (**case 1**)
- or the $G(X)$ curves associated with two distinct phases intercept each other (**case 2**)

then there exist two composition values X_1 and X_2 that verify eq. 24 (equality of chemical potentials in the two phases).

$$\frac{\partial G_{\text{phase 1}}(X = X_1)}{\partial X} = \frac{\partial G_{\text{phase 2}}(X = X_2)}{\partial X} \quad (24)$$

In other terms, a straight line, simultaneously tangent to the two phase $G(X)$ curves at compositions X_1 and X_2 , can be drawn. In case 1, the two phases are described by the same $G(X)$ function (see part II.3d)iv on miscibility gaps).

For compositions outside $[X_1 ; X_2]$, the system stable phases are those of lowest $G(X)$ values. When $X_1 < X < X_2$, the stable state of the system is a mixture of the two phases of respective compositions X_1 and X_2 . Their proportions can be assessed using the lever rule.

iv. *A first illustration of the tangent rule: case of miscibility gaps*

In many binary systems, the stable state can be a mixture of two phases that are yet described by the same $G(X)$ function. Such case is called a miscibility gap, or spinodal decomposition. The domain of existence of the gap can be assessed by means of application of the tangent rule on system $G(X)$ function.

Let us illustrate that with a binary A/B system placed at constant temperature (T_{eq}). In case of existence of a miscibility gap, the $G(X)$ curve of the binary solution presents two inflexion points, which makes the tangent rule applicable (see fig. 12a). The tangent line (**PQ**) shows the compositions of the two phases in equilibrium (X_P and X_Q) when $X_P < X < X_Q$.

In a physical mixture of composition ranging between X_P and X_Q (represented by point **M**), the formation of a single solution (point **N**) is favored, as $G_N < G_M$. However, the formation of two phases (represented by point **P** and **Q**) lowers the energy of the system (point **O**) which explains why the system stable state is not a single phase.

Consequently, below X_P , the stable state of the system is a A-rich single solution. Above X_Q , the system forms a B-rich single phase. Between X_P and X_Q , the system forms a mixture of these two phases (fig. 12b).

Solving eq. 24 at different temperature values permits the deduction of the compositions of the two phases in equilibrium in the miscibility gap. Joining up the corresponding $T(X)$ dots leads to the corresponding equilibrium curve (fig. 12c). It is worth noting that, as the two phases in equilibrium are described by the same $G(X)$ function, if these phase are solid, then the two solids have the same crystal structure.

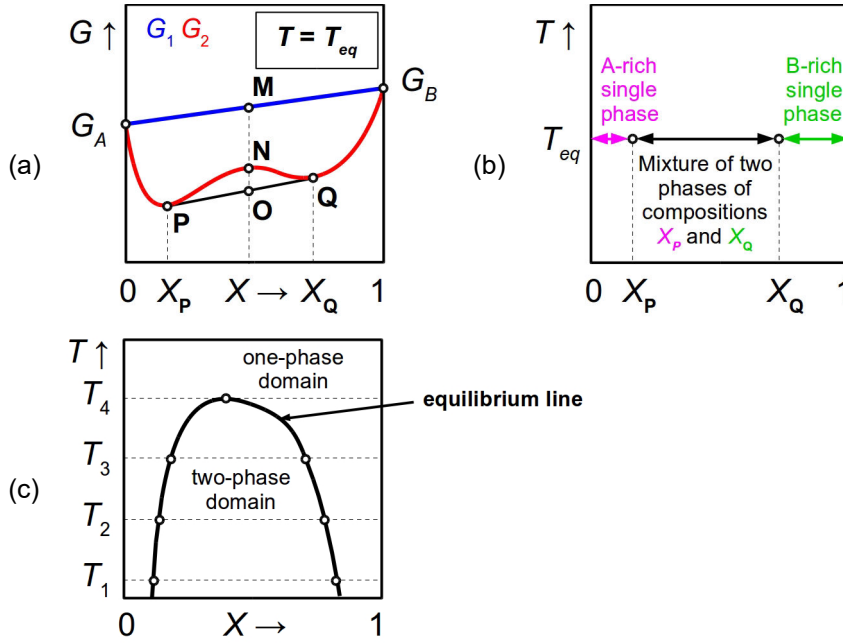


FIG. 12: **Miscibility gap** – (a) Isothermal Gibbs free energy curve; (b) phase stability domains at T_{eq} ; (c) phase stability domains at different temperatures

v. Two-phase equilibria

At a certain temperature, it is possible to observe binary equilibria between two phases described by separate $G(X)$ functions. Such equilibria can be rationalized by using the tangent rule applied to these functions.

Let us illustrate this concept on an ordinary A/B binary system (fig. 13). The two species consist in two different phases (“phase I” and “phase II”). At the equilibrium temperature (T_{eq}), phase I and II $G(X)$ functions present a common tangent straight line at points **O** and **P**. Consequently, in binary mixtures of composition $X_O < X < X_P$, the formation of two phases I and II of respective compositions X_O and X_P is favored, as the corresponding Gibbs energy (point **N**) is lower than that of the physical mixture (point **M**).

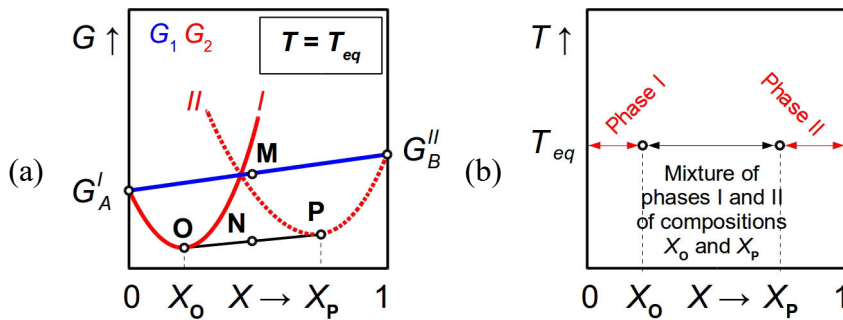


FIG. 13: **Two-phase domain** – a. Isothermal free energy curve; b. phase stability domains at the equilibrium temperature

Below X_O and above X_P , the stable states of the mixture are the single phases I and II, respectively.

vi. *Invariant equilibria*

In case of simultaneous stability of three different phases at a discrete temperature, there is a composition point at which the three phases coexist. This point is called “invariant” ($v = 0$), and exists at one single temperature (T_{inv}) and system composition value.

Let us consider a binary A/B equilibrium between three phases: I, II and III. The possible transformations of these three phases with respect to temperature can be classified into two categories: invariant reactions of type I and II.

In type-I invariant transformations, the two phases stable below T_{inv} associate with each other on heating to form a single phase above T_{inv} . In the case illustrated in fig. 14a, the corresponding reaction during heating is $I + II \rightarrow III$.

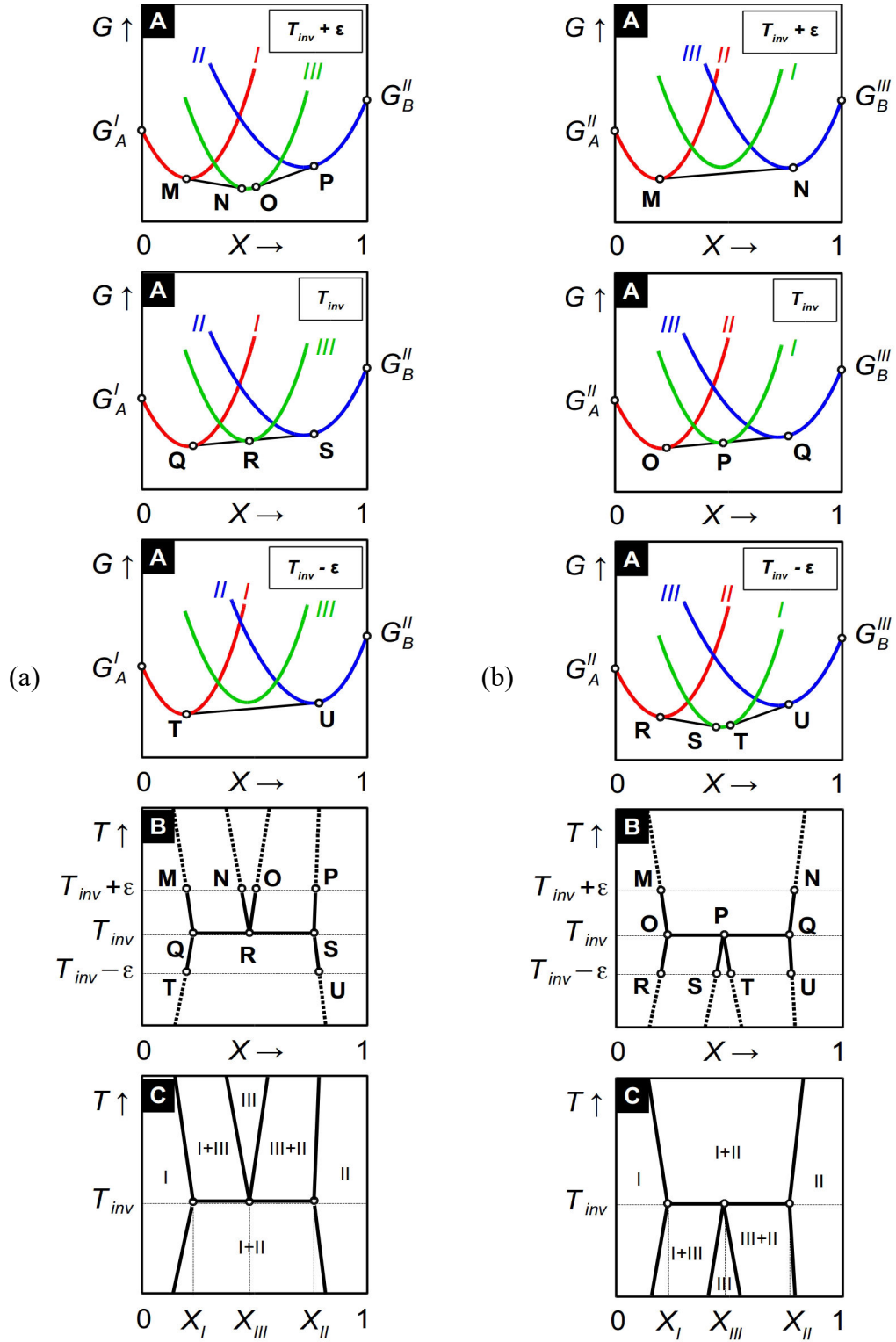
Conversely, in type-II invariant transformations, a single phase stable below T_{inv} discomposes into two phases above T_{inv} . In fig. 14b, the corresponding reaction is $I \rightarrow II + III$.

According to the nature of the phases involved in the invariant transformation, specific names are given to these transformations (see tab. 5). Many other transformations can be envisaged, but they are not often (or never) encountered. A recent paper attempted to give names to these transformations [40].

TAB. 5: Different possible invariant transformations involving solid phases (non-exhaustive list) – phases that are labeled with the same number (example: liquid 1 and liquid 1') indicate that miscibility gaps are involved in the considered transformation. The invariant reactions complying with this behavior are marked with asterisks (*).

Type	Nature of the phase			Name of the transformation
	I	II	III	
I (on heating, $I + II \rightarrow III$)	Solid 1	Solid 2	Liquid	Eutectic
	Solid 1	Solid 2	Solid 3	Eutectoid
	Solid	Liquid 1	Liquid 1'	Monotectic*
	Solid 1	Liquid	Solid 2	Metatectic
	Solid 1	Solid 2	Solid 2'	Monotectoid*
II (on heating, $I \rightarrow II + III$)	Solid 1	Liquid	Solid 2	Peritectic
	Liquid 1	Liquid 1'	Solid	Syntectic*
	Solid 1	Solid 2	Solid 3	Peritectoid
	Solid 1	Solid 2	Solid 2'	Syntectoid*

Fig. 14: **Invariant transformations in binary systems** - a. type I; b. type II. A. Phase free energies near the invariant transformation temperature; B. Projection of tangent points obtained after application of the tangent rule, and deduction of the equilibrium lines; C. Phase domains around the invariant transformation temperature. For the reason of clarity, the $G(X)$ functions of the physical mixtures are not represented.



e) Examples of binary phase diagrams

In this section, a selection of basic cases of solid-liquid binary equilibria are presented, in order to introduce new notions relevant for phase equilibria characterization and/or purification process development.

i. Complete miscibility in the solid and liquid states

The most simple binary systems are those in which the two components exhibit complete miscibility in the solid and liquid states. In other words, solid-liquid phase diagrams of such systems let appear only two one-phase domains: that of the solid (S) and that of the liquid (L). This implies the existence of one or more two-phase domains (S+L). These cases are illustrated in fig. 15.

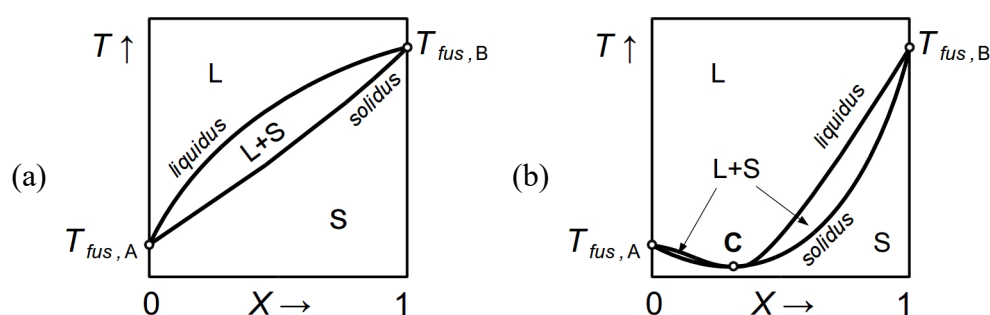


FIG. 15: **Binary phase diagrams of two hypothetical systems in which the components exhibit full miscibility in the solid and liquid states** – a. ordinary case; b. case of existence of a congruent point (C)

The curve associated with the melting of the solid phase is called “*solidus*”. That associated with the solidification of the liquid phase is the *liquidus*.

In some systems, it is possible to observe congruent points (e. g., points at which the equilibrium curves coincide – see fig. 15b). At the congruent point, the two phases in equilibrium have the same composition. However, the equilibrium lines should share the same horizontal tangent straight line at the congruent point, as shown in fig. 16 (Gibbs-Konovalov rule [41]).

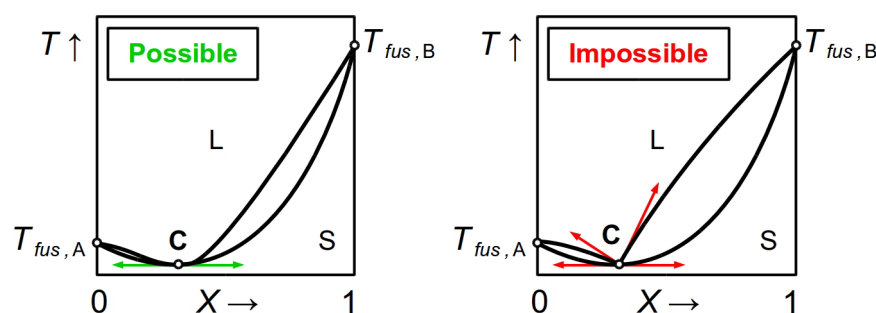


FIG. 16: **Illustration of Gibbs-Konovalov rule on congruent points**

ii. Binary invariant transformations

Systems in which the two components exhibit partial or no miscibility generally present miscibility gaps or invariant transformations. In this part, basic cases of binary phase diagrams involving common invariant reactions (eutectic, eutectoid, peritectic and peritectoid) are presented.

In fig. 17, examples of binary phase diagrams with type-I and -II invariant transformations are represented. During eutectic and eutectoid transformations (a, b), the two starting phases S_1 and S_2 give one single phase on heating (L in eutectic transformation, S_3 in eutectoid). Conversely, during peritectic and peritectoid transformations, the starting single solid phase S_1 gives two phases on heating ($L + S_2$ or $S_2 + S_3$, respectively). In cases (a) and (c), every solid phase has its own *liquidus* curve. Consequently, the *liquidus* of the systems are discontinuous. In addition, lines associated with equilibria between solid phases are called “*solvus*”.

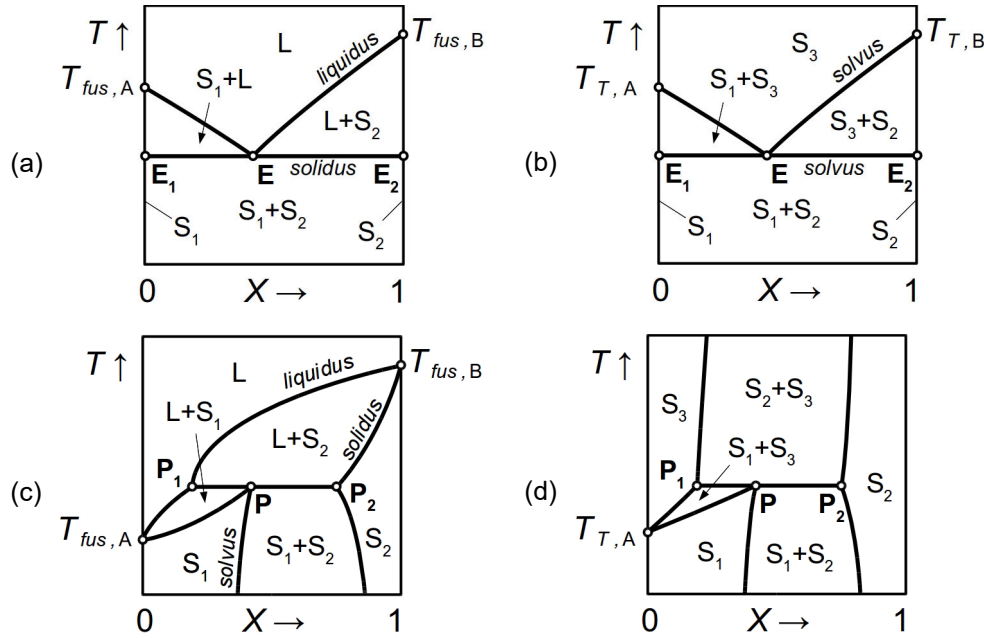


FIG. 17: **Simple binary phase diagrams representing invariant transformations –** (a) eutectic, (b) eutectoid, (c) peritectic, (d) peritectoid.

Segments E_1E and P_1P are called hypo-eutectic, -eutectoid, -peritectic or -peritectoid parts, according to the selected case. EE_2 and PP_2 correspond to hyper-eutectic, -eutectoid, -peritectic and -peritectoid parts.

Note that, in the solid phases involved in peritectic and peritectoid transformations, the two components necessarily exhibit partial miscibilities. The corresponding solid phase domains are surfaces, which is also called “partial solid solutions”. While not represented in fig. 17, partial solid solutions of more or less extent can be involved in eutectic and eutectoid transformations (fig. 18).

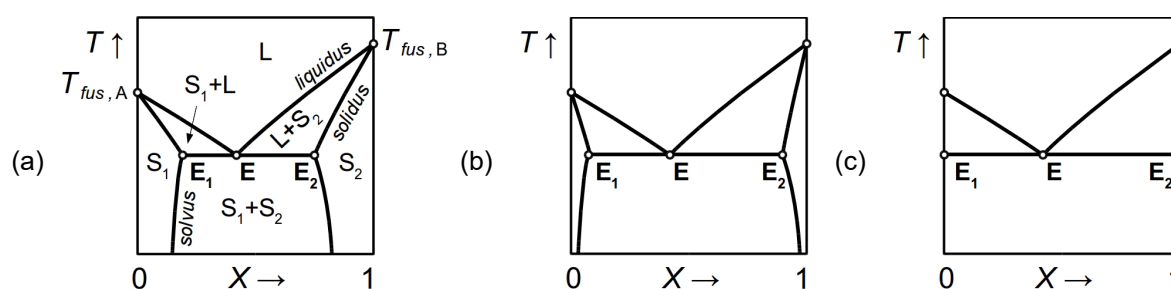


FIG. 18: **Binary phase diagrams with:** large (a), low (b) or no (c) stability domains of partial solid solutions.

The equilibrium lines near the invariant transformation temperature are submitted to strict rules, according to Schreinemaker [42]. Indeed, the tangents of these lines at the invariant temperature should lie in a two-phase domain (see fig. 19).

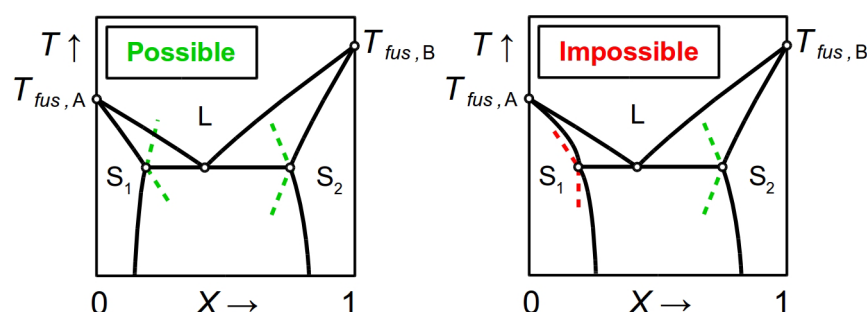


FIG. 19: **Illustration of Schreinemaker's rule in binary systems**

iii. Intermediate phases

In many systems, stable phases (other than liquid and that of the pure components) are susceptible to appear. They are called “*intermediate phases*”. If their stability stands on a very limited composition domain, they are generally called “*defined compounds*”, or “*co-crystals*” in the case of organic molecules.

Intermediate phases that exhibit a discrete composition are called “*stoichiometric compounds*”. Conversely, those exhibiting a stability over a certain composition range (*e. g.*, formation of partial solid solutions) are said “*non-stoichiometric*”.

Moreover, on heating, two types of behaviors are possible: **congruent** or **non-congruent melting**. A congruent-melting phase melts at one discrete temperature value and the composition of the liquid phase is the same as that of the solid. Conversely, on heating, non-congruent-melting phases decompose into two phases in a type-II invariant transformation (for example, a peritectic transformation).

Examples of phase diagrams involving intermediate compounds are shown in fig. 20.

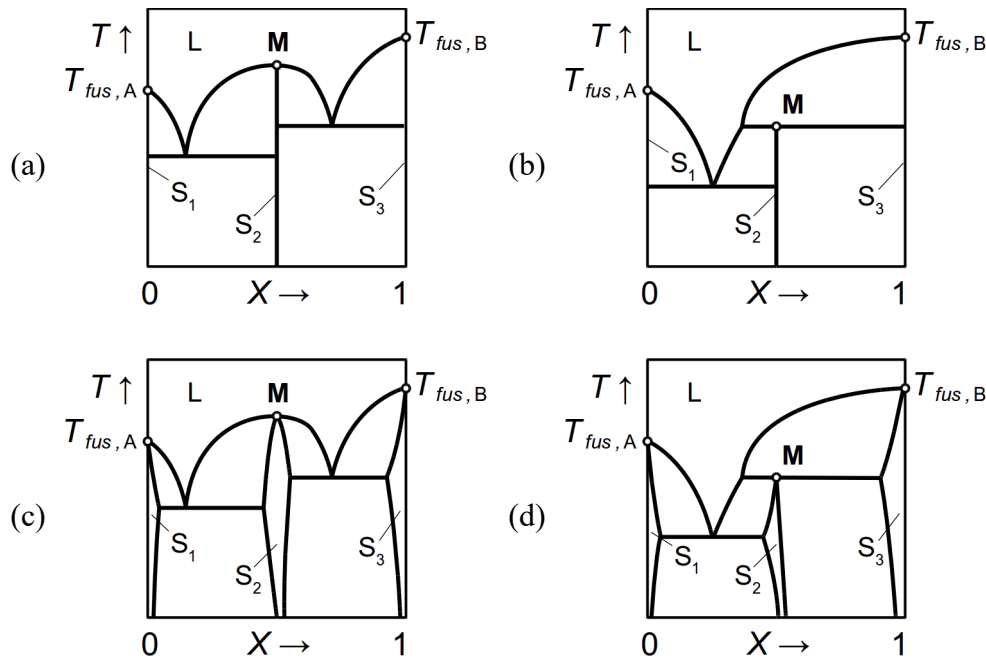


FIG. 20: **Examples of binary phase diagrams showing the existence of intermediate solid phases** – a. congruent melting stoichiometric compound; b. incongruent melting stoichiometric compound; c. congruent melting non-stoichiometric compound; d. incongruent melting non-stoichiometric compound. On every diagram, the melting point of the compound is represented by point **M**.

iv. Calorimetry of invariant transformations

On heating, invariant phase transformations are endothermic. The amount of heat absorbed by the system, Q , follows linear relationships with respect to its composition, as shown in fig. 21 for the case of type-I transformation. Q is maximal at the composition of the invariant point, null at the compositions of the boundary phases involved, and takes intermediate values otherwise. $Q(X)$ plots are called “*Tammann graphs*”, and allow the experimenter to determine the compositions of the three phases. This procedure can be applied to every type invariant reaction.

A demonstration of $Q(X)$ linearity is provided in appendix 2 (p. 76, case of the eutectic transformation).

Note that $Q(X)$ is generally measured in J g^{-1} , which requires to express compositions in **mass fractions**.

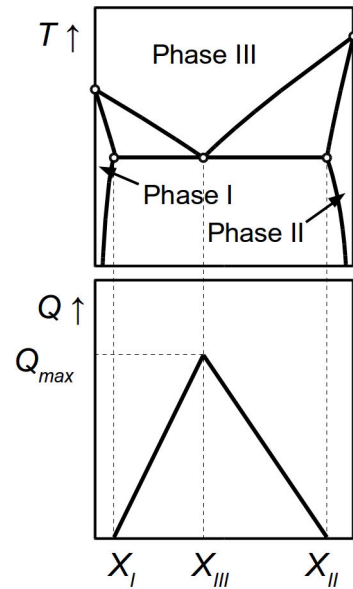


FIG. 21: **Tammann plot applied to an ordinary type-I invariant transformation**

4) Ternary systems at constant pressure and temperature

Ternary phase diagrams at constant pressure are prolongations of the constituting binary equilibria in a ternary composition/temperature space, as represented in fig. 22. In this section, the case of ternary equilibria at constant pressure and temperature is approached. Consequently, a focus on isothermal sections is attempted to introduce useful notions on crystallization processes.

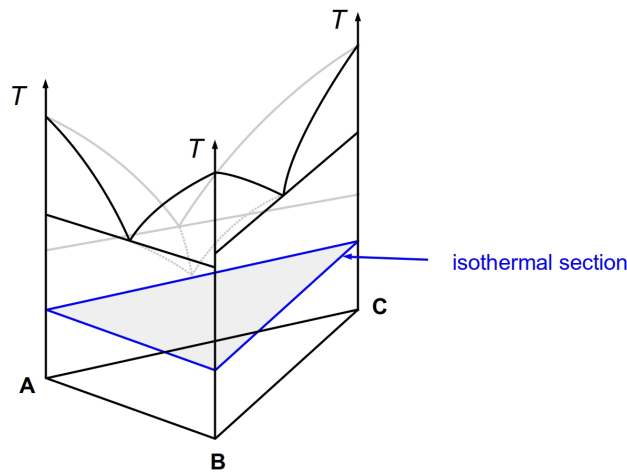


FIG. 22: Representation of a polythermic ternary phase diagram at constant pressure

a) Variance

In ternary systems ($c = 3$) in which equilibria are influenced by pressure and temperature ($N = 2$), the variance is given by $v = 5 - \phi$. Nevertheless, when both intensive variables are maintained constant, $k = 2$ and $v = 3 - \phi$. Therefore, variance equals 2 in one-phase domains, 1 in two-phase domains and 0 in three-phase domains. Here, the degree of freedom is related to the variables of composition of the system.

b) Variables of composition

In ternary systems, the composition is described by three variables: the (weight or molar) fractions of the three species. Let us consider a system made of three independent chemical species: A, B and C. Their molar fractions are:

$$X_A = \frac{n_A}{n_A + n_B + n_C} \quad (25)$$

$$X_B = \frac{n_B}{n_A + n_B + n_C} \quad (26)$$

$$X_C = \frac{n_C}{n_A + n_B + n_C} \quad (27)$$

Moreover, one has:

$$X_A + X_B + X_C = 1 \quad (28)$$

which means that **only two composition variables are independent**, because the third one is fixed by the others.

When variance equals 2 (*e. g.*, the system forms a single phase), the two composition variables can be changed without breaking the equilibrium. In a two-phase equilibrium ($\nu = 1$), the composition of one of the phases in equilibrium can be chosen, but that of the other phase will be fixed by the equilibrium. In three-phase invariant equilibria ($\nu = 0$), the compositions of the three phases are fixed by the equilibria; therefore, there is no degree of freedom.

c) Topological representation

The most conventional way to represent an isothermal and isobaric section of any ternary phase diagram is to use Gibbs' composition triangle [5,6,15], an equilateral triangle whose corners each represent a pure component of the system. The sides of the triangle are the corresponding binary composition axes. Nevertheless, a rotation direction must be fixed to obtain consistent reading of composition axis values. In this thesis, all the composition triangle axes will be described using a clockwise rotation direction.

Any ternary mixture of composition given by $\{X_A(\mathbf{M}), X_B(\mathbf{M}), X_C(\mathbf{M})\}$ can be represented by a point \mathbf{M} that is placed on the triangle according to the following rules, derived from homothety relationships:

$$X_A(\mathbf{M}) = \frac{\overline{MO}}{\overline{AO}}; X_B(\mathbf{M}) = \frac{\overline{MP}}{\overline{BP}}; X_C(\mathbf{M}) = \frac{\overline{MN}}{\overline{CN}} \quad (29)$$

\mathbf{N} , \mathbf{O} and \mathbf{P} being the points at which the \mathbf{CM} , \mathbf{AM} and \mathbf{BM} straight lines intercept the \mathbf{AB} , \mathbf{BC} and \mathbf{CA} lines (see fig. 23).

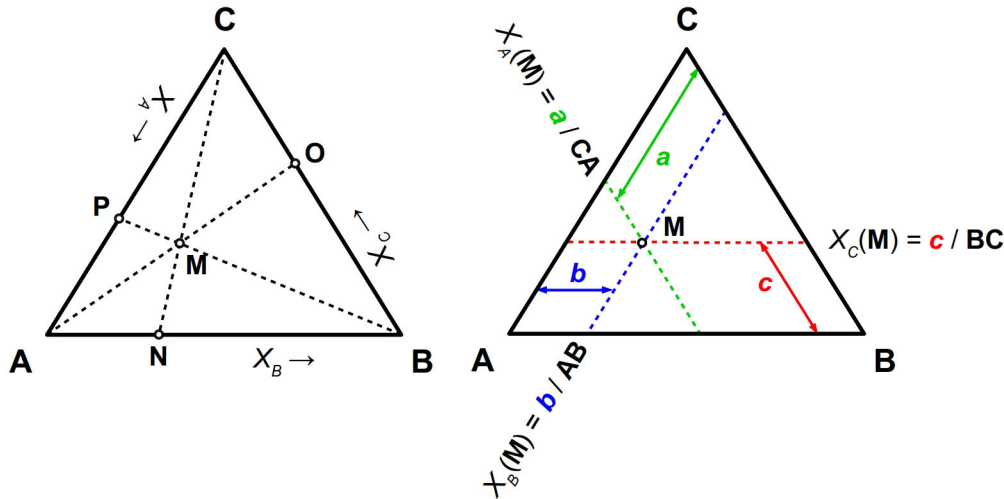
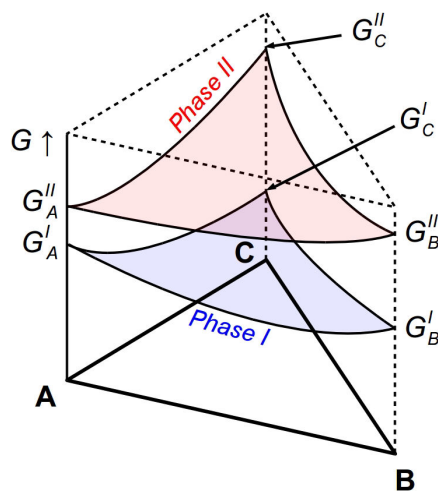


FIG. 23: Gibbs' composition triangle

d) Phase free energy

i. Generalities

The notions of phase free energy and components mixing by formation of solutions developed in the part related to binary systems can be extended to ternary ones. However, at constant temperature and pressure, G becomes a function of two independent variables – namely, X_A and $X_B - X_C$ being the complement. Therefore, $G(X_A, X_B)$ is a surface, and G functions can be represented in a three-sided prism whose base is the composition triangle, and height the G axis. The stable state of the system is the one that minimizes its free energy, and the tangent rule is still operative.



The most simple case is a system in which only one phase is stable, whatever the composition. This means that the G function associated with the stable phase is lower in value than that of all the other phases, as represented in fig. 24 – in which the ternary system appears as phase I, in the state of equilibrium.

In such cases, the composition of the phase in the state of equilibrium is the same as that of the system.

FIG. 24: **Example of phase free energy surfaces: case of one phase stable whatever the composition**

ii. Two-phase domains

At a given composition, in case of existence of a straight line of a plane: (i) that is simultaneously tangent to two different phase G functions, (ii) that minimizes the energy of the system (tangent rule); then the system stable state is a mixture of the two phases whose compositions are given by the tangent points coordinates (see example given in fig. 25).

The projection of the segment made by these two points on the base triangle is called “*tie line*” or “*conodal line*”. Any mixture whose composition lies on this line (represented here by point **M**) forms, in the state of equilibrium, two phases whose compositions are given by segment extremities (points **M**₁ and **M**₂). Moreover, their respective proportions can be calculated using the lever rule:

$$f_I = \frac{\overline{MM_2}}{\overline{M_1M_2}}; f_{II} = \frac{\overline{M_1M}}{\overline{M_1M_2}}; f_I + f_{II} = 1 \quad (30)$$

In a given two-phase equilibrium, there are an infinity of tangent lines that form a certain hull. The projection of this hull on the base triangle gives the range of stability of two-phase

mixtures. For the sake of clarity, only a few tie lines are generally represented on the composition triangle [5].

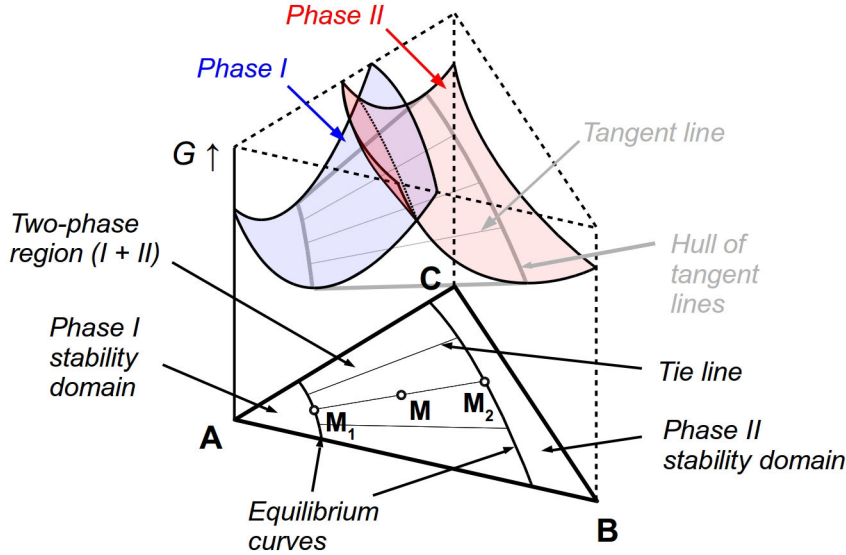


FIG. 25: **Example of phase free energy surfaces: case of existence of a two-phase domain**

iii. Three-phase domains

When a $G(X_A, X_B)$ plane:

- (i) is simultaneously tangent to three phase G functions,
- (ii) has a G value that minimizes the energy of the system;

then there exists a composition range in which the ternary system forms – in the state of equilibrium – the three corresponding phases whose compositions are given by the tangent points coordinates. Consequently, the three-phase domain is a triangle (see fig. 26a).

In addition, the following points can be deduced from rules applicable to G functions and phase stability (Palatnik-Landau rules [43], illustrated in fig. 26b):

- (i) on the composition triangle, the sides of the triangle domains that denotes the existence of three phases are concomitant to two-phase domains.
- (ii) the corners of the three-phase domains are concomitant to one- and two-phase domains.
- (iii) therefore, the two-phase domains are concomitant to three-phase (if applicable) and one-phase domains.

In the example shown in fig. 26a, when a ternary mixture presents a composition that lies in the three-phase domain (point **M**), the proportions of the three phases in equilibrium (points **N**, **O** and **P**, that correspond to phases I, II and III, respectively) can be calculated using the barycenter rule:

$$f_I(\mathbf{M}) = \frac{\overline{\mathbf{SM}}}{\overline{\mathbf{SN}}}; f_{II}(\mathbf{M}) = \frac{\overline{\mathbf{QM}}}{\overline{\mathbf{QO}}}; f_{III}(\mathbf{M}) = \frac{\overline{\mathbf{RM}}}{\overline{\mathbf{RP}}} \quad (31)$$

Eventually, according to Schreinemaker [44], the two-phase equilibrium curves are submitted to strict rules. Indeed, at every corner of a considered three-phase domain, the two-phase equilibrium line tangents must **both** lie in- or outside the three-phase domain triangle (see illustration in fig. 27).

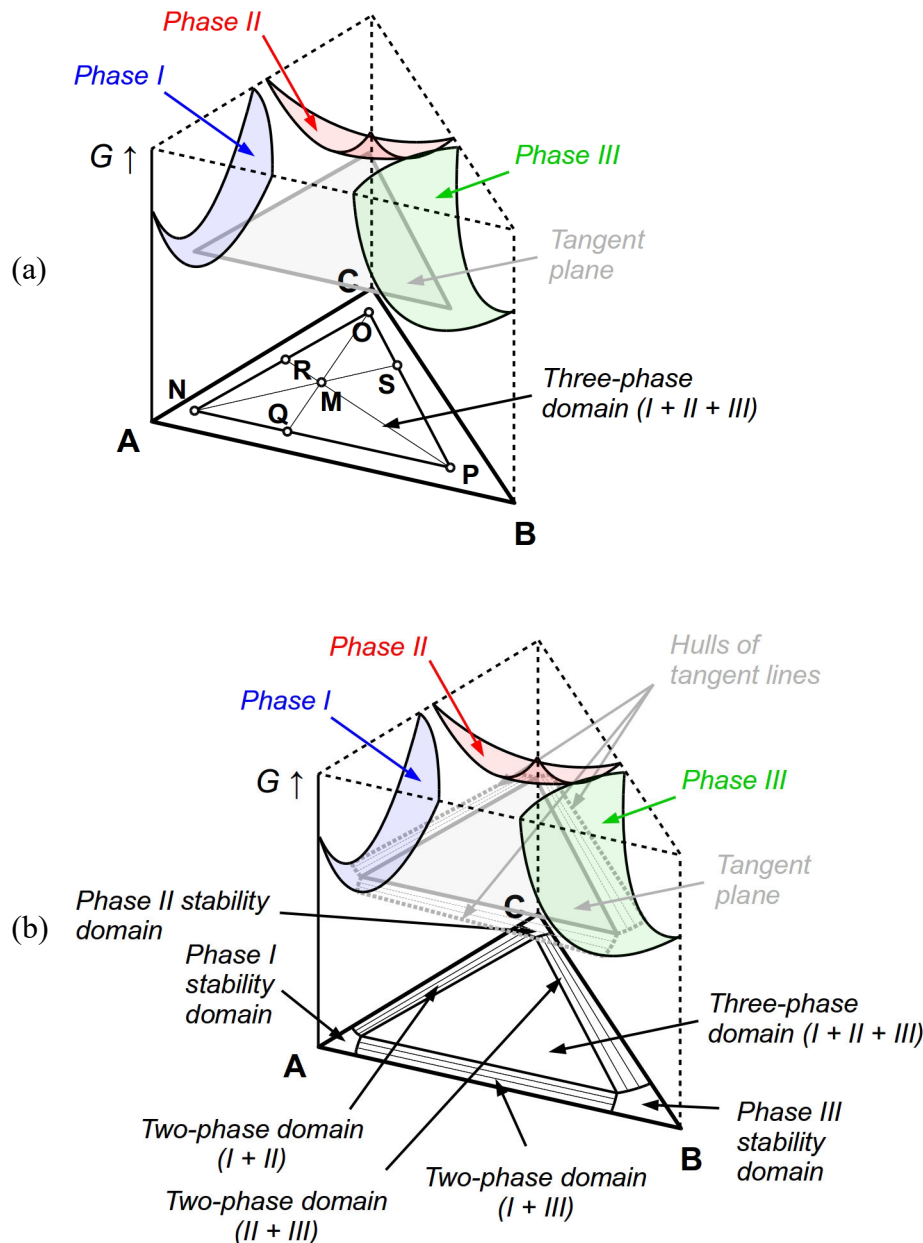


FIG. 26: **Example of phase free energy surfaces: case of existence of a three-phase domain** – a. representation of the three-phase domain on the base triangle; b. representation of one-, two-, and three-phase domains.

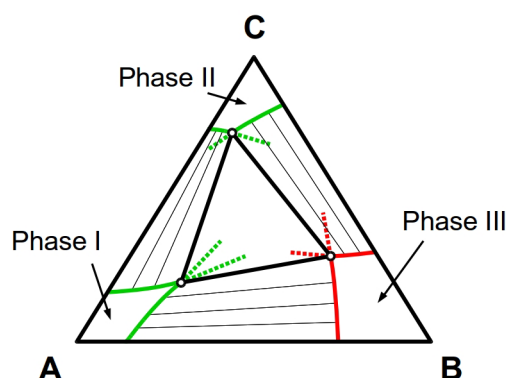


FIG. 27: **Example Illustration of Schreinemaker's rule on equilibrium lines in ternary systems** – green and red two-phase equilibrium lines denote possible and impossible cases, respectively.

e) From binary to ternary phase diagrams

In any A/B/C ternary system, knowledge on A/B, B/C and A/C phase equilibria is crucial to partially predict ternary equilibria at one considered equilibrium temperature (T_{eq}) [5]. Indeed, phase domain boundaries in binary phase diagrams can be projected on the corresponding sides of the composition triangle, which gives relevant data on phase domain boundaries in the ternary system. Then, provided that no additional ternary phase appears, the ternary phase diagram is generally an extrapolation of binary equilibrium lines. Let us illustrate that with a few examples.

The most simple case is a ternary system in which the three compounds exhibit complete miscibility in the solid and liquid states (see fig. 28). The projection of binary phase domain boundaries on the sides of the composition triangle, followed by the extrapolation of the solid-liquid equilibrium lines, gives a ternary phase diagram compatible with the three related binary ones.

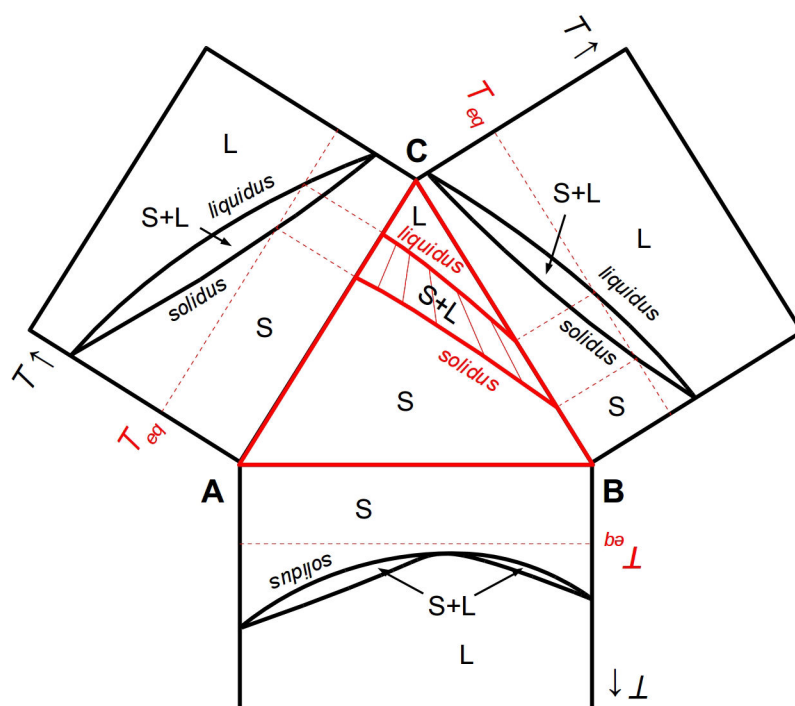


FIG. 28: Ternary phase diagram at T_{eq} compatible with the three related binary phase diagrams in case of complete miscibility in the solid and liquid state between the three components

In case of partial miscibility (or absence of miscibility) between the three components, binary phase diagrams at the equilibrium temperature let appear two-phase domains. Thus, the extrapolation of binary equilibria generally leads to the existence of three-phase domains in the ternary system, as represented in fig. 29.

It is worth noting that, at the equilibrium temperature, if partial solid or liquid solutions exist in at least one of the three binary phase diagrams, they will still have a domain of existence in the ternary system. In the example shown in fig. 29, the partial solid solution S_1 of the A/B diagram leads to S_1+L two-phase equilibria in the A/B/C ternary diagram.

This procedure can also be extended to systems in which a binary intermediate phase exists (see fig. 30). In this case, such phase still has a certain stability domain on the ternary phase diagram, but the extent of the latter cannot be predicted from binary equilibria.

In two-phase equilibria involving an intermediate binary solid phase and a liquid, two cases must be distinguished. Indeed, the intermediate phase can exhibit congruent or non-congruent solubility. In the first case, the addition of solvent does not change the nature of the solid phase until the solid is completely dissolved. Conversely, in the second one, the addition of solvent leads to a modification of the nature of the binary solid phase before all the solids are completely dissolved (see fig. 31).

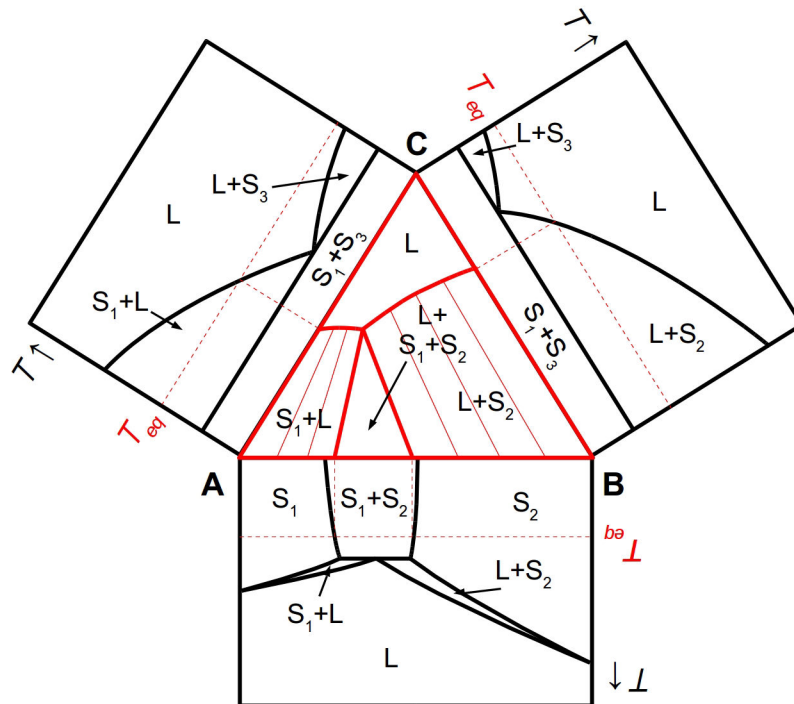


FIG. 29: Ternary phase diagram at T_{eq} compatible with the three related binary phase diagrams in case of partial miscibility in the solid state between the three components

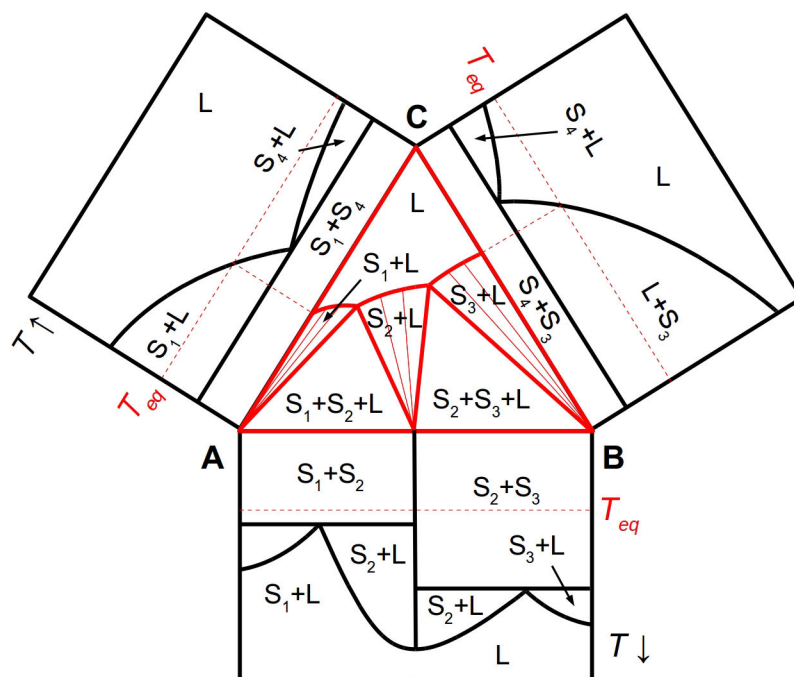


FIG. 30: Ternary phase diagram at T_{eq} compatible with the three related binary phase diagrams in case of existence of an intermediate binary phase (S_2)

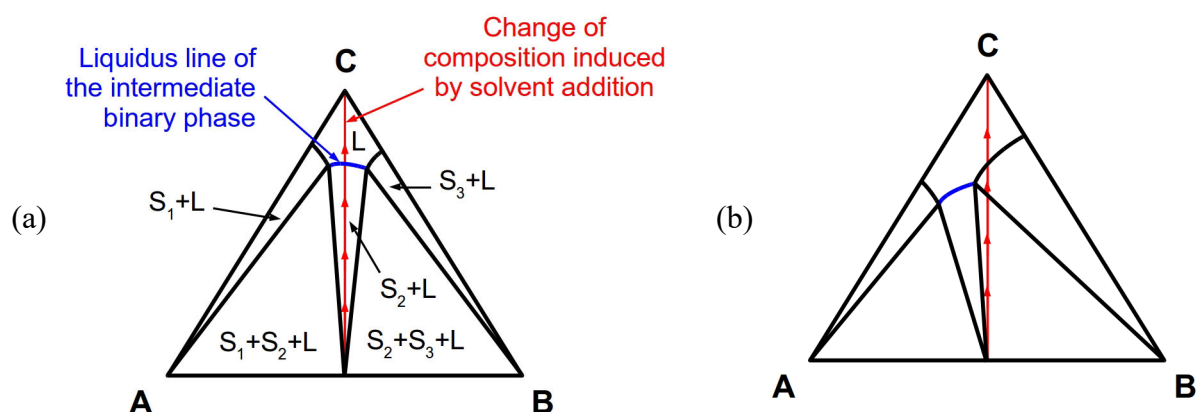


FIG. 31: **Solubility of binary intermediate phases in ternary systems** – a. congruent solubility; b. non-congruent solubility

From binary phase diagrams, there is no way to predict if the solubility of a binary intermediate phase is congruent or not. However, if the two components of which the intermediate phase is made exhibit very different solubility values in the solvent, then the probability of existence of a non-congruent solubility is high.

III. EXPERIMENTAL TECHNIQUES FOR MATERIAL AND PHASE EQUILIBRIA CHARACTERIZATION

In order to assess the behavior of materials containing one component or more, many tools can be employed. In this part, some experimental techniques that permit to characterize phase equilibria and phase transformations are presented.

1) Differential Scanning Calorimetry

Differential Scanning Calorimetry (DSC) is a comparative method that serves to assess the thermal behavior of a sample with respect to a reference [45–47]. Practically, two types of DSC analyses can be made: heat flux (HF) and power compensation DSC [48,49]. In this thesis, only HF-DSC is approached.

a) Principle of HF-DSC

HF-DSC consists in submitting two different systems (*e. g.*, a sample to analyze and a reference, generally made of air) sampled in separate pans to a controlled temperature program. The two pans are let in a small oven which is continuously supplied with a certain flow of gas (helium, nitrogen, argon...), heated (or cooled) by means of a specific thermal module. During the analysis, the temperature of the two pans is recorded, which serves to measure a difference of temperature (ΔT) between the sample and the reference. Then, the recorded signal is converted to specific heat flux absorbed by the sample (ϕ , eq. 32) using laws related to heat transfer – however, this step requires to perform a calibration of the system before starting analyses. The basic principle of the technique is represented in fig. 32.

$$\phi = \frac{\text{constant} \times \Delta T}{m_{\text{sample}}} \quad (32)$$

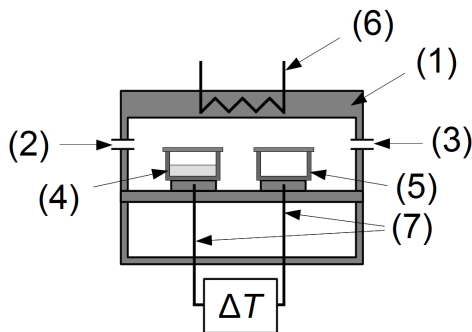


FIG. 32: **Representation of a HF-DSC calorimeter** – (1) oven, (2) carrier gas inlet, (3) carrier gas outlet, (4) sample pan, (5) reference pan, (6) heating/cooling module, (7) temperature sensors. In some devices, the heater/cooler can be placed up the oven.

The $\phi(t \text{ or } T)$ plots obtained after data recording are called “*thermograms*” or “*DSC figures*” (see fig. 33). Deviations from baseline occur when the sample undergoes a certain transformation (melting, glass transition, crystallization, etc). In this case, thermal peaks are obtained. In order to distinguish endothermic and exothermic transformations, it is necessary

to indicate the relative direction of the ϕ axis (with “*endo up*” or “*exo up*” annotations, for example).

Thermograms provide capital information such as: the temperature of occurrence of a certain thermal phenomenon associated with a transformation of the sample; the heat exchanged by the sample to perform such transformation – the latter can be assessed by integrating the specific heat flux vs. time signal.

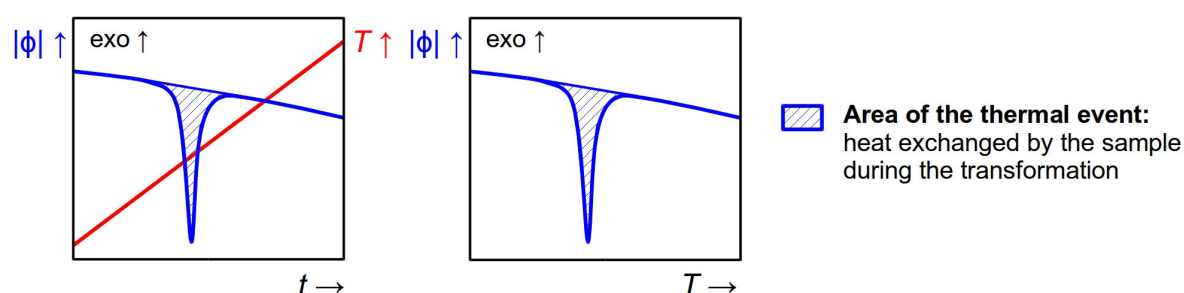


FIG. 33: Examples of thermogram representations

b) Signal delay

During the occurrence of a sample transformation that should occur at one discrete temperature (*e. g.*, a first order transition such as melting), ideal DSC figures should lead to discrete thermal peaks. In practice, this is not experimentally observed. Indeed, due to the thermal resistivity of the pans, the sample and the carrier gas, thermal diffusion engenders a certain delay [50]. Consequently, 1st order-related thermal events generally appear as peaks exhibiting a certain width (fig. 34).

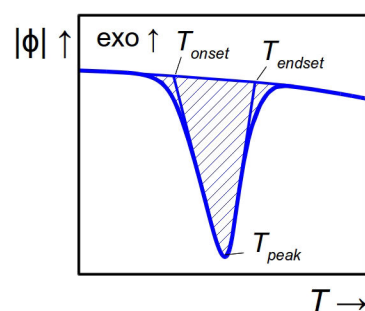


FIG. 34: Main characteristics of a DSC peak

The onset temperature (*e. g.*, the temperature at which the signal deviates from baseline) corresponds to the discrete temperature at which the 1st order transition occurs in the sample. Peak and endset temperatures (see fig. 34) are not representative of the occurrence of such transformation. They result from heat absorption or release delay associated with thermal diffusion in the system, which is influenced by many parameters: carrier gas, mass of sample, heating rate, pan material, etc.

c) Characterization of binary phase equilibria

DSC is an important technique in the field of phase equilibria study [51]. Indeed, it permits to evidence phase transformations in a sample with respect to temperature, which serves to deduce capital information related to solid-solid transitions, melting phenomena, invariant transformations, etc. In this paragraph, a brief presentation of the relationships between binary phase diagrams and sample thermograms is made.

i. Binary systems with complete miscibility in the solid and liquid states

During the analysis of binary mixtures of mixed crystals up to the melt, the obtained thermograms exhibit one single peak whose width depends on the extent of the two-phase L+S domain.

For one considered mixture, peak onset temperature (T_{onset}) corresponds to the *solidus* point. Generally, the temperature at which the peak has the largest intensity (T_{peak}) – rather than the endset temperature (T_{endset}) – is chosen as *liquidus* point. Indeed, due to thermal delays, choosing T_{endset} would lead to an overestimation of *liquidus* points [51].

ii. Binary system involving invariant transformations

During the analysis of binary mixtures that undergo invariant transformations, the thermograms obtained exhibit typical aspects, similar to that presented in fig. 35 (example of a binary system with existence of a eutectic transformation). As shown on this figure, superposition of thermograms of mixtures of different compositions is particularly convenient for the detection of invariant transformations.

Nevertheless, it is worth noting that low-enthalpy transformations (such as that associated with *solvus* points, or invariant transformations involving only solid phases) are generally hard to detect due to the lack of sensitivity of HT-DSC for such transformations.

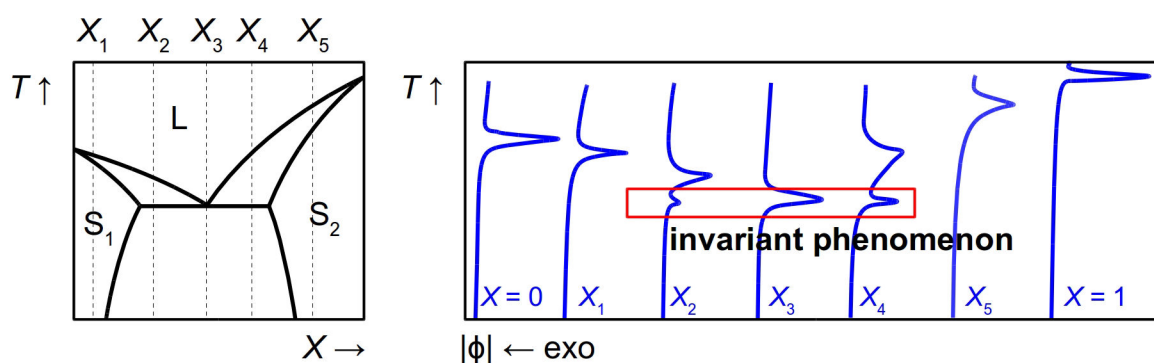


FIG. 35: Typical thermograms of binary mixtures showing eutectic transformations

To characterize invariant transformations from thermograms, the integration of peaks associated with the invariant reaction serves to plot Tammann graphs (see part II.3)e)iv). However, performing such plots requires these peak to be well resolved [52]. Generally, it is hard to find good experimental conditions to separate the peaks associated with the invariant transformation and the *liquidus* points, especially for peritectic reactions [51]. In this case,

several approaches can be chosen to tackle the problem: (i) is to analyze more samples exhibiting different compositions, in order to estimate with a sufficient accuracy the compositions of the three phases involved in the transformation, (ii) to perform peak deconvolution, (iii) to change the mass of analyzed sample, (iv) or to reduce the heating rate.

2) X-Ray Powder Diffraction

X-Ray Powder Diffraction (XRPD) is a powerful tool to perform structural analyses of crystallized samples [53,54]: it offers the possibility to identify and discriminate solid phases, which provides relevant information for phase diagrams assessment.

a) Solid phase crystal structure

In the solid state², chemical objects are periodically distributed in space by successive translations, in the three dimensions of space, of a unit cell. The latter is described by: (i) its lattice (*e. g.*, the axis system), (ii) the pattern, which corresponds to the lowest object that constitutes the crystal after application of lattice-associated translation operations.

The lattice presents six different parameters:

- the lengths of its unit vectors (a, b, c),
- the angles between them: $\alpha = (\vec{b}; \vec{c}), \beta = (\vec{a}; \vec{c}), \gamma = (\vec{a}; \vec{b})$.

Every atom that constitutes the pattern has its own coordinates in the lattice system: x_i, y_i and z_i . It is characterized by a single vector, $\vec{r}_i = x_i \cdot \vec{a} + y_i \cdot \vec{b} + z_i \cdot \vec{c}$.

An example of unit cell is represented in fig. 36. It contains only one object – here, an atom represented by a white sphere.

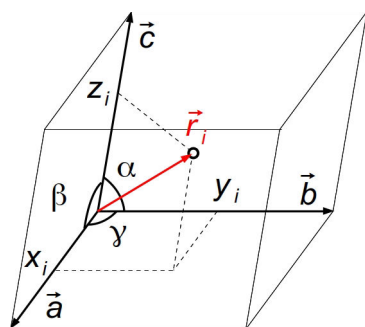


FIG. 36: Representation of an ordinary unit cell containing one atom (white circle)

b) Principle of PXRD

i. Description of the measurement procedure, Bragg's condition

During XRPD measurements, an X-Ray source produces a focused monochromatic beam that irradiates a powder sample with a certain incidence angle, ω . Besides, a detector measures the intensity of the beam diffracted by the sample at the 2θ angle, that is twice as larger as the ω one. The θ and 2θ angles are continuously varied during the measurement thanks to a

2. Here, "solid state" designates crystallized compounds, and excludes glassy state.

goniometer circle. The sample diffracts the incident beam when Bragg's condition is satisfied [54]:

$$2d_{hkl}\sin\theta = n\lambda \quad (33)$$

d_{hkl} is the distance between the hkl diffracting planes, n the order of diffraction (positive integer) and λ the incident beam wavelength.

At the end of the measurement, the recorded data are represented in diffracted beam intensity vs. 2θ angle values plots which are called “*diffraction patterns*”.

The basic principle of XRPD is represented in fig. 37.

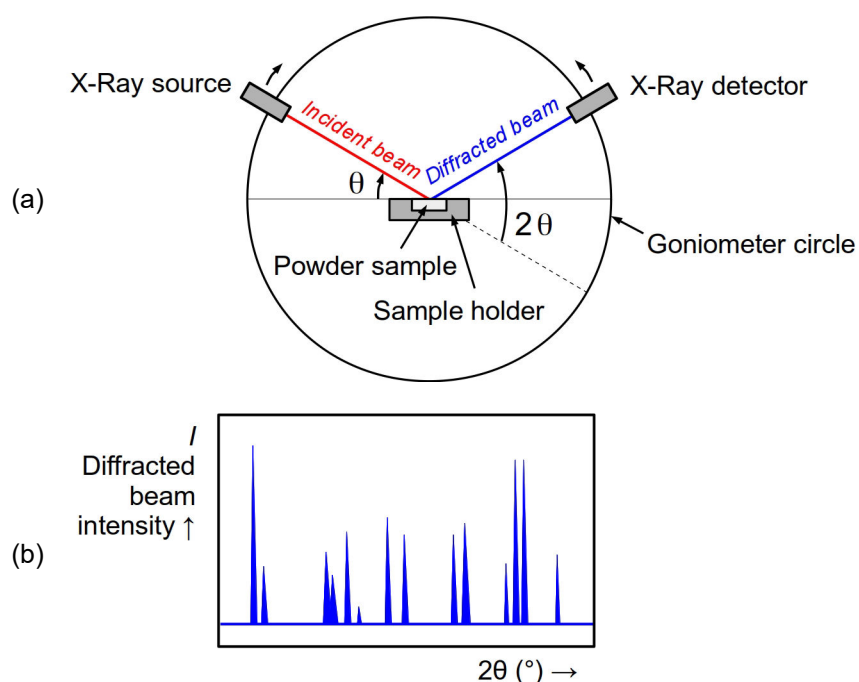


FIG. 37: **Basic principle of XRPD** – (a) experimental setup used in this thesis; (b) example of diffraction pattern

c) Application to phase identification

As a given crystalline phase is characterized by a certain unit cell (including the properties of the lattice and the pattern), and has its own diffraction pattern – with specific diffraction peaks. The diffraction pattern of a powder sample containing a mixture of phases corresponds to a superposition of the patterns associated with every phase. Therefore, XRPD is a helpful tool to characterize solid phases whatever the order of the system. An example of use of XRPD for phase identification purposes in a binary system is presented in fig. 38.

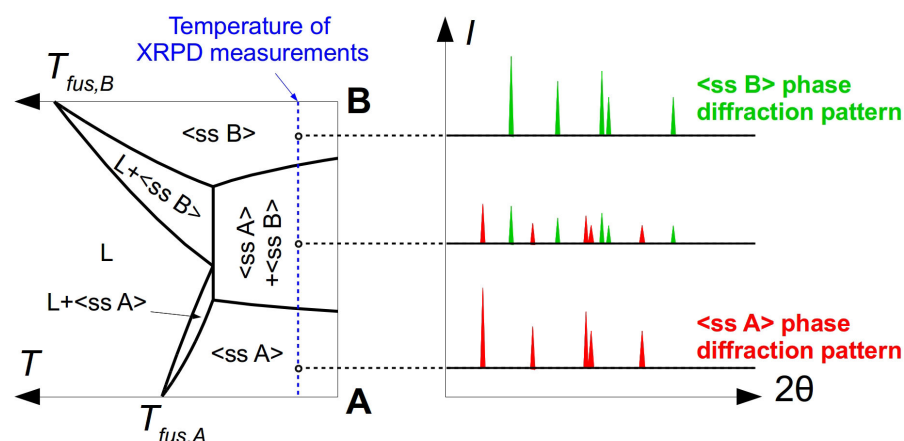


FIG. 38: **Application of XRPD to phase identification in a binary system** – left: binary phase diagram, right: XRPD diffraction patterns

Consequently, XRPD provides data complementary to that obtained using DSC: for a considered sample, it ensures the identification of the solid phases that are involved in the transformations observed in DSC. However, XRPD is not the only method that can give structural information about the phases that constitute a sample. Other methods, such as Second Harmonic Generation [55], Infrared Spectroscopy or Nuclear Magnetic Resonance are particularly convenient to discriminate certain types of solid phases.

3) Analysis of chemical composition

In case of equilibria involving at least two phases that can be separated, the chemical analysis of each phase provides relevant data to characterize the equilibrium. In particular, such analyses are generally performed to study isothermal sections of ternary phase diagrams: they are helpful to determine phase compositions in solid-liquid equilibria, and, subsequently, the corresponding tie lines in two-phase domains. Of course, chemical analyses should be cross-checked with data obtained using complementary phase characterization tools (XRPD, ...).

However, studying solid-liquid ternary equilibria can be complicated. Indeed, analyzing phase compositions requires to separate the solid(s) from the liquid. Nevertheless, there is no way to determine the exact composition of the solid(s), as it is impossible to completely remove the adhering saturated liquid from crystal surface, and the traces of that liquid (e. g., the wet residues) can bring their own contribution to solid composition measurement – in this case, the measured composition of solid(s) slightly deviates from the true composition value. To bypass that, Schreinemaker proposed a method – Schreinemaker's method of wet residues [56] – to determine the composition of the solid(s) in equilibrium with the saturated liquid, provided that the global composition of the starting mixture is known. Assuming that there is no miscibility between the solvent and the two other species in the solid state, the composition of the solid(s) can be calculated according to eq. 34:

$$X_{B,S} = \frac{X_{B,L}X_{C,0} - X_{B,0}X_{C,L}}{X_{C,0} - X_{C,L}} \quad (34)$$

$X_{C,0}$ and $X_{B,0}$ being the fractions of solvent and B species in the starting mixture; and $X_{C,L}$ and $X_{B,L}$ the fractions of solvent and B species in the liquid phase in equilibrium with the solid(s). An graphical representation of this equation is provided in fig. 39.

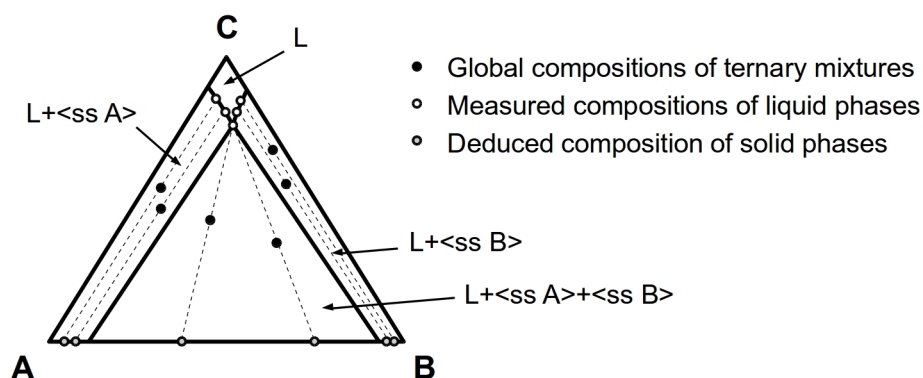


FIG. 39: Illustration of Schreinemaker's method of wet residues

4) The problem of sample preparation

The study of stable phase equilibria by means of any appropriate characterization method requires the elaboration of starting samples that must be in the state of equilibrium. Otherwise, the interpretation of data recorded during sample characterization can be particularly tedious and difficult, which does not facilitate the construction of the phase diagram.

The preparation of stable binary mixtures can be complicated. Indeed, the preparation method should permit the formation of the stable phase(s) starting from physical mixtures of the two species. In this view, many preparation methods can be envisaged: (i) the complete dissolution of binary physical mixtures in an appropriate solvent, followed by the recrystallization of the solid phases by solvent slow evaporation; (ii) the solidification of binary physical mixtures from the molten state; (iii) the grinding of physical mixtures; (iv) the recrystallization of physical mixtures in any solvent, followed by a separation of the solid phase(s) from the saturated liquid, (v) application of annealing treatments to physical mixtures, etc. These procedures can also be applied to form stable mixtures of higher order (ternary, quaternary, ...). Of course, there is no specific procedure to obtain stable mixtures. It is a matter of trial-and-errors.

IV. TECHNIQUES FOR MATERIAL CHEMICAL PURIFICATION AND PURITY ASSESSMENT

Most of purification procedures are based on phase-separation processes that take advantage of phase equilibria between the species to purify and its impurities. In this section, a short review of the most common purification techniques is presented. As monitoring the purifying effect of a specific method requires the use of analytical techniques, a brief presentation of analytical tools is also provided.

1) Methods for chemical purification

Many methods can be employed to separate the different species of a mixtures. The main ones can be classified into two categories: chromatographic techniques [57–59], and phase-separation based processes. Among the latter, distillation [60–62], liquid-liquid extraction [62–65], crystallization from gas phase (sublimation-condensation) [66], melt crystallization [67,68] and solvent-assisted crystallization [69,70] are the most used at the laboratory and industrial scales. However, their respective efficiencies depend on phase equilibria between the different species involved in the processes, and these methods present different advantages and drawbacks that are summarized in tab. 6.

TAB. 6: **Non-exhaustive list of purification methods with their advantages and drawbacks**

Method	Advantages	Drawbacks
Preparative chromatography	<ul style="list-style-type: none"> Offers many variants and optimization possibilities Exhibits large purifying effect when optimized 	<ul style="list-style-type: none"> Requires tedious optimization of experimental conditions Induces high costs (column, solvents, ...) Requires the use of ultrapure mobile phases Not productive at the laboratory scale
Distillation	<ul style="list-style-type: none"> Exhibits large efficiency at separating species exhibiting volatilities that are different enough Presents many parameters that can be adapted for optimization purposes 	<ul style="list-style-type: none"> Requires to operate under reduce pressure to deal with heavy compounds
Liquid-liquid extraction	<ul style="list-style-type: none"> Particularly efficient at separating chemical species of opposite polarities Can be achieved using basic laboratory equipment 	<ul style="list-style-type: none"> Unable at separating species exhibiting similar polarities Restricted to the use of non-miscible solvents (generally, water and an organic non-polar solvent)
Sublimation-condensation	<ul style="list-style-type: none"> Efficient at separating species exhibiting vapor pressures that are different enough Does not pollute the sample of interest by addition of a solvent Appropriate to grow single crystals Applicable to molecules that degrade upon heating 	<ul style="list-style-type: none"> Generally requires to operate under reduced pressure Requires specific laboratory equipment

Melt crystallization	<ul style="list-style-type: none"> • Offers many variants exhibiting various purifying effects • Appropriate to grow single crystals 	<ul style="list-style-type: none"> • Requires the molecules to be stable in the molten state
Solvent-assisted crystallization	<ul style="list-style-type: none"> • Simple technique Can be achieved using basic laboratory equipment • Applicable to molecules that degrade upon heating 	<ul style="list-style-type: none"> • Can lead to several issues related to polymorphism

2) Methods for chemical composition assessment

To determine the composition of a sample, it is necessary to employ analytical methods. However, there a large panel of techniques that can be combined if appropriate, according to the nature of the targeted solutes. Generally, analytical methods can be divided into two categories: (i) those that permit global molar purity assessment (Differential Scanning Calorimetry [71], Titrimetric and gravimetric analysis [72], Electrical resistivity measurement [73], Refractive index measurement [74–76], ...), (ii) those providing extended details on sample composition, with data on the levels of every component (chromatography [77,78], spectroscopy [79], ...). A brief summary of method advantages and drawbacks is proposed in tab. 7.

Tab. 7: **Non-exhaustive list of analytical methods with their advantages and drawbacks**

Method	Advantages	Drawbacks
Chromatography	<ul style="list-style-type: none"> • Appropriate for multicomponent analysis • Appropriate for non-targeted analyses, when coupled with mass spectrometry • Low detection thresholds when coupled with appropriate detector(s) 	<ul style="list-style-type: none"> • Requires optimization of experimental setup (column, mobile phase, detector...)
Molecular spectrophotometry	<ul style="list-style-type: none"> • Simple measurement procedures • Low detection thresholds on sensitive molecules 	<ul style="list-style-type: none"> • Leads to large errors on quantified solute amounts in case of multicomponent analysis • Inappropriate for non-targeted analyses • Requires the targeted molecules to present chromophores
Atomic spectroscopy	<ul style="list-style-type: none"> • Simple measurement procedures • Appropriate for elemental analysis • Low detection thresholds 	<ul style="list-style-type: none"> • Expansive apparatuses • Requires the application of tedious sample preparation procedures • Unable at quantifying molecular species
Differential Scanning Calorimetry	<ul style="list-style-type: none"> • Permits to measure high purity values (up to 99.999 mole %) 	<ul style="list-style-type: none"> • Applicable to one specific case: presence of only one impurity that decreases the melting point of the major component • Inappropriate for multicomponent analysis • Leads to large errors when the amount of impurity exceeds 1 mole %

Electrical resistivity measurement	<ul style="list-style-type: none">• Simple measurement procedure• Permits to measure high purity values	<ul style="list-style-type: none">• Only leads to global molar purity values• Sensitive to defects in the sample
Titrimetric and gravimetric analysis	<ul style="list-style-type: none">• Simple techniques	<ul style="list-style-type: none">• Inappropriate for non-targeted analyses• Requires the targeted species to react with the titrating solution

V. CONCLUSION

In this chapter, theoretical and practical basic notions on phase equilibria were developed in order to introduce the phenomena at the origin of chemical species separation. As seen in the different parts, many phase-separation based processes can be set up in order to concentrate and/or isolate different chemical species from mixtures of components. However, the large possibilities offered by phase equilibria to reach such goals make purification method development complicated:

- (i) the appropriate phase-separation process(es) must be selected, applied and, if appropriate, combined in the right order, in order to reach the purity requirements.
- (ii) the purity of samples – and the purifying effect of the process(es) applied to separate chemical species – must be monitored by means of one or more appropriate analytical methods.

These two focus points can be more or less difficult to deal with, according to the complexity (*e. g.*, the number of chemical species, and their behavior during application of phase-separation processes) of the starting sample.

The major topic of this thesis is the purification of Phenanthrene, a model compound, solid in normal conditions, and that contains many impurities exhibiting different thermodynamic behaviors. In the next chapter, a review of Phenanthrene system is attempted in order to introduce and summarize the problematics and the state of the art related to its purification.

VI. APPENDICES

1) Phase transitions in unary systems

As seen in part II.2, pure compounds can undergo phase transitions [80]. In this section, a few elements on this phenomenon are given in order to help at understanding the related concepts and the associated mechanisms [81–85]. Here, only phase transitions involving two solid phases are approached (melting, vaporisation and sublimation phenomena are not described).

a) Displacive and reconstructive phase transitions

According to crystal structure changes occurring during phase transitions, the latter can be classified into several categories. However, several criteria can be established to perform such classification. Consequently, there are many ways to sort phase transitions, and some of them are controversial. In this section, two kinds of transitions are described: displacive and reconstructive phase transitions. These notions are widely agreed in the field of material science.

During **displacive phase transitions** [86], the structural changes in the solid state are generally of minor magnitude: the chemical interactions between the different molecules are not broken, but the lengths of interactive bounds and/or the orientation of the molecules is/are slightly changed (below 0.1 Å for the lengths). Generally, these transitions are associated with small latent heats (a few J·g⁻¹), and small discontinuities of material physical quantities at the transition point. Moreover, the crystal structures of the two phases involved in the transformation generally exhibit group-subgroup relationships.

Conversely, **reconstructive transitions** [87] involve a breaking of intermolecular interactions in the solid state, which yields large structural changes. Thus, there is generally no clear relationship between the two phases crystal structures. During the occurrence of such transformations, the changes associated with material physical properties at the transition point are important. Consequently, reconstructive transitions go hand in hand with large latent heats (more than 10 J·g⁻¹). Empirical observations shown that these transitions are submitted to systematic thermal hysteresis – in contrast with displacive transitions.

b) Order-disorder transitions

In many cases, solid-solid phase transitions can be approached in terms of crystal structure order. Indeed, many species present phase transitions from an ordered low-temperature phase to a disordered high-temperature phase – these transitions are called “*order-disorder transitions*” [88].

Disorders have been classified into many categories. However, two main types of disorder exist: (i) **static disorder**, in which the molecules in the crystal structure are slightly vibrating due to thermal energy. Nevertheless, no change – with respect to time – of molecule configuration, orientation or position in the crystal lattice occur in static-disordered phases. (ii) **dynamic disorder**, that denotes the existence of continuous thermal motions inside the

molecules in the solid state. Part of molecules, as well as the whole molecules, can be affected by such motions. Dynamic disorder is generally induced by motion of alkyl chains, changes of molecule configuration, rotation of the molecule along a certain axis, etc.

Generally, the ordered and disordered phase crystal structures exhibit group-subgroup relationship. In this case, the ordered phase exhibits low symmetry, and the number of symmetry elements is increased in the disordered phase. Such transitions can be considered as being displacive transitions. Nevertheless, other cases of order-disorder transitions between two phases that do not exhibit such relationship are known. These transitions are reconstructive³.

Many series, such as that of ammonium halides [89,90], are known to undergo order-disorder transitions. This series has been previously intensely studied. Among it, ammonium chloride (NH_4Cl) and deuterated ammonium chloride (ND_4Cl) were found to exhibit order-disorder transitions [91] involving similar solid phases (see fig. 40a,b). As shown in fig. 40b, NH_4^+ or ND_4^+ ions exhibit dynamic disorder in the disordered phase, whereas they do not undergo any motion in the ordered phases. As revealed by structural studies on NH_4Cl and ND_4Cl during transition from the ferro-ordered (F) phase to the disordered (D) phase (fig. 40c), the two compounds exhibit distinct transition behaviors. Indeed, NH_4Cl lattice parameter undergoes a discontinuity at the transition temperature. Moreover, a thermal hysteresis was clearly evidenced, which means that the material went through a reconstructive-like order-disorder transition. Conversely, ND_4Cl lattice parameter was continuous during the transition, without existence of thermal hysteresis. Thus, ND_4Cl underwent a displacive-like transition.

On the base of many experimental observations, another classification of phase transitions was proposed by Ehrenfest. This was made in order to separate these transitions according to the evolution of material physical quantities around transition point.

3. Melting, sublimation and vaporization can be considered, to a certain extent, as order-disorder transitions. As the starting phase undergoes a complete deconstruction of molecular packing, these transformations can be considered as being somewhat reconstructive.

$$\frac{C_p}{T} = - \left(\frac{\partial^2 G}{\partial T^2} \right)_p = \left(\frac{\partial S}{\partial T} \right)_p = \frac{1}{T} \left(\frac{\partial H}{\partial T} \right)_p \quad (36)$$

Therefore, $H(T)$, $S(T)$ and $C_p(T)$ functions follow different behaviors according to the transition order. Examples of $H(T)$ and $C_p(T)$ curves associated with 1st and 2nd order transitions are presented in fig. 42. The most remarkable difference between 1st and 2nd order transitions is that 1st order ones are always associated to a latent heat ($\Delta H_{T,I-II}$), whereas 2nd order ones do not present such property.

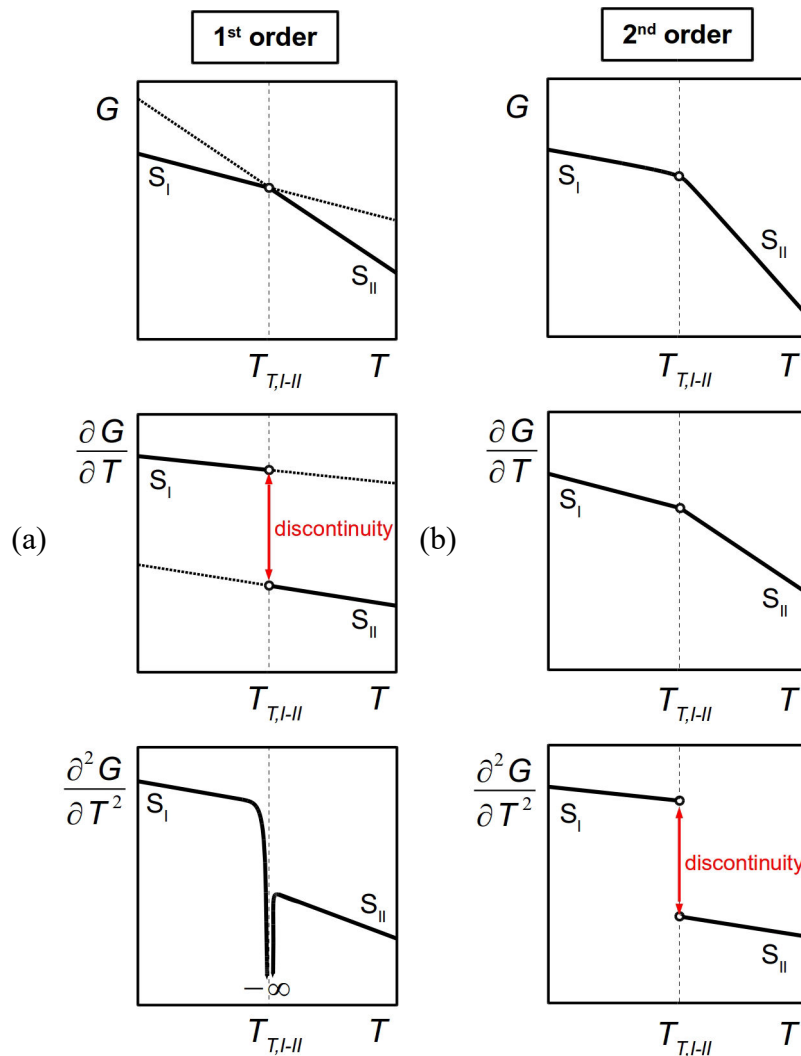


FIG. 41: Evolution of system molar free energy with respect to temperature (at constant pressure) during phase transitions – a. 1st order transition; b. 2nd order transition

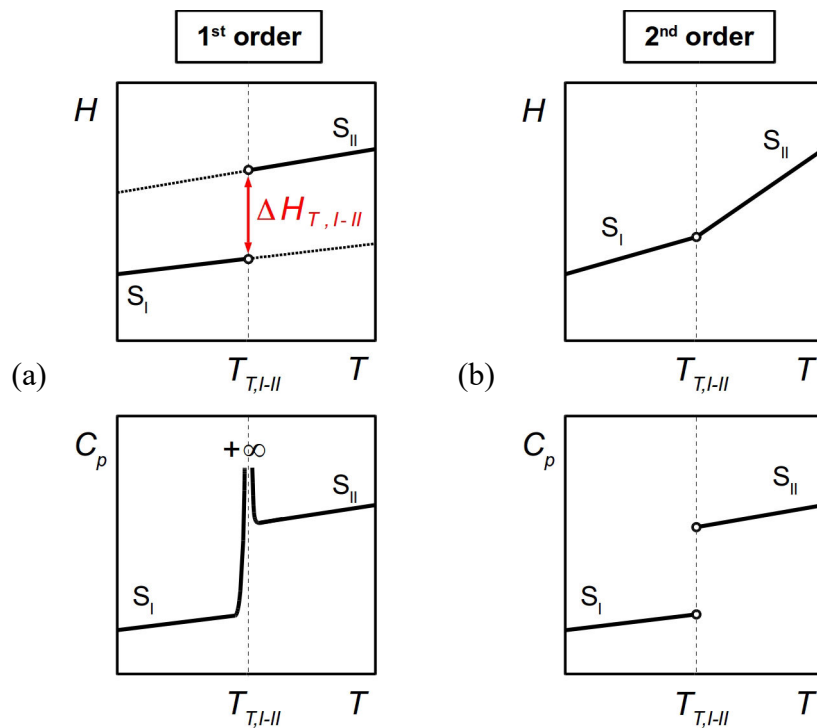


FIG. 42: Evolution of system molar enthalpy and heat capacity with respect to temperature (at constant pressure) during phase transitions – a. 1st order transition; b. 2nd order transition

Order of phase transitions has been the topic of a large debate for many years. Indeed, some researchers questioned the existence of 2nd order transitions [92,93], and the physical meaning associated with such concept. Experimentally, the measurement of H or C_p is generally biased by some device-related perturbations. Consequently, the criteria for classification of transitions has been limited to the existence of a latent heat and a thermal hysteresis (1st order) and the existence of a single C_p jump without existence of a latent heat nor hysteresis (2nd order).

2) Calorimetry of the eutectic transformation

Let us consider the following type-I invariant transformation: phase I + phase II \rightarrow phase III. At the invariant temperature, phases I, II and III respective compositions are X_I , X_{II} and X_{III} .

If the composition of the system ranges between X_I and X_{III} , the enthalpies of a binary mixture just below and above the invariant transformation are given by:

$$\begin{aligned} H(X)_{T_{inv}+\varepsilon} &= f_I H_I + f_{III} H_{III} \\ H(X)_{T_{inv}-\varepsilon} &= f_I H_I + f_{II} H_{II} \end{aligned} \quad (37)$$

H_I , H_{II} and H_{III} being the respective enthalpies of the three phases, and f_I , f_{II} and f_{III} their fractions. ε is a positive infinitesimal amount of temperature. Applying the lever rule to express f_I , f_{II} and f_{III} yields:

$$\begin{aligned} H(X)_{T_{inv}+\varepsilon} &= \left(\frac{X_{III}-X}{X_{III}-X_I} \right) H_I + \left(\frac{X-X_I}{X_{III}-X_I} \right) H_{III} \\ H(X)_{T_{inv}-\varepsilon} &= \left(\frac{X_{II}-X}{X_{II}-X_I} \right) H_I + \left(\frac{X-X_I}{X_{II}-X_I} \right) H_{II} \end{aligned} \quad (38)$$

Thus, the amount of molar heat (Q) absorbed by the mixture during the invariant transformation is:

$$\begin{aligned} Q(X) &= H(X)_{T_{inv}+\varepsilon} - H(X)_{T_{inv}-\varepsilon} \\ &= X \left(\frac{H_{III}-H_I}{X_{III}-X_I} + \frac{H_I-H_{II}}{X_{II}-X_I} \right) + \frac{X_{III}H_I - X_I H_{III}}{X_{III}-X_I} + \frac{X_I H_{II} - X_{II} H_I}{X_{II}-X_I} \end{aligned} \quad (39)$$

If $X_{III} < X < X_{II}$, then one has:

$$\begin{aligned} H(X)_{T_{inv}+\varepsilon} &= f_{III} H_{III} + f_{II} H_{II} \\ H(X)_{T_{inv}-\varepsilon} &= f_I H_I + f_{II} H_{II} \end{aligned} \quad (40)$$

Applying the lever rule gives:

$$\begin{aligned} H(X)_{T_{inv}+\varepsilon} &= \left(\frac{X_{II}-X}{X_{II}-X_{III}} \right) H_{III} + \left(\frac{X-X_{III}}{X_{II}-X_{III}} \right) H_{II} \\ H(X)_{T_{inv}-\varepsilon} &= \left(\frac{X_{II}-X}{X_{II}-X_I} \right) H_I + \left(\frac{X-X_I}{X_{II}-X_I} \right) H_{II} \end{aligned} \quad (41)$$

Then, the molar heat absorbed by the mixture during the invariant transformation becomes:

$$Q(X) = X \left(\frac{H_{II}-H_{III}}{X_{II}-X_{III}} + \frac{H_I-H_{II}}{X_{II}-X_I} \right) + \frac{X_{II}H_{III}-X_{III}H_{II}}{X_{II}-X_{III}} + \frac{X_I H_{II} - X_{II} H_I}{X_{II}-X_I} \quad (42)$$

Consequently:

(i) $Q = 0$ if $X = X_I$.

(ii) $Q = 0$ when $X = X_{II}$.

(iii) if $X = X_{III}$, the amount of heat is maximal and equals:

$$Q_{max} = H_{III} - H_I \left(\frac{X_{II} - X_{III}}{X_{II} - X_I} \right) - H_{II} \left(\frac{X_{III} - X_I}{X_{II} - X_I} \right) \quad (43)$$

Calorimetric measurements generally give $Q(X)$ values expressed in J g⁻¹. In this case, these relationships can be used to determine the compositions of the three phases provided that the composition values are expressed in mass fractions.

VII. REFERENCES

- [1] E.A. Guggenheim, *Thermodynamics: An advanced treatment for chemists and physicist*, North-Holland Publishing Company, Amsterdam, Pays-Bas, 1949.
- [2] R. Clausius, Ueber eine veränderte Form des zweiten Hauptsatzes der mechanischen Wärmetheorie, *Ann. Phys.* 169 (1854) 481–506. doi:10.1002/andp.18541691202.
- [3] L. Boltzmann, Ueber die Natur der Gasmoleküle, *Ann. Phys.* 236 (1877) 175–176. doi:10.1002/andp.18772360120.
- [4] D.L. Anderson, *Theory of the Earth*, Blackwell Scientific Publications, Boston, MA, 1989. <http://resolver.caltech.edu/CaltechBOOK:1989.001> (accessed January 26, 2017).
- [5] H.A.J. Oonk, M.T. Calvet, *Equilibrium between phases of matter. [1]: Phenomenology and thermodynamics*, Springer, Dordrecht, 2008.
- [6] D.A. Porter, K.E. Easterling, M. Sherif, *Phase Transformations in Metals and Alloys*, Third Edition (Revised Reprint), CRC Press, 2009.
- [7] D. Cavallo, D. Mileva, G. Portale, L. Zhang, L. Balzano, G.C. Alfonso, R. Androsch, Mesophase-Mediated Crystallization of Poly(butylene-2,6-naphthalate): An Example of Ostwald's Rule of Stages, *ACS Macro Lett.* 1 (2012) 1051–1055. doi:10.1021/mz300349z.
- [8] S.-Y. Chung, Y.-M. Kim, J.-G. Kim, Y.-J. Kim, Multiphase transformation and Ostwald's rule of stages during crystallization of a metal phosphate, *Nat. Phys.* 5 (2009) 68–73. doi:10.1038/nphys1148.
- [9] J. Nývlt, The Ostwald Rule of Stages, *Cryst. Res. Technol.* 30 (1995) 443–449. doi:10.1002/crat.2170300402.
- [10] W. Ostwald, Studien über die Bildung und Umwandlung fester Körper, *Z. Phys. Chem.* 22 (1897) 289–330.
- [11] T. Threlfall, Structural and Thermodynamic Explanations of Ostwald's Rule, *Org. Process Res. Dev.* 7 (2003) 1017–1027. doi:10.1021/op030026l.
- [12] M.M. Ayass, A. Abi Mansour, M. Al-Ghoul, Alternating Metastable/Stable Pattern in the Mercuric Iodide Crystal Formation Outside the Ostwald Rule of Stages, *J. Phys. Chem. A.* 118 (2014) 7725–7731. doi:10.1021/jp5058034.
- [13] J.C. Burley, M.J. Duer, R.S. Stein, R.M. Vrcelj, Enforcing Ostwald's rule of stages: Isolation of paracetamol forms III and II, *Eur. J. Pharm. Sci.* 31 (2007) 271–276. doi:10.1016/j.ejps.2007.04.002.
- [14] V. Dureisseix, M. Sanselme, Y. Robin, G. Coquerel, Two Concomitant Polymorphs of 1,2-Naphthoquinone-2-semicarbazone, *Cryst. Growth Des.* 9 (2009) 3438–3443. doi:10.1021/cg801361m.
- [15] J.W. Gibbs, *On the Equilibrium of Heterogeneous Substances*, Connecticut Academy of Arts and Sciences, 1874.
- [16] F. a. H. Schreinemakers, In-, mono- and divariant equilibria I, *K. Ned. Akad. Van Wet. Proc. Ser. B Phys. Sci.* 18 (1915) 116–126.
- [17] Allotropes of carbon, Wikipedia. (2017). https://en.wikipedia.org/w/index.php?title=Allotropes_of_carbon&oldid=772463861 (accessed March 31, 2017).
- [18] P. Gustafson, An evaluation of the thermodynamic properties and the P, T phase diagram of carbon, *Carbon.* 24 (1986) 169–176. doi:10.1016/0008-6223(86)90113-2.
- [19] A. Burger, R. Ramberger, On the polymorphism of pharmaceuticals and other molecular crystals. I, *Microchim. Acta.* 72 (1979) 259–271. doi:10.1007/BF01197379.
- [20] A. Burger, R. Ramberger, On the polymorphism of pharmaceuticals and other molecular crystals. II, *Microchim. Acta.* 72 (1979) 273–316. doi:10.1007/BF01197380.
- [21] M. Barrio, E. Maccaroni, I.B. Rietveld, L. Malpezzi, N. Masciocchi, R. Céolin, J. Tamarit, Pressure–temperature state diagram for the phase relationships between benfluorex hydrochloride forms I and II: A case of enantiotropic behavior, *J. Pharm. Sci.* 101 (2012) 1073–1078. doi:10.1002/jps.22821.
- [22] J.-O. Henck, M. Kuhnert-Brandstatter, Demonstration of the terms enantiotropy and monotropy in polymorphism research exemplified by flurbiprofen, *J. Pharm. Sci.* 88 (1999) 103–108. doi:10.1021/js9801945.
- [23] R. Céolin, J.-L. Tamarit, M. Barrio, D.O. López, B. Nicolai, N. Veglio, M.-A. Perrin, P. Espeau, Overall monotropic behavior of a metastable phase of biclotymol, 2,2'-methylenebis(4-chloro-3-methyl-isopropylphenol), inferred from experimental and topological construction of the related P-T state diagram, *J. Pharm. Sci.* 97 (2008) 3927–3941. doi:10.1002/jps.21285.
- [24] M.-A. Perrin, M. Bauer, M. Barrio, J.-L. Tamarit, R. Céolin, I.B. Rietveld, Rimobant dimorphism and its pressure–temperature phase diagram: A delicate case of overall monotropic behavior, *J. Pharm. Sci.* 102 (2013) 2311–2321. doi:10.1002/jps.23612.

- [25] R. Céolin, I.B. Rietveld, The topological phase diagram of cimetidine: A case of overall monotropy, *Ann. Pharm. Fr.* (2017). doi:10.1016/j.pharma.2016.11.002.
- [26] J.V. Parambil, S.K. Poornachary, S.J. Hinder, R.B.H. Tan, J.Y.Y. Heng, Establishing template-induced polymorphic domains for API crystallisation: the case of carbamazepine, *CrystEngComm*. 17 (2015) 6384–6392. doi:10.1039/C5CE01080B.
- [27] C. Capacci-Daniel, K.J. Gaskell, J.A. Swift, Nucleation and Growth of Metastable Polymorphs on Siloxane Monolayer Templates, *Cryst. Growth Des.* 10 (2010) 952–962. doi:10.1021/cg9012697.
- [28] D. Bi, C. Yi, J. Luo, J.-D. Décoppet, F. Zhang, S.M. Zakeeruddin, X. Li, A. Hagfeldt, M. Grätzel, Polymer-templated nucleation and crystal growth of perovskite films for solar cells with efficiency greater than 21%, *Nat. Energy*. 1 (2016) 16142. doi:10.1038/nenergy.2016.142.
- [29] E. Pechkova, C. Nicolini, Protein nucleation and crystallization by homologous protein thin film template, *J. Cell. Biochem.* 85 (2002) 243–251. doi:10.1002/jcb.10123.
- [30] J.L. Quon, K. Chadwick, G.P.F. Wood, I. Sheu, B.K. Brettmann, A.S. Myerson, B.L. Trout, Templated Nucleation of Acetaminophen on Spherical Excipient Agglomerates, *Langmuir*. 29 (2013) 3292–3300. doi:10.1021/la3041083.
- [31] A. Caridi, S.A. Kulkarni, G. Di Profio, E. Curcio, J.H. ter Horst, Template-Induced Nucleation of Isonicotinamide Polymorphs, *Cryst. Growth Des.* 14 (2014) 1135–1141. doi:10.1021/cg401605m.
- [32] N. Kubota, Effect of Impurities on the Growth Kinetics of Crystals, *Cryst. Res. Technol.* 36 (2001) 749–769. doi:10.1002/1521-4079(200110)36:8/10<749::AID-CRAT749>3.0.CO;2-#.
- [33] N. Kubota, J.W. Mullin, A kinetic model for crystal growth from aqueous solution in the presence of impurity, *J. Cryst. Growth*. 152 (1995) 203–208. doi:10.1016/0022-0248(95)00128-X.
- [34] J.V. Parambil, S.K. Poornachary, R.B.H. Tan, J.Y.Y. Heng, Influence of solvent polarity and supersaturation on template-induced nucleation of carbamazepine crystal polymorphs, *J. Cryst. Growth*. (2016). doi:10.1016/j.jcrysgro.2016.09.058.
- [35] J.W. Mullin, 5 - Nucleation, in: *Cryst. Fourth Ed.*, Butterworth-Heinemann, Oxford, 2001: pp. 181–215. doi:10.1016/B978-075064833-2/50007-3.
- [36] G.A. Stephenson, R.A. Forbes, S.M. Reutzel-Edens, Characterization of the solid state: quantitative issues, *Adv. Drug Deliv. Rev.* 48 (2001) 67–90. doi:10.1016/S0169-409X(01)00099-0.
- [37] A.W. Newman, S.R. Byrn, Solid-state analysis of the active pharmaceutical ingredient in drug products, *Drug Discov. Today*. 8 (2003) 898–905. doi:10.1016/S1359-6446(03)02832-0.
- [38] G.G.Z. Zhang, D. Law, E.A. Schmitt, Y. Qiu, Phase transformation considerations during process development and manufacture of solid oral dosage forms, *Adv. Drug Deliv. Rev.* 56 (2004) 371–390. doi:10.1016/j.addr.2003.10.009.
- [39] W. Hume-Rothery, R.E. Smallman, C.W. Haworth, The structure of metals and alloys, *Metals & Metallurgy Trust*, 1969. <https://books.google.fr/books?id=sfcNAQAIAAJ>.
- [40] B. Legendre, F. Querniard, Glossary for Binary Phase Diagram Reactions, *J. Phase Equilibria Diffus.* 35 (2014) 11–14. doi:10.1007/s11669-013-0266-6.
- [41] D.A. Goodman, J.W. Cahn, L.H. Bennett, The centennial of the Gibbs-Konovalov rule for congruent points, *Bull. Alloy Phase Diagr.* 2 (1981) 29–34. doi:10.1007/BF02873696.
- [42] J.E. Ricci, The phase rule and heterogeneous equilibrium, D. Van Nostrand Company, Inc., New York, 1951.
- [43] M. Hillert, Phase Equilibria, Phase Diagrams and Phase Transformations: Their Thermodynamic Basis, Cambridge University Press, 2007. <https://books.google.fr/books?id=juk4cxteC1AC>.
- [44] A.D. Pelton, Proof of Schreinemaker's rule for general phase diagram sections, *J. Phase Equilibria*. 16 (1995) 501–503. doi:10.1007/BF02646718.
- [45] M.E. Brown, Differential thermal analysis (DTA) and differential scanning calorimetry (DSC), in: *Introd. Therm. Anal.*, Springer Netherlands, 1988: pp. 23–49. doi:10.1007/978-94-009-1219-9_4.
- [46] J. Grenet, B. Legendre, Analyse calorimétrique différentielle à balayage (DSC), *Tech. Ing. Base documentaire : TIB384DUO* (2010). <http://www.techniques-ingenieur.fr/base-documentaire/mesures-analyses-th1/methodes-thermiques-d-analyse-42384210/analyse-calorimetrique-differentielle-a-balayage-dsc-p1205/>.
- [47] D.G.W.H. Höhne, D.W. Hemminger, D.H.-J. Flammersheim, Theoretical Fundamentals of Differential Scanning Calorimeters, in: *Differ. Scanning Calorim.*, Springer Berlin Heidelberg, 1996: pp. 21–40. doi:10.1007/978-3-662-03302-9_3.
- [48] D.G.W.H. Höhne, D.W. Hemminger, D.H.-J. Flammersheim, Types of Differential Scanning Calorimeters, in: *Differ. Scanning Calorim.*, Springer Berlin Heidelberg, 1996: pp. 7–20. doi:10.1007/978-3-662-03302-9_2.
- [49] D.G.W.H. Höhne, D.W. Hemminger, D.H.-J. Flammersheim, Introduction, in: *Differ. Scanning Calorim.*, Springer Berlin Heidelberg, 1996: pp. 1–6. doi:10.1007/978-3-662-03302-9_1.

- [50] D.G.W.H. Höhne, D.W. Hemminger, D.H.-J. Flammersheim, The DSC Curve, in: Differ. Scanning Calorim., Springer Berlin Heidelberg, 1996: pp. 81–104. doi:10.1007/978-3-662-03302-9_5.
- [51] L. Rycerz, Practical remarks concerning phase diagrams determination on the basis of differential scanning calorimetry measurements, *J. Therm. Anal. Calorim.* 113 (2013) 231–238. doi:10.1007/s10973-013-3097-0.
- [52] L. Yuan, S. Clevers, N. Couvrat, Y. Cartigny, V. Dupray, G. Coquerel, Precise Urea/Water Eutectic Composition by Temperature-Resolved Second Harmonic Generation, *Chem. Eng. Technol.* 39 (2016) 1326–1332. doi:10.1002/ceat.201600032.
- [53] P. Gravereau, Introduction à la pratique de la diffraction des rayons X par les poudres, lecture, Sciences Chimiques, 2011. <https://cel.archives-ouvertes.fr/cel-00671294/document> (accessed February 10, 2017).
- [54] J.-J. Rousseau, A. Gibaud, Cristallographie géométrique et radiocristallographie: cours et exercices corrigés, Dunod, Paris, 2007.
- [55] F. Simon, S. Clevers, V. Dupray, G. Coquerel, Relevance of the Second Harmonic Generation to Characterize Crystalline Samples, *Chem. Eng. Technol.* 38 (2015) 971–983. doi:10.1002/ceat.201400756.
- [56] H. Schott, A Mathematical Extrapolation for The Method of Wet Residues, *J. Chem. Eng. Data.* 6 (1961) 324–324. doi:10.1021/je00103a002.
- [57] K. Hostettmann, A. Marston, M. Hostettmann, Preparative Chromatography Techniques, Springer Berlin Heidelberg, Berlin, Heidelberg, 1998. doi:10.1007/978-3-662-03631-0.
- [58] H. Schmidt-Traub, Preparative Chromatography: of Fine Chemicals and Pharmaceutical Agents, John Wiley & Sons, 2006.
- [59] M. Juza, M. Mazzotti, M. Morbidelli, Simulated moving-bed chromatography and its application to chirotechnology, *Trends Biotechnol.* 18 (2000) 108–118. doi:10.1016/S0167-7799(99)01419-5.
- [60] J.G. Stichlmair, J.R. Fair, Distillation: principles and practices, Wiley-VCH, New York, 1998.
- [61] M.F. Doherty, J.D. Perkins, On the dynamics of distillation processes—I, *Chem. Eng. Sci.* 33 (1978) 281–301. doi:10.1016/0009-2509(78)80086-4.
- [62] C. Geankoplis, Transport Processes and Separation Process Principles (Includes Unit Operations) Fourth Edition, Fourth, Prentice Hall Press, Upper Saddle River, NJ, USA, 2003.
- [63] J. Rydberg, Solvent Extraction Principles and Practice, Revised and Expanded, CRC Press, 2004.
- [64] R. Marsili, Flavor, Fragrance, and Odor Analysis, CRC Press, 2001.
- [65] S. Macchietto, O. Odele, O. Omatsone, Design on optimal solvents for liquid-liquid extraction and gas absorption processes, *Chem. Eng. Res. Des.* 68 (1990) 429–433.
- [66] W.L.F. Armarego, C.L.L. Chai, Purification of Laboratory Chemicals, Butterworth-Heinemann, 2013.
- [67] C.M. van't Land, Industrial crystallization of melts, Dekker, New York, 2005.
- [68] J. Ulrich, H. Glade, eds., Melt crystallization: fundamentals, equipment and applications, Shaker, Aachen, 2003.
- [69] G. Coquerel, Crystallization of molecular systems from solution: phase diagrams, supersaturation and other basic concepts, *Chem. Soc. Rev.* 43 (2014) 2286–2300. doi:10.1039/C3CS60359H.
- [70] J.W. Mullin, 7 - Recrystallization, in: Cryst. Fourth Ed., Butterworth-Heinemann, Oxford, 2001: pp. 289–314. doi:10.1016/B978-075064833-2/50009-7.
- [71] M.E. Brown, Purity determination using DSC, in: Introd. Therm. Anal., Springer Netherlands, 1988: pp. 152–162. doi:10.1007/978-94-009-1219-9_14.
- [72] E.M. Rattenbury, Introductory Titrimetric and Gravimetric Analysis: The Commonwealth and International Library: Chemistry Division, Elsevier Science, 2016. <https://books.google.fr/books?id=7-IPDAAAQBAJ>.
- [73] R.A. Ribeiro, S.L. Bud'ko, C. Petrovic, P.C. Canfield, Effects of stoichiometry, purity, etching and distilling on resistance of MgB₂ pellets and wire segments, *Phys. C Supercond.* 382 (2002) 194–202. doi:10.1016/S0921-4534(02)01840-3.
- [74] M.I. Aralaguppi, C.V. Jadar, T.M. Aminabhavi, Density, Refractive Index, Viscosity, and Speed of Sound in Binary Mixtures of Cyclohexanone with Hexane, Heptane, Octane, Nonane, Decane, Dodecane, and 2,2,4-Trimethylpentane, *J. Chem. Eng. Data.* 44 (1999) 435–440. doi:10.1021/je9802266.
- [75] T.M. Aminabhavi, V.B. Patil, M.I. Aralaguppi, H.T.S. Phayde, Density, Viscosity, and Refractive Index of the Binary Mixtures of Cyclohexane with Hexane, Heptane, Octane, Nonane, and Decane at (298.15, 303.15, and 308.15) K, *J. Chem. Eng. Data.* 41 (1996) 521–525. doi:10.1021/je950279c.
- [76] M.I. Aralaguppi, C.V. Jadar, T.M. Aminabhavi, Density, Viscosity, Refractive Index, and Speed of Sound in Binary Mixtures of Acrylonitrile with Methanol, Ethanol, Propan-1-ol, Butan-1-ol, Pentan-1-ol, Hexan-1-ol, Heptan-1-ol, and Butan-2-ol, *J. Chem. Eng. Data.* 44 (1999) 216–221. doi:10.1021/je9802219.
- [77] R.L. Grob, E.F. Barry, eds., Modern practice of gas chromatography, 4. ed, Wiley-Interscience, Hoboken, NJ, 2004.

- [78] G. Gutnikov, H. Engelhardt, *High Performance Liquid Chromatography*, Springer Berlin Heidelberg, 2012. <https://books.google.fr/books?id=slHxC AAAQBAJ>.
- [79] G.L. David, *Analytical Chemistry*, Universities Press, 2001.
- [80] P. Papon, J. Leblond, P.H.E. Meijer, eds., *The Physics of Phase Transitions*, Springer Berlin Heidelberg, Berlin, Heidelberg, 2006. doi:10.1007/3-540-33390-8.
- [81] Y.V. Mnyukh, Molecular Mechanism of Polymorphic Transitions, *Mol. Cryst. Liq. Cryst.* 52 (1979) 163–199. doi:10.1080/00268947908071732.
- [82] Y.V. Mnyukh, N.A. Panfilova, Polymorphic transitions in molecular crystals—II. Mechanism of molecular rearrangement at ‘contact’ interface, *J. Phys. Chem. Solids.* 34 (1973) 159–170. doi:10.1016/0022-3697(73)90073-5.
- [83] Y.V. Mnyukh, N.A. Panfilova, N.N. Petropavlov, N.S. Uchvatova, Polymorphic transitions in molecular crystals—III, *J. Phys. Chem. Solids.* 36 (1975) 127–144. doi:10.1016/0022-3697(75)90003-7.
- [84] Y. Mnyukh, Mechanism and kinetics of phase transitions and other reactions in solids, *ArXiv11101654 Phys.* (2011). <http://arxiv.org/abs/1110.1654> (accessed April 19, 2017).
- [85] F.H. Herbstein, On the mechanism of some first-order enantiotropic solid-state phase transitions: from Simon through Ubbelohde to Mnyukh, *Acta Crystallogr. B.* 62 (2006) 341–383. doi:10.1107/S0108768106008640.
- [86] T. Malcherek, Displacive phase transitions, in: G. Papp, T.G. Weiszbürg, R. Miletich (Eds.), *Miner. Behav. Extreme Cond.*, Mineralogical society of Great Britain and Ireland, London, 2005: pp. 139–171. doi:10.1180/EMU-notes.7.6.
- [87] P. Tolédano, V. Dmitriev, *Reconstructive Phase Transitions In Crystals and Quasicrystals*, World Scientific, 1996. https://books.google.fr/books/about/Reconstructive_Phase_Transitions.html?hl=fr&id=T-3sCgAAQBAJ (accessed March 29, 2017).
- [88] M.J. de Oliveira, Order-Disorder Transition, in: *Equilib. Thermodyn.*, Springer Berlin Heidelberg, 2013: pp. 207–223. doi:10.1007/978-3-642-36549-2_12.
- [89] V.-G. Vaks, V.E. Schneider, On the theory of phase transitions in the ammonium halides, *Phys. Status Solidi A.* 35 (1976) 61–72. doi:10.1002/pssa.2210350107.
- [90] R. Stevenson, Phase Transitions in the Ammonium Halides, *J. Chem. Phys.* 34 (1961) 1757–1762. doi:10.1063/1.1701074.
- [91] O.H. Seeck, D. Hupfeld, H. Krull, M. Tolan, W. Press, Order-disorder transition of ND₄Cl and NH₄Cl, *Phys. Rev. B.* 58 (1998) 623–632. doi:10.1103/PhysRevB.58.623.
- [92] G. Jaeger, The Ehrenfest Classification of Phase Transitions: Introduction and Evolution, *Arch. Hist. Exact Sci.* 53 (1998) 51–81. doi:10.1007/s004070050021.
- [93] T. Sauer, A Look Back at the Ehrenfest Classification. Translation and Commentary of Ehrenfest’s 1933 paper introducing the notion of phase transitions of different order, *ArXiv161203062 Phys.* (2016). <http://arxiv.org/abs/1612.03062> (accessed March 29, 2017).

Chapter II

The Phenanthrene system

Chapter II

THE PHENANTHRENE SYSTEM

TABLE OF CONTENTS

NOMENCLATURE.....	86
I. INTRODUCTION.....	87
II. PHENANTHRENE SOLID STATE.....	89
1) An overview of Phenanthrene solid state landscape.....	89
2) The order-disorder solid-solid transition in Phenanthrene.....	89
3) Impact of Phenanthrene purity on its solid-solid transition.....	93
III. STATE OF THE ART ON PHENANTHRENE PURIFICATION AND ANALYSIS.....	95
1) State of the art on Phenanthrene purification.....	95
a) Purification using phase-separation based methods.....	96
i. Purification by distillation.....	96
ii. Purification by solvent-assisted recrystallization.....	96
iii. Purification by vacuum sublimation.....	97
iv. Purification by melt crystallization (Zone Melting).....	97
b) Purification by impurity chemical transformation.....	97
c) Purification by preparative liquid chromatography.....	98
d) Summary.....	99
2) State of the art on Phenanthrene purity assessment.....	99
a) Analytical Gas Chromatography.....	99
b) Infrared spectroscopy.....	100
c) Summary.....	100
IV. IMPLICATIONS OF PHENANTHRENE SYSTEM REINVESTIGATION.....	101
V. REFERENCES.....	102

NOMENCLATURE

Abbreviations

API	Active Pharmaceutical Ingredient
DSC	Differential Scanning Calorimetry
GC	Gas Chromatography
HP	High pressure
HT	High temperature
IR	Infrared
LT	Low temperature
PAH	Polycyclic Aromatic Hydrocarbon
POP	Persistent Organic Pollutant
SHG	Second Harmonic Generation
UV	Ultraviolet
XRPD	X-Ray Powder Diffraction

I. INTRODUCTION

Phenanthrene molecule ($C_{14}H_{10}$, of molar mass $178.23 \text{ g}\cdot\text{mol}^{-1}$, and represented in fig. 1) belongs to polycyclic aromatic hydrocarbons (PAH) class¹. This compound is naturally present in oil and is industrially produced by extraction from coal tar residues. Besides that, Phenanthrene is also a persistent organic pollutant (POP) that is generated by incomplete combustion or organic matter during various processes: fuel/wood combustion in cars, plants and chimneys, food cooking, cigarette smoking, etc. Even if its biological activity has not been fully characterized up to now, the compound is suspected to have a certain toxicity, including potential carcinogenic effects. However, due to lack of data, it has not been classified by official health agencies as carcinogen, but GHS² data on Phenanthrene (tab. 1) clearly associate the molecule with many hazards.

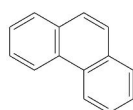


FIG. 1: Phenanthrene topological formula

TAB. 1: GHS data on Phenanthrene

Caution pictograms	
Risk phrases	H302, H315, H319, H335, H410, P261, P273, P305, P338, P351, P501

Phenanthrene molecule presents many industrial applications:

- (i) it is produced and used as standard in order to obtain reference samples for the detection and quantification of the compound in different matrices: foods, environmental samples, etc.
- (ii) it is used as base for the synthesis of many drugs, including colorants, explosive materials, active pharmaceutical ingredients (APIs) [1], electrical conductors [2,3], photo-luminescent materials [4], etc.

For these reasons, Phenanthrene is easily accessible from many suppliers that provide different grades: technical, for synthesis, standard, etc.

Besides the extraction from tar coals, Phenanthrene can be prepared by synthesis from different chemicals, and several preparation procedures have been reported in the literature for many years [5–10]. However, due to its environmental toxicity, many researches were previously conducted in order to study chemical reactions to eliminate Phenanthrene from contaminated soils. In this framework, the reactivity of the molecule offered many possibilities to reach that goal.

1. PAHs are organic compounds containing more than one aromatic rings that are generally fused.

2. Abbreviation for *Globally Harmonised System of Classification and Labelling of Chemicals*, a European official organism.

In the solid state, Phenanthrene exhibits a certain electrical conductivity that is due to electron mobility inside the crystals. Consequently, the compound also belongs to organic semiconductor class. However, the electronic properties of solid Phenanthrene were found to exhibit a strong dependence with respect to temperature [11]. Complementary investigations showed that this observation was due to the existence of a solid-solid phase transition occurring at $\sim 65\text{-}70\text{ }^{\circ}\text{C}$ [12]. However, this transition was found to present unusual phenomena. Moreover, the impurities of Phenanthrene were highlighted to have a significant influence on this phase transition.

In this chapter, a brief presentation of knowledge on Phenanthrene solid state is made. In a first part, the known solid phases of the compound are described. Then, a summary of the studies made on the solid-solid transition, in view of assessing its mechanism at the molecular scale, is exposed. In a third part, the known issues related to the purity of the compound and its influence on the transition are presented. Eventually, the state of the art on Phenanthrene purification and analysis is summarized, in order to introduce the problematics related to the access to ultrapure grade.

II. PHENANTHRENE SOLID STATE

1) An overview of Phenanthrene solid state landscape

Many – more or less recent – studies on Phenanthrene solid phases have been previously performed and published in the literature. A short review permits to highlight the existence of three known polymorphs. Two of them were obtained and characterized at atmospheric pressure: the low and high temperature (LT, HT) crystalline forms of this compound, whose respective structures were determined by Petricek *et al.* [13]. The third one was obtained at room temperature under high pressure (HP, 700 MPa) by Fabbiani *et al.* [14]. The crystallographic characteristics of these phases are summarized in tab. 2, and the crystal structures are shown in fig. 2.

TAB. 2: Crystallographic data on Phenanthrene solid phases

	LT phase	HT phase	HP phase
Crystal lattice	Monoclinic	Monoclinic	Monoclinic
Space group	$P2_1$	$P2_1/c$	$P2_1/n$
a (Å)	8.441(2)	8.506(2)	12.937(3)
b (Å)	6.140(1)	6.215(2)	3.822(1)
c (Å)	9.438(1)	9.525(2)	17.693(6)
β (°)	97.96(1)	98.73(2)	99.13
Unit-cell volume (Å ³)	484.4(1)	497.7(2)	863.7(1)
Molecules per unit cell	2	2	4
Density (g·cm ⁻³)	1.222	1.189	1.371
Temperature (°C)	21	71	20
Pressure (MPa)	0,1	0,1	700

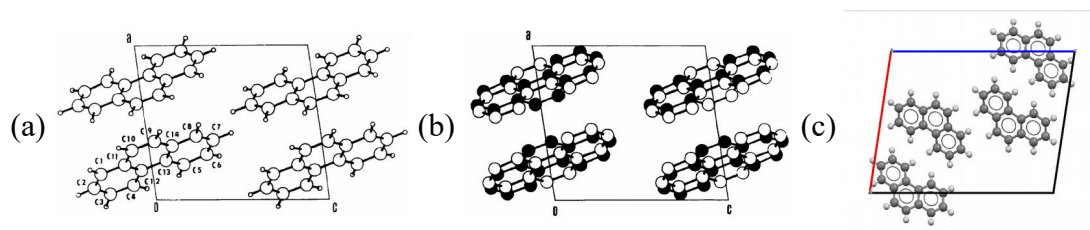


FIG. 2: Projection of Phenanthrene unit cell contents along the b axis, from Petricek *et al.* [13] and Fabbiani *et al.* [14] – a. LT phase; b. HT phase; c. HP phase

2) The order-disorder solid-solid transition in Phenanthrene

According to their crystal structures, Phenanthrene LT and HT phases exhibit group-subgroup relationship. Indeed, in the LT form, the molecules are almost static and do not undergo detectable dynamic disorder. Conversely, in the HT one, Phenanthrene molecules occupy the same positions as in the LT phase, but they are subject to rotational/orientational dynamic disorder, as showed by fig. 2b. This disorder induces a slight increase of the unit-cell parameters (with respect to those of the LT form), leading to a low decrease of solid density (see tab. 2). Moreover, it generates new symmetry elements. Among them, the existence of inversion centers is the most remarkable difference with the LT phase.

In 1966, Matsumoto shown, by means of calorimetric and structural studies, that a reversible transition between the LT and HT phases of Phenanthrene occurred at 65-70 °C (1 atm) [12]. Thus, at atmospheric pressure, the two phases are enantiotropically related. In addition, the HT phase was found to melt at ~ 98-100 °C.

Due to the high similarity of the LT and HT phases, both of them present close XRPD patterns, as shown in fig. 3. However, due to the gain of symmetry, LT phase characteristic peaks at ~ 15 and 20.5 ° vanish after the transition to the HT form.

Besides, the monitoring of Phenanthrene solid-solid transition by means of DSC highlighted that the latter could be associated by a small – but significant – latent heat of a few $\text{J}\cdot\text{g}^{-1}$ (fig. 4). According to the different theories on phase transitions developed in chapter I appendices, this indicates the existence of a 1st order contribution to this phase transformation.

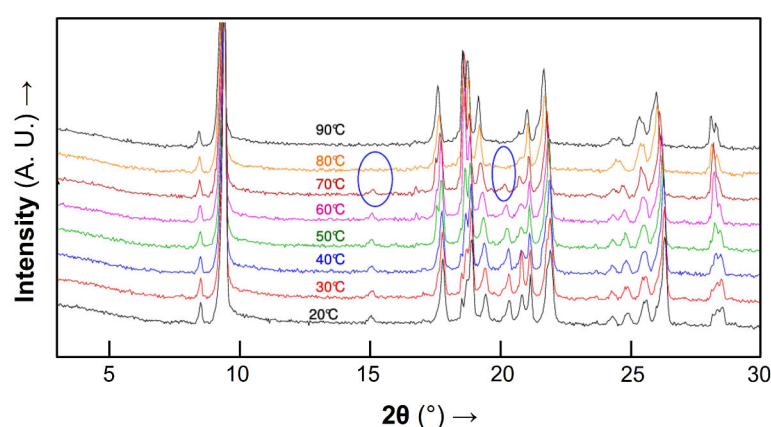


FIG. 3: **Monitoring of Phenanthrene solid-solid transition by Temperature-Resolved XRPD**, from Couvrat [15].

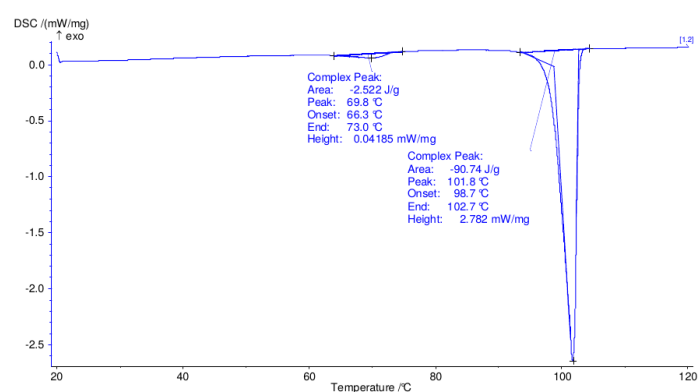


FIG. 4: **Monitoring of Phenanthrene phase transitions on heating by DSC**, from Couvrat [15].

Nevertheless, other studies performed using complementary techniques showed the unusual character of this transition. As the HT and LT phases are centro- and non-centrosymmetric, they can be distinguished by means of Second Harmonic Generation (SHG³) experiments. In

3. During application of SHG measurements on crystals, a laser beam of wavelength λ irradiates the sample. If the latter is made of a non-centrosymmetric phase, a part of the incident beam is converted to an emitted beam of wavelength $\lambda/2$. Conversely, if the sample contains only centrosymmetric phase, no conversion of incident beam occurs. SHG intensity corresponds to the intensity of the emitted beam.

1976, Dougherty and Kurz monitored the transition using this technique [16]. Their results, shown in fig. 5a, highlighted the progressive decrease of SHG signal intensity on heating from room temperature to $\sim 70^\circ\text{C}$ – temperature at which the SHG positive character of Phenanthrene completely vanished, thus indicating the complete conversion of the LT phase to the HT one. These observations corroborated those previously made by Matsumoto and Fukuda in 1967 [17] (fig. 5b). Indeed, their monitoring of the height of Phenanthrene LT phase ($10\bar{2}$) plane XRPD peak ($2\theta = 20.5^\circ$) with respect to temperature led to similar conclusions.

From these results, some doubts on the order of the transition raised, as well as the question of the possible existence of a 2nd order contribution to the transition. This question was also justified by the continuous aspect of Phenanthrene crystal lattice parameters around the transition temperature, as evidenced by Matsumoto and Fukuda (fig. 6). However, no data on potential thermal hysteresis were presented by the authors of the study.

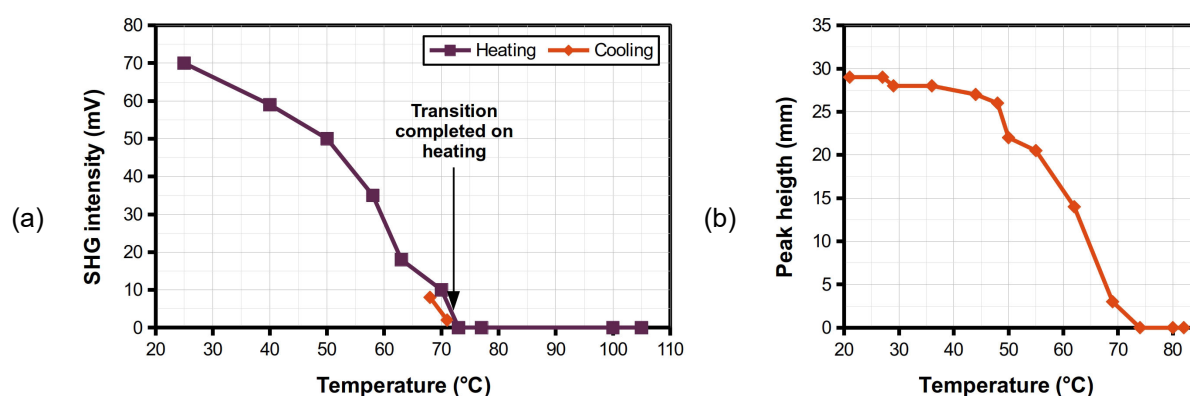


FIG. 5: **Monitoring of Phenanthrene solid-solid transition** – (a) by means of SHG (adapted from Dougherty and Kurz paper [16]); (b) by means of XRPD: intensity of ($10\bar{2}$) plane diffraction peak vs. temperature on heating (adapted from Matsumoto and Fukuda paper [17]).

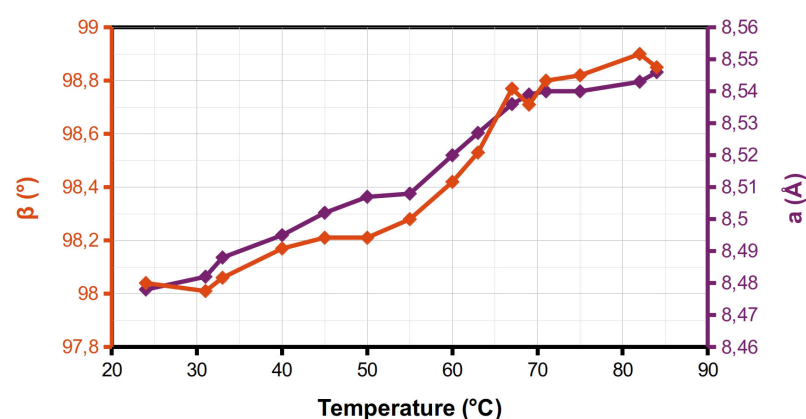


FIG. 6: **Evolution of Phenanthrene crystal lattice parameters with respect to temperature on heating**, adapted from Matsumoto and Fukuda paper [17].

In another study, Matsumoto monitored the evolution of Phenanthrene crystal resistance with respect to temperature by applying several gradual heating and cooling steps on the sample. The results, shown in fig. 7, highlighted two unusual phenomena:

- (i) on the one hand, on heating, a change of slope of $\log(\text{resistance})$ vs T function could be observed at $\sim 56^\circ\text{C}$, but it remained continuous around the point of slope change. The phenomenon was reversible on cooling, and no thermal hysteresis was observed.
- (ii) on the other hand, a discontinuity of $\log(\text{resistance})$ vs T function was evidenced at $65\text{--}70^\circ\text{C}$. The phenomenon was reversible on cooling, but a certain thermal hysteresis was observed. Nevertheless, on cooling, it occurred at higher temperature values than on heating, which is unusual.

These observations might indicate the potential occurrence of two successive and reversible phase transitions in a narrow temperature range. Nevertheless, both of them seem to exhibit different orders.

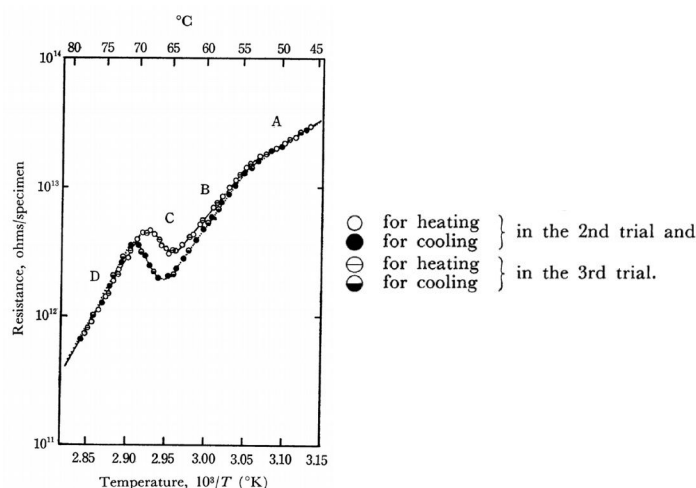


FIG. 7: **Evolution of Phenanthrene crystal resistance with respect to temperature**, from Matsumoto [11].

Complementary structural studies made by Petříček *et al.* [13] showed that, on heating, phenanthrene molecules in the LT phase undergo a progressive increase of orientational disorder until reaching the complete conversion of the phase to the HT one. This study suggested the formation of disordered clusters in the LT phase, and the increase of the number of clusters on heating.

All these solid-solid transition mechanism characterization studies performed on Phenanthrene samples highlighted unusual behaviors. Up to now, the mechanism of the transition, at the molecular scale, has not been fully characterized. Moreover, in other studies, the chemical purity of the compound was found to severely impact the transition.

3) Impact of Phenanthrene purity on its solid-solid transition

Besides the unusual character of Phenanthrene solid-solid transition, another point was found to exhibit a critical influence on the behavior of the molecule in the solid state. Indeed, the chemical purity of the solid has a strong impact on the transition, as well as the melting point of the compound. This paragraph aims at summarizing the main studies related to the influence of Phenanthrene purity on its transition.

In a recent study, Couvrat *et al.* showed the significant influence of Phenanthrene chemical purity on its solid-solid transition [18]. Indeed, DSC experiments made on samples provided by different suppliers highlighted significant changes in transition temperature and latent heat, according to the purity (see fig. 8).

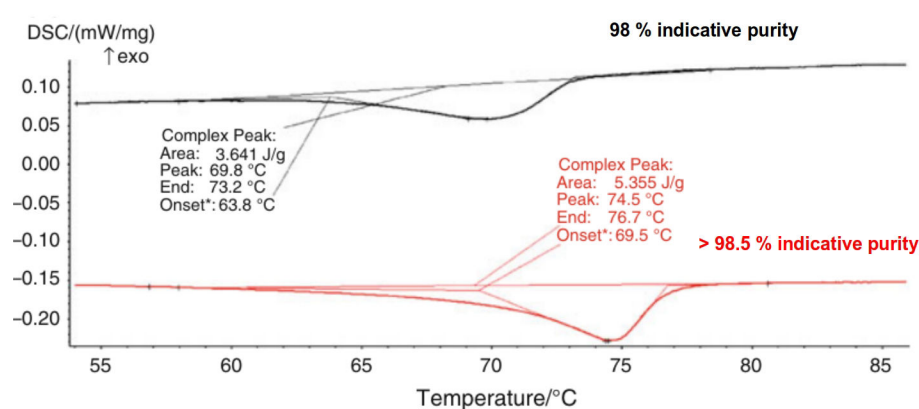


FIG. 8: **DSC thermograms of Phenanthrene samples of different chemical purities**, adapted from Couvrat *et al.* paper [18].

In another study, Gloistein *et al.* tried to assess the influence of several impurities of Phenanthrene on its transition [19]. Among them, Anthracene and Carbazole were found to stabilize the HT phase at room temperature with moderate impurity levels (*e. g.*, 3.7 mol. % for Anthracene and 6.0 mol. % for Carbazole).

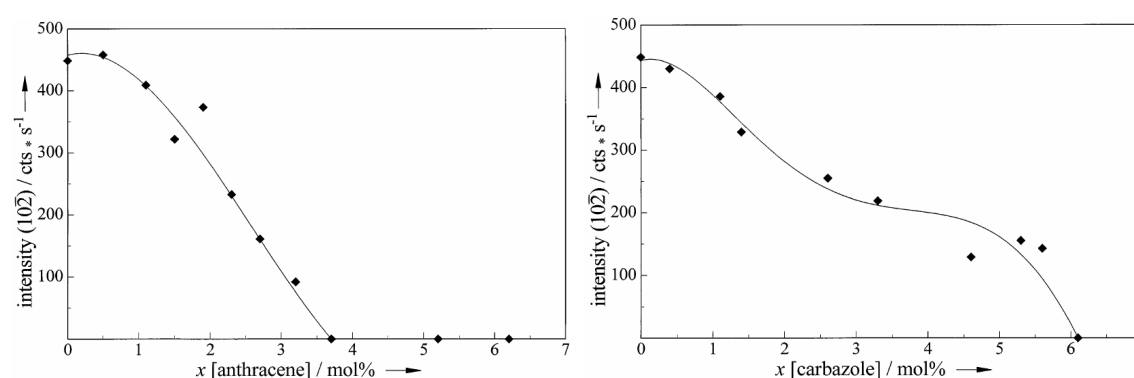


FIG. 9: **Evolution of Phenanthrene (102) LT phase plane diffraction peak intensity at room temperature with respect to Anthracene (left) and Carbazole (right) levels in the sample**, from Gloistein *et al.* [19].

These two studies highlighted that Phenanthrene chemical purity was a critical parameter to which a particular attention should be paid before studying the solid-solid transition. Indeed,

one question of major importance raises from these observations: is the unusual character of the transition related to the pure compound itself or due to the presence of impurities in the material? As this interrogation remains unanswered for now, it calls for supplementary solid-solid transition studies on ultrapure Phenanthrene. Therefore, purification methods have to be developed and applied to the compound in order to reach that goal. Nevertheless, this implies two major tasks: (i) the development and optimization of these purification procedures to reach 99.9 mole % purity; (ii) the elaboration of analytical methods to assess the purifying effect of these procedures. In the next paragraphs, a brief presentation of the state of the art on Phenanthrene purification and analysis is made to expose the know-how on these two points.

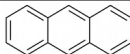
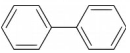
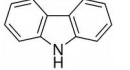
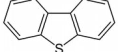
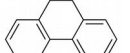
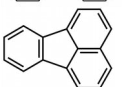
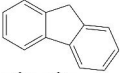
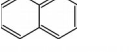
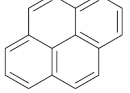
III. STATE OF THE ART ON PHENANTHRENE PURIFICATION AND ANALYSIS

Up to now, many purification procedures to remove different impurities from Phenanthrene samples were described in the literature. The purifying effect of these procedures was assessed by means of several analytical methods that were more or less precisely depicted. The different procedures exhibited various selectivity, according to the impurities. In this part, a review of the literature is presented to summarize the know-how in Phenanthrene purification and analysis.

1) State of the art on Phenanthrene purification

As a product from coal tar, Phenanthrene generally contains impurities that also belong to PAHs. Among them, 9 different chemical species were previously identified, as indicated by tab. 3 entries. However, the presence (or not) and levels of these different impurities change according to the supplier and the purity grade.

TAB. 3: Impurities generally found in commercial Phenanthrene samples

Impurity	Topological formula	Raw formula	Molecular weight (g·mol ⁻¹)	References
Anthracene		C ₁₄ H ₁₀	178.23	[18,20–28]
Biphenyl		C ₁₂ H ₁₀	154.21	[21]
Carbazole		C ₁₂ H ₉ N	167.21	[18,22,23,25,26]
Dibenzothiophene		C ₁₂ H ₈ S	184.26	[18,20,21]
Dihydrophenanthrene		C ₁₄ H ₁₂	180.25	[20,21]
Fluoranthene		C ₁₆ H ₁₀	202.26	[21]
Fluorene		C ₁₃ H ₁₀	166.22	[18,20–23,25]
Naphthalene		C ₁₀ H ₈	128.17	[21,24]
Pyrene		C ₁₆ H ₁₀	202.25	[21]

As revealed by their molecular structures, the different impurities can be classified into several categories:

- (i) those that contain only carbon and hydrogen, and exhibit full aromaticity: Anthracene, Biphenyl, Fluoranthene, Naphthalene and Pyrene.
- (ii) those that contain heteroatoms: Carbazole and Dibenzothiophene.

- (iii) those that are made of carbon and hydrogen, but that do not exhibit full aromaticity: Dihydrophenanthrene and Fluorene.

According to the cited literature, many purification methods were described to separate Phenanthrene from these impurities. In this section, a short review of published results is attempted and discussed.

a) Purification using phase-separation based methods

Many phase-separation based methods were previously applied to Phenanthrene in order to separate this compound from its impurities. Among them, distillation, melt crystallization, sublimation and solvent-assisted crystallization were the most employed ones.

i. Purification by distillation

In 1951, Feldman *et al.* reported the purification of Phenanthrene by means of azeotropic distillation [22]. Raw impure Phenanthrene was first treated by means of chemical reactions to remove some major impurities. At the end of this first step, treated Phenanthrene was found to contain Fluorene and Carbazole. An azeotropic distillation of the product using Ethylene Glycol as solvent gave different distillate fractions containing Phenanthrene with low amounts of Fluorene. Conversely, the residue was found to be mainly made of Carbazole. This impurity was completely removed from Phenanthrene by this procedure that was patented the next year [23].

In 1974, McArdle and Sherwood attempted the removal of Phenanthrene impurities by means of vacuum distillation [21]. The product – initially solid – was distilled at low pressure using basic laboratory equipment. The first and last 10 % distillate fractions were discarded. The product recovered from the distillate was analyzed. The results showed that this method was particularly efficient at removing Fluorene. Similar results were reported by Runsheng *et al.* in 2010 [25].

ii. Purification by solvent-assisted recrystallization

In many studies dealing with the purification of Phenanthrene, solvent-assisted crystallization procedures were applied and combined to other methods to remove the impurities. While many papers describe recrystallization steps – involving classical laboratory solvents and equipments – they do not give any quantitative data about their purifying effect [29,30]. However, a few other publications give more detailed information on that [24,26]. In these studies, the recrystallization solvent was supercritical CO₂.

In their study, Sako *et al.* showed that, using this procedure, it was possible to separate Phenanthrene from Naphthalene in a binary starting mixture in which the two components had the same mass fractions [24].

Besides, Esmailzadeh *et al.* showed that the recrystallization of a ternary mixture made of 40 % Anthracene, 40 % Phenanthrene and 20 % Carbazole (in mass fractions) in supercritical CO₂ led to the precipitation of a solid enriched in Phenanthrene (~ 82 %) and impoverished in Anthracene (~ 12 %) and Carbazole (~ 6 %) [26].

iii. Purification by vacuum sublimation

In several studies, vacuum sublimation was employed to purify Phenanthrene [29,31,32]. However, no quantitative data on the purifying effect of this method was provided by the authors of the corresponding papers.

iv. Purification by melt crystallization (Zone Melting)

The “reference” method used to purify Phenanthrene (*e. g.*, the purification method that was almost systematically used across the different studies) was Zone Melting⁴, a variant of melt crystallization. In this method, an ingot made of the solid to purify is submitted to a local heating, which leads to the generation of a small molten zone. The latter is then displaced from one end of the sample to the other. According to the difference between their solubilities in the molten zone and in the solid slice that recrystallizes at every slight displacement of the zone, the impurities can be displaced towards the different ends of the sample – more details on this technique are provided in chapter IV. The molten zone pass can be repeated as many times as desired, in order to amplify impurity concentration at ingots ends.

Due to Phenanthrene stability upon melting, this technique has been widely used to purify the molecule [20,21,27,28]. Moreover, it is worth noting that, to date, many suppliers (TCI Chemicals, Sigma-Aldrich, etc) provide commercial zone refined Phenanthrene, which shows that this technique is still a reference method for the preparation of high-purity samples of this molecule.

Quantitative data on the purifying effect of this method showed that Zone Melting is particularly efficient at displacing Naphthalene, Biphenyl, Dihydrophenanthrene, Dibenzothiophene [21]. Similar observations were made for impurity Anthracene [21,27]. While efficient at removing these impurities from Phenanthrene, the technique exhibited more moderate efficiency with respect to Fluorene, whose solubility values in the liquid and solid phases were found to be similar [21].

After application of several number zone passes, the authors of the different studies could demonstrate that the technique dropped the levels of several impurities below the detection thresholds of their analytical methods (generally, below 1 ppm impurity in Phenanthrene). This was the only method that permitted to reach such results. However, its major drawback is its productivity: performing large numbers of zone passes requires much time, which is probably the main limitation of Zone Melting.

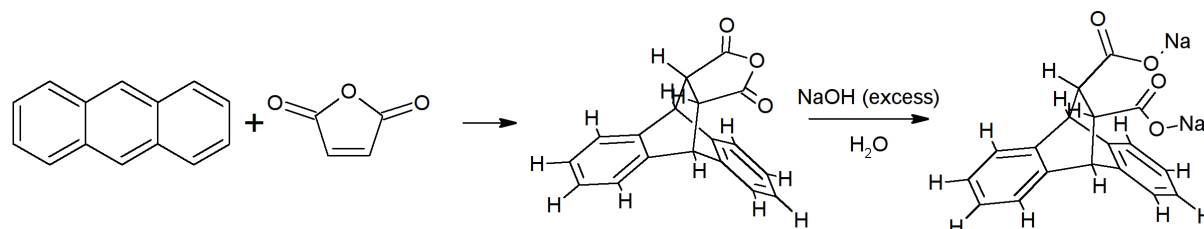
b) Purification by impurity chemical transformation

Thanks to the difference in chemical reactivity between Phenanthrene impurities, the latter can be specifically modified in order to change their properties and their ability at being removed from the target compound.

The most typical example is that of Anthracene, that exhibits the reactivity of dienes. Consequently, it is possible to convert this impurity to its Diels-Alder products using any appropriate dienophile reactant – Phenanthrene, that has almost no Diels-Alder reactivity [33], should not undergo any similar transformation. One of the related chemical transformations is

4. Also called “Zone Refining”.

the reaction with Maleic Anhydride, that is known to form with Anthracene the corresponding Diels-Alder adduct [34] (see scheme 1). The latter can react with water in alkaline-pH medium, leading to the formation of a salt extractable by liquid-liquid extraction.



SCHEME 1: Reaction of Anthracene with Maleic Anhydride, followed by Sodium salt formation

In 1974, McArdle and Sherwood performed a treatment of Phenanthrene with Maleic Anhydride. The Anthracene/Maleic Anhydride Diels-Alder adduct was removed by successive reactive extractions with 3M aqueous NaOH solutions [21]. According to the authors of the study, this procedure was able to reduce Anthracene level in Phenanthrene below the limit of detection of their analytical method (< 1 ppm). Note that this procedure was also employed by Feldman *et al.* [22], leading to similar purifying effects.

In their study, McArdle and Sherwood showed that other chemical treatments were also able to remove other impurities from Phenanthrene:

- (i) the exposure of Phenanthrene samples to molten Sodium was found to convert Dibenzothiophene to Biphenyl. The latter was removed from the target compound by means of Zone Melting which was found to remove Biphenyl more easily than Dibenzothiophene. However, another paper showed the reactivity of Phenanthrene with alkali metals [35], which can cause the formation of undesirable impurities.
- (ii) treatment of Phenanthrene with Raney Nickel led to the partial elimination of Dibenzothiophene. Nevertheless, a new unidentified impurity was generated by this procedure.
- (iii) treatment of Phenanthrene with molten Potassium Hydroxide led to the reduction of Fluorene level below the limit of detection of the analytical method (1 ppm).

c) Purification by preparative liquid chromatography

Besides the techniques previously mentioned, preparative liquid chromatography was also used in several studies to purify Phenanthrene. However, only one recent study, conducted by Couvrat, gave quantitative figures on its purifying effect [18]. After application of the technique, Phenanthrene main impurity levels (Fluorene, Dibenzothiophene, Anthracene and Carbazole) were reduced below the detection thresholds of the analytical method employed (~ 0.01 wt. % impurity in Phenanthrene). However, this procedure was applied to a starting Phenanthrene sample that exhibited low impurity contents. The purifying effect of the method was not assessed on Phenanthrene samples containing more impurities. Moreover, the main drawback of this method is its productivity, as several days were required to obtain only 10 mg of purified Phenanthrene.

d) Summary

As shown in this part, many purification procedures were described to remove impurities from Phenanthrene samples, which offers a certain freedom of choice. In several studies, two (or more) different methods were combined in order to increase the purity of the molecule. However, only two methods (solvent assisted recrystallization and zone melting) based on discrimination in the solid state were reported and supported by quantitative data on their purifying effects. Moreover, most of these studies were conducted many years ago, which calls for a critical re-evaluation of their efficiency.

2) State of the art on Phenanthrene purity assessment

In order to assess the purifying effects of the different methods described above, several analytical methods were reported by the researchers who led the corresponding studies. The aim of this paragraph is to present them and to discuss their efficiency.

a) Analytical Gas Chromatography

Due to their favorable vapor pressures, Phenanthrene and its organic impurities can be analyzed by means of Gas Chromatography (GC). This method was widely used to determine impurity levels in Phenanthrene samples. However, in their study, McArdle *et al.* used a packed column in order to separate the interest chemical species [21]. In these conditions, Anthracene could not be separated from Phenanthrene, which prevented from its quantification using GC. Moreover, typical chromatograms obtained by the authors (fig. 10) showed broad solute peaks, which is generally not suitable for trace analysis. In their case, several peaks (E, F) were not sufficiently resolved to perform specific impurity quantification. The impurity detection thresholds were 0.0001 wt. % for almost all the impurities, except Dibenzothiophene (0.01 wt. %). Note that no detailed information was provided by the authors about the chromatographic conditions (carrier gas, temperature program, sample preparation...).

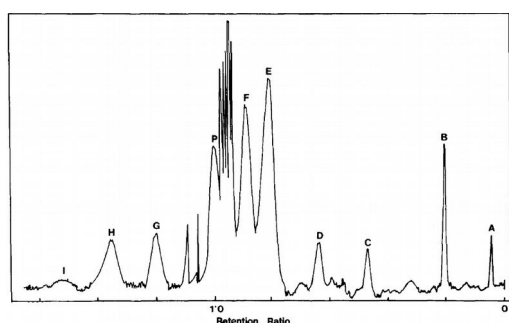


FIG. 10: **Typical low-resolution GC chromatogram of Phenanthrene samples using packed columns**, from McArdle *et al.* [21]. A. Naphthalene, B. Biphenyl, C. Fluorene, D. Dihydrophenanthrene, E. Unknown impurity, F. Dibenzothiophene, P. Phenanthrene, G. Fluoranthene, H. Pyrene.

More recently, Couvrat *et al.* resorted to GC to analyze Phenanthrene [18]. However, they used capillary columns, that are known to be more efficient⁵ than packed ones. The resulting

5. Efficient columns give thin peaks, which generally improves the resolution between the bands of solutes that exhibit close retention times.

chromatograms exhibited more resolved solute peaks, which led to the improvement of impurity quantification specificity. However, the detection thresholds of this method were higher (~ 0.01 wt. %) than those obtained by McArdle *et al.* using low-resolution GC.

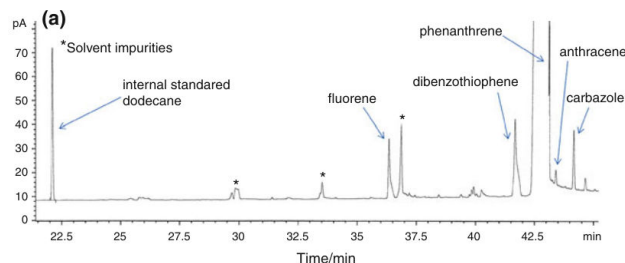


FIG. 11: Typical capillary-GC chromatogram of Phenanthrene, from Couvrat *et al.* [18].

b) Infrared spectroscopy

During the studies conducted by Matsumoto *et al.* and McArdle *et al.*, Anthracene was not resolvable from Phenanthrene in Gas Chromatography. Consequently, this impurity was quantified by spectroscopic analyses.

In Matsumoto study [27], Anthracene levels were determined by Infrared (IR) absorption spectroscopy. Indeed, this impurity presents a strong absorption band at 882 cm^{-1} whereas Phenanthrene does not absorb at this wavenumber. Consequently, a specific quantification of this impurity was possible, and the detection threshold was $\sim 10^{-5}$ mol/mol.

In their study, McArdle *et al.* quantified this impurity by means of ultraviolet (UV) absorption spectroscopy. A similar limit of detection was obtained using this method [21].

c) Summary

Two major outcomes were highlighted during the previous studies on Phenanthrene analysis:

- (i) First, thanks to their high capacity, packed GC columns permitted the detection of impurities at very low levels – that were sufficient to measure ultrapurity values. However, this method was not efficient enough to quantify all the impurities by one shot: Anthracene and Dibenzothiophene peaks were not sufficiently resolved to perform specific quantification by GC, and this method had to be combined with spectroscopic analyses to determine the levels of all the detectable impurities.
- (ii) Secondly, thanks to their high efficiency, capillary GC columns offered a better resolution of Phenanthrene impurity peaks, which made possible their quantification by one single analysis. Nevertheless, these columns exhibit lower capacities than those of packed ones, which means that the analyzable mass of sample was lower. Consequently, the detection thresholds were higher. Even if the chromatographic conditions described by Couvrat *et al.* are sufficient to measure ultrapurity, they do not permit the measurement of purity values higher than 99.9(9) %. Therefore, this chromatographic method should be refined and optimized to reach that goal.

IV. IMPLICATIONS OF PHENANTHRENE SYSTEM REINVESTIGATION

As mentioned in this chapter:

(i) at atmospheric pressure, Phenanthrene presents two different phases whose stability is reversed at $\sim 65\text{-}70\text{ }^{\circ}\text{C}$. The LT phase is ordered, and the HT one exhibits dynamic disorder.

(ii) studies on the transition between the two phases mentioned previously highlighted its unusual character: SHG monitoring shown the progressive conversion of the LT form to the HT on heating, and electrical resistance measurements suggested the potential occurrence of two separate transitions of different orders in a narrow temperature range. They raised the question of the mechanism of the transition, which was, up to now, not resolved.

(iii) studies on Phenanthrene chemical purity shown that this parameters had a large influence on the solid-solid transition temperature. They raised the question of the origin of the unusual character of the transition: Phenanthrene molecule itself, or its impurities?

These two questions have to be answered by studies on ultrapure Phenanthrene samples, which implies:

(i) the development and optimization of purification processes to obtain 99.9 mole % purity product,

(ii) the measurement of impurity contents in Phenanthrene, at levels sufficiently low to assess the purity of ultrapure samples.

Consequently, the next chapter aims at presenting works dedicated to the development of an analytical method for Phenanthrene impurity levels quantification in one single shot (with a particular attention paid to the detection thresholds, in order to measure ultrapurity).

Then, chapter IV will present works on Phenanthrene ultrapurification by means of crystallization.

V. REFERENCES

- [1] K. Wang, Y. Hu, Y. Liu, N. Mi, Z. Fan, Y. Liu, Q. Wang, Design, Synthesis, and Antiviral Evaluation of Phenanthrene-Based Tylophorine Derivatives as Potential Antiviral Agents, *J. Agric. Food Chem.* 58 (2010) 12337–12342. doi:10.1021/jf103440s.
- [2] M.J. Sienkowska, J.M. Farrar, F. Zhang, S. Kusuma, P.A. Heiney, P. Kaszynski, Liquid crystalline behavior of tetraaryl derivatives of benzo[c]cinnoline, tetraazapyrene, phenanthrene, and pyrene: the effect of heteroatom and substitution pattern on phase stability, *J. Mater. Chem.* 17 (2007) 1399–1411. doi:10.1039/B615545F.
- [3] X.F. Wang, Y.J. Yan, Z. Gui, R.H. Liu, J.J. Ying, X.G. Luo, X.H. Chen, Superconductivity in $\text{Ba}_{1-x}\text{Sr}_x\text{Phenanthrene}$ ($\text{A}=\text{Sr}, \text{Ba}$), *Phys. Rev. B.* 84 (2011) 214523. doi:10.1103/PhysRevB.84.214523.
- [4] J. Li, G. Hu, N. Wang, T. Hu, Q. Wen, P. Lu, Y. Wang, Oligo(3,6-phenanthrene ethynyls): Synthesis, Characterization, and Photoluminescence, *J. Org. Chem.* 78 (2013) 3001–3008. doi:10.1021/jo302825r.
- [5] S. Menon, D. Sinha-Mahapatra, J.W. Herndon, Synthesis of phenanthrene derivatives through the net [5+5]-cycloaddition of prenylated carbene complexes with 2-alkynylbenzaldehyde derivatives, *Tetrahedron.* 63 (2007) 8788–8793. doi:10.1016/j.tet.2007.06.032.
- [6] L.F. Fieser, E.B. Hershberg, A NEW PHENANTHRENE SYNTHESIS, *J. Am. Chem. Soc.* 57 (1935) 1508–1509. doi:10.1021/ja01311a503.
- [7] C. Brown, B.J. Sikkell, C.F. Carvalho, M.V. Sargent, A new phenanthrene synthesis, *J. Chem. Soc. [Perkin 1].* (1982) 3007–3010. doi:10.1039/P19820003007.
- [8] S.F. Dyke, A.R. Marshall, J.P. Watson, Aspects of aryne chemistry—I: A phenanthrene synthesis, *Tetrahedron.* 22 (1966) 2515–2521. doi:10.1016/S0040-4020(01)99043-X.
- [9] A. Matsumoto, *Iron-Catalyzed Synthesis of Fused Aromatic Compounds via C–H Bond Activation*, Springer, 2014.
- [10] A. Matsumoto, L. Ilies, E. Nakamura, Phenanthrene Synthesis by Iron-Catalyzed [4 + 2] Benzannulation between Alkyne and Biaryl or 2-Alkenylphenyl Grignard Reagent, *J. Am. Chem. Soc.* 133 (2011) 6557–6559. doi:10.1021/ja201931e.
- [11] S. Matsumoto, Unusual Behaviors in Electrical Conductivity of Phenanthrene Crystal, *Bull. Chem. Soc. Jpn.* 40 (1967) 2749–2753. doi:10.1246/bcsj.40.2749.
- [12] S. Matsumoto, A Phase Transition in Phenanthrene Crystal, *Bull. Chem. Soc. Jpn.* 39 (1966) 1811–1813. doi:10.1246/bcsj.39.1811.
- [13] V. Petříček, I. Císařová, L. Hummel, J. Kroupa, B. Březina, Orientational disorder in phenanthrene. Structure determination at 248, 295, 339 and 344 K, *Acta Crystallogr. B.* 46 (1990) 830–832. doi:10.1107/S0108768190007510.
- [14] F.P.A. Fabbiani, D.R. Allan, W.I.F. David, S.A. Moggach, S. Parsons, C.R. Pulham, High-pressure recrystallisation—a route to new polymorphs and solvates, *CrystEngComm.* 6 (2004) 505–511. doi:10.1039/B406631F.
- [15] N. Couvrat, Four case studies on the impact of the heterogeneous equilibria on physicochemical behaviours of organic solids, European PhD thesis, Université de Rouen, 2011. <http://www.theses.fr/s149502>.
- [16] J.P. Dougherty, S.K. Kurtz, A second harmonic analyzer for the detection of non-centrosymmetry, *J. Appl. Crystallogr.* 9 (1976) 145–158. doi:10.1107/S0021889876010789.
- [17] S. Matsumoto, T. Fukuda, An X-ray Study on the Phase Transition of Phenanthrene Crystal, *Bull. Chem. Soc. Jpn.* 40 (1967) 743–746. doi:10.1246/bcsj.40.743.
- [18] N. Couvrat, A. Burel, S. Tisse, Y. Cartigny, G. Coquerel, Combining zone melting and preparative chromatography to purify Phenanthrene, *J. Therm. Anal. Calorim.* 112 (2013) 293–300. doi:10.1007/s10973-012-2746-z.
- [19] U. Glostein, M. Epple, H.K. Cammenga, Influencing the Solid-Solid Phase Transition in Phenanthrene by Suitable Doping, *Z. Für Phys. Chem.* 214 (2009) 379. doi:10.1524/zpch.2000.214.3.379.
- [20] B. McArdle, J. Sherwood, The purity and purification of organic materials, *Chem. Ind.* (1985) 268–274.
- [21] B.J. McArdle, J.N. Sherwood, A.C. Damask, The growth and perfection of phenanthrene single crystals, *J. Cryst. Growth.* 22 (1974) 193–200. doi:10.1016/0022-0248(74)90094-3.
- [22] J. Feldman, P. Pantages, M. Orchin, Purification and Freezing Point of Phenanthrene, *J. Am. Chem. Soc.* 73 (1951) 4341–4343. doi:10.1021/ja01153a091.
- [23] F. Julian, O. Milton, F. Julian, O. Milton, Purification of phenanthrene by azeotropic distillation, 1951. <https://www.google.com/patents/US2590096> (accessed April 25, 2017).

- [24] T. Sako, M. Sato, S. Yamane, Purification of Polycyclic Aromatic Compounds Using Retrograde Crystallization in Supercritical Carbon Dioxide, *J. Chem. Eng. Jpn.* 23 (1990) 770–772. doi:10.1252/jcej.23.770.
- [25] Y. Runsheng, L. Zuyu, W. Zhizhong, Study of Purification of Phenanthrene from Phenanthrene Waste, *Indian J. Sci. Technol.* 3 (2010) 1148–1150. doi:10.17485/ijst/2010/v3i12/29850.
- [26] F. Esmailzadeh, I. Goodarznia, Supercritical Extraction of Phenanthrene in the Crossover Region, *J. Chem. Eng. Data.* 50 (2005) 49–51. doi:10.1021/je049872x.
- [27] S. Matsumoto, Zone-Refining of Phenanthrene and Studies on the Purity, *Bull. Chem. Soc. Jpn.* 41 (1968) 2792–2794. doi:10.1246/bcsj.41.2792.
- [28] M.J. Joncich, D.R. Bailey, Zone Melting and Differential Thermal Analysis of Some Organic Compounds, *Anal. Chem.* 32 (1960) 1578–1581. doi:10.1021/ac60168a010.
- [29] H. Ringel, A.C. Damask, R.A. Arndt, The Heat Capacity Anomaly in Phenanthrene; Effects of Deuteration, Purification and Dissolution, *Mol. Cryst.* 3 (1967) 145–147. doi:10.1080/15421406708083923.
- [30] L.C. Daniels, A.O. Jaeger, S. Co, Purification of crude aromatic compounds, 1929. <https://www.google.com/patents/US1892772> (accessed April 25, 2017).
- [31] R.A. Arndt, A.C. Damask, Heat-Capacity Anomaly in Phenanthrene, *J. Chem. Phys.* 45 (1966) 755–756. doi:10.1063/1.1727640.
- [32] N. Karl, Organic Semiconductors: Purification and Crystal Growth, *Mol. Cryst. Liq. Cryst. Inc. Nonlinear Opt.* 171 (1989) 157–177. doi:10.1080/00268948908065793.
- [33] D. Biermann, W. Schmidt, Diels-Alder reactivity of polycyclic aromatic hydrocarbons. 1. Acenes and benzologs, *J. Am. Chem. Soc.* 102 (1980) 3163–3173. doi:10.1021/ja00529a046.
- [34] M.C. Kloetzel, The Diels-Alder Reaction with Maleic Anhydride, in: John Wiley & Sons, Inc. (Ed.), *Org. React.*, John Wiley & Sons, Inc., Hoboken, NJ, USA, 2011: pp. 1–59. doi:10.1002/0471264180.or004.01.
- [35] A. Jeanes, R. Adams, The Addition of Alkali Metals to Phenanthrene, *J. Am. Chem. Soc.* 59 (1937) 2608–2622. doi:10.1021/ja01291a041.

Chapter III
Development of an analytical method to assess
Phenanthrene purity

Chapter III

DEVELOPMENT OF AN ANALYTICAL METHOD TO ASSESS PHENANTHRENE PURITY

TABLE OF CONTENTS

NOMENCLATURE.....	109
I. INTRODUCTION.....	111
II. BASIC NOTIONS ON GAS CHROMATOGRAPHY.....	113
1) Basic principle of the technique	113
2) Characteristics of a chromatogram	114
a) The elution peak.....	114
b) Column efficiency.....	114
c) Apparent retention factor.....	115
d) Column apparent selectivity.....	115
e) Peak resolution.....	115
3) Characteristics of a column	116
a) Technology.....	116
b) Dimensions.....	116
c) Phase ratio.....	116
d) Hold-up time.....	117
4) Characteristics of a column flow	117
a) Carrier gas local velocity.....	117
b) Carrier gas average velocity.....	119
c) Column flow.....	119
d) Carrier gas viscosity.....	119
5) Solute elution thermodynamics	120
a) Introduction.....	120
i. Equilibrium constant.....	121
ii. Solute retention factor.....	121
b) Impact of temperature on solute partitioning.....	121
c) Solute retention time.....	122
6) Kinetic phenomena during solute elution	122
a) Solute diffusion in the gas phase.....	122
b) Solute diffusion in the stationary phase.....	123
c) Local plate height.....	123
7) Gas Chromatograph modules: injectors and detectors	125
a) Split/splitless injector.....	125
b) Detectors.....	126
i. Flame Ionization Detector.....	126
ii. Mass Spectrometer Detectors.....	126
8) Comprehensive two-dimensional techniques	127
III. RETENTION TIME PREDICTION IN CAPILLARY GAS CHROMATOGRAPHY...	130
1) Introduction	130

2) Development of a new retention model.....	132
a) New theoretical expression of solute retention factor.....	132
b) Estimation of model parameters.....	135
i. Determination of column phase ratio.....	135
ii. Determination of solute partition parameters.....	136
3) Validation of the new retention model.....	137
a) Introduction.....	137
b) Materials and methods.....	137
i. Chemicals.....	137
ii. Chromatographic conditions.....	137
iii. Optimization and prediction procedures.....	138
c) Results and discussion.....	139
i. Column phase ratio determination.....	139
ii. Solute partition parameters determination.....	140
iii. Retention time prediction in one-dimensional GC.....	144
iv. Retention time prediction in FM-GC×GC.....	147
d) Conclusions.....	150
IV. IMPURITY QUANTIFICATION IN PHENANTHRENE.....	152
1) Introduction.....	152
2) Analytical method.....	152
a) Capillary GC-FID conditions.....	152
b) Impurity level determination.....	153
i. FID calibration.....	153
ii. Impurity quantification.....	154
3) Validation of the method.....	154
a) Assessment of injection volume repeatability.....	154
b) FID response factors.....	155
c) Testing the method on Phenanthrene samples.....	156
i. Analysis of technical-grade Phenanthrene.....	156
ii. Analysis of synthesis grade Phenanthrene (Alfa Aesar).....	159
iii. Analysis of synthesis grade Phenanthrene (Sigma-Aldrich, lot 1).....	160
iv. Analysis of synthesis grade Phenanthrene (Sigma-Aldrich, lot 2).....	162
d) Conclusion.....	163
4) General conclusion.....	164
V. APPENDICES.....	165
1) Experimental retention time values for model parameter estimation.....	165
a) Column phase ratio determination.....	165
b) Solute partition parameter determination.....	166
2) Analysis of Phenanthrene by GC-MSD.....	167
VI. REFERENCES.....	168

NOMENCLATURE

Abbreviations

FID	Flame Ionization Detector
FM	Flow Modulation
GC	Gas Chromatograph(y)
GC×GC	Comprehensive two-dimensional Gas Chromatography
HPLC	High Performance Liquid Chromatography
MP	Mobile phase
MSD	Mass Spectrometer Detector
PAH	Polycyclic Aromatic Hydrocarbon
SP	Stationary Phase
TM	Thermal Modulation
UVD	Ultraviolet Detector
WCOT	Wall Coated Open Tubular (capillary column)

Symbols (expressed in international system units)

$C_{p,i}$	$[\text{J}\cdot\text{mol}^{-1}\cdot\text{K}^{-1}]$	Solute heat capacity
D_i	$[\text{m}^2\cdot\text{s}^{-1}]$	Solute diffusion coefficient
d	$[\text{m}]$	Column internal diameter
d_p	$[\text{m}]$	Particle diameter
e	$[\text{m}]$	Stationary phase film thickness
F	$[\text{m}^3\cdot\text{s}^{-1}]$	Column volumetric outlet flow
G_i	$[\text{J}\cdot\text{mol}^{-1}]$	Solute Gibbs molar free energy
H_i	$[\text{J}\cdot\text{mol}^{-1}]$	Solute molar enthalpy
h	$[\text{m}]$	Column local plate height
\bar{h}	$[\text{m}]$	Column average plate height
K_i	$[-]$	Solute partition equilibrium constant
k_i	$[-]$	Solute retention factor
k_{iapp}	$[-]$	Solute apparent retention factor
L	$[\text{m}]$	Column length
LD_i	$[\text{kg}\cdot\text{m}^{-3}]$	Limit of detection of a solute
LQ_i	$[\text{kg}\cdot\text{m}^{-3}]$	Limit of quantification of a solute
M_i	$[\text{kg}\cdot\text{mol}^{-1}]$	Molar mass
N	$[-]$	Number of Carbon atoms
N_i	$[-]$	Column efficiency
P	$[-]$	Column pressure ratio
p	$[\text{Pa}]$	Pressure
R	$[\text{J}\cdot\text{mol}^{-1}\cdot\text{K}^{-1}]$	Gas constant
R_s	$[-]$	Peak resolution
RF	$[\text{signal unit}\cdot\text{kg}^{-1}]$	Response factor
S_i	$[\text{J}\cdot\text{mol}^{-1}\cdot\text{K}^{-1}]$	Solute molar entropy

SSD	$[s^2]$	Sum of squares of deviations
T	$[K]$	Temperature
t	$[s]$	Time
t_0	$[s]$	Column holdup time
U_i	$[J \cdot mol^{-1}]$	Solute molar internal energy
V_i	$[m^3 \cdot mol^{-1}]$	Solute molar volume
v	$[m^3]$	Phase volume

Greek symbols (expressed in international system units)

α_{app}	$[-]$	Column apparent selectivity
α_i	$[m^3 \cdot mol^{-1} \cdot K^{-1}]$	Solute molar coefficient of expansion
β	$[-]$	Column phase ratio
Δ	$[-]$	Difference between the stationary and mobile phases
δ_i	$[s]$	Peak width at half height
η	$[Pa \cdot s]$	Viscosity
κ	$[m^2]$	Flow permeability
σ_i	$[s]$	Peak standard deviation
χ_i	$[m^3 \cdot mol^{-1} \cdot Pa^{-1}]$	Solute molar compressibility

Note: in this chapter, all the quantities are expressed in the international system units, unless specified.

I. INTRODUCTION

As stated in the previous chapter, many analytical methods can be envisaged to analyze Phenanthrene samples. Due to the large number of impurities to quantify, separative methods (*e. g.*, gas chromatography, GC) were judiciously selected during previous works on Phenanthrene purification. However, due to their low efficiency, packed GC columns that were used [1] made the employment of other complementary methods (IR and/or UV spectroscopy) compulsory, in order to quantify non-resolved impurities such as Anthracene. In this case, the preparation of samples for purity determination is tedious, which is not suitable when many analyses must be performed.

Thanks to technical progresses, many chromatographic variants can be envisaged to tackle the problem of Phenanthrene purity assessment. Among them, classical GC, using capillary columns, can be raised. Such columns generally exhibit sufficient efficiencies to obtain thin and high chromatographic peaks, which offers, with respect to packed-column GC: (i) an improvement of the separation of the species to quantify; (ii) a decrease of the detection thresholds.

However, appropriate detectors must be chosen to quantify the solutes after elution. Among them, Flame Ionization (FIDs) and Mass Spectrometer (MSDs) detectors are widely employed due to their sensitivity with respect to almost all the organic molecules. Moreover, MSDs offer an access to solute molecular formula, or even chemical structure, which permits their identification.

In this thesis, quantification of impurities in Phenanthrene is targeted. As the final aim of this work is to produce ultrapure samples of this molecule (*e. g.*, samples exhibiting purities larger than 99.9 mole %), an analytical method, able at measuring such high purities, must be developed. Consequently, capillary-column GC-FID was selected to quantify impurity levels in Phenanthrene. The present chapter aims at explaining the different steps of the development of a method using this technique. All the measurements were cross-checked with capillary-column GC-MSD experiments in view of increasing the degree of certainty on impurity identities.

In this work, the development of the analytical method was performed in separate steps:

- the elaboration of a retention thermodynamic model, in order to predict solute retention times in given chromatographic conditions.
- some internal validation of the analytical method, once the separation is optimized using the predictive model previously developed. Solute response factors, peak resolutions and detection thresholds were assessed in order to estimate the maximum purity that can be measured in case of absence of impurity detection.
- eventually, various commercial Phenanthrene samples, provided by different suppliers and exhibiting different purity grades, were analyzed using the method developed in this work, to test its reliability.

Before introducing the results, some basic notions on Gas Chromatography are presented, in order to help the reader at understanding the theoretical and experimental developments introduced in this chapter.

II. BASIC NOTIONS ON GAS CHROMATOGRAPHY

1) Basic principle of the technique

Classical Gas Chromatography (GC) devices can be described according to fig. 1. They are made of several modules: a pressurized carrier gas bottle, a pneumatic control module, an injector, a column (and its oven), a detector and a recorder.

During a chromatographic process, a certain pressure of carrier gas (Helium, Nitrogen or Hydrogen) is set at the head of a tubular column, which permits the generation of a gas flow through the column. Conventionally, the carrier gas is called “*mobile phase*” (MP).

If capillary, the column contains a certain amount of stationary phase (SP) which is generally a liquid polymer coated on its internal wall.

Any liquid or gaseous sample can be analyzed by introduction of a certain amount in the injector by means of a glass syringe. During the injection, the sample is vaporized and transported by the carrier gas. The different solutes undergo successive partition equilibria between the MP and the SP. According to these partition equilibria, the solutes travel at different rates in the column (elution process), which permits their separation. To optimize the separation with a given column, the operator can change: (i) the MP velocity, (ii) the column oven temperature program.

After elution, solutes reach the detector that generates a signal whose intensity is generally proportional to the amount of solute detected. Consequently, after detector calibration, the species of interest can be quantified. The record intensity vs. analysis time is called “*chromatogram*”.

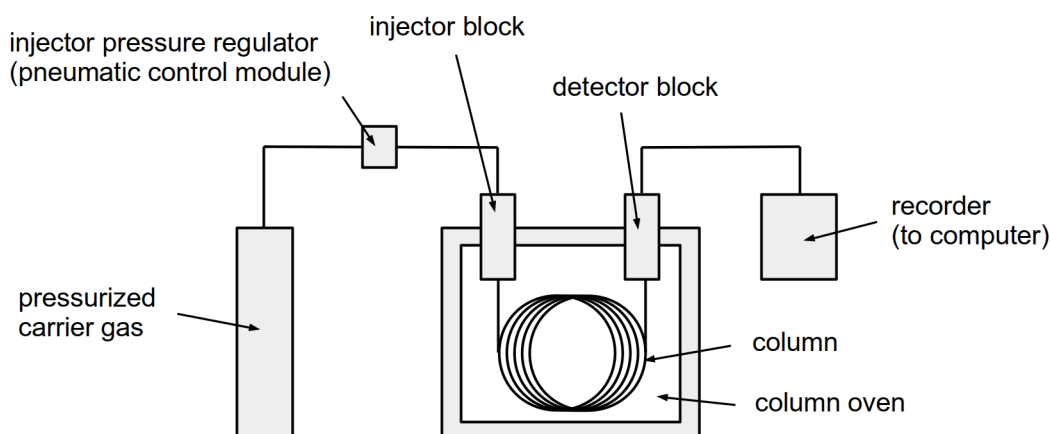


FIG. 1: Schematic representation of a Gas Chromatograph

2) Characteristics of a chromatogram

a) The elution peak

Basically, the process of solute elution can be approached using the plate theory [2]. In the latter, it is assumed that the column behaves as a cascade of biphasic reactors (the MP and SP being the two phases) between which solute partition occurs. At every displacement of solute induced by the MP, new partition equilibria take place. Due to this phenomenon and to diffusion of solutes, a certain broadening of solute bands is engendered. At the end of the process, the different solutes generally elute as Gaussian peaks whose parameters are their retention times ($t_{R,i}$) and their standard deviation (σ_i) (see eq. 1).

$$y_i(t) = y_0 + \frac{C_i \times RF_i}{\sigma_i \sqrt{2\pi}} \exp\left(-\frac{1}{2} \times \left[\frac{t - t_{R,i}}{\sigma_i}\right]^2\right) \quad (1)$$

$y_i(t)$ being signal intensity, y_0 signal baseline intensity, C_i the concentration of the solute, RF_i the detector response factor, and t time. A graphical representation of the function is presented in fig. 2.

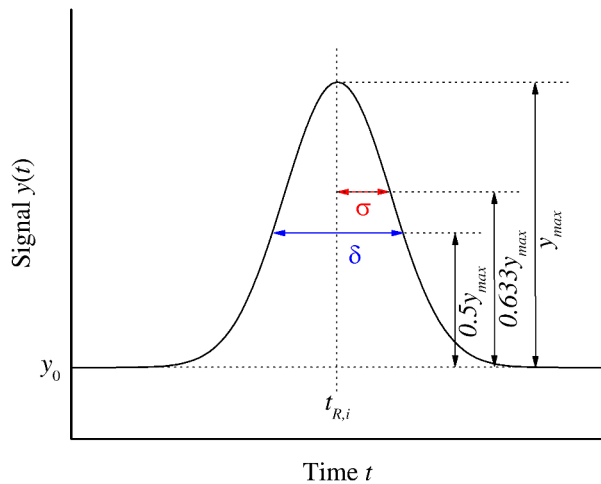


FIG. 2: Characteristics of the elution peak

b) Column efficiency

The efficiency of a column with respect to a solute, N_i , is defined by eq. 2:

$$N_i = \left(\frac{t_{R,i}}{\sigma_i}\right)^2 = 5.54 \times \left(\frac{t_{R,i}}{\delta_i}\right)^2 \quad (2)$$

δ_i being peak width at half intensity.

Generally, column efficiency is also called “*number of plates*”. N_i quantifies the ability of a column at generating plates during solute elution. From N_i , the column average plate height, \bar{h}_i , can be calculated using the following relationship, in which L designates column length:

$$\bar{h}_i = \frac{L}{N_i} \quad (3)$$

In practice, large N_i (or low \bar{h}_i) values can be associated with thin peaks, which is suitable for two reasons: (i) fine peaks offer more space for other peaks on the chromatogram (concept of peak capacity); (ii) due to the properties of Gaussian function, fine peaks are more intense, which make them easier to integrate after detection (suitable for trace analysis).

c) Apparent retention factor

The apparent retention (or capacity) factor of a column with respect to a solute, $k_{app,i}$, is defined by eq. 4:

$$k_{app,i} = \frac{t_{R,i} - t_0}{t_0} \quad (4)$$

t_0 being the hold-up time of the column (e. g., the retention time of a non-retained compound).

Physically, it corresponds to the ratio of the times spent by the solute in the SP and in the MP. Solute apparent retention factors are necessarily higher than 0.

d) Column apparent selectivity

The apparent selectivity of a column with reference to two solutes ($\alpha_{app,j/i}$, j being the more retained solute) can be estimated using eq. 5:

$$\alpha_{app,j/i} = \frac{k_{app,j}}{k_{app,i}} = \frac{t_{R,j} - t_0}{t_{R,i} - t_0} \quad (5)$$

This quantity is related to the ability of a column to separate two solutes. Nevertheless, selectivity higher than unity does not necessarily mean that the considered solutes are separated. Indeed, this criteria only takes solute retention times into account, but not widths of their peaks. This is why the concept of resolution is more relevant to describe the separation between two solutes.

e) Peak resolution

The resolution ($R_{s,j/i}$, j being the more retained solute) between two solute Gaussian peaks can be calculated using eq. 6:

$$R_{s,j/i} = 1.18 \times \left(\frac{t_{R,j} - t_{R,i}}{\delta_i + \delta_j} \right) \quad (6)$$

When non-selective detectors are used, the resolution between two peaks should be higher than 1.5 in order to quantify the related solutes. Indeed, this value corresponds to a recovering percentage of 2% – generally considered as acceptable for specific quantification in analytical chemistry. Obtaining good resolutions requires to adapt chromatographic conditions to compromise column efficiency and selectivity, as shown by fig. 3. Indeed, for a given selectivity, sufficient column efficiency leads to thin and well-resolved peaks (a). Conversely, low efficiency leads to broad and non-resolved peaks (b), which requires the use of a selective detector to integrate solute peaks and perform quantification.

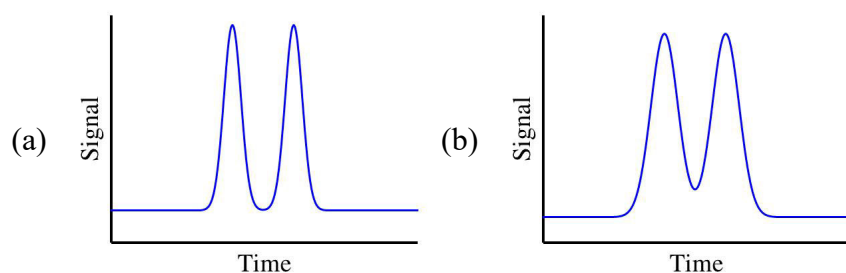


FIG. 3: **Illustration of the concept of peak resolution** – (a) two well-resolved peaks with complete return to baseline, (b) two non-resolved peaks with incomplete return to baseline, that denote partial coelution of the two solutes.

3) Characteristics of a column

Capillary columns can be described using several characteristics that are listed in this paragraph.

a) Technology

Capillary columns used in this work are known as “*wall coated open tubular*” (WCOT). A schematic representation of a transversal cut of this kind of column is made in fig. 4.

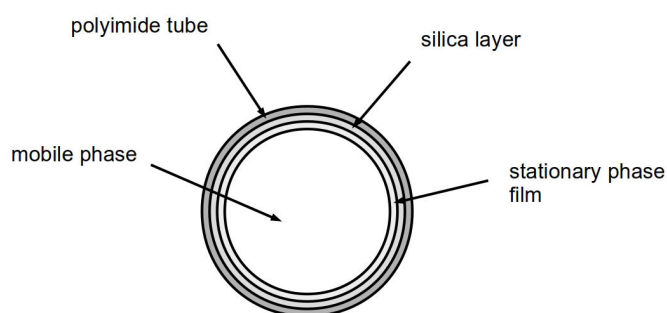


FIG. 4: **Schematic transversal cuts of chromatographic columns** – left: capillary column, right: packed column

Capillary WCOT columns are open fused-silica tubes whose external wall is coated with a polyimide film. The internal wall is coated with a SP film. The major part of the tube is made of void, which permits carrier gas flowing.

b) Dimensions

Capillary WCOT columns have three characteristic dimensions: their length (L), their internal diameter (d), and their stationary phase film thickness (e). Conventional dimensions are: $5 \leq L \leq 60$ m, $0.10 \leq d \leq 0.53$ mm and $0.05 \leq e \leq 8$ μ m [3].

c) Phase ratio

The phase ratio (β) of a column corresponds to the ratio of the volume of SP (v_{SP}) and that occupied by the MP (v_{MP}) [4,5].

$$\beta = \frac{v_{SP}}{v_{MP}} \quad (7)$$

In the case of capillary columns, phase ratio can be estimated using eq. 8:

$$\beta \approx \frac{d}{4 \times e} \text{ when } e \ll d \quad (8)$$

d) Hold-up time

The hold-up time of a column corresponds to the retention time of an unretained solute. It is generally noted t_0 . Its mathematical expression is given by the following relationship [6], where x is the position in the column and u carrier gas velocity.

$$t_0 = \int_0^L \frac{dx}{u(x)} \quad (9)$$

4) Characteristics of a column flow

a) Carrier gas local velocity

The local velocity of the MP through a tubular pipe can be estimated using Darcy's law [5]:

$$u(x) = -\frac{\kappa}{\eta} \times \frac{dp}{dx} \quad (10)$$

κ being column permeability, η MP viscosity and p pressure.

Conservation of carrier gas mass flow through the column leads to:

$$p(x) \times u(x) = p_{outlet} \times u_{outlet} \quad (11)$$

p_{outlet} and u_{outlet} being carrier gas pressure and velocity at column outlet, respectively.

Combining eqs. 10 and 11 yields:

$$-\frac{\kappa}{\eta} \times p(x) \times dp = p_{outlet} \times u_{outlet} \times dx \quad (12)$$

Integrating this equation and applying $x = L$ leads to:

$$u_{outlet} = \frac{\kappa \times p_{outlet}}{2 \times \eta \times L} \times (P^2 - 1) \quad (13)$$

where P is the column pressure ratio: $P = p_{inlet} / p_{outlet}$, p_{inlet} being column head pressure.

In capillary columns, κ can be expressed using eq. 14 [5]:

$$\kappa = \frac{d^2}{32} \quad (14)$$

Besides, combining eqs. 10, 11 and 13 permits an expression of the pressure profile along the column (eq. 15). A graphical representation of this function is made in fig. 5.

$$p(x) = p_{outlet} \times \sqrt{P^2 - \frac{x}{L} \times (P^2 - 1)} \quad (15)$$

Consequently, eqs. 11 and 15 permit to express the theoretical profile of carrier gas velocity along a column (eq. 16). The graphical representation of this equation is provided in fig. 6.

$$u(x) = \frac{u_{outlet}}{\sqrt{P^2 - \frac{x}{L} \times (P^2 - 1)}} \quad (16)$$

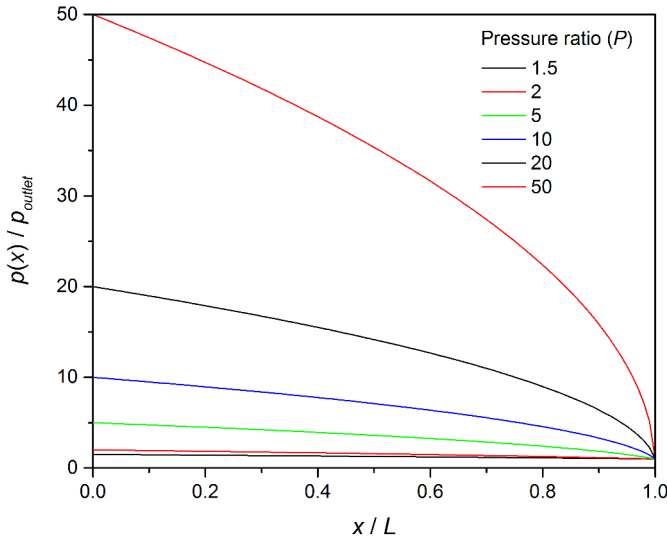


FIG. 5: **Theoretical pressure profiles in a tubular GC column** – calculated using eq. 15 for several pressure ratio values

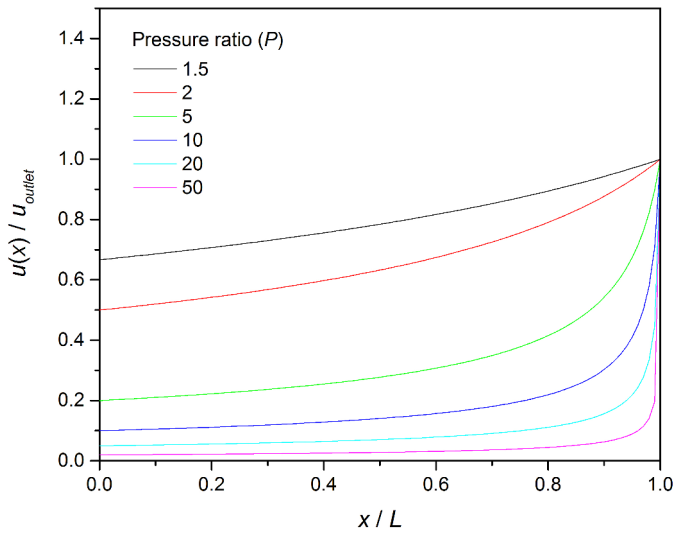


FIG. 6: **Theoretical carrier gas velocity profiles in a tubular GC column** – calculated using eq. 16 for several pressure ratio values

Starting from eqs. 13–14, the gas outlet velocity can be expressed according to eq. 17 for capillary ones.

$$u_{outlet} = \frac{d^2 \times p_{outlet}}{64 \times \eta \times L} \times (P^2 - 1) \quad (17)$$

Consequently, the detailed expression of carrier gas velocity profile becomes eq. 18:

$$u(x) = \frac{d^2}{64\eta L} \frac{p_{outlet}(P^2 - 1)}{\sqrt{P^2 - \frac{x}{L}(P^2 - 1)}} \quad (18)$$

b) Carrier gas average velocity

The average velocity of the carrier gas in a column can be estimated using eq. 19 [3–5,7]:

$$\bar{u} = \frac{L}{t_0} \quad (19)$$

In practice, this quantity can be calculated by measuring the hold-up time of the column. However, a theoretical expression taking the extremity pressures into account permits an indirect estimation of \bar{u} , as shown by eq. 20 (capillary ones) [5].

$$\bar{u} = \frac{3d^2}{128\eta L} \frac{(p_{inlet}^2 - p_{outlet}^2)^2}{(p_{inlet}^3 - p_{outlet}^3)} \quad (20)$$

A simpler – but equivalent – expression can be employed to estimate the average carrier gas velocity in a capillary column [4]:

$$\bar{u} = \frac{d^2}{32\eta L} (p_{inlet} - p_{outlet}) \quad (21)$$

c) Column flow

For capillary columns, the carrier gas outlet volumetric flow, F , can be calculated using Poiseuille's equation [4]:

$$F = \frac{\pi d^4}{256\eta L} \left(\frac{p_{inlet}^2 - p_{outlet}^2}{p_{outlet}} \right) \quad (22)$$

Basically, chromatographic analyses performed in constant flow and variable temperature mode require the injector pneumatic control module to regulate column inlet pressure to counterbalance viscosity changes induced by modifications of temperature.

d) Carrier gas viscosity

As previously mentioned, carrier gas viscosity has a significant impact on its flow. Indeed, large viscosity values induce high flow resistance. Moreover, gas viscosity is increased as temperature increases. To illustrate that, viscosity values of different gases are represented in fig. 7. Generally, the viscosity of a gas can be expressed according to eq. 23 [8]:

$$\eta(T) = a_0 T^{a_1} \quad (23)$$

a_0 and a_1 being gas-related parameters (see tab. 1).

Tab. 1: **Parameters of eq. 23 for different carrier gases** [8] – the viscosity values calculated using these data are expressed in $\mu\text{Pa}\cdot\text{s}$

	He	N ₂	H ₂
a_0	0.4978	0.2841	0.1851
a_1	0.646	0.725	0.680

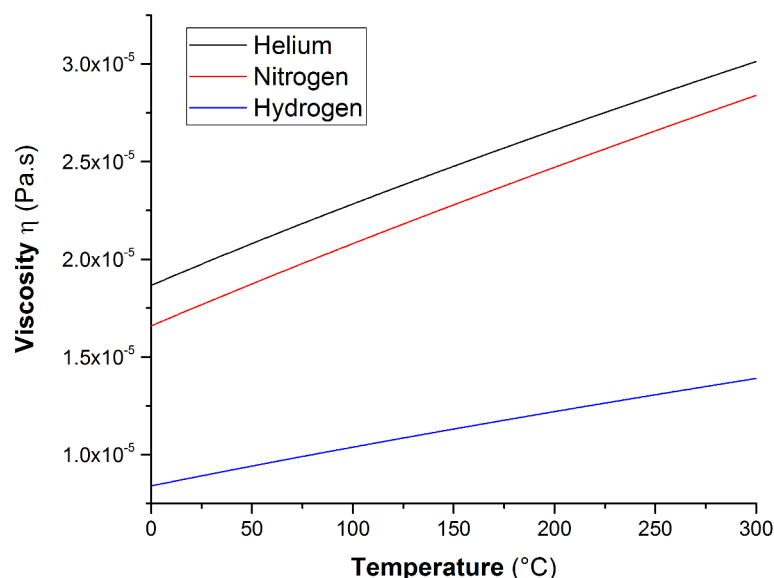


FIG. 7: **Viscosity of different carrier gas with respect to temperature**, calculated using eq. 23.

This figure shows that hydrogen is the gas that exhibits the lowest flow resistance. Conversely, helium is the most viscous one.

Note that more extended models serve to carrier gas viscosity values. Among them, the most used was that developed by Hawkes [9].

5) Solute elution thermodynamics

a) Introduction

As mentioned previously, the process of elution yields from successive displacements of solute partition equilibria between the MP and the SP – this process occurs in the different plates of the column. Let us consider the equilibrium associated with solute partition:

$$i_{(MP)} \leftrightarrow i_{(SP)}$$

This partition transformation can be described using several thermodynamic quantities listed below.

i. Equilibrium constant

The equilibrium constant associated with solute partition transformation is given by the following equation [4,5]:

$$K_i = \frac{[i]_{SP}}{[i]_{MP}} \quad (24)$$

$[i]_{SP}$ and $[i]_{MP}$ being solute concentrations in the SP and MP, respectively. In the case of infinite dilution hypothesis (*e. g.*, the amount of solute introduced in the column does not exceed column capacity), K_i does not depend on solute amount. When this hypothesis is not true, concave or convex partition isotherms can govern solute partitioning. In this case, elution peaks are not Gaussian, but exhibit significant peak fronting or tailing, respectively.

ii. Solute retention factor

This quantity is derived from the equilibrium constant expression. It is defined as the ratio of the mass of solute contained by the SP and that contained by the MP in the state of equilibrium [4,5]:

$$k_i = \frac{m_{i,SP}}{m_{i,MP}} \quad (25)$$

Using column phase ratio (eq. 7) and partition constant (eq. 24) definitions, this relationship can be rewritten as follows:

$$k_i = \frac{K_i}{\beta} \quad (26)$$

b) Impact of temperature on solute partitioning

The equilibrium constant temperature dependency is governed by the following relationship:

$$K_i = \exp\left(\frac{-\Delta G_i}{RT}\right) \quad (27)$$

where ΔG_i is the difference of solute molar Gibbs free energy in the SP and the MP in the state of equilibrium ($\Delta G_i = G_{i,MP} - G_{i,SP}$). R is the gas constant.

Using thermodynamic relationships, one can introduce ΔH_i and ΔS_i , the enthalpy and entropy associated with solute partitioning ($\Delta H_i = H_{i,MP} - H_{i,SP}$ and $\Delta S_i = S_{i,MP} - S_{i,SP}$). As:

$$\Delta G_i = \Delta H_i - T \Delta S_i \quad (28)$$

then the equilibrium constant becomes:

$$K_i = \exp\left(\frac{-\Delta H_i}{RT} + \frac{\Delta S_i}{R}\right) \quad (29)$$

Combining eqs. 29 and 26 yields:

$$k_i = \exp\left(\frac{-\Delta G_i}{RT} - \ln \beta\right) = \exp\left(\frac{-\Delta H_i}{RT} + \frac{\Delta S_i}{R} - \ln \beta\right) \quad (30)$$

This model equation, known as linear Van't Hoff relationship, assumes that ΔH_i and ΔS_i are constant with respect to temperature [6]. These two quantities are both negative. In addition, eq. 30 shows that temperature has a major impact on retention factor values. At low temperatures, these values are generally high, which means that solutes are preferentially dissolved in the SP, and are, consequently, more retained by the column. Conversely, increasing temperature decreases retention factors, and solutes are less retained. The selectivity of a column with respect to two solutes depends on their ΔH_i and ΔS_i values, and temperature has to be optimized to (i) make solute retention factors different enough to obtain a good separation, (ii) make solutes eluting in the minimum analysis time.

c) Solute retention time

Thanks to a mathematical analysis of the elution process, the retention time of a solute can be defined using the following integral [10]:

$$t_{R,i} = \int_0^L \left(\frac{1+k_i}{u(x_i)} \right) dx_i \quad (31)$$

This integral confirms that solute retention time depends on the successive values taken by the retention factor during the analysis, as well as on local carrier gas velocity at its successive positions in the column.

6) Kinetic phenomena during solute elution

During elution, solute band in the column undergoes broadening phenomena. These phenomena occur due to multiple sources: axial molecular diffusion of solutes, mass transfer by diffusion, etc. Thus, they limit the number of apparent equilibria occurring inside the column during elution, which means that they impact local plate height.

a) Solute diffusion in the gas phase

The coefficient of diffusion of solute in the MP (in $\text{cm}^2 \cdot \text{s}^{-1}$) can be estimated from Fuller *et al.* model equation [11]:

$$D_{i,MP} = \frac{0.00125 \times T^{1.75} \times \sqrt{\frac{1}{M_i} + \frac{1}{M_j}}}{p \left(\left(\sum_l v_{l,i} \right)^{\frac{1}{3}} + \left(\sum_m v_{m,j} \right)^{\frac{1}{3}} \right)} \quad (32)$$

where:

T	temperature (K)
M_i	solute molar mass ($\text{g} \cdot \text{mol}^{-1}$)
M_j	carrier gas molar mass ($\text{g} \cdot \text{mol}^{-1}$)
p	pressure (atm)
$v_{l,i}$	solute atomic diffusion volume increment (cm^3)
$v_{m,j}$	carrier gas atomic diffusion volume increment (cm^3)

The atomic diffusion volume increment values can be estimated using tab. 2 entries:

TAB. 2: Diffusion volume increment values for Fuller et al. equation, in cm^3

Atom or molecule	Diffusion volume increment	Atom or molecule	Diffusion volume increment
C	16.5	Aromatic or heterocyclic rings	-20.2
H	1.98	H ₂	7.07
O	5.48	He	2.88
N	5.69	N ₂	17.9
Cl	19.5	O ₂	16.6
S	17.0		

Hence, using these data, diffusion coefficients of solutes in MP can be predicted using their structure and the related diffusion volume increment values.

b) Solute diffusion in the stationary phase

The coefficient of diffusion of a solute in the stationary phase can be estimated using Wilke and Chang relationship [12] which gives approximate values for solutes in solution in a solvent (here, the SP):

$$D_{i,SP} = 7.4 \times 10^{-10} \frac{\sqrt{\Psi_{SP} M_{SP} T}}{\eta_{SP} V_i^{0.6}} \text{ in } \text{m}^2 \cdot \text{s}^{-1} \quad (33)$$

where:

Ψ_{SP}	constant related to molecular associations in the SP
M_{SP}	molecular weight of the SP ($\text{kg} \cdot \text{mol}^{-1}$)
η_{SP}	SP viscosity ($\text{Pa} \cdot \text{s}$)
V_i	molar volume of the solute ($\text{m}^3 \cdot \text{mol}^{-1}$)

Applying this equation to solutes in a stationary phase is not easy, as it requires knowledge on SP properties. An approximation made by Snijders *et al.* permits a simpler estimation of $D_{i,SP}$, according to the following relationship [10]:

$$D_{i,SP} = \frac{D_{i,MP}}{50000} \quad (34)$$

$D_{i,MP}$ being easily accessible from eq. 32.

c) Local plate height

The mathematical analysis of plate theory, combined to many studies dealing with solute band broadening, permitted to estimate local plate height in capillary columns as a function of local carrier gas velocity and solute retention factor, using Golay equation [5]:

$$h_i = \frac{2 D_{i,MP}}{u} + \frac{(1 + 6k_i + 11k_i^2)}{96(1 + k_i)^2} \frac{d^2}{D_{i,MP}} u + \frac{6k_i}{(1 + k_i)^2} \frac{e^2}{D_{i,SP}} u \quad (35)$$

Eq. 35 can be easily used for prediction purposes, as the different parameters can be estimated from experimental measurements and Fuller *et al.* and Snijders *et al.* equations.

This equation indicates that a minimum plate height value can be obtained at an optimal MP velocity, u_{opt} . This quantity can be analytically expressed by solving $dH_i / du = 0$. It is suitable to set gas velocity at its optimum value to obtain the thinnest possible peaks.

For capillary columns, the minimal attainable plate height is:

$$h_{i,min} = \frac{d}{2 \times (1+k_i)} \sqrt{\frac{1+6k_i+11k_i^2}{3}} \quad (36)$$

and the corresponding optimal carrier gas velocity is:

$$u_{i,opt} = \frac{8 D_{i,MP} (1+k_i)}{d} \sqrt{\frac{3}{1+6k_i+11k_i^2}} \quad (37)$$

In capillary columns, the variation of plate height with carrier gas velocity as constant temperature generally follows the behavior shown in fig. 8. As revealed by the graph, the optimal gas velocity is maximal using Hydrogen, which makes its use suitable as it permits “rapid” analyses.

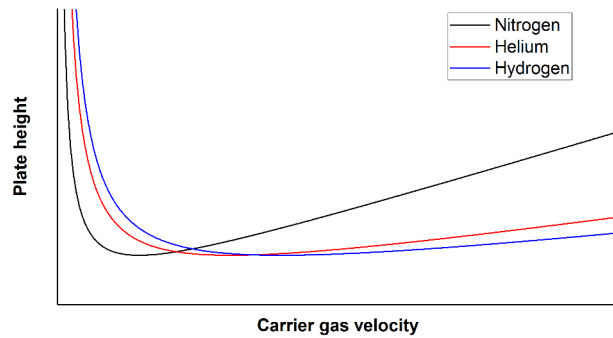


FIG. 8: Qualitative variation of plate height in capillary columns with respect to carrier gas velocity for various carrier gases

7) Gas Chromatograph modules: injectors and detectors

In this section, a brief description of the different GC device modules used in this thesis is presented.

a) Split/splitless injector

Split/splitless injectors are specifically dedicated to capillary columns, and are the most used for classical GC applications. Due to capillary column low capacity, it is necessary to avoid overloading in order to obtain thin and high peaks. In this case, this injector is generally used in “*split*” mode.

During the injection of a liquid sample by means of a glass syringe, vaporization occurs in a heated glass liner. The injector is supplied by a certain flow of carrier gas that is divided into two parts: the column and split flows. Consequently, the gas generated by sample vaporization is split into two parts: one of them is introduced in the column whereas the other exits the injector towards the split vent, thanks to the split flow. This serves: (i) to introduce a reduced fraction of the sample injected instead of overloading the column with the entire injected sample amount (fig. 9), (ii) to reduce the time spent by the solutes in the injector, to minimize band broadening during the injection.

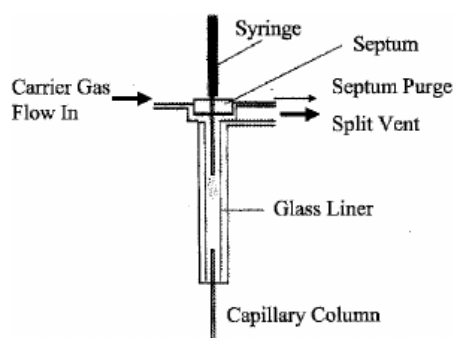


FIG. 9: **Schematic representation of a split/splitless injector** – from [4].

Of course, the column and split flows can be set by the operator, as they are regulated by means of dedicated pneumatic control modules. At constant column flow, the amount of sample introduced in the column decreases as the split flow increases. The fraction of injected sample introduced in the column, FI, is given by the following relationship:

$$FI = \frac{\text{column flow}}{\text{column flow} + \text{split flow}} \quad (38)$$

Of course, the split flow can be set as 0, which means that the entire injected sample is introduced in the column. In this case, the injector is in “*splitless*” mode.

b) Detectors

According to the targeted solutes, appropriate detection modules should be chosen. Indeed, some types of detectors are dedicated to the detection of specific classes of compounds, such as molecules containing sulfur, phosphorus and halide elements.

However, some detectors are said “universal” as they are able to generate signals for every molecule. Among them, FIDs permit the detection of almost every organic species (almost universal detector). In addition, MSDs are sensitive to all the organic species that can be ionized and allow the solutes to be identified. These two detectors are presented below.

i. Flame Ionization Detector

FIDs equip most of the conventional GCs, due to their ability at detecting all the organic species (except volatile little molecules such as CO₂, Formaldehyde, etc). They simply consist in burning the eluting solutes in a continuous flame supplied with Hydrogen and air, which generates ions that are collected by electrodes. Consequently, an electric signal is generated. Its intensity is proportional to the mass flow of eluting solute. The principle scheme of this detector is presented in fig. 10.

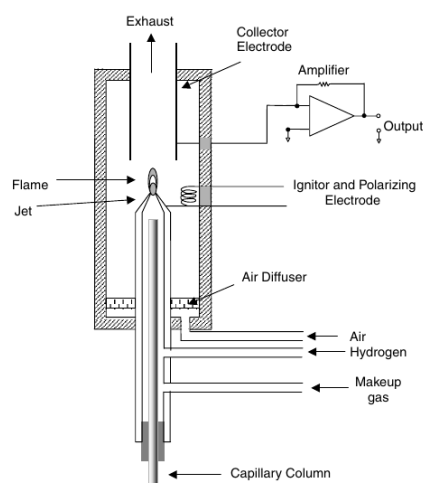


FIG. 10: **Schematic representation of a Flame Ionization Detector** – from [4].

The main advantage of FIDs is that their response factor with respect to organic solute remain constant over several magnitudes of order of concentration.

ii. Mass Spectrometer Detectors

MSD can be declined under many variants. They consist in ionizing the eluting solute using any appropriate means. The ions generated are then introduced in an analyzer that permits their discrimination in terms of mass over charge ratio (m/z). The detection of the analyzed ions gives mass spectra, that consist in plotting the abundance of ions as a function of m/z .

During GC-MSD analyses, the MSD determines the mass spectra of the eluting MP every τ seconds, τ being the acquisition frequency that depends on the targeted m/z range set by the operator. At a given retention time value, the chromatographic signal corresponds to the sum of the abundances of the different collected ions (Total Ion Current, TIC).

In classical MSD coupled with GC, ions are produced by exposure of eluting solutes to an electron beam (electron impact). This engenders the fragmentation of the molecules into several ions. When the electron beam energy is set at 70 eV, the fragmentation is reproducible if Helium is used as carrier gas. Consequently, the mass spectra obtained after ion analysis in the MSD are reproducible too. This has a major interest for solute identification: the user can obtain the mass spectrum associated with a chromatographic peak to make a comparison with database entries.

8) Comprehensive two-dimensional techniques

Classical GC is based on solute separation by means of a single chromatographic column. However, in some cases, the analysis of complex samples containing large number of solutes becomes difficult. Indeed, one column can be insufficient to separate all the components, which prevent from their quantification.

In order to bypass this issue, comprehensive two-dimensional GC techniques (GC×GC) were developed. These techniques have known a wide spread during the past years. They consist in taking advantage of combination of two separate capillary columns that exhibit appropriate selectivity values. The solutes eluting from the first column are trapped in a modulation device, that re-injects the solutes into the second column every t_{mod} seconds, t_{mod} being the modulation period whose duration is generally a few seconds. Conventionally, the first column (also called “*primary column*” or “*1st dimension column*”) is long (10-30 m) and the second one (“*secondary column*”, “*2nd dimension column*”) is short (1-5 m). Note that the two columns can be placed in the same oven, or in two separate independent ovens.

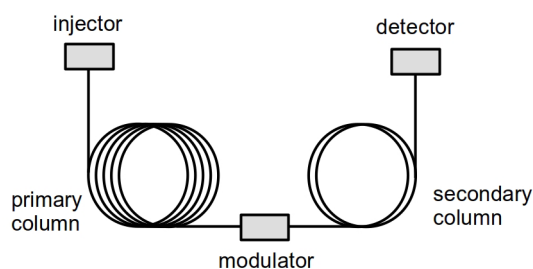


FIG. 11: Schematic principle of GC×GC

Up to now, several types of modulators were developed. Among them, thermal modulators (TM) are basically simple: the two columns are connected in series thanks to a connect-union and share the same carrier gas flow. Solutes eluting from the primary column are trapped by means of cold jets of cooling liquid and are re-injected into the secondary one by stopping the jet. As the efficiency of the modulation strongly depends on the vapor pressures of the solutes, more robust modulators based on valve switching were then developed. These modulators are called “flow modulators” (FM).

The principle of FMs is different. The primary and secondary column flows are independently regulated by means of two separate pneumatic control modules – one at the injector that sets pressure p_{inj} at primary column head, and one at the modulator that sets pressure p_{mod} at the

modulator. The primary column flow is generally low ($0.1\text{--}1\text{ mL min}^{-1}$), conversely to the secondary column one ($15\text{--}50\text{ mL min}^{-1}$, according to column dimensions). The two columns are linked by the modulator that is made of a sampling loop and whose extremities are connected to a switching valve (fig. 12). The modulation period is divided into two parts: (i) the fill (or collection) cycle, during which the switching valve is set as to impose p_{mod} at the modulation loop outlet; (ii) the flush (or re-injection) cycle, during which the valve switches to impose p_{mod} at the modulation loop inlet. Consequently, during the fill cycle, solutes eluting from the primary column are collected by the loop during a few seconds. Conversely, during the flush cycle, collected solutes are rapidly re-injected into the secondary column.

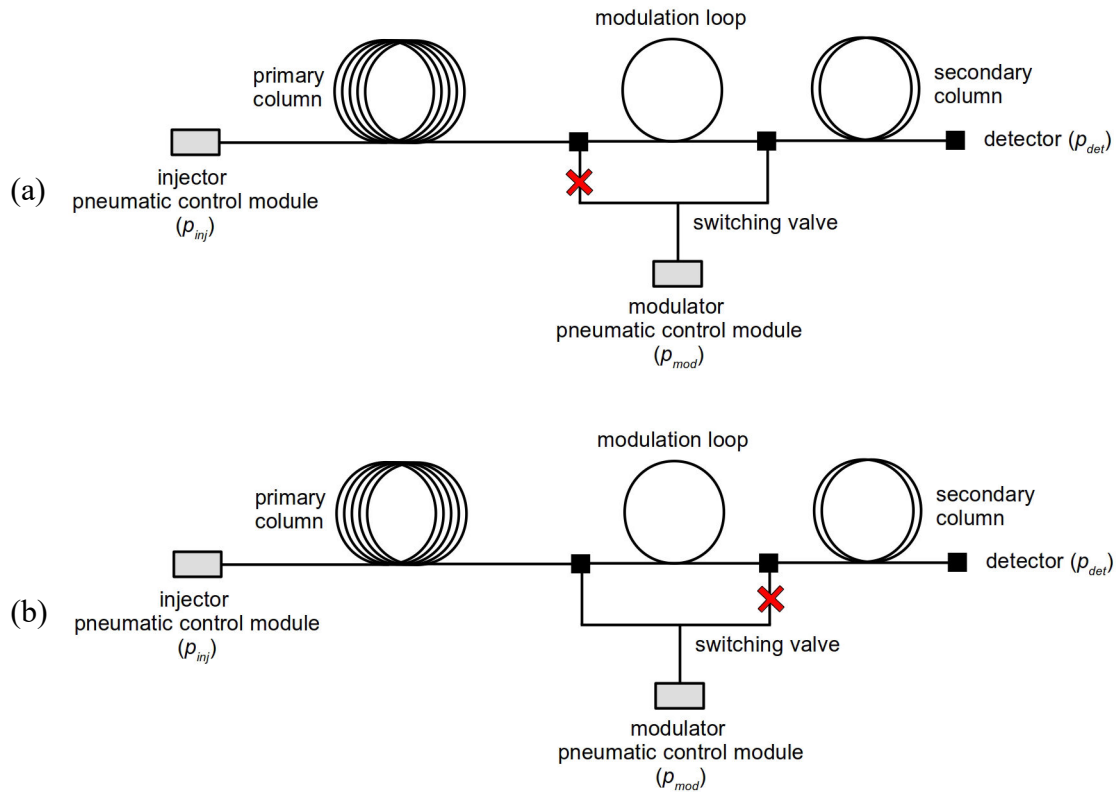


FIG. 12: **Schematic principle of FM-GC×GC (Forward Fill Flush, Capillary Flow Technology from Agilent)** – (a) fill cycle, (b) flush cycle.

Note that p_{inj} and p_{mod} are set according to column flows using Poiseuille's equation:

$$p_{inj} = \sqrt{\frac{256 \eta_1 L_1}{\pi d_1^4} \frac{T_1}{T_0} p_0 F_1 + \frac{256 \eta_2 L_2}{\pi d_2^4} \frac{T_2}{T_0} p_0 F_2 + p_{det}^2} \quad (39)$$

$$p_{mod} = \sqrt{\frac{256 \eta_2 L_2}{\pi d_2^4} \frac{T_2}{T_0} p_0 F_2 + p_{det}^2} \quad (40)$$

where

p_0 and T_0 are reference pressure and temperature (1 atm, 298.15 K)
 T_1 and T_2 are primary and secondary column temperatures, respectively

η_1 and η_2 are MP viscosity in the primary and secondary columns, respectively
 L_1 and L_2 are primary and secondary column lengths, respectively
 d_1 and d_2 are primary and secondary column internal diameters, respectively
 F_1 and F_2 are primary and secondary column outlet volumetric flows, respectively
 and p_{det} the detector pressure¹

The one-dimensional resulting chromatograms are complex. The signal is split every t_{mod} seconds in order to construct corresponding two-dimension chromatograms [13] (fig. 13), which is generally represented as contour plot.

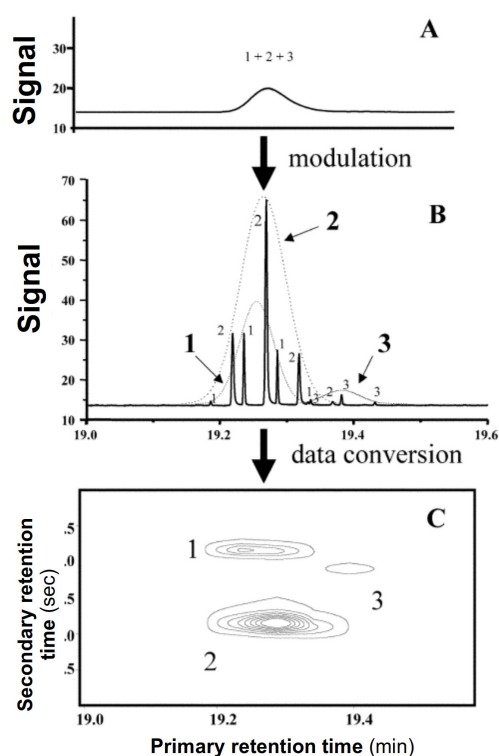


FIG. 13: **Two-dimension chromatogram** – adapted from [13]. A. one-dimensional GC chromatogram: the technique was unable at separating 3 different solutes, B. one-dimensional signal of GC×GC analysis of the same sample: the technique permitted the separation of the three compounds, C. reconstructed two-dimension chromatogram.

Note that, in order to obtain good separation of solutes during analysis of complex mixtures, appropriate chromatographic conditions should be found in order to maximize method peak capacity (concept of column orthogonality [14–17]). This can be attempted by combining several approaches: (i) the choice of two columns exhibiting different selectivity, (ii) the optimization of column flows, (iii) the elaboration of an appropriate temperature program [14].

1. When a FID is used as detector, $p_{det} = 1$ atm.

III. RETENTION TIME PREDICTION IN CAPILLARY GAS CHROMATOGRAPHY

1) Introduction

Development of chromatographic methods dedicated to complex matrices analysis implies many issues: sample preparation (extraction, sampling, etc. [18]), separation [19] and detection. In GC, obtaining good separations (*e. g.*, sufficient resolutions permitting the specific detection of every solute) requires to optimize experimental conditions. First, an appropriate column must be chosen. Then, a compromise between injection, temperature program and carrier gas velocity (or flow) must be found to meet analytical requirements: (i) good resolutions between the peaks of solutes of interest must be obtained – in case of non-resolved peaks, using selective detectors can help at obtaining specific signals; (ii) sufficient column efficiency (*e. g.*, number of plates) should be reached to contribute to the improvement of resolution and to maximize peak heights, which helps at decreasing detection thresholds.

In this context, developing optimal separation for samples containing many solutes is not easy, and trial-and-errors approaches do not always lead to the targeted results. In past years, many authors have developed computer-assisted retention time prediction procedures in order to help at developing separations [6,10,20–23]. The principle of these procedures is simple. First, retention thermodynamic parameters of solutes associated with a given column are estimated. This part can be achieved using retention indices [10], for example, or by estimating retention parameters from experimental retention time measurements in given conditions [20,22]. Once known, these parameters can be used in calculation programs that predict retention times of solutes according to input experimental conditions (temperature program, carrier gas flow or inlet pressure, column dimensions) using retention models and their parameters.

Most of the retention time prediction studies published in the literature describe procedures applied to one-dimensional GC [10,20–22]. However, a recent paper from Barcaru *et al.* presents a successful extension of the existing prediction procedure to TM-GC×GC [23]. In this paper, the authors pointed out that some corrections would be required to apply their procedure to FM-GC×GC. Indeed, the flows of the two columns are independently regulated using two separate pneumatic control modules (see part II.8, p. 127). In addition, column flows are generally very different: up to 1 mL min⁻¹ in the 1st dimension, and up to 30 mL min⁻¹ in the 2nd one. According to eqs. 39 and 40 (p. 128), column head pressures necessary to generate such flows can be substantial according to column dimensions, carrier gas and temperature (up to ~ 1000 kPa gauge pressure).

These considerations indicate that during their elution, solutes undergo significant pressure decreases (see fig. 5, p 118). It is well known that pressure is a physical factor that can impact thermodynamic equilibria, especially those involving simultaneously two condensed and gas

phases. As a consequence, it should impact solute partitioning between the two phases of a column, and this factor should be taken into account in retention models for accurate predictions. During preliminary experiments, solute apparent retention factors (defined by eq. 4, p 115) in isothermal mode were found to change with respect to column head pressure (see fig. 14). Such observation is not compatible with the classical retention model, according to eq. 30 (p. 121), which justifies the development of a new model taking pressure into account.

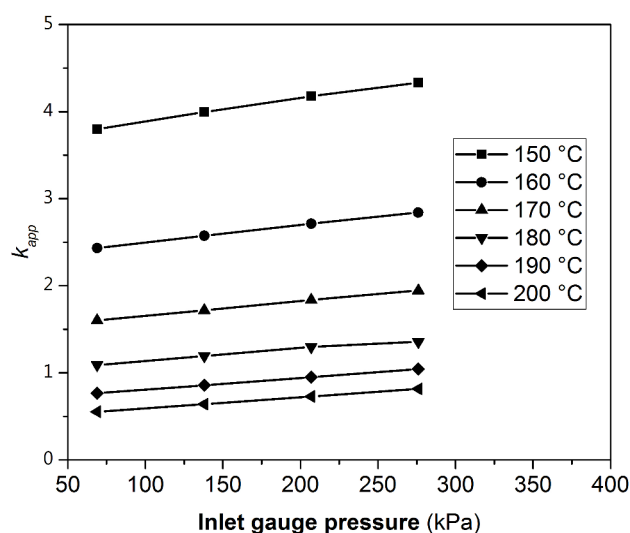


FIG. 14: **Isothermal apparent retention factors of *n*-heneicosane at different temperatures and column inlet pressures** – chromatographic conditions: 0,2 μL injection volume, solution containing 500 $\text{mg}\cdot\text{L}^{-1}$ *n*-heneicosane in dichloromethane, carrier gas: hydrogen, detector: FID, inlet split flow: 30 $\text{mL}\cdot\text{min}^{-1}$. Column: SLB-IL60 (30 m \times 0.25 mm \times 0.20 μm).

Up to now only a few papers have described the impact of pressure on solute retention [24,25]. Nevertheless, no application of these studies to retention time prediction was made. All the retention models used for prediction considered temperature as the only variable impacting solute retention.

Therefore, this work aims at providing some contribution on prediction of retention times by taking both effects of temperature and pressure on solute retention.

In a first part, the retention model was developed. Then, the parameters of this model were estimated from experimental measurements to determine: (i) column phase ratio values, (ii) solute partition thermodynamic parameters. Two different columns were tested: Agilent DB-35MS and Sigma-Aldrich SLB-IL60. 11 model compounds (*e. g.*, Phenanthrene and some of its impurities) were used for the study. The same procedure was applied using the classical retention model (eq. 30, p 121). Eventually, the two models were used for retention time prediction purposes. The accuracy of predicted retention time values was assessed by experimental measurements in GC and FM-GC \times GC and the results were discussed.

2) Development of a new retention model

a) New theoretical expression of solute retention factor

According to eq. 31 (p. 122), prediction of solute retention time requires knowledge on k_i values. Consequently, one has to express the different parameters associated with solute partition (ΔG_i).

Considering that pressure impacts solute free energy, the first principle of thermodynamics gives the following relationship:

$$G_i = U_i + pV_i - TS_i \quad (41)$$

U_i and V_i being solute molar internal energy and volume, respectively.

Therefore, in every local equilibrium², the difference of solute free energy between the two phases can be rewritten as follows:

$$\Delta G_i = \Delta U_i + p \Delta V_i - T \Delta S_i \text{ in J} \cdot \text{mol}^{-1} \quad (42)$$

with

$$\Delta U_i = U_{i,SP} - U_{i,MP} \text{ (J} \cdot \text{mol}^{-1})$$

$$\Delta V_i = V_{i,SP} - V_{i,MP} \text{ (m}^3 \cdot \text{mol}^{-1})$$

Consequently, the retention factor of a solute becomes:

$$k_i = \exp \left(-\frac{\Delta U_i}{RT} - p \frac{\Delta V_i}{RT} + \frac{\Delta S_i}{R} - \ln \beta \right) \quad (43)$$

Nevertheless, using this model equation to predict solute retention times implies that the three parameters (ΔU_i , ΔV_i , and ΔS_i) do not vary with respect to the two variables (*e. g.*, p and T). This assumption could be not true, especially for the ΔV_i term. Indeed, it partially depends on solute molar volume in the gas phase, and this quantity is theoretically largely impacted by pressure and temperature, according to ideal gas law. Therefore, it is suitable to estimate the variation of ΔU_i , ΔV_i , and ΔS_i as a function of p and T in order to obtain an expression of ΔG_i that would describe accurately solute partitioning in extended temperature-pressure ranges.

The three parameters involved in eq. 43 correspond to the differences of solute state functions (*e. g.*, U_i , V_i and S_i) between the SP and the MP. The variation of any state function with respect to p and T is governed by the following relationship:

$$f(p, T) = f(p_0, T_0) + \int_{p_0, T_0}^{p, T} df \quad (44)$$

$f(p_0, T_0)$ being the value taken by f in arbitrary reference conditions (p_0, T_0), and df the differential of $f(p, T)$:

$$df = \left(\frac{\partial f}{\partial p} \right)_T dp + \left(\frac{\partial f}{\partial T} \right)_p dT \quad (45)$$

2. In a given plate, pressure and temperature are considered as being homogeneous in space.

Integrating eq. 44 yields:

$$f(p, T) = f(p_0, T_0) + \int_{p_0}^p (df)_{T_0} + \int_{T_0}^T (df)_p = \int_{p_0}^p \left(\frac{\partial f}{\partial p} \right)_{T_0} dp + \int_{p_0}^p \left(\frac{\partial f}{\partial T} \right)_p dT \quad (46)$$

Then it can be applied to the three state functions previously mentioned:

$$U_i(p, T) = U_i(p_0, T_0) + \int_{p_0}^p \left(\frac{\partial U_i}{\partial p} \right)_{T_0} dp + \int_{T_0}^T \left(\frac{\partial U_i}{\partial T} \right)_p dT \quad (47)$$

$$V_i(p, T) = V_i(p_0, T_0) + \int_{p_0}^p \left(\frac{\partial V_i}{\partial p} \right)_{T_0} dp + \int_{T_0}^T \left(\frac{\partial V_i}{\partial T} \right)_p dT \quad (48)$$

$$S_i(p, T) = S_i(p_0, T_0) + \int_{p_0}^p \left(\frac{\partial S_i}{\partial p} \right)_{T_0} dp + \int_{T_0}^T \left(\frac{\partial S_i}{\partial T} \right)_p dT \quad (49)$$

The partial derivatives involved in eqs. 47–49 can be re-expressed using the following thermodynamic identities [26]:

$$\frac{\partial U_i}{\partial T} = C_{p,i} - \alpha_i p \quad (50) \quad \left| \quad \frac{\partial V_i}{\partial p} = -\chi_i \quad (53)$$

$$\frac{\partial U_i}{\partial p} = -\alpha_i T + \chi_i p \quad (51) \quad \left| \quad \frac{\partial S_i}{\partial T} = \frac{C_{p,i}}{T} \quad (54)$$

$$\frac{\partial V_i}{\partial T} = \alpha_i \quad (52) \quad \left| \quad \frac{\partial S_i}{\partial p} = -\alpha_i \quad (55)$$

α_i , χ_i and $C_{p,i}$ being new thermodynamic parameters:

α_i : solute molar coefficient of thermal expansion ($\partial V_i / \partial T$, $\text{m}^3 \cdot \text{mol}^{-1} \cdot \text{K}^{-1}$)

χ_i : solute molar compressibility ($\partial V_i / \partial p$, $\text{m}^3 \cdot \text{mol}^{-1} \cdot \text{Pa}^{-1}$)

$C_{p,i}$: solute molar heat capacity ($\partial H_i / \partial T$, $\text{J} \cdot \text{mol}^{-1} \cdot \text{K}^{-1}$)

In more comprehensive terms, α_i is the increase of solute molar volume engendered by an infinitesimal increase of temperature at constant pressure. χ_i is the increase of solute molar volume engendered by an infinitesimal increase of pressure at constant temperature. $C_{p,i}$ is the increase of solute molar enthalpy which occurs when temperature is slightly increased at constant pressure. α_i and χ_i values of gases are generally higher than those of liquids and solids [27]. Conversely, $C_{p,i}$ values associated with liquids are higher than those of gases. By analogy, solutes should behave like gases in the mobile phase and like liquids in the stationary one.

Assuming that the differences of solute $U_i(p_0, T_0)$, $V_i(p_0, T_0)$, $S_i(p_0, T_0)$, α_i , χ_i and $C_{p,i}$ values between the SP and MP remain constant with respect to p and T , a combination of eqs. 47–55 leads to the three following relationships:

$$\Delta U_i(p, T) = \Delta U_i(p_0, T_0) - \Delta \alpha_i T_0 \int_{p_0}^p dp + \Delta \chi_i \int_{p_0}^p p dp + \Delta C_{p,i} \int_{T_0}^T dt - \Delta \alpha_i p \int_{T_0}^T dT \quad (56)$$

$$\Delta V_i(p, T) = \Delta V_i(p_0, T_0) - \Delta \chi_i \int_{p_0}^p dp + \Delta \alpha_i \int_{T_0}^T dT \quad (57)$$

$$\Delta S_i(p, T) = \Delta S_i(p_0, T_0) - \Delta \alpha_i \int_{p_0}^p dp + \Delta C_{p,i} \int_{T_0}^T \frac{dT}{T} \quad (58)$$

where

$$\begin{aligned} \Delta U_i(p, T) &= U_{i,SP}(p, T) - U_{i,MP}(p, T) \quad (\text{J} \cdot \text{mol}^{-1}) \\ \Delta V_i(p, T) &= V_{i,SP}(p, T) - V_{i,MP}(p, T) \quad (\text{m}^3 \cdot \text{mol}^{-1}) \\ \Delta S_i(p, T) &= S_{i,SP}(p, T) - S_{i,MP}(p, T) \quad (\text{J} \cdot \text{mol}^{-1} \cdot \text{K}^{-1}) \\ \Delta \alpha_i &= \alpha_{i,SP} - \alpha_{i,MP} \quad (\text{m}^3 \cdot \text{mol}^{-1} \cdot \text{K}^{-1}) \\ \Delta \chi_i &= \chi_{i,SP} - \chi_{i,MP} \quad (\text{m}^3 \cdot \text{mol}^{-1} \cdot \text{Pa}^{-1}) \\ \Delta C_{p,i} &= C_{p,i,SP} - C_{p,i,MP} \quad (\text{J} \cdot \text{mol}^{-1} \cdot \text{K}^{-1}) \end{aligned}$$

For the reasons mentioned above, solute $\Delta \alpha_i$ and $\Delta \chi_i$ values should be negative. Conversely, $\Delta C_{p,i}$ values should be positive. Due to the large velocity of molecules in gases and to their large degree of freedom, their molar internal energy and entropy should be higher in the MP than in the SP. Thus, $\Delta U_i(p_0, T_0)$ and $\Delta S_i(p_0, T_0)$ values are expected to be negative. Nevertheless, $\Delta V_i(p_0, T_0)$ signs should be largely impacted by the arbitrarily set reference values p_0 and T_0 .

Integration of equations 56–58 gives:

$$\Delta U_i(p, T) = \Delta U_i(p_0, T_0) + \Delta \alpha_i p_0 T_0 - \frac{1}{2} \Delta \chi_i p_0^2 - \Delta C_{p,i} T_0 + \Delta C_{p,i} T - \Delta \alpha_i p T + \frac{1}{2} \Delta \chi_i p^2 \quad (59)$$

$$\Delta V_i(p, T) = \Delta V_i(p_0, T_0) + \Delta \chi_i p_0 - \Delta \alpha_i T_0 + \Delta \alpha_i T - \Delta \chi_i p \quad (60)$$

$$\Delta S_i(p, T) = -\Delta S_i(p_0, T_0) T - \Delta \alpha_i p_0 T + \Delta C_{p,i} T \ln T_0 - \Delta C_{p,i} T \ln T + \Delta \alpha_i p T \quad (61)$$

Consequently, the expression of ΔG_i (given by eq. 42) becomes:

$$\begin{aligned} \Delta G_i(p, T) &= \Delta U_i(p_0, T_0) + \Delta \alpha_i p_0 T_0 - \frac{1}{2} \Delta \chi_i p_0^2 - \Delta C_{p,i} T_0 \\ &+ (\Delta C_{p,i} - \Delta S_i(p_0, T_0) - \Delta \alpha_i p_0 + \Delta C_{p,i} \ln T_0) T - \Delta C_{p,i} T \ln T + \Delta \alpha_i p T \\ &+ (\Delta V_i(p_0, T_0) + \Delta \chi_i p_0 - \Delta \alpha_i T_0) p - \frac{1}{2} \Delta \chi_i p^2 \end{aligned} \quad (62)$$

Then, by combining eqs. 43, 59, 60 and 61 ($k_i = \exp(-\Delta G_i/RT - \ln \beta)$), a new expression of solute retention factor can be established:

$$k_i = \exp \left(\frac{A_i}{T} + B_i + C_i \frac{p}{T} + D_i p + E_i \ln T + F_i \frac{p^2}{T} - \ln \beta \right) \quad (63)$$

where:

$$A_i = \frac{-\Delta U_i(p_0, T_0) - \Delta \alpha_i p_0 T_0 + \frac{1}{2} \Delta \chi_i p_0^2 + \Delta C_{p,i} T_0}{R} \quad \text{in K}$$

$$\begin{aligned}
B_i &= \frac{\Delta S_i(p_0, T_0) - \Delta C_{p,i} + \Delta \alpha_i p_0 - \Delta C_{p,i} \ln T_0}{R} \\
C_i &= \frac{-\Delta V_i(p_0, T_0) - \Delta \chi_i p_0 + \Delta \alpha_i T_0}{R} \text{ in K} \cdot \text{Pa}^{-1} \\
D_i &= -\frac{\Delta \alpha_i}{R} \text{ in Pa}^{-1} \\
E_i &= -\frac{\Delta C_{p,i}}{R} \\
F_i &= \frac{1}{2} \frac{\Delta \chi_i}{R} \text{ in K} \cdot \text{Pa}^{-2}
\end{aligned}$$

In eq. 63, p can be calculated using eq. 15 (p. 117).

The model equation described above contains 7 parameters. 6 of them (*e. g.*, $\Delta U_i(p_0, T_0)$, $\Delta V_i(p_0, T_0)$, $\Delta S_i(p_0, T_0)$, $\Delta \alpha_i$, $\Delta \chi_i$ and $\Delta C_{p,i}$) are only related to solute partitioning, and the other (*e. g.*, β) only depends on column dimensions (eq. 8, p. 117). Of course, to simplify the problem, it is possible to assume that $\Delta S_i(p_0, T_0) / R - \ln \beta$ is a constant. In this case, only 6 parameters (instead of 7) govern this model. The operator is free to choose to make this simplification or not.

Applying this new model to retention time prediction requires knowledge on its parameters. In the next paragraph, a brief description of a procedure to estimate these parameters is made.

b) Estimation of model parameters

The general procedure to estimate the parameters of a model is to measure the quantity expressed by the model (here: solute retention time) in known conditions (here: column dimensions, carrier gas, column temperature and inlet pressure). Then, the parameters must be optimized by successive iterations in order to minimize the sum of squares of deviations (*SSD*) between the values calculated using the model equation and those experimentally measured. For every solute, the *SSD* can be calculated using the following relationship:

$$SSD_i = \sum (t_{R,i,calc} - t_{R,i,exp})^2 \quad (64)$$

$t_{R,i,calc}$ values can be numerically estimated from eq. 31 (p. 122), in which the chosen k_i expression depends on the considered model (*e. g.*, eq. 30 (p. 121) for the classical one, and eq. 63 for the extended one developed in this study). Various methods and procedures can be used to perform the optimizations. Among them, the Nelder-Mead algorithm [28] is probably the most known and used.

In this study, it was chosen to consider $\Delta S_i(p_0, T_0)$ and β as two separate constants. In other terms, two separate optimizations were performed: a first one to estimate column phase ratio (made only once per column), and a second one to determine solute partition parameters (repeated for every solute).

i. Determination of column phase ratio

One way to estimate a column phase ratio (β) is to study the retention of an homologous series of solutes. Indeed, according to group contribution theory [29], the free energy

associated with one molecule can be segmented into as many contributions as there are chemical groups on this molecule – each group having its own contribution. In the case of n -alkanes, their free energy can be considered as being proportional to their number of carbon atoms. Therefore, we have:

$$\Delta G_N = N \times \Delta G_C \quad (65)$$

ΔG_N being the difference of free energy between the SP and the MP related to a n -alkane containing N carbon atoms, and ΔG_C the contribution of one $-\text{CH}_2$ or $-\text{CH}_3$ group. Note that, in this model, contributions of methyl and methylene groups are supposed to be equivalent.

From eq. 65 implicitly follow the same relationships for all ΔG_N sub-parameters:

$$\begin{aligned} \Delta U_N(p_0, T_0) &= N \times \Delta U_C(p_0, T_0) \\ \Delta V_N(p_0, T_0) &= N \times \Delta V_C(p_0, T_0) \\ \Delta S_N(p_0, T_0) &= N \times \Delta S_C(p_0, T_0) \\ \Delta \alpha_N &= N \times \Delta \alpha_C \\ \Delta \chi_N &= N \times \Delta \chi_C \\ \Delta C_{p,N} &= N \times \Delta C_{p,C} \end{aligned}$$

From these considerations, n -alkane free energy associated with solute dissolution in the SP becomes:

$$k_N = \exp\left(-N \times \frac{\Delta G_C}{RT} - \ln \beta\right) \quad (66)$$

Therefore, the calculated retention time associated with an n -alkane can be estimated using eq. 67 (classical model) or 68 (extended one).

$$t_{R,calc}(N, T) = \int_0^L \frac{1 + \exp\left(N \times \left[\frac{-\Delta H_C}{RT} + \frac{\Delta S_C}{R}\right] - \ln \beta\right)}{u(x_N)} dx_N \quad (67)$$

$$t_{R,calc}(N, T) = \int_0^L \frac{1 + \exp\left(N \times \left[\frac{A_C}{T} + B_C + C_C \frac{p}{T} + D_C p + E_C \ln T + F_C \frac{p^2}{T}\right] - \ln \beta\right)}{u(x_N)} dx_N \quad (68)$$

Consequently, retention times of different n -alkanes can be measured at several temperature and inlet pressure values. Then, n -alkane partition parameters, as well as column phase ratio can be determined by minimizing the SSD between calculated (eq. 67 or 68) and the experimental retention times, using N and T (classical model) or N , p and T (extended one) as variables.

ii. Determination of solute partition parameters

Once β is known, its optimized value can be set as known constant for upcoming solute partition parameters optimization. Then, the latter can be estimated solute-by-solute by minimizing the SSD between calculated and experimental retention time values. Only two parameters need for optimization using the classical model, and six for the extended one.

3) Validation of the new retention model

a) Introduction

In the previous part, a new retention model, taking into account the combined impacts of temperature and pressure on solute partitioning, was developed. It is necessary to test its accuracy at predicting solute retention times in various operating conditions.

In this part, an experimental assessment of the new model is developed. In a first time, the phase ratio values of two different columns was estimated from experimental measurements on *n*-alkanes, according to the procedure described in part III.2)b)i, p. 135. Then, the partition parameters of 11 different solutes on these two columns were determined. These solutes³ were chosen as model compounds in order to help at developing a separation of Phenanthrene and its impurities. Eventually, all the determined parameters were used for retention time prediction purposes in temperature-programmed analyses in GC and FM-GC×GC. The accuracy of the predicted retention times was assessed by comparison with experimental values obtained in the considered conditions. This procedure was also attempted using the classical retention model, in order to compare the results obtained and to select the best one in terms of performance.

b) Materials and methods

i. Chemicals

The following products were used for the determination of column phase ratios:

A solution containing 100 ppm of every of the following *n*-alkanes was prepared in Dichloromethane (VWR Chemicals): *n*-nonadecane (C19, 99 %), *n*-eicosane (C20, 99 %), *n*-heneicosane (C21, 99 %), *n*-docosane (C22, 99 %), *n*-tricosane (C23, 99 %) and *n*-tetracosane (C24, 99 %). All were purchased from Alfa Aesar.

For the determination of solute partition parameters, a solution containing 50 ppm of every of these 11 solutes was prepared in Acetone (HPLC grade, purchased from VWR Chemicals): Fluorene (98+ %), 1-methylfluorene (99 %), Dibenzothiophene (98 %), Phenanthrene (98 %) were obtained from Alfa Aesar. 9,10-dihydrophenanthrene (94 %), Anthracene (99 %), Carbazole (> 95 %), 2-methylanthracene (97 %), 9-methylanthracene (98 %), and 9,10-dimethylanthracene (99 %) were purchased from Sigma-Aldrich. 9,10-dihydroanthracene (98 %) was obtained from TCI Chemicals.

ii. Chromatographic conditions

GC and FM-GC×GC experiments were performed on an Agilent 7890B Series Gas Chromatograph, equipped with: a split/splitless injector whose temperature was set at 300 °C; a FID (300 °C) and an Agilent G4513A autosampler (0.5 µL injection volume). Hydrogen was used as carrier gas. Two columns were selected for the separations: SLB-IL60 30 m ×

3. The chosen solutes are: Fluorene*, 9,10-dihydroanthracene*, 9,10-dihydrophenanthrene*, 1-methylfluorene*, Dibenzothiophene*, Phenanthrene, Anthracene*, Carbazole*, 2-methylanthracene**, 9-methylanthracene**, 9,10-dimethylanthracene**. * impurities found in commercial Phenanthrene samples, ** compounds chosen in order to model methylated derivatives of Phenanthrene and Anthracene.

0.25 mm \times 0.20 μ m (Sigma-Aldrich, indicative dimensions) and DB-35MS 30 m \times 0.25 mm \times 0.25 μ m (Agilent, indicative dimensions). The actual column lengths were carefully determined: 32.4 m for the SLB-IL60 one and 29.0 m for the DB-35MS one for GC experiments; and 4.97 m (SLB-IL60) and 28.35 m (DB-35MS) for FM-GC \times GC experiments. Note that the short columns were cuts of the long ones.

FM-GC \times GC analyses were performed using a one plate Agilent Forward Fill Flush flow modulator. The modulation period and inject time were set at 5 and 0.2 s, respectively.

iii. Optimization and prediction procedures

Numerical calculations were performed on Scilab 5.5.2 software. Optimization procedures were carried out using the *fminsearch* function (Nelder-Mead algorithm). Hydrogen viscosity values were calculated using Hawkes model equations [9].

For retention time prediction, a simple procedure to calculate eq. 31 (p. 122) is to divide the analysis into short dt steps. During every step, solute displacement can be estimated according to the following equivalent equation [6]:

$$\frac{dx_i}{dt} = \frac{u(x_i)}{1+k_i} \quad (69)$$

Before starting the first integration step, the position of the solute, the time of analysis, the temperature and (if appropriate) the local pressure should be initialized according to the input data (column dimensions, temperature program, integration step duration, etc). Then, the retention factor of the solute during the first integration step should be calculated using the appropriate model equation. From there, solute displacement can be estimated according to the following relationship:

$$dx_i = \frac{u(x_i)}{1+k_i} dt \quad (70)$$

At the end of the step, solute position, analysis time, column temperature, local velocity and pressure must be updated. If the new position of the solute is lower than column length, then a new integration step should be started. Otherwise, the actual analysis time corresponds to the predicted retention time (see fig. 15).

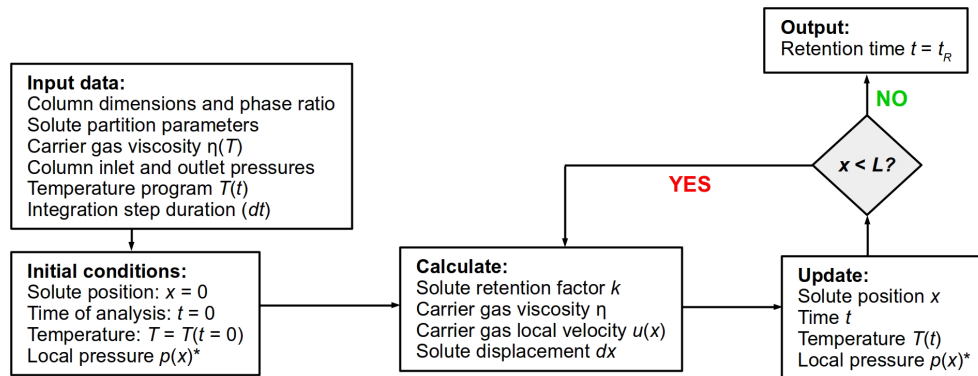


FIG. 15: **Algorithm for retention time prediction in one-dimensional GC** – * required only when the extended retention model is chosen to express k .

To predict retention times in FM-GC×GC, a similar procedure can be applied (fig. 16).

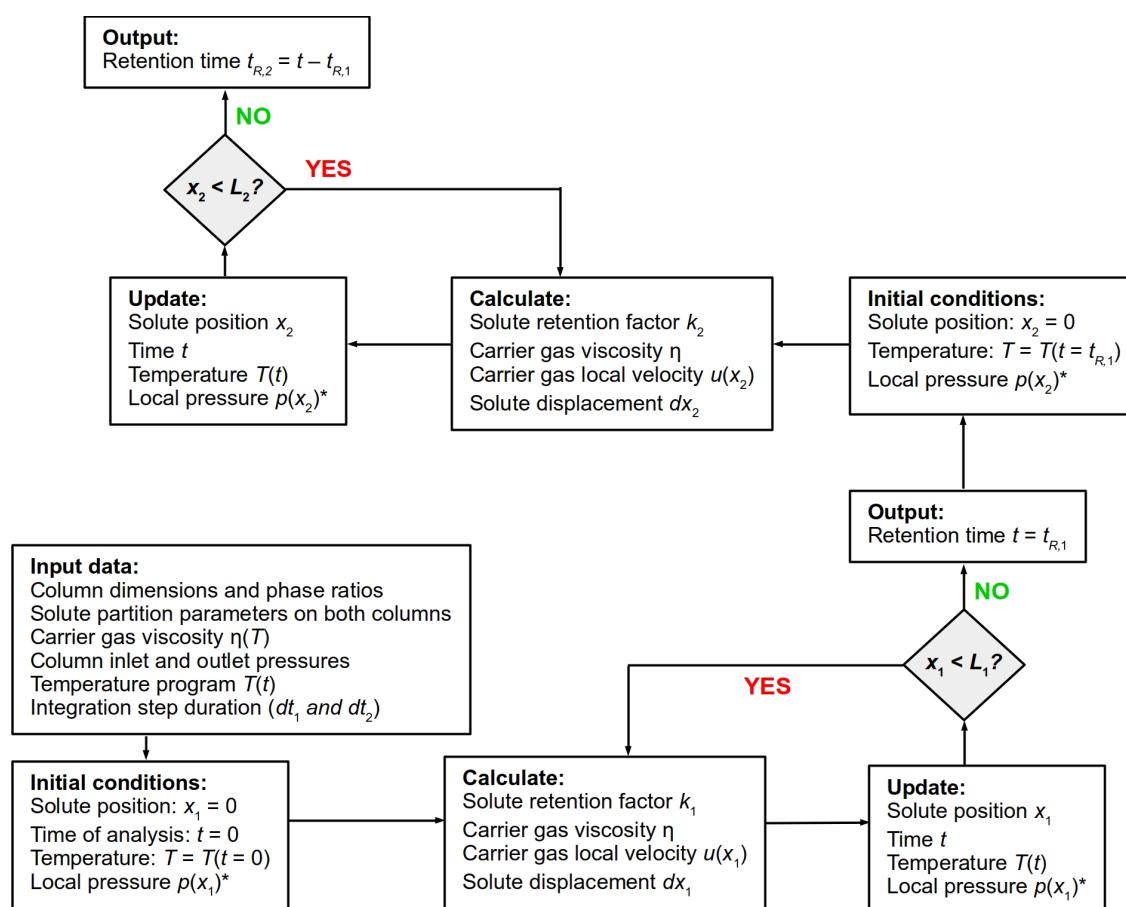


FIG. 16: **Algorithm for retention time prediction in FM-GC×GC** – * required only when the extended retention model is chosen to express k . Subscripts 1 and 2 designate primary and secondary columns. In this algorithm, the two columns are placed in the same oven, so, at a given time, carrier gas viscosity is the same in both dimensions.

c) Results and discussion

i. Column phase ratio determination

Two column phase ratios were determined by studying the retention of a series of 6 n -alkanes (from $N = 19$ to $N = 24$) on the SLB-IL60 (32.4 m × 0.25 mm × 0.25 μm) and DB-35ms (29 m × 0.25 mm × 0.25 μm) columns. The n -alkanes were analyzed at constant column head pressure and in isothermal mode. 4 different inlet pressures were applied: 68.9, 138, 207 and 276 kPa hydrogen gauge pressure. For every tested inlet pressure, the mixture of n -alkanes was analyzed at 6 different temperatures:

- SLB-IL60: 150, 160, 170, 180, 190 and 200 °C,
- DB-35ms: 200, 210, 220, 230, 240 and 250 °C.

The n -alkane retention times were measured in the conditions mentioned above (numerical values are given in tabs. S1-2, appendix 1, p. 165). Then, the n -alkane partition parameters

and column phase ratios were optimized (p_0 and T_0 were arbitrarily set at 101 325 Pa and 298.15 K, respectively) to minimize the SSD between calculated and observed retention time values. Eqs. 67 and 68 were used as model equations to estimate calculated retention times. The optimized values are entered in tab. 3.

TAB. 3: **Optimized values of n -alkane partition parameters and column phase ratios**

	SLB-IL60	DB-35ms
β value calculated from nominal dimensions	313	250
<i>Classical model</i> (model equation: eq. 67)		
ΔH_C (J·mol ⁻¹)	-3193	-3310
ΔS_C (J·mol ⁻¹ ·K ⁻¹)	-4.517	-3.911
β	563	535
R²	0.9998	0.9998
<i>Extended model</i> (model equation: eq. 68) $p_0 = 101\,325$ Pa, $T_0 = 298.15$ K		
$\Delta U_C(p_0, T_0)$ (J·mol ⁻¹)	-4461	-4642
$\Delta V_C(p_0, T_0)$ (m ³ ·mol ⁻¹)	1.96×10^{-4}	2.65×10^{-4}
$\Delta S_C(p_0, T_0)$ (J·mol ⁻¹ ·K ⁻¹)	-7.938	-7.274
$\Delta \alpha_C$ (m ³ ·mol ⁻¹ ·K ⁻¹)	-1.68×10^{-6}	-1.60×10^{-6}
$\Delta \chi_C$ (m ³ ·mol ⁻¹ ·Pa ⁻¹)	-4.32×10^{-11}	-1.07×10^{-11}
$\Delta C_{p,C}$ (J·mol ⁻¹ ·K ⁻¹)	8.585	6.563
β	563	535
R²	0.99994	0.99995

According to the R^2 values obtained after optimization of model parameters, the experimental data fit well with both models. Nevertheless, a slightly better fit is observed using the extended one, as the R^2 values are closer to unity.

No significant difference can be observed on phase ratio values whatever the model used to optimize them. Using eq. 8 (p. 117), it is possible to deduce SP film thickness for both columns: 0.11 (SLB-IL60) and 0.12 μm (DB-35ms). Surprisingly, these values are much lower than those indicated by the manufacturers, which might be explained by two hypotheses:

- the two columns underwent SP film thickness decreases during their anterior uses, which might be due to phase bleeding phenomena at high temperatures.
- some parts of the SP films are not permeable to carrier gas (which can be attributed, for example, to their high reticulation). In other words, solute partitioning cannot occur in these parts. Consequently, the optimized phase ratio values are only apparent values which are only related to SP film available to solute partition.

Further studies are required to validate one of these hypotheses. Direct measurement of film thicknesses should help at dealing with that point.

The optimized phase ratio values were set as known constant for the upcoming optimization of solute retention parameters.

ii. Solute partition parameters determination

The partition parameters of the 11 solutes were determined by minimizing the SSD between calculated and experimental retention time values observed using the SLB-IL60 and DB-35ms

columns. The calculated values were obtained using eq. 31 (p. 122), in which the retention factor was calculated using eq. 30 (p. 121, classical model) or eq. 63 (p. 134, extended one). The experimental values were acquired by setting different inlet gauge pressures (68.9, 138, 207 and 376 kPa hydrogen) and in isothermal mode, according to the temperature values listed below:

- SLB-IL60: 180, 190, 200, 210 and 220 °C,
- DB-35ms: 150, 160, 170, 180 and 190 °C.

The experimental values of retention times are provided in tabs. S3-4 (appendix 1, p. 165).

The optimized partition parameters of these solutes can be found in tabs. 4 (classical model) and 5 (extended one).

Tab. 4: **Optimized solute partition parameter values** (classical model)

SLB-IL60 ($\beta = 562, L = 32.4$ m)			
Solute	ΔH (J·mol ⁻¹)	ΔS (J·mol ⁻¹ ·K ⁻¹)	R ²
Fluorene	-55329	-56.59	0.9996
9,10-dihydroanthracene	-57413	-60.09	0.9997
9,10-dihydrophenanthrene	-57287	-59.57	0.9997
1-methylfluorene	-59696	-62.55	0.9998
Dibenzothiophene	-60995	-61.19	0.99992
Phenanthrene	-63455	-63.92	0.99995
Anthracene	-63743	-64.29	0.99995
Carbazole	-75765	-76.20	0.99998
2-methylanthracene	-67693	-69.70	0.99996
9-methylanthracene	-68031	-69.50	0.99997
9,10-dimethylanthracene	-72127	-74.50	0.99998
DB-35ms ($\beta = 535, L = 29.0$ m)			
Solute	ΔH (J·mol ⁻¹)	ΔS (J·mol ⁻¹ ·K ⁻¹)	R ²
Fluorene	-54681	-57.92	0.99995
9,10-dihydroanthracene	-58428	-63.12	0.99995
9,10-dihydrophenanthrene	-58462	-62.50	0.99994
1-methylfluorene	-59213	-64.03	0.99996
Dibenzothiophene	-59929	-63.06	0.99997
Phenanthrene	-60817	-64.07	0.99997
Anthracene	-61198	-64.60	0.99997
Carbazole	-65387	-71.18	0.99996
2-methylanthracene	-65270	-70.05	0.99996
9-methylanthracene	-66389	-70.44	0.99997
9,10-dimethylanthracene	-71437	-75.96	0.99998

The good R² values indicate that the experimental data fit well with both models. Nevertheless, significantly better adjusted correlation coefficients were obtained using the extended model. In tab. 4, the signs of the adjusted parameter values conform to those observed in the literature [10,20,22]. Moreover, the signs associated with parameter values indicated in tab. 5 also conform to expectations.

- Indeed, solute molar internal energy, entropy and thermal expansivity were expected to be higher in the MP than in the SP. Therefore, negative values of optimized $\Delta U_i(p_0, T_0)$, $\Delta S_i(p_0, T_0)$ and $\Delta \alpha_i$ parameters are logical.
- In addition, in the chosen reference conditions (25 °C, 1 atm), the studied solutes were strongly retained by the column, which means that they were preferentially dissolved in the SP in the state of equilibrium. Consequently, their molar volumes were probably higher in the SP than in the MP. It is therefore logical to observe positive values for the $\Delta V_i(p_0, T_0)$ parameter. It is worth noting that setting other reference conditions would have changed the values – for example, at high temperature and low pressure reference values, $\Delta V_i(p_0, T_0)$ values would have been negative, probably.
- The values of solute $\Delta \chi_i$ were systematically negative on the DB-35ms column, and randomly distributed around 0 on the SLB-IL60 one. It is hard to predict qualitatively the values of solute compressibility in each phase, as it should depend on solute and SP molecular structures.
- The optimized $\Delta C_{p,i}$ were all positive, which means that solute $C_{p,i}$ values were higher in the SP than in the MP, as expected.

Using the data provided in tabs. 4–5, it is possible to calculate the absolute values of ΔU_i (eq. 59, p. 134), ΔV_i (eq. 60) and ΔS_i (eq. 61) as a function of pressure and temperature. A plot of these 3 functions applied to Phenanthrene on the DB-35ms column is represented in fig. 17.

As revealed by fig. 17, pressure has a slight impact on Phenanthrene ΔU_i and ΔS_i values. Indeed, these two quantities exhibit strong variations with respect to temperature, but their change (at constant temperature) with respect to pressure is moderate. Conversely, Phenanthrene ΔV_i exhibits strong pressure and temperature dependencies. Note that these observations can also be made on the other solutes, using both tested columns.

TAB. 5: Optimized solute partition parameter values (extended model)

Solute	$\Delta U(p_0, T_0)$ (J·mol ⁻¹)	$\Delta V(p_0, T_0)$ (m ³ ·mol ⁻¹)	$\Delta S(p_0, T_0)$ (J·mol ⁻¹ ·K ⁻¹)	$\Delta\alpha$ (m ³ ·mol ⁻¹ ·K ⁻¹)	$\Delta\chi$ (m ³ ·mol ⁻¹ ·Pa ⁻¹)	ΔC_p (J·mol ⁻¹ ·K ⁻¹)	R ²
SLB-IL60 ($\beta = 562$, $L = 32.4$ m)							
Fluorene	-76023	6.8065×10^{-3}	-109.2	-4.7757×10^{-5}	-5.5543×10^{-10}	109.3	0.999995
9,10-dihydroanthracene	-79712	6.9164×10^{-3}	-116.9	-4.6944×10^{-5}	3.7137×10^{-10}	118.9	0.999996
9,10-dihydrophenanthrene	-79200	6.4003×10^{-3}	-115.5	-4.3917×10^{-5}	-6.1506×10^{-11}	117.4	0.999996
1-methylfluorene	-79760	5.3601×10^{-3}	-114.0	-3.5820×10^{-5}	5.9945×10^{-10}	108.7	0.999997
Dibenzothiophene	-77863	3.6985×10^{-3}	-104.7	-2.3990×10^{-5}	6.2011×10^{-10}	92.90	0.999998
Phenanthrene	-79679	3.1528×10^{-3}	-105.9	-1.9581×10^{-5}	1.0670×10^{-9}	90.25	0.999998
Anthracene	-80929	3.2843×10^{-3}	-108.8	-2.0667×10^{-5}	6.3647×10^{-10}	95.66	0.999998
Carbazole	-84482	2.7406×10^{-3}	-113.3	-1.6413×10^{-5}	1.0129×10^{-9}	94.51	0.999998
2-methylantracene	-84417	2.6465×10^{-3}	-112.1	-1.5397×10^{-5}	1.5077×10^{-9}	92.36	0.999998
9-methylantracene	-86423	1.4573×10^{-3}	-112.0	-9.3185×10^{-6}	-4.1736×10^{-10}	81.99	0.999998
9,10-dimethylantracene	-88326	9.7298×10^{-4}	-109.3	-5.3623×10^{-6}	3.4993×10^{-10}	72.79	0.999998
DB-35ms ($\beta = 535$, $L = 29.0$ m)							
Fluorene	-67519	9.4037×10^{-4}	-92.94	-9.7795×10^{-6}	-1.5490×10^{-9}	89.26	0.999998
9,10-dihydroanthracene	-72876	8.2536×10^{-4}	-102.6	-7.8584×10^{-6}	-1.0512×10^{-9}	101.4	1.000000
9,10-dihydrophenanthrene	-75054	3.9312×10^{-4}	-108.0	-5.2396×10^{-6}	-1.7644×10^{-9}	117.6	0.999999
1-methylfluorene	-72560	4.4690×10^{-4}	-100.6	-5.6747×10^{-6}	-2.0102×10^{-9}	94.29	0.999999
Dibenzothiophene	-72461	4.4525×10^{-4}	-97.42	-4.9338×10^{-6}	-1.4023×10^{-9}	88.60	1.000000
Phenanthrene	-73554	3.5211×10^{-4}	-99.03	-3.7180×10^{-6}	-8.9979×10^{-10}	90.41	1.000000
Anthracene	-73641	2.0399×10^{-4}	-98.81	-3.6976×10^{-6}	-2.0830×10^{-9}	88.47	0.999999
Carbazole	-80109	4.3625×10^{-4}	-111.6	-4.3297×10^{-6}	-1.2427×10^{-9}	104.7	1.000000
2-methylantracene	-79595	5.3724×10^{-4}	-109.3	-4.7192×10^{-6}	-8.0970×10^{-10}	101.7	1.000000
9-methylantracene	-79877	3.4637×10^{-4}	-107.5	-2.9033×10^{-6}	-3.6119×10^{-10}	96.25	1.000000
9,10-dimethylantracene	-83733	3.2211×10^{-4}	-109.7	-2.4438×10^{-6}	-6.8424×10^{-10}	88.01	1.000000

$p_0 = 101325$ Pa, $T_0 = 298.15$ K

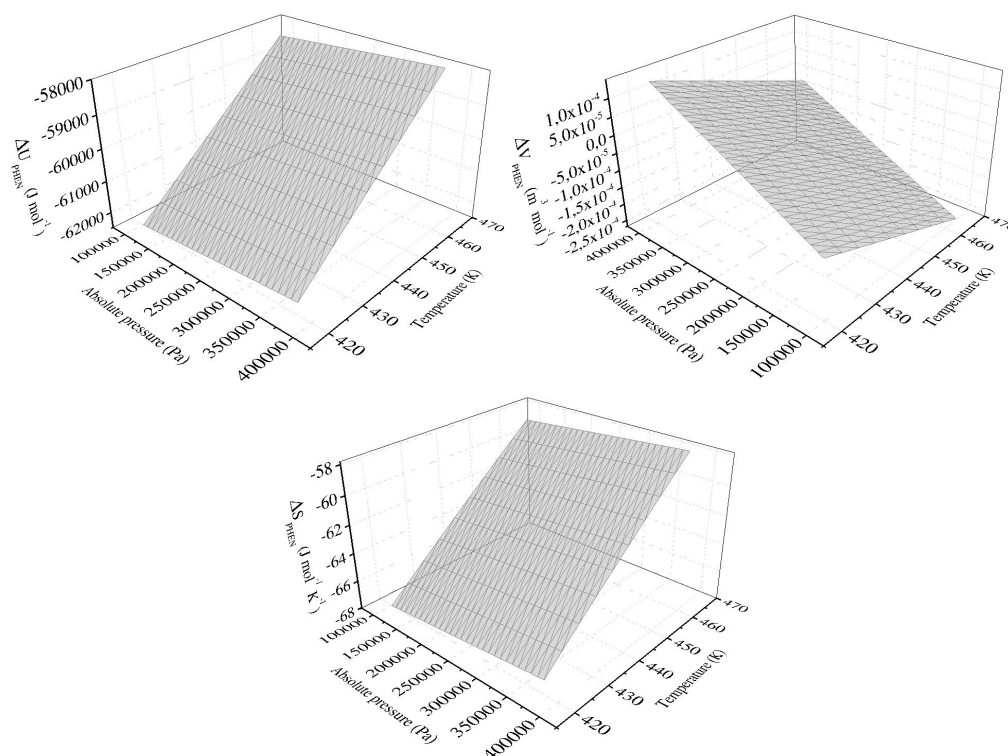


FIG. 17: Calculated Phenanthrene (PHEN) ΔU_i , ΔV_i and ΔS_i values on the DB-35ms column – ΔU_i and ΔS_i exhibit low pressure dependency, whereas ΔV_i is much more impacted by both quantities.

To conclude, this part of the study showed that the extended model developed in this work offers a better description of solute partitioning, as revealed by a comparison of adjusted R^2 values obtained using the two models. In addition, it introduces pressure effects on solute retention, which could serve at explaining the evolution of isothermal solute apparent retention factors with respect to column head pressure (fig. 14, p. 131). Nevertheless, even if developing models by increasing the number of parameters can increase the correlation with experimental data, one has to make sure that the adjusted parameter values are physically meaningful. In this part, we have qualitatively demonstrated that the values obtained were logical, but further confirmation is required to validate the new model. To perform that, a study of its ability at predicting solute retention times would be suitable. Based on that, a comparison of the results obtained with both models would help at highlighting the best one – and subsequently at validating (or not) the extended one. This is the aim of the two next paragraphs.

iii. Retention time prediction in one-dimensional GC

The retention times of the 11 tested solutes were predicted on the two columns, using the two models and the associated adjusted parameter values (tabs. 4–5). Four different sets of conditions were tested. For all of them, the same column temperature program was applied. First, a $10\text{ }^{\circ}\text{C}\cdot\text{min}^{-1}$ heating ramp was programmed from 100 to 150 $^{\circ}\text{C}$. Then, a 5 min isothermal step was set, and a second $10\text{ }^{\circ}\text{C}\cdot\text{min}^{-1}$ heating ramp was applied up to 250 $^{\circ}\text{C}$. 4 different inlet gauge pressure values were applied:

- Program 1: 103 kPa
- Program 2: 172 kPa
- Program 3: 241 kPa
- Program 4: 310 kPa

The retention time values acquired and predicted in these conditions can be found in tabs. 6 (SLB-IL60 column) and 7 (DB-35ms). Graphical representations of errors on predicted values (*e. g.*, difference between predicted and experimental retention times) are provided in fig. 18 (SLB-IL60) and 19 (DB-35ms).

TAB. 6: Experimental and predicted retention times on the SLB-IL60 column (in minutes)

Program	1			2			3			4		
	Exp.	Calc. (1)	Calc. (2)	Exp.	Calc. (1)	Calc. (2)	Exp.	Calc. (1)	Calc. (2)	Exp.	Calc. (1)	Calc. (2)
Fluorene	14.077	13.892	14.093	11.732	11.367	11.689	9.816	9.304	9.643	8.379	7.945	8.127
9,10-dihydroanthracene	14.710	14.568	14.739	12.538	12.264	12.527	10.919	10.480	10.811	9.404	8.927	9.167
9,10-dihydrophenanthrene	14.821	14.683	14.844	12.660	12.392	12.647	11.067	10.643	10.966	9.572	9.083	9.342
1-methylfluorene	15.948	15.864	15.961	13.958	13.801	13.947	12.616	12.378	12.556	11.508	11.177	11.369
Dibenzothiophene	17.775	17.730	17.784	15.860	15.792	15.855	14.654	14.557	14.628	13.738	13.615	13.688
Phenanthrene	18.858	18.813	18.870	16.993	16.950	16.995	15.847	15.794	15.839	15.005	14.940	14.984
Anthracene	18.961	18.913	18.977	17.098	17.057	17.107	15.958	15.908	15.956	15.120	15.061	15.104
2-methylanthracene	20.135	20.061	20.146	18.325	18.284	18.334	17.239	17.206	17.244	16.457	16.426	16.458
9-Methylanthracene	20.524	20.431	20.535	18.681	18.635	18.691	17.593	17.559	17.602	16.813	16.785	16.823
9,10-dimethylanthracene	22.220	22.040	22.204	20.028	19.952	20.030	18.965	18.916	18.971	18.211	18.178	18.219
Carbazole	26.526	26.158	26.506	22.838	22.628	22.824	21.229	21.099	21.228	20.319	20.236	20.325

Exp.: experimental, Calc.: calculated, (1): classical model, (2): extended model.

TAB. 7: Experimental and predicted retention times on the SLB-IL60 column (in minutes)

Program	1			2			3			4		
	Exp.	Calc. (1)	Calc. (2)	Exp.	Calc. (1)	Calc. (2)	Exp.	Calc. (1)	Calc. (2)	Exp.	Calc. (1)	Calc. (2)
Fluorene	11.300	11.288	11.341	8.243	8.175	8.257	6.773	6.701	6.773	5.942	5.869	5.930
9,10-dihydroanthracene	13.398	13.415	13.440	10.951	10.918	10.979	8.928	8.866	8.943	7.679	7.616	7.681
9,10-dihydrophenanthrene	13.806	13.823	13.854	11.474	11.448	11.510	9.521	9.449	9.550	8.153	8.081	8.166
1-methylfluorene	13.868	13.882	13.907	11.568	11.550	11.596	9.639	9.585	9.659	8.247	8.193	8.248
Dibenzothiophene	15.122	15.125	15.158	13.045	13.046	13.070	11.534	11.527	11.562	10.186	10.139	10.187
Phenanthrene	15.584	15.578	15.619	13.578	13.579	13.602	12.179	12.171	12.199	10.982	10.957	10.995
Anthracene	15.735	15.722	15.767	13.752	13.750	13.775	12.382	12.375	12.400	11.227	11.206	11.232
Carbazole	16.928	16.865	16.956	15.110	15.088	15.125	13.934	13.925	13.943	13.023	13.018	13.024
2-methylanthracene	17.289	17.217	17.321	15.473	15.446	15.491	14.309	14.302	14.323	13.418	13.420	13.428
9-Methylanthracene	18.130	18.021	18.160	16.342	16.290	16.356	15.223	15.196	15.232	14.384	14.375	14.395
9,10-dimethylanthracene	20.205	19.954	20.208	18.465	18.314	18.462	17.414	17.313	17.410	16.658	16.588	16.652

Exp.: experimental, Calc.: calculated, (1): classical model, (2): extended model.

According to the values given in tabs. 6–7 and figs. 18–19, the classical model permitted the prediction of retention times with an honest accuracy on both columns. Indeed, the errors ranged from 1 to 29 s, which is a honorable result. However, large deviations were generally observed for the most (Fluorene, 9,10-dihydroanthracene and 9,10-dihydrophenanthrene) and least (9,10-dimethylanthracene) volatile solutes. Besides, the use of the extended model led to a significant decrease of errors on predicted retention times (maximum error of 15 s, and most of errors ranged from 0 to 3 s). In addition, the deviations on volatile or heavy solutes retention times were significantly decreased. It is worth noting that the classical model systematically led to the underestimation of solute retention times, whereas the extended one gave values more or less distributed around the experimental ones.

Consequently, these results show the relevance of using the extended model developed in this work to describe solute retention and predict retention times. Indeed, a good fit with experimental data was observed, and additionally, it provides an excellent accuracy on prediction. However, one supplementary way to compare the two models is to test their accuracy on prediction in FM-GC×GC, which was attempted in the next part.

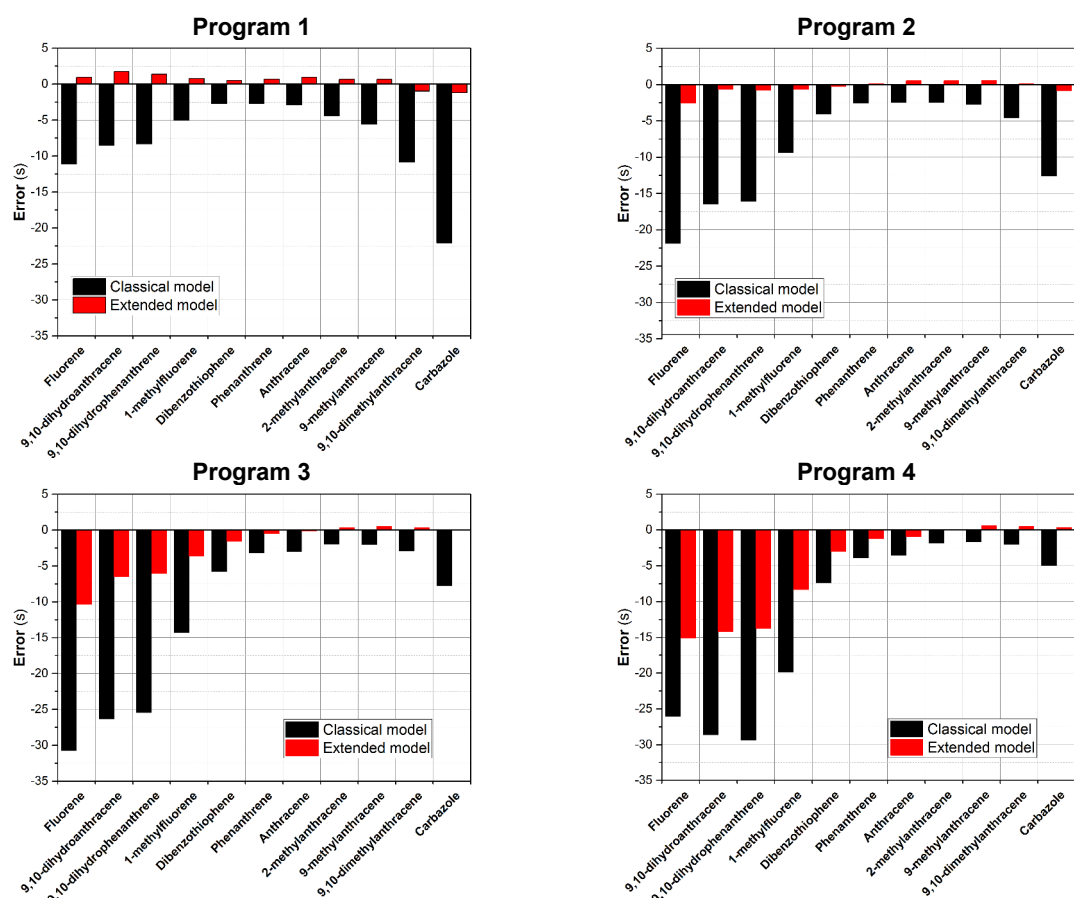


FIG. 18: Errors on predicted retention times using the SLB-IL60 column

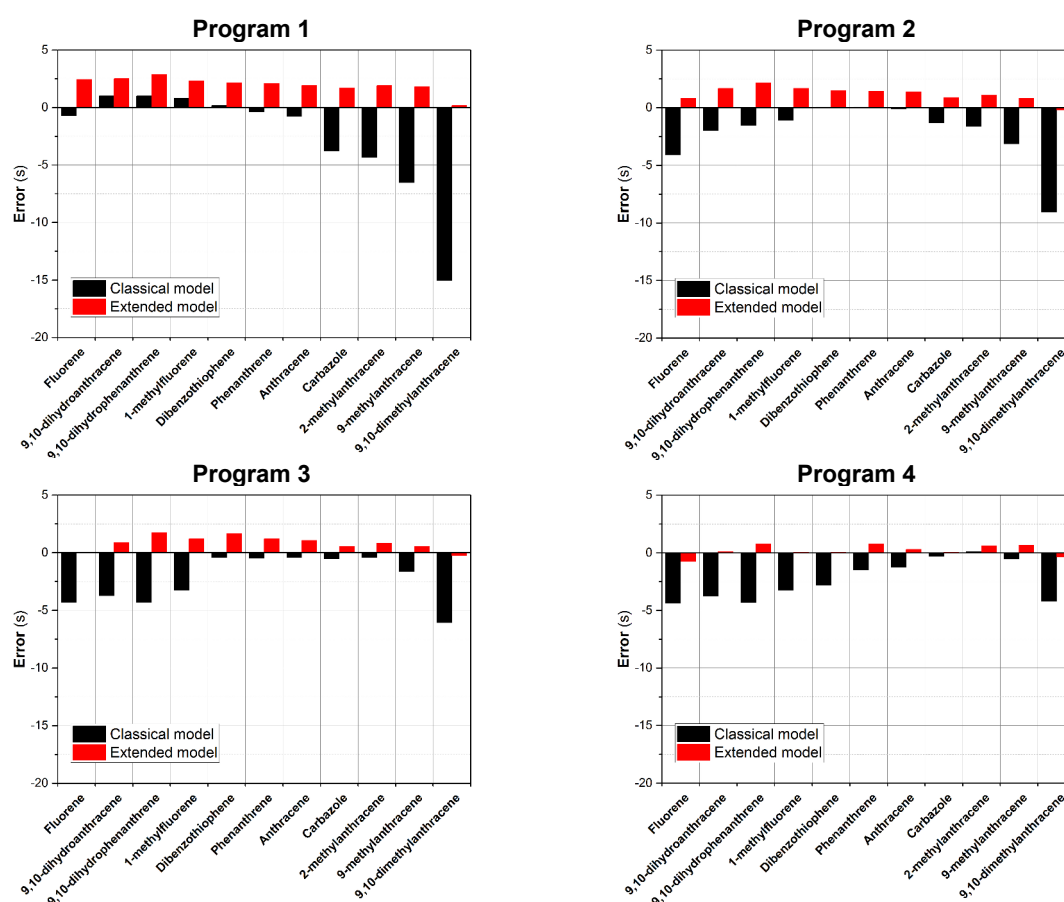


FIG. 19: Errors on predicted retention times using the DB-35ms column

iv. Retention time prediction in FM-GC×GC

The retention times of the 11 tested solutes were predicted in constant pressure mode, using the DB-35ms (28.35 m) and SLB-IL60 (4.97 m) columns as primary and secondary columns. The gauge pressures at the injector and the modulator were set at 228 and 217 kPa, respectively. Four different temperature programs were tested:

- Program 1: $5\text{ }^{\circ}\text{C}\cdot\text{min}^{-1}$ heating ramp from 100 to $250\text{ }^{\circ}\text{C}$, then isothermal step,
- Program 2: $10\text{ }^{\circ}\text{C}\cdot\text{min}^{-1}$ heating ramp from 100 to $250\text{ }^{\circ}\text{C}$, then isothermal step,
- Program 3: $15\text{ }^{\circ}\text{C}\cdot\text{min}^{-1}$ heating ramp from 100 to $250\text{ }^{\circ}\text{C}$, then isothermal step,
- Program 4: $20\text{ }^{\circ}\text{C}\cdot\text{min}^{-1}$ heating ramp from 100 to $250\text{ }^{\circ}\text{C}$, then isothermal step.

The values of retention times acquired in these conditions are entered in tabs. 8 (1st dimension) and 9 (2nd dimension). Additionally, the errors on predicted primary and secondary retention times are graphically represented in figs. 20 and 21, respectively.

Note that Carbazole calculated 2nd dimension retention times were systematically larger than the modulation period (*e. g.*, 5 s), which was caused by wraparound phenomenon [30]. Therefore, the calculated values were corrected by removing 5 s to each of them.

TAB. 8: Experimental and predicted primary retention times in FM-GC×GC (in minutes)

Program	1			2			3			4		
	Exp.	Calc. (1)	Calc. (2)	Exp.	Calc. (1)	Calc. (2)	Exp.	Calc. (1)	Calc. (2)	Exp.	Calc. (1)	Calc. (2)
Fluorene	31.583	31.138	31.758	22.833	22.150	22.932	19.917	19.153	19.990	18.500	17.655	18.518
9,10-dihydroanthracene	34.417	33.630	34.543	24.917	23.987	25.087	21.833	20.772	21.935	20.250	19.163	20.358
9,10-dihydrophenanthrene	35.250	34.430	35.543	25.583	24.665	26.003	22.417	21.410	22.823	20.917	19.782	21.232
1-methylfluorene	35.250	34.353	35.237	25.667	24.557	25.613	22.500	21.290	22.407	20.917	19.658	20.802
Dibenzothiophene	38.250	37.055	38.208	28.167	26.887	28.217	24.833	23.497	24.887	23.250	21.802	23.222
Phenanthrene	39.333	38.033	39.305	29.083	27.720	29.172	25.750	24.282	25.793	24.083	22.562	24.105
Anthracene	39.750	38.340	39.617	29.417	27.977	29.430	26.083	24.522	26.035	24.417	22.795	24.337
Carbazole	42.917	40.908	42.833	32.167	30.130	32.258	28.667	26.538	28.733	26.917	24.742	26.972
2-methylanthracene	44.250	42.207	44.343	33.417	31.348	33.692	29.917	27.730	30.140	28.167	25.920	28.365
9-Methylanthracene	47.833	45.378	47.868	36.833	34.312	36.995	33.167	30.622	33.372	31.417	28.777	31.560
9,10-dimethylanthracene	60.000	55.750	59.637	48.417	44.173	48.240	44.583	40.315	44.442	42.667	38.387	42.542

Exp.: experimental, Calc.: calculated, (1): classical model, (2): extended model.

TAB. 9: Experimental and predicted secondary retention times in FM-GC×GC (in seconds)

Program	1			2			3			4		
	Exp.	Calc. (1)	Calc. (2)	Exp.	Calc. (1)	Calc. (2)	Exp.	Calc. (1)	Calc. (2)	Exp.	Calc. (1)	Calc. (2)
Fluorene	1.500	1.384	1.468	1.490	1.384	1.468	1.480	1.384	1.468	1.470	1.384	1.468
9,10-dihydroanthracene	1.535	1.417	1.508	1.525	1.417	1.508	1.515	1.417	1.508	1.510	1.417	1.508
9,10-dihydrophenanthrene	1.560	1.437	1.528	1.690	1.437	1.528	1.675	1.437	1.528	1.530	1.437	1.528
1-methylfluorene	1.700	1.567	1.662	1.545	1.567	1.662	1.535	1.567	1.662	1.660	1.567	1.662
Dibenzothiophene	2.155	1.996	2.111	2.135	1.996	2.111	2.115	1.996	2.111	2.095	1.996	2.111
Phenanthrene	2.485	2.307	2.439	2.460	2.307	2.439	2.435	2.307	2.439	2.410	2.307	2.439
Anthracene	2.525	2.340	2.483	2.495	2.340	2.483	2.470	2.340	2.483	2.445	2.340	2.483
Carbazole	2.025	1.531	1.859	1.920	1.531	1.859	1.805	1.531	1.859	1.725	1.531	1.859
2-methylanthracene	3.010	2.781	2.951	2.965	2.781	2.951	2.935	2.781	2.951	2.900	2.781	2.951
9-Methylanthracene	3.230	2.989	3.171	3.180	2.989	3.171	3.145	2.989	3.171	3.115	2.989	3.171
9,10-dimethylanthracene	4.160	3.864	4.076	4.105	3.864	4.076	4.055	3.864	4.076	4.015	3.864	4.076

Exp.: experimental, Calc.: calculated, (1): classical model, (2): extended model.

As shown by the data provided in tabs. 8–9 and figs. 20–21, retention times predicted using the classical model were systematically lower than the experimental values in both dimensions. Moreover, very large deviations (up to 257 s) on primary retention time values were observed for the least volatile solutes. Deviations were also high in the 2nd dimension (up to 0.5 s). Conversely, values predicted using the extended model were closer than the experimental ones. Indeed, the maximal errors were 25 s in the 1st dimension and 0.17 s in the 2nd one.

Note that even if they underwent a small pressure drop in the primary column (11 kPa), solute were exposed to high pressure values, which means that their partition did not occur by the same way as if they would have been exposed to the same column pressure ratio with an outlet pressure of 1 atm.

In this part, it was shown that retention times in FM-GC×GC can be predicted with an excellent accuracy using the extended model, whereas the classical one led to larger errors. This brings a supplementary proof of the relevance of taking pressure into account to describe solute partitioning, and validates the model developed in this chapter.

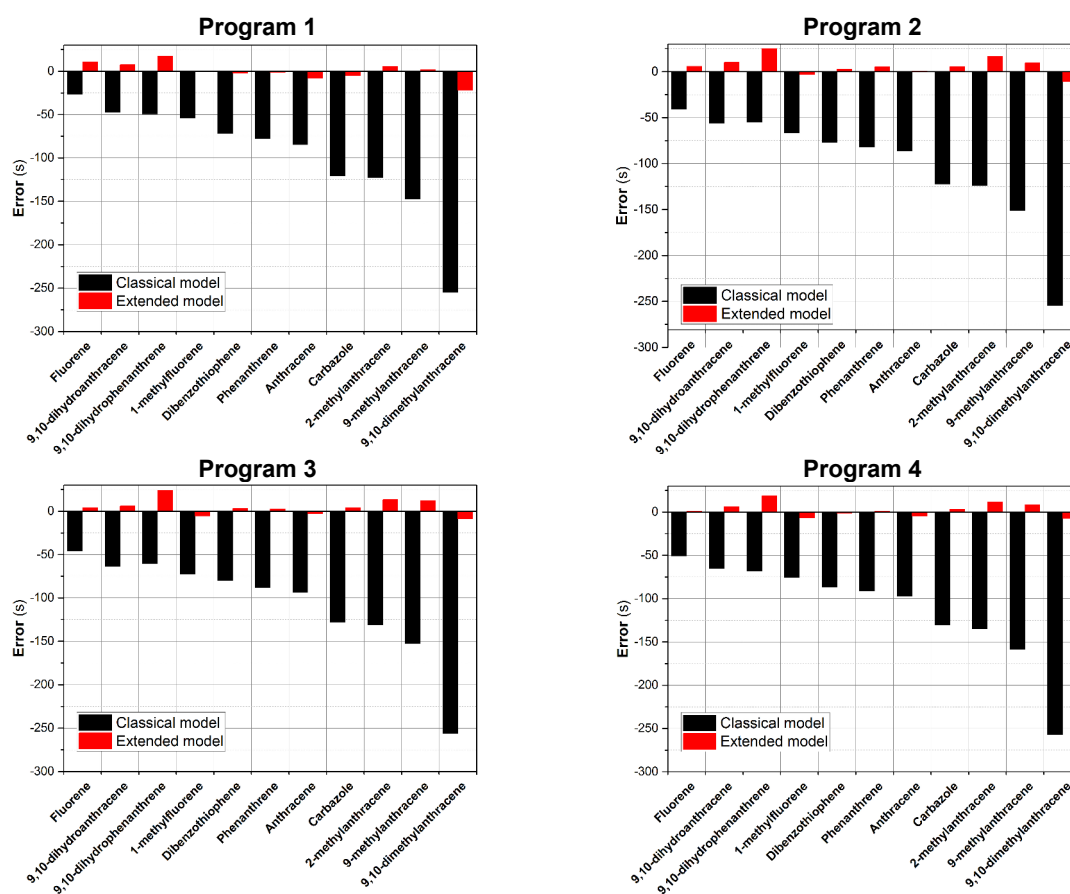


FIG. 20: Errors on predicted primary retention times in FM-GC×GC

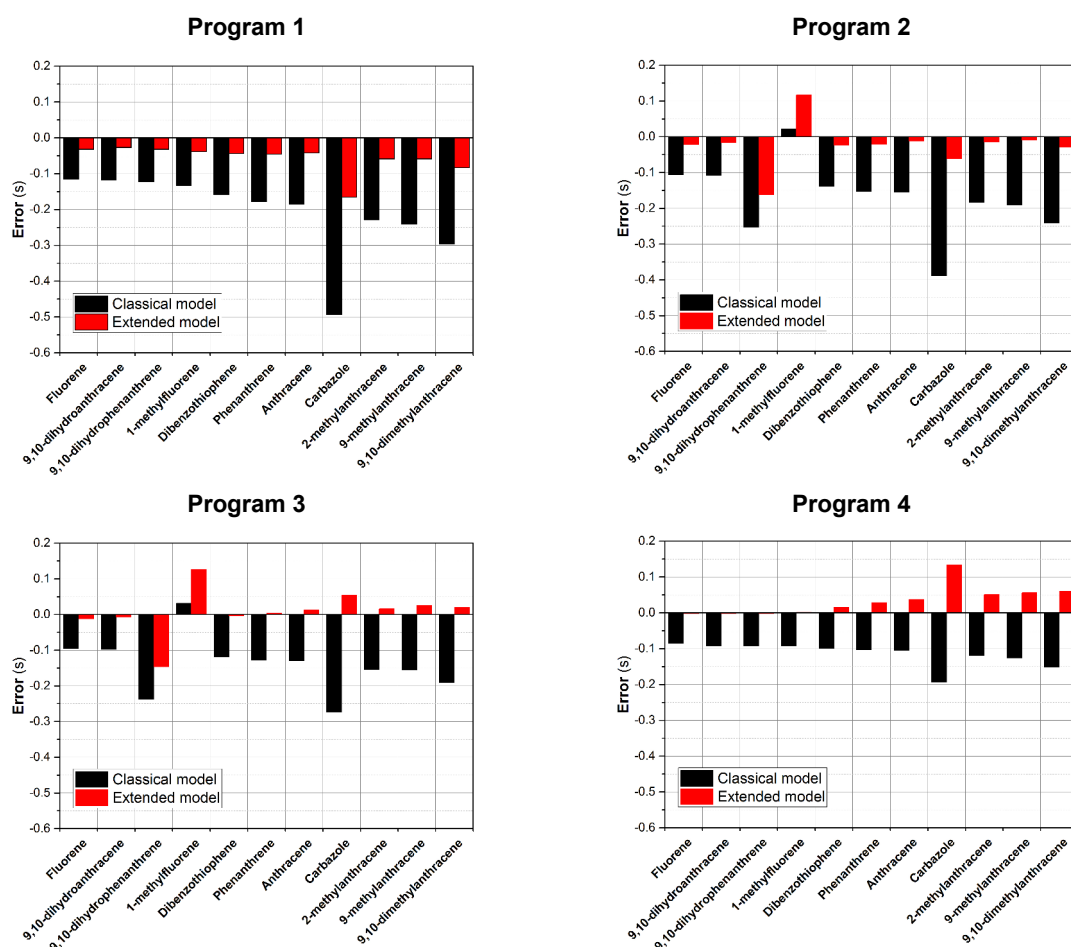


FIG. 21: Errors on predicted 2nd dimension retention times in FM-GC \times GC

d) Conclusions

In this work, the impact of pressure on solute partitioning in capillary GC was successfully demonstrated. A new model equation was developed to describe solute retention factor as a function of pressure and temperature, and deviations from ideal behaviors with respect to these two variables were taken into account.

This model was applied to solute retention time prediction in GC and FM-GC \times GC and gave very good accuracies on predicted values. The comparison with the classical model shown that the extended one was clearly more efficient, especially for retention time prediction in FM-GC \times GC. Therefore, it can serve as a supplementary tool to optimize solute separation using this technique in order to obtain satisfying peak capacities.

It is worth noting that applying this retention time prediction method to every solute of a complex mixture would be time-costing. Therefore, choosing one or two model compounds per family of solute should be sufficient to develop the required separation.

The two models presented in this study were also applied to SP film thickness estimation, and systematically led to values lower than those indicated by the manufacturers – whatever the

considered model. Two hypotheses were proposed to explain these results, but further work is required to validate one of them.

Additionally, it is well known that solute elution order changes can be observed by column temperature modification, especially when polar or chiral columns are used [31,32]. This new model opens up a theoretical justification for a potential other kind of elution order reversion associated with carrier gas velocity – at a given temperature, the elution order of two solutes could be inverted by changing the inlet pressure. Obviously, this requires the pressure-related partition parameters of these solutes to be favorable to such behavior. As far as we know, such observations have not been reported in the literature up to now. But any future evidence of this kind of reversion could be justified using this model.

IV. IMPURITY QUANTIFICATION IN PHENANTHRENE

1) Introduction

Thanks to the model developed in the previous part, appropriate chromatographic conditions were selected in order to separate Phenanthrene and its impurities. During preliminary tests, the most critical couple (*e. g.*, Phenanthrene-Anthracene) was found to be more resolved using a DB-35ms column. Consequently, a simple one-dimensional GC-FID method was developed using this column.

In this part, the validation of the method is presented. In a first time, FID calibration was performed. In order to choose the calibration method (*e. g.*, external or internal standard calibration), the repeatability of injection volume was assessed before determining FID response factors. Then, a particular attention was paid to the detection thresholds of the method, in order to estimate the minimal detectable levels of impurity in Phenanthrene samples. The method was then tested on commercial samples purchased from different suppliers and that were used for purification experiments in this thesis. Eventually, some tests were performed using a packed column, in order to compare the performance with respect to the capillary one and to justify the use of a capillary column.

2) Analytical method

a) Capillary GC-FID conditions

The analytical method was developed on an Agilent 7890B Series Gas Chromatograph equipped with a split/splitless injector and a Flame Ionization Detector. The injector and detector temperatures were set at 300 °C. The inlet split flow was set at 20 mL·min⁻¹. An Agilent DB-35ms (30 m × 0.25 mm × 0.25 µm) column was used for the separations. Hydrogen was chosen as carrier gas (2.0 mL·min⁻¹ column flow, which corresponded to an average velocity of ~ 60 cm·s⁻¹ at the beginning of the analysis). The FID was supplied with 30 and 300 mL·min⁻¹ hydrogen and air, respectively. The acquisition frequency was 200 Hz. The injections were performed using an Agilent G4513A autosampler. The injection volume was set at 1 µL (amount of sample analyzed: ~ 0.8 µg). Before and after every injection, the syringe was washed 5 times with acetone, and was washed 3 times with the sample solution. The temperature program was set as follows: isothermal step at 100 °C for 10 min, then heating ramp at 5 °C·min⁻¹ up to 270 °C, then isothermal step for 20 min.

The injector was set in split mode in order to avoid column overloading and to prevent from low resolution of Anthracene peak.

b) Impurity level determination

Impurity level determination requires: (i) prior identification of the impurities, which was attempted by GC-MSD, and which permitted the determination of FID response factors with respect to the different solutes, (ii) analysis of Phenanthrene samples.

*i. FID calibration***Determination of FID response factors:**

After checking the repeatability of the injection volume, FID was calibrated according to the external standard calibration method.

Standard solutions were prepared in HPLC grade Acetone (VWR Chemicals). The following solutes were put together in the solutions: Naphthalene, Biphenyl (98 %, Acros Organics) Fluorene, 9,10-dihydroanthracene, 9,10-dihydrophenanthrene, Dibenzothiophene, Anthracene and Carbazole⁴. Solute concentrations were ranging from 10 to 180 ppm. Every solution was analyzed twice. For every chromatogram obtained after the analyses, impurity peaks were integrated to determine their area. The response factors were determined by modeling the results by the following equation:

$$A_i = RF_i \times C_i \quad (71)$$

where:

A_i	impurity peak area (pA·s)
RF_i	FID response factor (pA·s·ppm ⁻¹)
C_i	impurity concentration in the standard solution (ppm)

Determination of FID detection thresholds:

Solute detection and quantification thresholds were determined from a study of baseline noise. Blank runs permitted to measure baseline standard deviation ($\sigma_{baseline} = 0,02934$ pA). Heights of detectable (h_{LD}) and quantifiable (h_{LQ}) solute peak were estimated by multiplying $\sigma_{baseline}$ by 3 and 10, respectively, which led to 0,0880 and 0,2934 pA values. Starting from eq. 1 (p. 114), these values could be converted to concentrations to determine the limits of detection (LD) and quantification (LQ) using the following relationships:

$$LD_i = \frac{h_{LD} \times \sigma_i \times \sqrt{2\pi}}{RF_i} \text{ in ppm} \quad (72)$$

$$LQ_i = \frac{h_{LQ} \times \sigma_i \times \sqrt{2\pi}}{RF_i} \text{ in ppm} \quad (73)$$

σ_i being solute peak standard deviation, which was supposed independent from solute concentration. This quantity was determined using the data obtained during injection of standard solutions.

4. Except Biphenyl, the provenances of solutes are the same as described in part III.3)b)i (p. 137).

ii. Impurity quantification

Samples were prepared by dissolution of ~ 10 mg of Phenanthrene in ~ 1 g of HPLC grade Acetone (VWR Chemicals) in order to obtain ~ 10 000 ppm solutions. Every sample was prepared twice. The prepared solutions were analyzed once.

For every chromatogram, impurity peaks were integrated to determine their area. Impurity concentration in the sample was determined using eq. 71. Impurity level in the sample was then determined using the following relationship:

$$X_i = \frac{C_i}{C_{sample}} \quad (74)$$

As two replicates were made for every sample, impurity level in Phenanthrene was calculated using eq. 75:

$$\bar{X}_i = \frac{X_{i,1} + X_{i,2}}{2} \quad (75)$$

The interval confidence on impurity level was determined with a degree of certainty of 95 % according to the following equation (Student law):

$$IC(\bar{X}_i) = \frac{a_2 \times s}{\sqrt{2}} \quad (76)$$

a_2 being the corresponding Student coefficient and s the standard deviation on \bar{X}_i .

3) Validation of the method

a) Assessment of injection volume repeatability

In order to choose the method of FID calibration (external or internal standard calibration), the repeatability of injection volume was assessed.

A solution containing ~ 30 ppm of 6 different solutes was injected 5 times in the conditions described in part IV.2)a (p. 152). The chromatograms were treated to obtain impurity peak areas (their values are entered in tab. 10). For every solute, the mean peak areas, the corresponding standard deviations and coefficients of variation were also calculated. The ratios between solute and Naphthalene peak areas are entered in tab. 11.

TAB. 10: Solute peak areas (pA·s) obtained after 5 successive injections

Solute	Rank of injection					Mean area	Standard deviation	Coefficient of variation (%)
	1	2	3	4	5			
Naphthalene	155,59	155,67	155,85	155,59	155,74	155,69	0,10	0,06
Biphenyl	164,08	164,12	164,42	164,12	164,34	164,21	0,14	0,08
Fluorene	150,96	150,83	151,43	150,77	151,37	151,07	0,28	0,18
9,10-dihydroanthracene	152,06	151,90	152,39	152,00	152,50	152,17	0,23	0,15
9,10-dihydrophenanthrene	156,35	156,13	156,76	156,25	156,78	156,45	0,27	0,17
1-methylfluorene	159,94	159,72	160,23	159,78	160,28	159,99	0,23	0,14

The coefficients of variation on solute areas observed in tab. 10 are very low (below 1 %), which indicates that the injection volume was clearly repeatable. Those observed on area ratios (tab. 11) are slightly lower, but the order of magnitude remains similar.

Thus, there is no particular interest at introducing an internal standard in every solution: this would induce a supplementary task during solution preparation without significant improvement of result accuracy. Consequently, in this work, impurity quantification was performed using the external standard calibration method.

TAB. 11: **Ratios of solute peak areas obtained after 5 successive injections** – Naphthalene peak was used as reference (internal standard)

Solute	Rank of injection					Mean area ratio	Standard deviation	Coefficient of variation (%)
	1	2	3	4	5			
Biphenyl	1,055	1,054	1,055	1,055	1,055	1,055	0,0003	0,03
Fluorene	0,970	0,969	0,972	0,969	0,972	0,970	0,0013	0,13
9,10-dihydroanthracene	0,977	0,976	0,978	0,977	0,979	0,977	0,0011	0,11
9,10-dihydrophenanthrene	1,005	1,003	1,006	1,004	1,007	1,005	0,0013	0,13
1-methylfluorene	1,028	1,026	1,028	1,027	1,029	1,028	0,0011	0,11

b) FID response factors

The calibration data associated with the selected compounds are entered in tab. 12. For every one of them, similar response factors (around $0.9 \text{ pA} \cdot \text{s} \cdot \text{ppm}^{-1}$) were observed, except for compounds containing heteroatoms (*e. g.*, Dibenzothiophene and Carbazole, whose response factors were lower than those of the other solutes). As high numbers of plates were obtained for all solutes, the resulting thin peaks led to calculated limits of detection and of quantification around 0.25 and 0.80 ppm, respectively, which corresponds to 0.003 and 0.008 wt. % in Phenanthrene samples (10 000 ppm sample solutions). As they permit the detection of traces below 0.1 %⁵, these values comply with the requested criteria and therefore validate the use of this method to determine Phenanthrene purity.

TAB. 12: **Results of FID calibration**

Solute	Retention time (min)	Peak standard deviation (min)	Response factor (pA s ppm^{-1})	R ²	Limit of detection (ppm)	Limit of quantification (ppm)
Naphthalene	8.44	1.643	0.8945	0.99996	0.41	1.35
Biphenyl	17.16	1.090	0.9346	0.99997	0.26	0.86
Fluorene	23.53	0.988	0.9064	0.99997	0.24	0.80
9,10-dihydroanthracene	25.85	0.969	0.9042	0.99997	0.24	0.79
9,10-dihydrophenanthrene	26.35	0.971	0.9221	0.99997	0.23	0.78
1-methylfluorene	26.43	0.966	0.9226	0.99998	0.23	0.77
Dibenzothiophene	28.07	0.973	0.7732	0.99998	0.28	0.93
Anthracene	28.93	0.984	0.9140	0.99998	0.24	0.79
Carbazole	30.71	0.942	0.8401	0.99998	0.25	0.83

5. In other words, such detection thresholds permit ultrapurity measurements.

Injection of solutions containing these impurities in levels distributed from 0.001 to 1 ppm shown that they could be actually detected starting from ~ 0.01 ppm, which corresponds to ~ 0.0001 wt. % level in Phenanthrene samples. Consequently, during upcoming quantification procedures, the detection and quantification thresholds were considered as being 0.01 and $10 \times 0.01 / 3 = 0.033$ ppm.

c) Testing the method on Phenanthrene samples

The selected chromatographic conditions were applied during the analysis of several Phenanthrene samples, in order to test its reliability. Samples of different purity grades and purchased from different suppliers were analyzed: (i) in the conditions described in part IV.2)a (p. 152), (ii) in GC-MSD according to the conditions described in appendix 2 (p. 167), in order to identify the impurities. Peak resolutions were measured to determine the ability of impurities at being quantified. Impurities were then quantified using the external standard method described in the previous paragraphs.

i. Analysis of technical-grade Phenanthrene

First, technical grade Phenanthrene (Alfa Aesar, 90 % indicative purity) was analyzed. The different peaks detected and the identity of the corresponding impurities are listed in tab. 13, as well as peak width at half height and peak resolution. The chromatogram is shown in fig. 22.

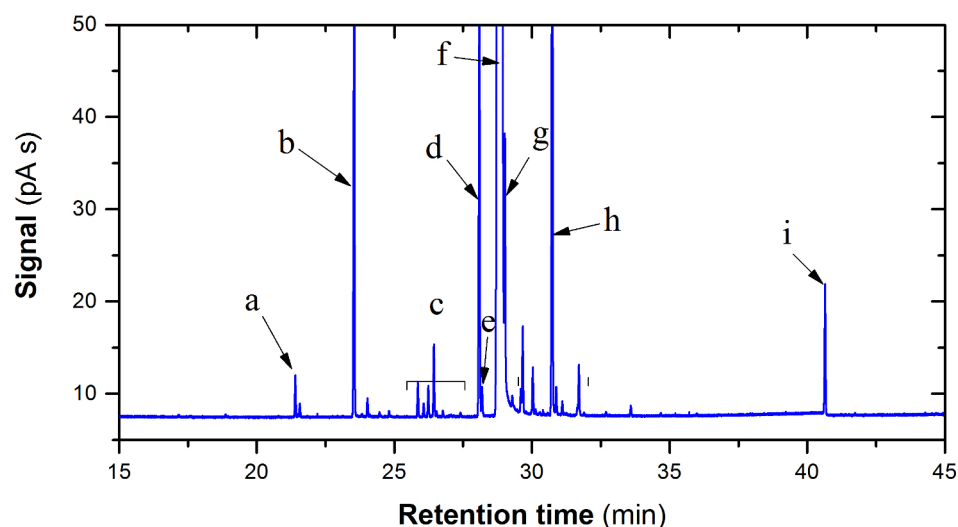


FIG. 22: GC-FID chromatogram of technical grade Phenanthrene – a. butenedioic acid, dibutyl ester; b. Fluorene; c. Dihydrophenanthrenes, dihydroanthracenes, tetrahydrophenanthrenes, tetrahydroanthracenes; d. Dibenzothiophene; e. Naphthothiophene 1; f. Phenanthrene; g. Anthracene; h. Carbazole; i. Anthracene/Maleic Anhydride Diels Alder adduct.

TAB. 13: Chromatographic data for technical grade Phenanthrene analysis

Impurity	Retention time in GC-FID (min)	Peak width at half height (min)	Peak resolution	Impurity level (wt. %)
Biphenyl	17.19	0.0401	--	0.0071 ± 0.0004
Methylnaphthalene*	18.88	0.0370	21.9	0.0068 ± 0.0002
Butenedioic acid, dibutyl ester*	21.42	0.0361	34.8	0.158 ± 0.008
Dibenzofuran	21.59	0.0341	2.42	0.0451 ± 0.0002

Impurity	Retention time in GC-FID (min)	Peak width at half height (min)	Peak resolution	Impurity level (wt. %)
Fluorene	23.56	0.0406	26.37	1.692 ± 0.0002
Methylbiphenyl*	24.04	0.0398	5.97	0.054 ± 0.002
Xanthene	24.47	0.0367	5.62	0.017 ± 0.005
Fluorene isomer*	24.82	0.0356	4.84	0.018 ± 0.002
9,10-dihydroanthracene	25.87	0.0366	14.5	0.099 ± 0.005
Dihydro-anthracene or -phenanthrene*	26.08	0.0355	2.91	0.0365 ± 0.0003
Dihydro-anthracene or -phenanthrene*	26.25	0.0348	2.42	0.087 ± 0.002
1-methylfluorene	26.45	0.0392	2.70	0.209 ± 0.003
Tetrahydro-anthracene or -phenanthrene*	26.78	0.0418	4.07	0.017 ± 0.002
Tetrahydro-anthracene or -phenanthrene*	27.42	0.0417	7.66	0.012 ± 0.001
Dibenzothiophene	28.10	0.0460	7.75	1.78 ± 0.04
Naphthothiophene 1*	28.20	0.0470	1.08	0.114 ± 0.003
Anthracene	29.03	0.0460	--**	0.554 ± 0.005
Unknown impurity	29.29	0.0421	2.95	0.0446 ± 0.0002
Benzoquinoline*	29.61	0.0315	4.35	0.0639 ± 0.0004
Naphthothiophene 2*	29.68	0.0404	0.97	0.297 ± 0.004
Methyl-dibenzothiophene or -naphthothiophene*	30.05	0.0374	4.76	0.17 ± 0.02
Carbazole	30.76	0.0393	9.26	2.8 ± 0.2
Methyl-phenanthrene or -anthracene*	30.90	0.0336	1.92	0.0831 ± 0.0008
Methyl-phenanthrene or -anthracene*	31.12	0.0414	2.93	0.036 ± 0.004
Methyl-phenanthrene or -anthracene*	31.72	0.0412	7.26	0.157 ± 0.009
Methylcarbazole*	32.71	0.0344	13.1	0.012 ± 0.002
9,10-phenanthrenequinone	33.61	0.0371	12.6	0.04 ± 0.02
Anthracene/Maleic Anhydride Diels Alder adduct	40.66	0.0399	91.6	0.55 ± 0.09
			Total	9.2 ± 0.4

* Unidentified isomer, ** in the case of Anthracene, the resolution could not be calculated as Phenanthrene peak was not Gaussian. However, a qualitative assessment of the separation highlighted that a specific integration of Anthracene peak was possible in these conditions. Further proof is available in fig. 23 (p. 159).

As revealed by tab. 13 entries, technical grade Phenanthrene contains many impurities (29). Thanks to GC-MSD experiments, most of them could be identified. However, many impurities were found to be isomers, and no complete identification of these isomers could be performed by injection of standards. Indeed, the identity of some isomers of Dihydrophenanthrene, Dihydroanthracene, Tetrahydrophenanthrene, Tetrahydroanthracene, Naphthothiophene and methylated derivatives of Carbazole, Phenanthrene and Anthracene could not be strictly determined. In addition, one impurity (retention time: 29.29 min) could not be identified by means of its mass spectrum.

As many of these impurities were not available as standards, the FID could not be calibrated for them. Consequently, the corresponding FID response factors were estimated thanks to Saint Laumer *et al.* relationship [33]:

$$RF_i = \frac{-0.071 + \frac{8,57}{10000} \times \Delta H_{comb,i} + 0,127 \times n_{benz,i}}{-0.071 + \frac{8,57}{10000} \times \Delta H_{comb,ref} + 0,127 \times n_{benz,ref}} \times \frac{MW_{ref}}{MW_i} \times RF_{ref} \quad (77)$$

i being the compound for which the FID was not calibrated, and ref a chosen reference solute for which the FID was calibrated. Solute combustion enthalpy, ΔH_{comb} , can be estimated using eq. 78:

$$\Delta H_{comb} = 11.06 + 103.57 \times n_C + 21.85 \times n_H - 47.18 \times n_O + 7.46 \times n_N + 74.67 \times n_S \quad (78)$$

where

MW	solute molecular weight
n_{benz}	number of benzene rings in the solute
n_C	number of carbon atoms in the solute
n_H	number of hydrogen atoms in the solute
n_O	number of oxygen atoms in the solute
n_N	number of nitrogen atoms in the solute
n_S	number of sulfur atoms in the solute

Thanks to these formula, the response factors entered in tab. 14 were estimated, which served to their quantification (impurity levels given in tab. 13).

TAB. 14: Predicted FID response factor for several Phenanthrene impurities

Impurity	Predicted response factor (pA s ppm ⁻¹)	Reference compound
Methylnaphthalene	0.8890	Naphthalene
Butenedioic acid, dibutyl ester	0.6778	Naphthalene
Dibenzofuran	0.8102	Dibenzothiophene
Methylbiphenyl	0.9315	Biphenyl
Xanthene	0.8169	Dihydroanthracene
Tetrahydro-phenanthrene or -anthracene	0.9289	Dihydroanthracene
Benzoquinoline	0.8909	Carbazole
Methyl-dibenzothiophene or -naphthothiophene	0.8037	Dibenzothiophene
Methyl-phenanthrene or -anthracene	0.9094	Anthracene
Methylcarbazole	0.8579	Carbazole
Anthracene/Maleic Anhydride Diels Alder adduct	0.6827	Dihydroanthracene

One can note that some impurities were not completely separated, as shown by their peak resolution (< 1.5). First, the couple Dibenzothiophene/Naphthothiophene (1st isomer) was not sufficiently resolved to permit the complete return to baseline. Similar observations can be made for the couples Phenanthrene/Anthracene (qualitative assessment of Anthracene peak resolution) and Benzoquinoline/Naphthothiophene (2nd isomer). However, these impurities could be quantified after signal integration by peak splitting.

In addition, the FID response factor for the unidentified impurity (29.29 min) could not be predicted. In this work, the lowest encountered RF value was chosen for this impurity (*e. g.*, 0.6778 pA s ppm⁻¹).

Eventually, the retention time of Anthracene on the sample chromatogram (*e. g.*, 29.03 min) was a bit higher than that observed during FID calibration (28.93 min). Consequently, to confirm the identity of the impurity associated with this peak, analyses of the same sample without and with addition of a low amount of Anthracene was performed. The chromatograms confirmed that the peak eluting at 29.03 min was Anthracene (see fig. 23).

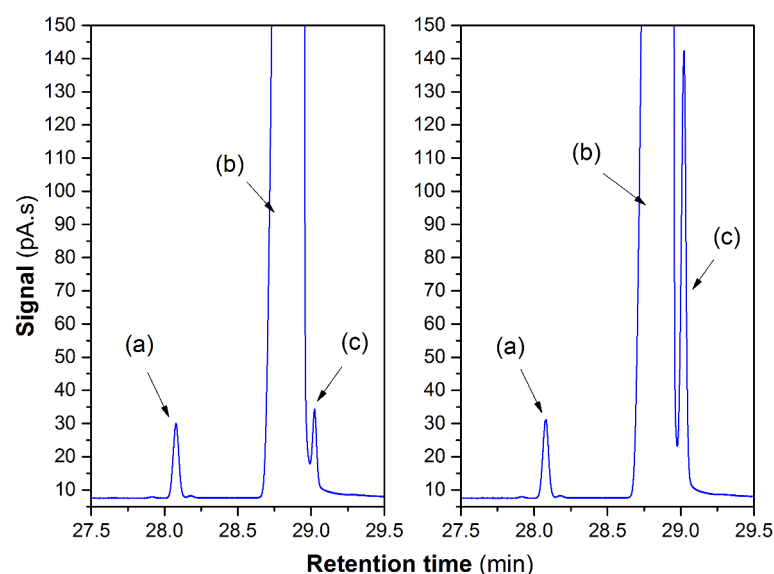


FIG. 23: **GC-FID chromatogram of technical grade Phenanthrene** – without (left) and with (right) addition of Anthracene, (a) Dibenzothiophene; (b) Phenanthrene; (c) Anthracene

Eventually, the chemical purity of this batch was measured at 90.8 wt. %, which is close to the indicative value given by Alfa Aesar.

ii. *Analysis of synthesis grade Phenanthrene (Alfa Aesar)*

Synthesis grade Phenanthrene provided by Alfa Aesar (98 % indicative purity) was analyzed by GC-FID and GC-MSD. GC-FID chromatographic data on this sample are entered in tab. 15. The chromatogram is shown in fig. 24.

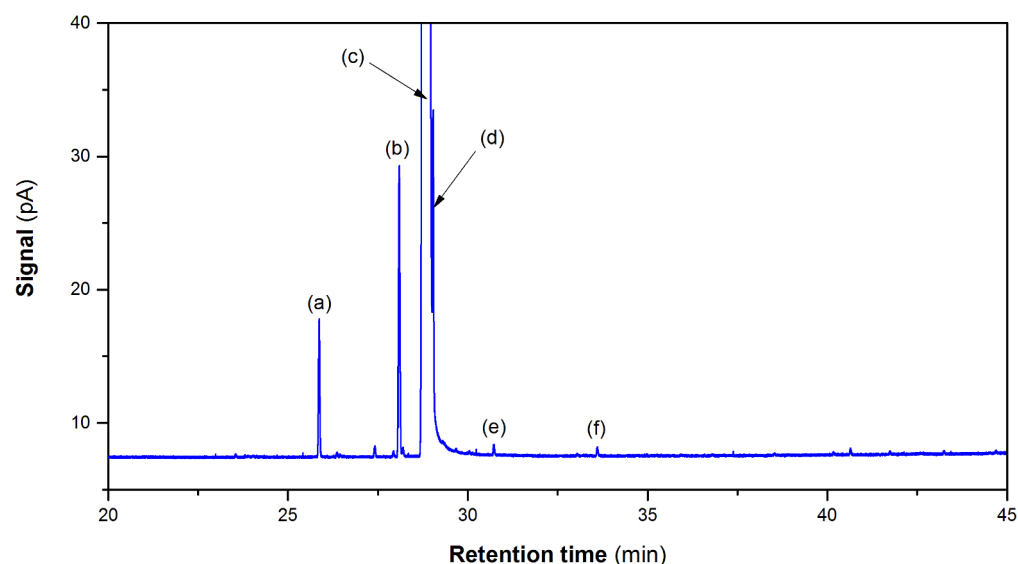


FIG. 24: **GC-FID chromatogram of synthesis grade Phenanthrene** – Alfa Aesar, 98 % indicative purity. (a) 9,10-dihydroanthracene, (b) Dibenzothiophene, (c) Phenanthrene, (d) Anthracene, (e) Carbazole, (f) Phenanthrenequinone.

TAB. 15: Chromatographic data for synthesis grade Phenanthrene analysis – Alfa Aesar, 98 % indicative purity

Impurity	Retention time in GC-FID (min)	Peak width at half height (min)	Peak resolution	Impurity level (wt. %)
Fluorene	23.56	0.0346	--	0.0052 ± 0.0003
9,10-dihydroanthracene	25.87	0.0366	32.44	0.285 ± 0.007
9,10-dihydrophenanthrene	26.37	0.0305	7.45	0.0077 ± 0.0001
1-methylfluorene	26.44	0.0317	1.13	0.0039 ± 0.0001
Tetrahydro-anthracene or -phenanthrene*	27.42	0.0416	13.4	0.022 ± 0.001
Dihydro-anthracene or -phenanthrene*	27.94	0.0420	6.22	0.012 ± 0.001
Dibenzothiophene	28.10	0.0462	1.81	0.809 ± 0.007
Naphthothiophene 1*	28.20	0.0451	1.10	0.025 ± 0.001
Anthracene	29.04	0.0309	--	0.393 ± 0.008
Naphthothiophene 2*	29.68	0.0398	9.05	0.008 ± 0.001
Methyl-dibenzothiophene or -naphthothiophene*	30.05	0.0374	4.79	0.006 ± 0.002
Carbazole	30.73	0.0386	8.95	0.0229 ± 0.0005
9,10-phenanthrenequinone	33.61	0.0388	37.2	0.021 ± 0.002
Anthracene/Maleic Anhydride Diels Alder adduct	40.65	0.0401	89.2	0.015 ± 0.004
			Total	1.64 ± 0.04

As shown by tab. 15 entries, synthesis grade Phenanthrene contains less impurities than technical grade one. Indeed, only 14 impurities were detected. 4 of them could not be strictly identified by means of injection of standards. Consequently, the identity of some isomers (highlighted in tab. 15 by asterisks) was not determined.

This sample contains 3 major impurities: 9,10-dihydroanthracene, Dibenzothiophene and Anthracene. All the other impurities were detected at low levels.

Two couples were not fully resolved (9,10-dihydroanthracene/1-methylfluorene and Dibenzothiophene/Naphthothiophene 1), but the corresponding impurities could be easily quantified by splitting peaks.

The chemical purity of this lot was assessed as being 98.36 wt. %, which conforms to indicative value provided by the manufacturer.

iii. Analysis of synthesis grade Phenanthrene (Sigma-Aldrich, lot 1)

Synthesis grade Phenanthrene provided by Sigma-Aldrich (98 % indicative purity) was analyzed according to the same procedure as described previously. GC-FID chromatographic data on this sample are entered in tab. 15. The chromatogram is shown in fig. 24.

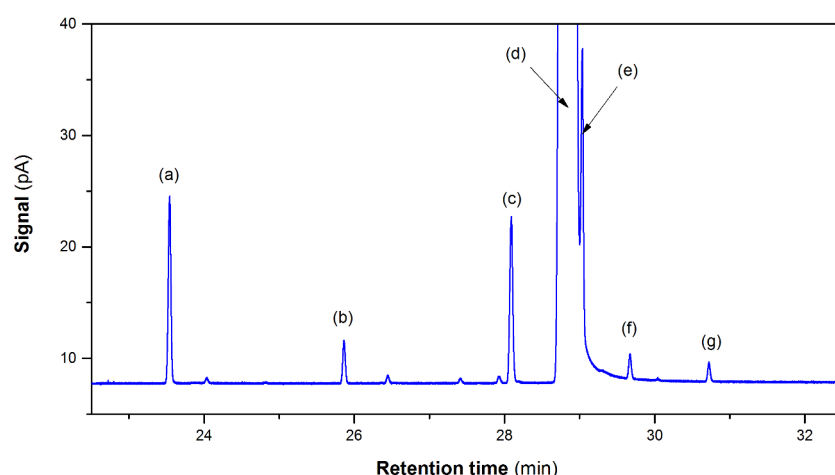


FIG. 25: **GC-FID chromatogram of synthesis grade Phenanthrene** – Sigma-Aldrich, lot 1, 98 % indicative purity. (a) Fluorene, (b) 9,10-dihydroanthracene, (c) Dibenzothiophene, (d) Phenanthrene, (e) Anthracene, (f) Naphthothiophene 2, (g) Carbazole

TAB. 16: **Chromatographic data for synthesis grade Phenanthrene analysis** – Sigma-Aldrich, lot 1, 98 % indicative purity.

Impurity	Retention time in GC-FID (min)	Peak width at half height (min)	Peak resolution	Impurity level (wt. %)
Fluorene	23.55	0.0413	--	0.46 ± 0.02
Methylbiphenyl*	24.04	0.0381	6.17	0.012 ± 0.002
9,10-dihydroanthracene	25.86	0.0328	25.7	0.102 ± 0.004
1-methylfluorene	26.45	0.0411	7.98	0.0180 ± 0.0007
Tetrahydro-anthracene or -phenanthrene*	27.41	0.0410	11.7	0.0114 ± 0.0003
Dihydro-anthracene or -phenanthrene*	27.93	0.0451	6.04	0.017 ± 0.002
Dibenzothiophene	28.09	0.0472	1.73	0.55 ± 0.02
Naphthothiophene 1*	28.19	0.0420	1.12	0.0061 ± 0.0001
Anthracene	29.04	0.0325	--	0.49 ± 0.01
Naphthothiophene 2*	29.67	0.0370	9.06	0.068 ± 0.001
Methyl-dibenzothiophene or -naphthothiophene*	30.03	0.0361	4.92	0.004 ± 0.001
Carbazole	30.72	0.0401	9.06	0.049 ± 0.002
Total				1.79 ± 0.06

In this sample, 13 impurities were detected. GC-MSD experiments served to determine the nature of these impurities, but not their exact identity (in case of isomers that could not be identified by injection of standards, see asterisks in tab. 16).

Except the Dibenzothiophene/Naphthothiophene 1 couple, all the peaks were sufficiently resolved for permitting the quantification of the corresponding impurities. For the non-resolved couple, peak splitting was applied to determine the levels.

The chemical purity was assessed as being 98.11 wt. %, which is close to the indicative purity value given by the manufacturer.

iv. *Analysis of synthesis grade Phenanthrene (Sigma-Aldrich, lot 2)*

Another synthesis grade Phenanthrene lot provided by Sigma-Aldrich was submitted to the same procedure of impurity identification and quantification. The GC-FID chromatogram is shown in fig. 26. Chromatographic data and impurity identities are entered in tab. 17.

Tab. 17: **Chromatographic data for synthesis grade Phenanthrene analysis** – Sigma-Aldrich, lot 2, 98 % indicative purity.

Impurity	Retention time in GC-FID (min)	Peak width at half height (min)	Peak resolution	Impurity level (wt. %)
Fluorene	23.54	0.0306	--	0.0051 ± 0.0005
9,10-dihydroanthracene	25.87	0.0395	33.2	0.31 ± 0.03
9,10-dihydrophenanthrene	26.36	0.0369	6.41	0.0085 ± 0.0002
1-methylfluorene	26.45	0.0304	1.34	0.0038 ± 0.0002
Tetrahydro-anthracene or -phenanthrene*	27.42	0.0390	14.0	0.023 ± 0.003
Dihydro-anthracene or -phenanthrene*	27.93	0.0404	6.42	0.012 ± 0.002
Dibenzothiophene	28.10	0.0457	1.97	0.87 ± 0.04
Naphthothiophene 1*	28.20	0.0484	1.06	0.029 ± 0.002
Anthracene	29.04	0.0309	--	0.409 ± 0.003
Naphthothiophene 2*	29.68	0.0404	8.98	0.0081 ± 0.0004
Methyl-dibenzothiophene or -naphthothiophene*	30.05	0.0327	5.06	0.0061 ± 0.0004
Carbazole	30.73	0.0408	9.25	0.023 ± 0.002
9,10-phenanthrenequinone	33.60	0.0394	35.8	0.023 ± 0.005
Anthracene/Maleic Anhydride Diels Alder adduct	40.64	0.0408	87.8	0.019 ± 0.004
Total				1.75 ± 0.08

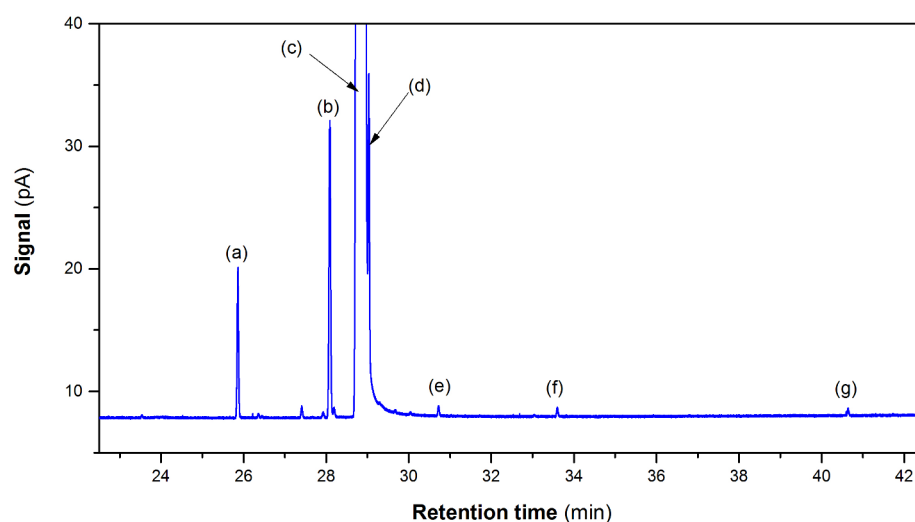


Fig. 26: **GC-FID chromatogram of synthesis grade Phenanthrene** – Sigma-Aldrich, lot 2, 98 % indicative purity. (a) 9,10-dihydroanthracene, (b) Dibenzothiophene, (c) Phenanthrene, (d) Anthracene, (e) Carbazole, (f) 9,10-phenanthrenequinone, (g) Anthracene/Maleic Anhydride Diels Alder adduct

For this Phenanthrene lot, most of the impurity peaks were well-resolved. Only two couples were not fully separated: 9,10-dihydrophenanthrene/1-methylfluorene and Dibenzothiophene/Naphthothiophene. These 4 impurities could be quantified by peak splitting.

This lot present 3 major impurities: 9,10-dihydroanthracene, Dibenzothiophene and Anthracene.

The purity of this sample was 98.25 wt. %, which complies with the indicative purity value given by the manufacturer.

d) Conclusion

In this part of the work, chromatographic conditions for the separation of Phenanthrene and its impurities were successfully established.

Various impurities were detected. Most of them were fused aromatic rings derivatives. Many isomers were detected, but their exact identity could not be determined by injection of standards, due to commercial unavailability or expansiveness. Consequently, their FID response factors were predicted using Saint Laumer *et al.* equation [33].

A few couples of impurity peaks were not sufficiently resolved to permit their specific quantification. However, integration by peak splitting was used to obtain reasonable estimations of their levels during quantification.

The detection thresholds were low enough to permit the measurement of ultrapurity in Phenanthrene.

4) General conclusion

In this chapter, a GC-FID method was developed in order to determine impurity levels in Phenanthrene samples. The chromatographic conditions were established thanks to a retention time prediction procedure, using a new retention model developed in the frame of this thesis.

The new retention model was presented during the 13th ISCC and GC×GC symposium in Riva del Garda (Italy, 2016, oral communication). The results were published in *Journal of Chromatography A*, in the dedicated special issue, after classical peer-review procedure [34].

The method developed in this chapter was tested on various Phenanthrene samples provided by different suppliers and exhibiting different purity grades. The results highlighted the robustness of the method and its ability at quantifying Phenanthrene impurities with honorable accuracies, even is some impurity levels were quantified after peak splitting due to insufficient resolutions. Moreover, thanks to low detection thresholds (< 0.0001 wt. %), Phenanthrene can be announced as being ultrapure when no impurity is detected.

As the validation of this method was successful, it was used for impurity level monitoring in upcoming purification experiments presented in the next chapter.

V. APPENDICES

1) Experimental retention time values for model parameter estimation

a) Column phase ratio determination

Experimental values of *n*-alkane retention times on the SLB-IL60 and DB-35ms columns can be found in tabs. S1 and S2, respectively.

Tab. S1: *n*-alkane retention times on the SLB-IL60 column

Inlet gauge pressure (psi)		10.0	20.0	30.0	40.0
Inlet absolute pressure (kPa)		170	239	308	377
n-C19 retention times (min) – N = 19					
Temperature (°C)	150	4.162	2.178	1.514	1.178
	160	3.338	1.749	1.220	0.953
	170	2.816	1.481	1.037	0.812
	180	2.485	1.311	0.921	0.710
	190	2.273	1.201	0.846	0.667
	200	2.135	1.132	0.798	0.631
n-C20 retention times (min) – N = 20					
Temperature (°C)	150	5.352	2.793	1.935	1.500
	160	4.086	2.134	1.483	1.154
	170	3.296	1.728	1.206	0.942
	180	2.802	1.474	1.032	0.795
	190	2.486	1.311	0.921	0.725
	200	2.282	1.207	0.850	0.670
n-C21 retention times (min) – N = 21					
Temperature (°C)	150	7.074	3.683	2.544	1.966
	160	5.144	2.678	1.855	1.439
	170	3.962	2.070	1.440	1.121
	180	3.232	1.695	1.184	0.911
	190	2.772	1.458	1.021	0.802
	200	2.476	1.307	0.918	0.723
n-C22 retention times (min) – N = 22					
Temperature (°C)	150	9.560	4.965	3.421	2.638
	160	6.637	3.447	2.381	1.842
	170	4.884	2.544	1.765	1.370
	180	3.817	1.996	1.390	1.068
	190	3.152	1.654	1.156	0.904
	200	2.730	1.438	1.008	0.791
n-C23 retention times (min) – N = 23					
Temperature (°C)	150	13.135	6.810	4.683	3.604
	160	8.741	4.529	3.121	2.409
	170	6.157	3.199	2.213	1.713
	180	4.610	2.404	1.669	1.282
	190	3.660	1.915	1.334	1.041
	200	3.063	1.609	1.125	0.881
n-C24 retention times (min) – N = 24					
Temperature (°C)	150	18.264	9.450	6.489	4.987
	160	11.688	6.048	4.159	3.203
	170	7.908	4.100	2.829	2.185
	180	5.681	2.955	2.046	1.57
	190	4.334	2.262	1.571	1.223
	200	3.497	1.833	1.278	0.999

Tab. S2: *n*-alkane retention times on the DB-35ms column

Inlet gauge pressure (psi)		10.0	20.0	30.0	40.0
Inlet absolute pressure (kPa)		170	239	308	377
n-C19 retention times (min) – N = 19					
Temperature (°C)	200	4.068	2.130	1.482	1.155
	210	3.326	1.747	1.220	0.954
	220	2.821	1.486	1.042	0.817
	230	2.474	1.307	0.919	0.724
	240	2.232	1.182	0.834	0.659
	250	2.062	1.095	0.774	0.613
n-C20 retention times (min) – N = 20					
Temperature (°C)	200	5.335	2.784	1.931	1.498
	210	4.189	2.192	1.525	1.188
	220	3.421	1.796	1.254	0.98
	230	2.898	1.526	1.069	0.839
	240	2.538	1.340	0.942	0.742
	250	2.286	1.211	0.854	0.674
n-C21 retention times (min) – N = 21					
Temperature (°C)	200	7.177	3.735	2.583	1.998
	210	5.423	2.828	1.961	1.523
	220	4.263	2.230	1.551	1.208
	230	3.485	1.828	1.277	0.998
	240	2.954	1.555	1.089	0.855
	250	2.586	1.365	0.96	0.756
n-C22 retention times (min) – N = 22					
Temperature (°C)	200	9.850	5.112	3.527	2.722
	210	7.179	3.735	2.582	1.999
	220	5.443	2.838	1.968	1.528
	230	4.293	2.245	1.562	1.217
	240	3.519	1.846	1.289	1.008
	250	2.987	1.572	1.102	0.865
n-C23 retention times (min) – N = 23					
Temperature (°C)	200	13.714	7.109	4.894	3.771
	210	9.677	5.023	3.465	2.675
	220	7.092	3.688	2.551	1.975
	230	5.406	2.818	1.956	1.519
	240	4.285	2.241	1.559	1.216
	250	3.524	1.849	1.291	1.010
n-C24 retention times (min) – N = 24					
Temperature (°C)	200	19.303	9.988	6.868	5.282
	210	13.219	6.850	4.717	3.636
	220	9.392	4.876	3.365	2.599
	230	6.933	3.607	2.496	1.933
	240	5.320	2.775	1.926	1.497
	250	4.240	2.219	1.545	1.205

Experimental values of solute retention times on the SLB-IL60 and DB-35ms columns can be found in tabs. S3 and S4, respectively.

Elution order ↓		Retention times (min)																					
		Inlet gauge pressure (psi)																					
		Inlet absolute pressure (kPa)																					
		Temperature (°C)																					
Solute																							
1	Fluorene	8.974	4.664	3.219	2.483	7.030	3.656	2.534	1.964	5.677	2.965	2.060	1.603	4.728	2.474	1.722	1.344	4.051	2.138	1.491	1.170		
2	9,10-dibenzanthracene	10.030	5.202	3.587	2.766	7.726	4.014	2.780	2.151	6.146	3.207	2.226	1.730	5.050	2.639	1.836	1.433	4.274	2.254	1.571	1.233		
3	9,10-dihydrophenanthrene	10.081	5.333	3.664	2.874	7.912	4.111	2.846	2.202	6.289	3.280	2.277	1.769	5.160	2.696	1.874	1.460	4.360	2.298	1.600	1.253		
4	1-methylfluorene	13.118	6.793	4.605	3.603	9.863	5.115	3.534	2.729	7.654	3.983	2.758	2.138	6.130	3.195	2.216	1.723	5.061	2.662	1.849	1.445		
5	Dibenzanthracene	20.770	10.733	7.373	5.672	15.259	7.893	5.439	4.187	11.528	5.981	4.128	3.189	8.954	4.653	3.214	2.488	7.164	3.752	2.595	2.017		
6	Phenanthrene	28.154	14.528	9.972	7.666	20.258	10.463	7.200	5.536	14.966	7.756	5.345	4.122	11.380	5.899	4.067	3.142	8.889	4.647	3.209	2.487		
7	Anthracene	29.026	14.976	10.276	7.899	20.828	10.763	7.405	5.691	15.346	7.961	5.486	4.230	11.658	6.042	4.165	3.217	9.078	4.750	3.279	2.541		
8	2-methylanthracene	42.431	21.856	15.004	11.512	29.583	15.272	10.490	8.053	21.183	10.968	7.546	5.809	15.611	8.079	5.561	4.287	11.815	6.167	4.249	3.284		
9	9-methylanthracene	47.362	24.403	16.729	12.858	32.909	16.970	11.663	8.952	23.471	12.145	8.356	6.430	17.213	8.908	6.128	4.722	12.953	6.763	4.657	3.598		
10	dimethylanthracene	75.971	39.195	26.894	20.615	51.390	26.510	18.182	13.942	35.548	18.394	12.637	9.716	25.333	13.086	8.992	6.917	18.479	9.638	6.626	5.105		
11	Carbazole	160.810	82.926	56.811	43.591	105.940	54.587	37.435	28.691	71.544	36.883	25.310	19.441	49.402	25.501	17.488	13.430	34.893	18.190	12.481	9.595		

← Elution order	Inlet gauge pressure (psi)																			
	10.0	20.0	30.0	40.0	10.0	20.0	30.0	40.0	10.0	20.0	30.0	40.0	10.0	20.0	30.0	40.0	10.0	20.0	30.0	40.0
	Inlet absolute pressure (kPa)																			
	170	239	308	377	170	239	308	377	170	239	308	377	170	239	308	377	170	239	308	377
Temperature (°C)																				
150 150 150 150 160 160 160 160 170 170 170 170 180 180 180 180 190 190 190 190																				
Solute																				
Retention times (min)																				
1	Fluorene 13.179 6.823 4.685 3.598 9.686 5.004 3.438 2.645 7.334 3.801 2.615 2.009 5.741 2.978 2.050 1.580 4.640 2.414 1.665 1.282																			
2	9,10-dihydroanthracene 19.807 10.236 7.026 5.391 14.028 7.249 4.977 3.826 10.260 5.313 3.365 2.803 7.750 4.016 2.761 2.126 6.052 3.140 2.162 1.664																			
3	9,10-dihydroanthracene 21.692 11.223 7.700 5.903 15.302 7.912 5.432 4.176 11.163 5.770 3.969 3.051 8.422 4.364 2.996 2.305 6.536 3.385 2.330 1.792																			
4	1-methylanthracene 22.055 11.406 7.820 6.001 15.519 8.023 5.504 4.227 11.253 5.829 4.001 3.069 8.422 4.364 2.996 2.305 6.536 3.385 2.330 1.792																			
5	Dibenzophenone 20.923 15.468 10.602 8.136 18.807 7.738 5.665 4.924 7.713 5.297 4.064 3.110 5.697 3.913 3.009 8.368 4.341 2.985 2.284 1.804																			
6	Phenanthrene 33.938 17.532 12.027 9.228 23.419 12.099 8.298 6.372 16.658 8.609 5.910 4.535 12.184 6.304 4.329 3.329 9.198 4.761 3.274 2.513																			
7	Anthracene 35.406 18.317 12.551 9.628 24.387 12.595 8.640 6.630 17.252 8.931 6.131 4.704 12.601 6.520 4.477 3.442 9.482 4.908 3.375 2.559																			
8	Carbazole 52.191 26.954 18.464 14.161 34.752 17.949 12.313 9.445 23.867 12.336 8.458 6.493 16.885 8.739 5.995 4.606 12.335 6.380 4.384 3.367																			
9	2-methylanthracene 57.752 29.795 20.421 15.672 38.419 19.866 13.624 10.449 26.361 13.632 9.352 7.172 18.643 9.636 6.615 5.073 13.558 7.015 4.819 3.699																			
10	9-methylanthracene 75.338 38.867 26.659 20.465 49.657 25.660 17.581 13.494 33.743 17.444 11.962 9.179 23.554 12.194 8.356 6.416 16.947 8.754 6.011 4.613																			
11	9,10-dihydroanthracene 161.593 83.340 57.095 43.742 102.693 55.961 36.340 27.810 67.220 36.481 23.773 18.216 45.187 23.292 15.995 12.284 31.193 16.115 11.063 8.481																			

2) Analysis of Phenanthrene by GC-MSD

During GC-MSD experiments, the following chromatographic conditions were applied:

Analyses were run on a Thermo Trace Gas Chromatograph equipped with a split/splitless injector (300 °C), a Thermo AS3000 autosampler (10 µL syringe, 1 µL injection volume), an Agilent DB-35ms column (30 m × 0.25 mm × 0.25 µm) and a Thermo ITQ-900 Mass Spectrometer Detector.

Helium was used as carrier gas (1.0 mL·min⁻¹). The temperature program was: isothermal step at 100 °C for 10 min, then heating ramp at 5 °C·min⁻¹ up to 270 °C, then isothermal step for 20 min.

Before and after every injection, the syringe was washed 5 times with HPLC grade Acetone. The syringe was also washed 5 times with the sample solution.

The MSD transfer line and ion source temperatures were set at 300 and 200 °C, respectively. Solute were ionized by electronic impact (70 eV). Positive charge ions were scanned every 0.15 s from 50 to 300 m/z range.

Note that, in these conditions, solute elution order was assumed to be the same as that observed in GC-FID in the conditions described in part IV.2)a (p. 152).

Solute mass spectra were compared to NIST database entries (2007) to identify the impurities.

VI. REFERENCES

- [1] B.J. McArdle, J.N. Sherwood, A.C. Damask, The growth and perfection of phenanthrene single crystals, *J. Cryst. Growth*. 22 (1974) 193–200. doi:10.1016/0022-0248(74)90094-3.
- [2] W.-C. Lee, G.-J. Tsai, G.T. Tsao, Analysis of chromatography by plate theory, *Sep. Technol.* 3 (1993) 178–197. doi:10.1016/0956-9618(93)80018-M.
- [3] J. Tranchant, *Chromatographie en phase gazeuse*, Tech. Ing. (n.d.). <http://www.techniques-ingenieur.fr/ezproxy.normandie-univ.fr/base-documentaire/mesures-analyses-th1/chromatographie-et-techniques-separatives-42385210/chromatographie-en-phase-gazeuse-p1485/>.
- [4] R.L. Grob, E.F. Barry, eds., *Modern practice of gas chromatography*, 4. ed, Wiley-Interscience, Hoboken, NJ, 2004.
- [5] G. Guiochon, C.L. Guillemin, *Quantitative gas chromatography for laboratory analyses and on-line process control*, Elsevier, Amsterdam, 1988.
- [6] G. Castello, P. Moretti, S. Vezzani, Retention models for programmed gas chromatography, *J. Chromatogr. A*. 1216 (2009) 1607–1623. doi:10.1016/j.chroma.2008.11.049.
- [7] J. Tranchant, *Manuel pratique de chromatographie en phase gazeuse*, Elsevier Masson, 1995.
- [8] J.V. Hinshaw, L.S. Ettre, The variation of carrier gas viscosities with temperature, *J. High Resolut. Chromatogr.* 20 (1997) 471–481. doi:10.1002/jhrc.1240200903.
- [9] S.J. Hawkes, Viscosities of carrier gases at gas chromatograph temperatures and pressures, *Chromatographia*. 37 (1993) 399–401. doi:10.1007/BF02272255.
- [10] H. Snijders, H.-G. Janssen, C. Cramers, Optimization of temperature-programmed gas chromatographic separations I. Prediction of retention times and peak widths from retention indices, *J. Chromatogr. A*. 718 (1995) 339–355. doi:10.1016/0021-9673(95)00692-3.
- [11] E.N. Fuller, P.D. Schettler, J.C. Giddings, New method for prediction of binary gas-phase diffusion coefficients, *Ind. Eng. Chem.* 58 (1966) 18–27. doi:10.1021/ie50677a007.
- [12] C.R. Wilke, P. Chang, Correlation of diffusion coefficients in dilute solutions, *AIChE J.* 1 (1955) 264–270. doi:10.1002/aic.690010222.
- [13] D. Ryan, P. Marriott, Comprehensive two-dimensional gas chromatography, *Anal. Bioanal. Chem.* 376 (2003) 295–297. doi:10.1007/s00216-003-1934-x.
- [14] D. Ryan, P. Morrison, P. Marriott, Orthogonality considerations in comprehensive two-dimensional gas chromatography, *J. Chromatogr. A*. 1071 (2005) 47–53. doi:10.1016/j.chroma.2004.09.020.
- [15] C.J. Venkatramani, J. Xu, J.B. Phillips, Separation Orthogonality in Temperature-Programmed Comprehensive Two-Dimensional Gas Chromatography, *Anal. Chem.* 68 (1996) 1486–1492. doi:10.1021/ac951048b.
- [16] B. Omais, M. Courtiade, N. Charon, J. Ponthus, D. Thiébaud, Considerations on Orthogonality Duality in Comprehensive Two-Dimensional Gas Chromatography, *Anal. Chem.* 83 (2011) 7550–7554. doi:10.1021/ac201103e.
- [17] G. Semard, V. Peulon-Agasse, A. Bruchet, J.-P. Bouillon, P. Cardinaël, Convex hull: A new method to determine the separation space used and to optimize operating conditions for comprehensive two-dimensional gas chromatography, *J. Chromatogr. A*. 1217 (2010) 5449–5454. doi:10.1016/j.chroma.2010.06.048.
- [18] C. Nerín, C. Domeño, J. Salafranca, 3.38 - Advances in Sample Preparation of Environmental Solid Matrices, in: J. Pawliszyn (Ed.), *Compr. Sampl. Sample Prep.*, Academic Press, Oxford, 2012: pp. 783–796. doi:10.1016/B978-0-12-381373-2.00113-7.
- [19] C.J. King, *Separation Processes* (2nd ed.), Dover Publications, New York, 2013.
- [20] J. Randon, L. Maret, C. Ferronato, Gas chromatography–mass spectroscopy optimization by computer simulation, application to the analysis of 93 volatile organic compounds in workplace ambient air, *Anal. Chim. Acta*. 812 (2014) 258–264. doi:10.1016/j.aca.2014.01.016.
- [21] Z. Wu, Retention simulation in gas chromatography, *J. Chromatogr. A*. 840 (1999) 137–143. doi:10.1016/S0021-9673(99)00124-7.
- [22] F. Aldaeus, Y. Thewalim, A. Colmsjö, Prediction of retention times and peak widths in temperature-programmed gas chromatography using the finite element method, *J. Chromatogr. A*. 1216 (2009) 134–139. doi:10.1016/j.chroma.2008.11.038.
- [23] A. Barcaru, A. Anroedh-Sampat, H.-G. Janssen, G. Vivó-Truyols, Retention time prediction in temperature-programmed, comprehensive two-dimensional gas chromatography: Modeling and error assessment, *J. Chromatogr. A*. 1368 (2014) 190–198. doi:10.1016/j.chroma.2014.09.055.

- [24] A. Felinger, B. Boros, R. Ohmacht, Effect of pressure on retention factors in HPLC using a non-porous stationary phase, *Chromatographia*. 56 (2002) S61–S64. doi:10.1007/BF02494114.
- [25] M. Martin, G. Guiochon, Effects of high pressure in liquid chromatography, *J. Chromatogr. A*. 1090 (2005) 16–38. doi:10.1016/j.chroma.2005.06.005.
- [26] D.L. Anderson, Thermodynamics and Equations of State, in: *Theory Earth*, Blackwell Scientific Publications, Boston, 1989: pp. 79–102.
- [27] CRC Handbook of Chemistry and Physics, 97th Edition, CRC Press, W. M. Haynes, n.d.
- [28] A. Wouk, *New Computing Environments: Microcomputers in Large-scale Computing*, SIAM, 1987.
- [29] A. Fredenslund, *Vapor-Liquid Equilibria using UNIFAC*, Elsevier, Amsterdam, 1977.
- [30] T. Górecki, J. Harynuk, O. Panić, The evolution of comprehensive two-dimensional gas chromatography (GC×GC), *J. Sep. Sci.* 27 (2004) 359–379. doi:10.1002/jssc.200301650.
- [31] Z. Jiang, J. Crassous, V. Schurig, Gas-chromatographic separation of tri(hetero)halogenomethane enantiomers, *Chirality*. 17 (2005) 488–493. doi:10.1002/chir.20191.
- [32] J. Li, P.W. Carr, Extra-thermodynamic relationships in chromatography enthalpy-entropy compensation in gas chromatography, *J. Chromatogr. A*. 670 (1994) 105–116. doi:10.1016/0021-9673(94)80285-8.
- [33] J.-Y. de Saint Laumer, E. Cicchetti, P. Merle, J. Egger, A. Chaintreau, Quantification in Gas Chromatography: Prediction of Flame Ionization Detector Response Factors from Combustion Enthalpies and Molecular Structures, *Anal. Chem.* 82 (2010) 6457–6462. doi:10.1021/ac1006574.
- [34] A. Burel, M. Vaccaro, Y. Cartigny, S. Tisse, G. Coquerel, P. Cardinael, Retention modeling and retention time prediction in gas chromatography and flow-modulation comprehensive two-dimensional gas chromatography: The contribution of pressure on solute partition, *J. Chromatogr. A*. 1485 (2017) 101–119. doi:10.1016/j.chroma.2017.01.011.

Chapter IV

Ultrapurification of Phenanthrene by crystallization

Chapter IV

ULTRAPURIFICATION OF PHENANTHRENE BY CRYSTALLIZATION

TABLE OF CONTENTS

NOMENCLATURE.....	175
I. INTRODUCTION.....	176
II. PURIFICATION BY ZONE MELTING.....	180
1) Introduction	180
2) Basic notions on Zone Melting	180
a) Zone Melting modeling.....	181
b) Influence of phase equilibria and molten zone displacement rate.....	184
c) Summary.....	186
3) Presentation of a new prototype dedicated to organic solids	187
4) Phase equilibria between Phenanthrene and some of its impurities	189
a) Introduction.....	189
b) Experimental procedures.....	192
c) Study of the Phenanthrene/9,10-dihydroanthracene binary system.....	193
d) Re-investigation of the Phenanthrene-Carbazole binary system.....	195
e) Re-investigation of the Phenanthrene/Fluorene binary system.....	199
f) Re-investigation of the Phenanthrene/Dibenzothiophene binary system.....	202
g) Re-investigation of the Phenanthrene-Anthracene binary system.....	204
h) Summary.....	208
5) Zone Refinement of Phenanthrene samples	210
a) Validation of the SMS laboratory Zone Melting device efficiency.....	210
b) Attempt of Phenanthrene ultrapurification by Zone Melting.....	217
6) Conclusions	219
III. PURIFICATION BY VACUUM SUBLIMATION.....	220
1) Introduction	220
2) Development of a new gradient sublimier	222
a) Presentation of the first gradient sublimation prototype.....	222
b) Presentation of the new gradient sublimier designed in our laboratory.....	223
3) Phenanthrene purification experiments	224
4) Discussion, conclusion and outlooks	226
IV. PURIFICATION BY CO-CRYSTALLIZATION.....	227
1) Introduction	227
2) Phenanthrene known co-crystals	229
3) Screening of Phenanthrene new co-formers	231
a) Discovery of new Phenanthrene co-formers.....	231
b) Determination of the stoichiometry of new Phenanthrene co-crystals.....	235
c) Summary.....	235

4) Phenanthrene purification experiments.....	236
5) Discussion.....	241
6) Conclusions and outlooks.....	243
V. COMBINATORIAL APPROACHES.....	244
1) Introduction.....	244
2) Purification by co-crystallization and Zone Melting.....	245
a) Introduction.....	245
b) Experimental part.....	245
i. Phenanthrene pre-purification by co-crystallization.....	245
ii. Purification by Zone Melting.....	245
c) Results and discussion.....	246
d) Conclusion.....	248
3) Purification by chemical modification and crystallization.....	249
a) Introduction.....	249
b) Chemical reactivity of Phenanthrene impurities.....	249
i. Fluorene and its derivatives.....	249
ii. Dihydroanthracenes and dihydrophenanthrenes.....	249
iii. Dibenzothiophene and its derivatives.....	250
iv. Anthracene and its derivatives.....	250
v. Carbazole and its derivatives.....	251
vi. Summary.....	252
c) Purification of Phenanthrene by chemical treatments.....	253
i. Purification of Phenanthrene by treatment with Maleic Anhydride.....	253
ii. Purification of Phenanthrene by impurity alkylation and co-crystallization of treated product.....	254
iii. Purification of Phenanthrene by hydrogenation treatment and co-crystallization.....	259
d) Conclusion.....	263
VI. CONCLUSION.....	266
VII. APPENDICES.....	268
1) Supplementary bibliographic item.....	268
2) Methods.....	268
a) X-Ray Powder Diffraction.....	268
b) Differential Scanning Calorimetry.....	268
c) Analytical Gas Chromatography for ternary phase diagram investigations.....	268
3) Pre-purification of products for phase equilibria investigation.....	270
4) Composition data on ternary systems investigated in this work.....	271
5) Screening of Phenanthrene new co-formers.....	273
6) Determination of the stoichiometry of the discovered co-crystals.....	277
VIII. REFERENCES.....	281

NOMENCLATURE

Abbreviations

35DNBA	3,5-dinitrobenzoic acid
ANT	Anthracene
CARB	Carbazole
CC	Co-crystal
DBT	Dibenzothiophene
DHA	Dihydroanthracene
DSC	Differential Scanning Calorimetry
FID	Flame Ionization Detector
FLU	Fluorene
GC	Gas Chromatography
HT	High temperature
IP	Intermediate phase
L	Liquid
LT	Low temperature
MSD	Mass spectrometer detector
ss	Solid solution
wt	Weight
XRPD	X-Ray Powder Diffraction

Symbols

D	[m ² s ⁻¹]	Diffusion coefficient in molten zone
e	[m]	Molten zone thickness
j	[-]	Zone pass rank
k	[-]	Impurity effective segregation coefficient
k_0	[-]	Impurity equilibrium segregation coefficient
l	[m]	Ingot length
S	[m ²]	Ingot cross-section
v	[m s ⁻¹]	Molten zone translation rate
x	[m]	Position of molten zone solidification interface
X	[-]	Impurity mole fraction

Greek symbol

δ	[m]	Impurity diffusion layer length in the molten zone
----------	-----	--

I. INTRODUCTION

Due to unusual observations made on Phenanthrene solid-solid transition at atmospheric pressure (see chapter II), many questions raised about the related mechanism at the molecular scale. In particular, the origin (*e. g.*, Phenanthrene itself, or its impurities) of such an unusual transition is, up to now, unknown. Consequently, this point remains to be investigated, which requires the ultrapurification of the product (*e. g.*, the increase of molar purity above 99.9 %). The aim of this chapter is to propose crystallization procedures to reach this goal. In this view, chromatographic measurements were performed using the analytical method developed in chapter III, in order to monitor crystallization method purifying effects.

During the purification of an impure substance by crystallization from a liquid phase, two cases can be encountered:

- (i) The molecules of the species to purify self assembly to crystallize without impurities. The latter remain in the liquid phase.
- (ii) The molecules of the component of interest self assembly to form crystals, with random substitution or insertion of impurities in the available crystallographic sites. In this case, they form a solid solution. To observe that, the impurities should be structurally similar to the major component to ensure the stability of intermolecular bond network (substitution), or small enough to insert in crystallographic sites.

As previously stated in chapter I, the existence of a partial solid solution between the compound to purify and its impurities can be assessed by means of a simple solvent assisted recrystallization. If an impurity still remains in the recrystallized substance, then there exists a solid solution. In this case, they cannot be completely eliminated by this procedure.

In the case of Phenanthrene, a preliminary recrystallization test applied to technical-grade material¹ shown that most of its impurities were still present in the purified material. The chromatograms of Phenanthrene samples before and after recrystallization are shown in fig. 1, and the variation of impurity levels in tab. 1. The molecular structures of all the impurities mentioned in this chapter are shown in fig. 2.

Except Methylnaphthalene, Butenedioic acid dibutyl ester, Xanthene and one Tetrahydroanthracene or -phenanthrene, all the impurities were still detected in the recrystallized product, which indicates the existence of a solid solution of Phenanthrene. Consequently, other crystallization procedures should be developed and adapted in order to attempt their removal.

1. 2 g of Phenanthrene (Alfa Aesar, 90 % indicative purity, technical grade) was recrystallized at room temperature under magnetic stirring for 24 h in 2 g of HPLC grade Acetone (VWR Chemicals). The suspension was recovered by filtration over a 2-porosity glass filter. The crystals were washed with 10 mL of cold (0 °C) HPLC grade Methanol (VWR Chemicals) and were dried overnight at 50 °C. The impurity levels in Phenanthrene before and after recrystallization were determined by GC-FID. Impurity identities were determined using complementary GC-MSD experiments.

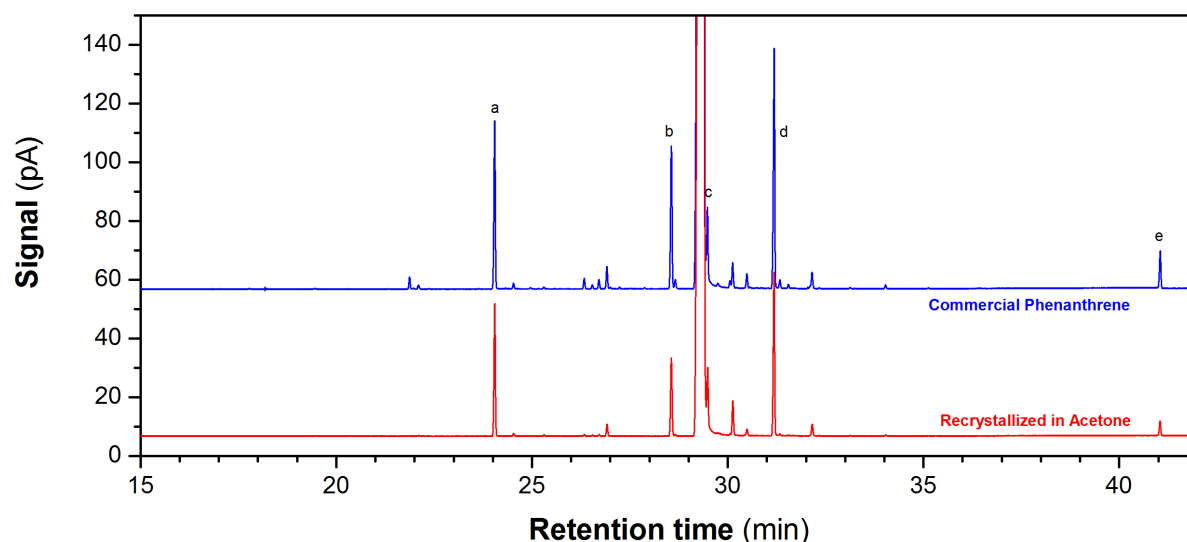


FIG. 1: **Normalized GC-FID chromatograms of technical grade Phenanthrene samples before and after recrystallization in Acetone** – major impurities: a. Fluorene, b. Dibenzothiophene, c. Anthracene, d. Carbazole, e. Anthracene/Maleic Anhydride Diels Alder adduct

TAB. 1: **Impurity levels (in wt. %) in technical grade Phenanthrene** – impurities are sorted by ascending elution order

Impurity	Commercial	Recrystallized in Acetone
Biphenyl	0.0071 ± 0.0004	ND
Methylnaphthalene*	0.0068 ± 0.0002	0.0047 ± 0.0003
Butenedioic acid, dibutyl ester*	0.158 ± 0.008	ND
Dibenzofuran	0.0451 ± 0.0002	0.0083 ± 0.0002
Fluorene	1.692 ± 0.0002	1.21 ± 0.02
Methylbiphenyl*	0.054 ± 0.002	0.0227 ± 0.0004
Xanthene	0.017 ± 0.005	ND
Fluorene isomer*	0.018 ± 0.002	0.0134 ± 0.0003
9,10-dihydroanthracene	0.099 ± 0.005	0.0154 ± 0.0005
Dihydroanthracene/phenanthrene*	0.0365 ± 0.0003	0.0099 ± 0.0003
Dihydroanthracene/phenanthrene*	0.087 ± 0.002	0.0143 ± 0.0004
9,10-dihydrophenanthrene	0.209 ± 0.003	0.104 ± 0.002
Tetrahydroanthracene/phenanthrene*	0.017 ± 0.002	ND
Tetrahydroanthracene/phenanthrene*	0.012 ± 0.001	0.0034 ± 0.0001
Dibenzothiophene	1.78 ± 0.04	0.91 ± 0.02
Naphthothiophene 1*	0.114 ± 0.003	0.023 ± 0.002
Anthracene	0.554 ± 0.005	0.37 ± 0.02
Unknown impurity	0.0446 ± 0.0002	0.022 ± 0.007
Benzoquinoline*	0.0639 ± 0.0004	0.0101 ± 0.0002
Naphthothiophene 2*	0.297 ± 0.004	0.365 ± 0.008
Methyldibenzothiophene/naphthothiophene*	0.17 ± 0.02	0.072 ± 0.004
Carbazole	2.8 ± 0.2	1.61 ± 0.03
Methylphenanthrene/anthracene (isomer 1)*	0.0831 ± 0.0008	0.0145 ± 0.0007
Methylphenanthrene/anthracene (isomer 2)*	0.036 ± 0.004	0.0056 ± 0.0005
Methylphenanthrene/anthracene (isomer 3)*	0.157 ± 0.009	0.111 ± 0.003
Methylcarbazole*	0.012 ± 0.002	0.005 ± 0.001
9,10-phenanthrenequinone	0.04 ± 0.02	0.0121 ± 0.0002
Anthracene/Maleic Anhydride Diels Alder adduct	0.55 ± 0.09	0.18 ± 0.02
Total	9.2 ± 0.4	5.1 ± 0.2

ND: Not detected (< 0.0001 wt. %) – *undetermined isomer²

2. GC-MSD complementary experiments allowed for determining the mass of the corresponding impurities, which provided partial knowledge on their chemical structures. In case of existence of isomers, no complete identification of them could be achieved by solely use of mass spectra, due to high similarities.

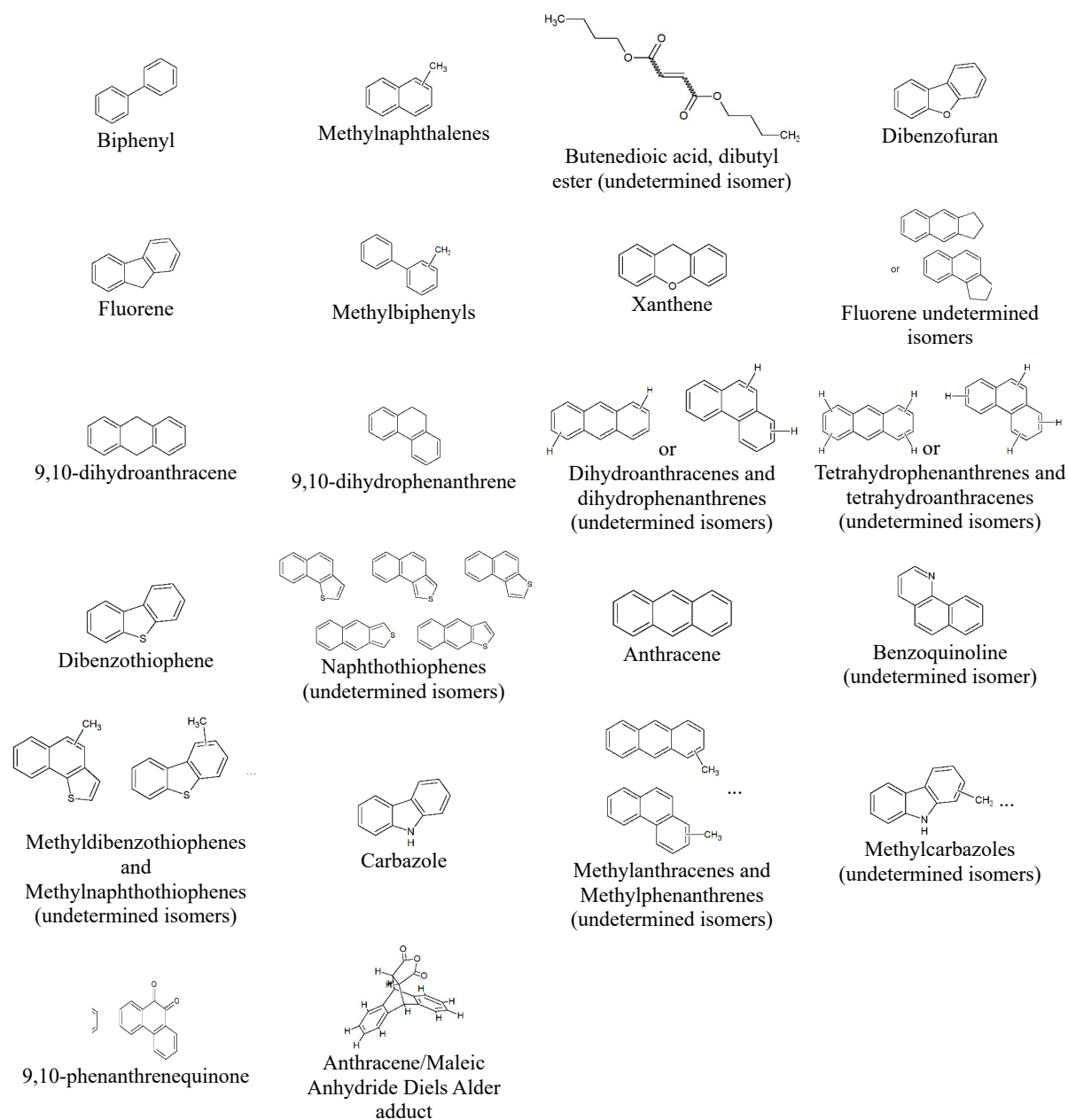


FIG. 2: **Molecular structures of Phenanthrene starting impurities mentioned in this chapter**

In this thesis, several pathways were investigated in view to reach ultrapure Phenanthrene. First, Zone Melting was applied to Phenanthrene, in order to benefit from multi-stage recrystallization from the melt and amplify impurity partial elimination as well as the number of zone passes is increased. In part II, this technique is presented into more details. A new prototype, designed in our laboratory, is also introduced. Validation and purification experiments are reported, and results are discussed with particular attention paid to phase equilibria between Phenanthrene and its impurities.

Thereafter, Phenanthrene purification was attempted by means of vacuum sublimation, using a gradient sublimator designed in our laboratory. Prototype and process developments are reported in part III, as well as the results on purification experiments.

Then, co-crystallization was tested on Phenanthrene and was found to exhibit an efficiency different to that of Zone Melting and simple recrystallization with respect to the different impurities. The different works related to the development of this technique, and its application to Phenanthrene, are reported in part IV.

Eventually, thanks to the key learnings highlighted during the previous parts, combinatorial approaches were attempted to access to ultrapure Phenanthrene. Two pathways were investigated: (i) purification by co-crystallization, followed by Zone Melting; (ii) purification by impurity chemical modification, followed by their elimination using co-crystallization. These works are reported in part V.

A discussion of the purifying effects of these procedures was attempted in a last part. A particular attention was paid to the relationship between impurity molecular structure and discrimination in the solid state during crystallization.

II. PURIFICATION BY ZONE MELTING

1) Introduction

Zone Melting is a well-known technique that serves to grow crystals from the melt. This method was invented and patented in the early 50's by William Gardner Pfann (1917-1982), an American engineer from Bell Labs company [1,2]. Many variants and applications were previously reported: purification of chemical species (in this case, Zone Melting is generally called "*zone refining*"); growth of ultrapure single crystals; design of semiconductors, etc [3]. In this thesis, the method was used to attempt Phenanthrene ultrapurification using a device developed by our team.

In this chapter, basic theoretical and applied notions on Zone Melting are provided in part 2. Then, a description of the prototype designed in our laboratory is made in part 3. Binary phase equilibria between Phenanthrene and its major impurities were (re-)investigated in part 4, in which the applicability of the method to Phenanthrene is also discussed. Eventually, purification experiments were performed in order to: (i) validate our device, (ii) attempt Phenanthrene ultrapurification. Results and discussion on these points are provided in part 5, before concluding on this method (part 6).

2) Basic notions on Zone Melting

At the time of its invention, Zone Melting (pictures shown in fig. 3) was some kind of revolution in the field of material science. Indeed, this method allowed to reach extremely high purity values for semi-conductive inorganic materials (Germanium, Silicone...) widely used to design transistors dedicated to telephones [4]. Indeed, the level of impurities in the treated substances could be decreased to 1 part per 10 billion (only 10^{-8} % impurity!). Such performance was clearly more interesting than those of the techniques that were used to attempt Silicone purification (pyro- and hydrometallurgy) before the introduction of Zone Melting. It also played a significant role in the rise of new efficient electronics-based technologies (microprocessors, etc) [5].

The principle of the technique can be summarized as follows: the substance to purify is molten and resolidified in a glass tube to form an ingot. Then, a molten zone is generated at one end of the ingot using a heating device. Subsequently, the zone is slowly displaced from one extremity to the other. According to the difference of impurity solubilities in the zone and the solid slice that recrystallizes at every displacement of the heater, impurities can be displaced towards the different ends of the ingot. Generally, one single zone pass is not sufficient to obtain high purity sample at a given part of the ingot. Therefore, several passes are generally performed to amplify impurity concentration at ingot ends until reaching purity specification.

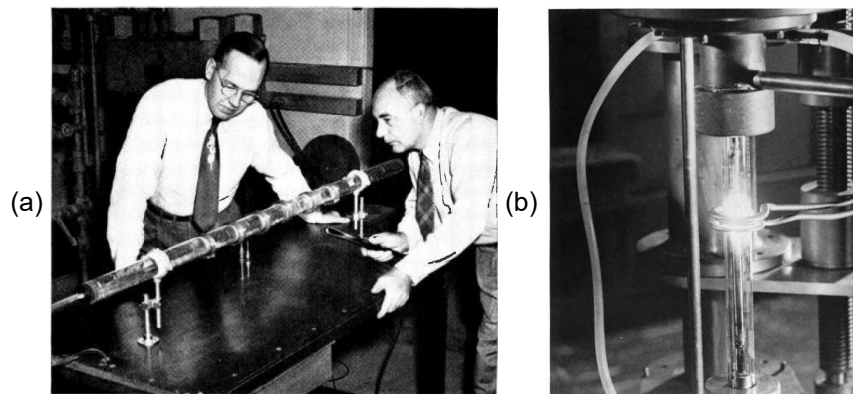


FIG. 3: **First Zone Melting devices** – (a) W. G. Pfann (left) presenting the technique to one of its co-workers, from *Radio & Television News* (1954) [4]; (b) picture of a vertical Zone Refiner, from *The Michigan Technic* (1959) [6].

a) Zone Melting modeling

The modeling of Zone Melting process is well documented [3]. Previous works detailed the prediction of impurity distribution profiles in the treated products after application of the technique.

The basic principle of Zone Melting is represented in fig. 4, in which are considered an ingot of length l , treated by means of a molten zone of thickness e . In the frame of reference of molten zone traveling, the solidification and melting interfaces are located at positions x and $x + e$, respectively.

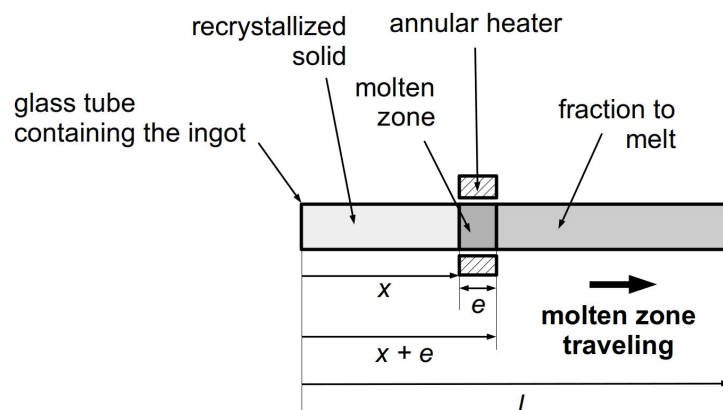


FIG. 4: **Schematic representation of a Zone Melting device**

Zone Melting process can be divided into two steps: when the solidification interface is located between $0 \leq x \leq l - e$, the molten zone remains constant in thickness and is continuously supplied with the fraction to melt at the melting interface. This step corresponds to “*pure Zone Melting*”. Conversely, when the melting interface reaches the end of the ingot ($l - e < x < l$), the zone length progressively decreases ($e = l - x$), as no matter income occurs. This solidification pathway is called “*normal freezing*”. Consequently, these two steps can be described using different matter balance equations.

Application of balance equations on molten zone served at establishing differential equations that relate impurity level as a function of the position in the treated ingot. Eqs. 1 and 2 should be applied in the $0 \leq x \leq l - e$ and $l - e < x < l$ regions, respectively.

$$\frac{dX_j(x)}{dx} = \frac{k}{e} [X_{j-1}(x+e) - X_j(x)] \text{ with } X_j(x=0) = \frac{k}{e} \int_{x=0}^{x=e} X_{j-1} \cdot dx \quad (1)$$

$$\frac{dX_j(x)}{dx} = \frac{(1-k) \cdot X_j(x)}{l-x} \quad (2)$$

with:

- X_j : impurity fraction in the resolidified fraction after molten zone pass of rank j
- X_{j-1} : impurity fraction in the resolidified fraction after molten zone pass of rank $j-1$
- k : impurity segregation coefficient

k , the impurity segregation coefficient, is the ratio of impurity fractions in the deposited solid and the molten zone:

$$k = \frac{X_j}{X_L} \quad (3)$$

In case of single-pass Zone Melting experiment, eqs. 1 and 2 can be re-expressed according to eqs. 4 and 5, assuming that:

- impurity segregation coefficient (k) does not change with the composition of the molten zone
- the starting ingot is homogeneous in composition and presents impurity fraction X_0 .

$$X_1(x) = X_0 \cdot \left[1 - (1-k) \exp\left(\frac{-k \cdot x}{e}\right) \right] \text{ with } 0 \leq x \leq l - e \quad (4)$$

$$X_1(x) = X_1(l-e) \cdot \left(\frac{l-x}{e} \right)^{(k-1)} \text{ with } l - e < x < l \quad (5)$$

Note that eq. 4 should be used to calculate $X_1(l - e)$, as required to apply eq. 5.

Applying these equations, impurity distribution profiles can be predicted for different parameter values (k, l, e). Examples of profiles are shown in fig. 5, in which different impurity segregation coefficient (k) values are taken, as well as several molten zone relative thickness (e / l) values. Note that eq. 5 is not defined at $x = l$, and exhibits a vertical asymptotic behavior.

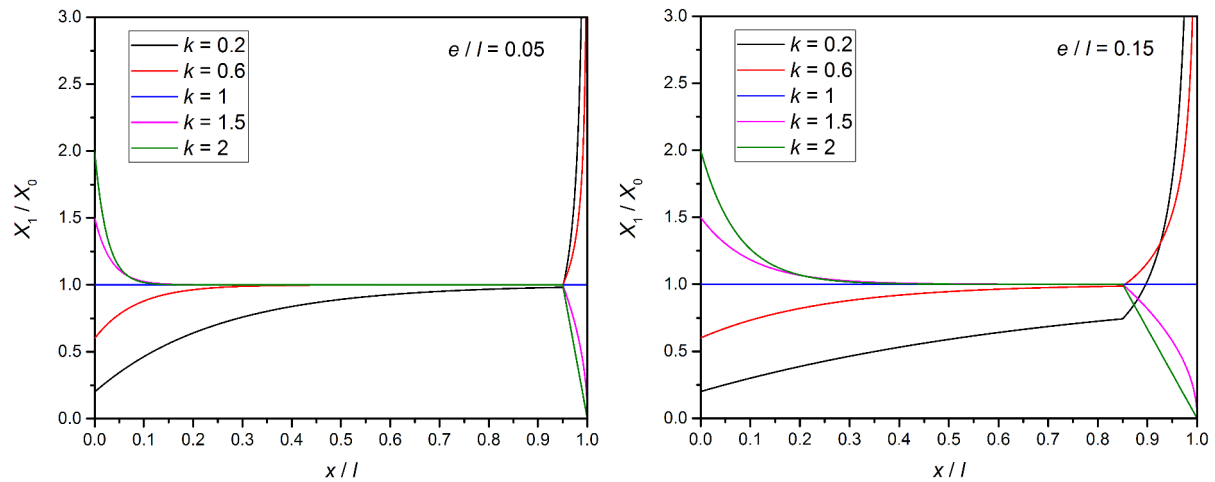


FIG. 5: **Theoretical impurity distribution profiles after one single zone pass, for various k and e values, calculated from eqs. 4 and 5.**

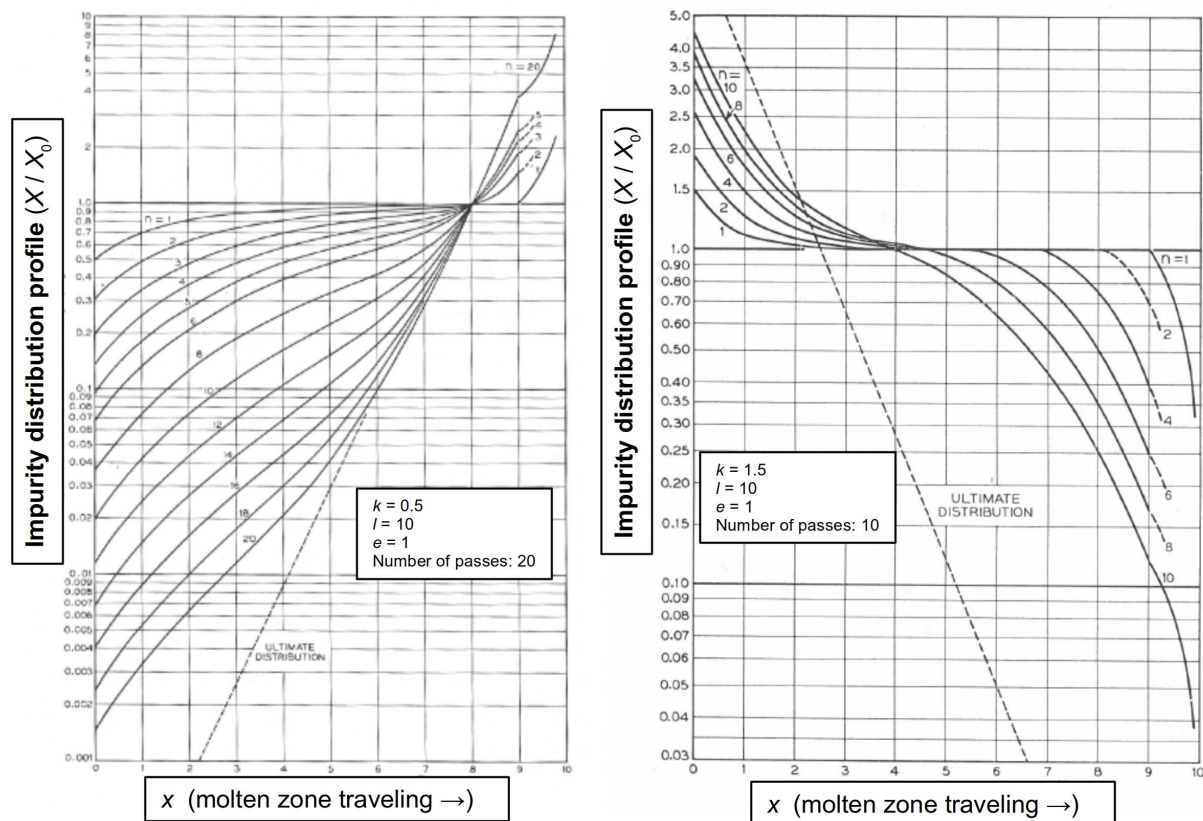


FIG. 6: **Theoretical impurity distribution profiles after multi-pass Zone Melting, adapted from Pfann [3].**

Fig. 5 qualitatively shows that impurities whose segregation coefficients are lower than unity are expected to be displaced towards the same direction as that of the molten zone during its traveling. Conversely, impurities whose k values are higher than 1 should be displaced

towards the opposite direction. Eventually, the molten zone does not have any influence on impurities exhibiting k values of 1, which means that the use of this method is irrelevant to remove such impurities.

It is worth noting that the farthest from unity the segregation coefficient is, the more efficient Zone Melting becomes. Moreover, by maintaining the other parameters constant, an increase of molten zone relative thickness (e / l) value allows to displace a larger amount of impurity by one single zone pass.

Performing more than one single zone pass serves at amplifying impurity displacements, as shown by impurity distribution profiles calculated from eqs. 1 and 2 and shown in fig. 6. In the example shown in the right part, 20 passes are expected to divide impurity level by almost three orders of magnitude in the $x = 0$ region (with reference to the starting sample).

Several studies have been previously performed in order to optimize Zone Melting process on various samples by computer-assisted procedures [7–12]. In most of them, impurity segregation coefficients were estimated from experimental measurements of distribution profiles in known conditions. Their values were then used for distribution prediction purposes. The experimental results were generally close to the predicted ones, which indicates that this model gives accurate results. However, more sophisticated models, taking various effects into account (thermal diffusion, transitional regime...), were also developed [13–15].

b) Influence of phase equilibria and molten zone displacement rate

As mentioned previously, k values have a large influence on the efficiency of Zone Melting at displacing the impurities towards ingot ends. However, they largely depend on the translation rate v of the zone. Indeed, at very low rates, the ratio between impurity levels in the deposited solid and in the zone is close to the equilibrium segregation coefficient – the most favorable case. At larger rates, the recrystallized solid slice rejects the impurity more rapidly than it can diffuse in the zone. Consequently, the zone is not homogeneous anymore (see fig. 7 for illustration), which modifies k . This problem was widely studied by Burton, Prim and Slichter [16], who proposed eq. 6 to express k dependency with respect to v .

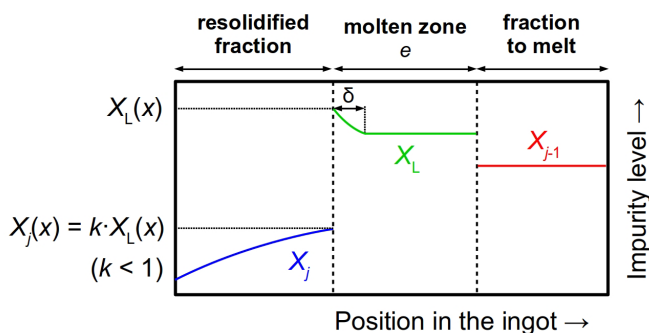


FIG. 7: Illustration of biased segregation occurring at large zone displacement rates

$$k = \frac{k_0}{k_0 + (1 - k_0) \exp\left(-v \frac{\delta}{D}\right)} \quad (6)$$

k_0 being the impurity segregation coefficient when $v \rightarrow 0$ (e. g., the equilibrium segregation coefficient), δ the impurity diffusion layer length in the molten zone at the solidification interface, and D the impurity diffusion coefficient in the molten zone. The $v\delta / D$ term can be seen as the “normalized growth velocity” at the solidification interface [17]. As δ and D are independent from v , a plot of k ($v\delta / D$) function (fig. 8) for different k_0 values shows that increasing the zone translation rate engenders a modification of the effective impurity segregation coefficient. The latter tends towards unity as well as v is increased, which means that Zone Melting has no effect on impurity displacement when the zone translation rate is too large.

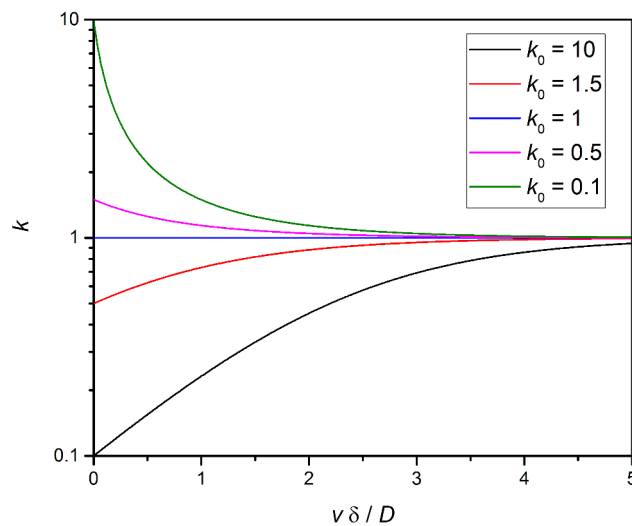


FIG. 8: **Theoretical evolution of impurity segregation coefficient with respect to the normalized growth velocity**

Of course, the lower v is, the larger the segregation becomes. Consequently, Zone Melting efficiency should be maximal when $v \rightarrow 0$. As it costs much time, imposing such translation rates is, of course, not suitable. Therefore, a compromise between v and the effective segregation coefficient k should be found to obtain desirable purifying effects by Zone Melting. However, several ways to improve molten zone homogeneity were proposed to avoid process efficiency decrease at large displacement rates. Among them, the rotation of the ingot along the cylindrical axis exhibited interesting results for the purification of Germanium by this technique (see appendix 1, p. 268).

Besides, every impurity k_0 value can be estimated from the binary phase diagram between the compound to purify and the considered impurity (fig. 9). However, two separate cases should be envisaged:

- If the impurity decreases the melting point of the compound to purify, then $k_0 < 1$ and the zone is richer in impurity than the solid phase. Consequently, the impurity

concentration in the deposited solid is lower than in zone, which corresponds to a displacement towards the same direction as that of the zone.

- Conversely, if the impurity increases the melting point of the compound to purify ($k_0 > 1$), then the deposited solid is always richer in impurity than the zone is, which means that the impurity is displaced towards the opposite direction.

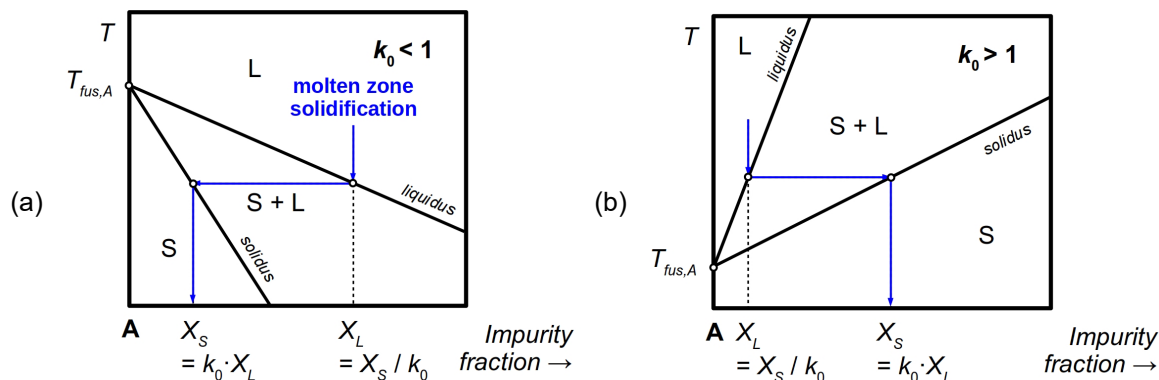


FIG. 9: **Extraction of impurity k_0 value from binary phase diagrams between the compound to purify (A) and the impurity –**

(a) impurity decreasing the melting point of the compound to purify ($k_0 < 1$);

(b) impurity increasing the melting point ($k_0 > 1$)

Consequently, if the compound to purify presents several impurities exhibiting opposite behaviors during the solidification of the molten zone, the purifying effect of the method is limited. More zone passes should be performed in order to amplify impurity concentration at the different ends of the ingot, and, therefore, to obtain a purer intermediate part.

c) Summary

Zone Melting is a melt-crystallization technique that provides many applications: crystal growth, semiconductor doping, purification, etc. The process is driven by thermodynamics (*e. g.*, phase equilibria between the species involved in the treated sample \rightarrow impurity k_0 values) and kinetics (impurity diffusion in the zone).

In this thesis, the technique was applied to Phenanthrene purification. As no device was commercially available, a prototype dedicated to the purification of organic solids was built in our laboratory. A brief presentation of the prototype is made in the next part.

3) Presentation of a new prototype dedicated to organic solids

For many years, purification of organic species has been one of the main research topics of the SMS laboratory. Consequently, the laboratory bought and/or developed new devices dedicated to this task. Among them, a new Zone Melting prototype was developed according to our specifications, and was built by Normalab (Lintot, France) with the support of CRCT of the CNRS through the CRISTECH network (Pascal Lejay coordinator).

A global view of the prototype is proposed in fig. 10. The apparatus is made of two main parts: (i) the Zone Melting device itself, (ii) the control box, that allows the experimenter to adjust the different operating parameters.

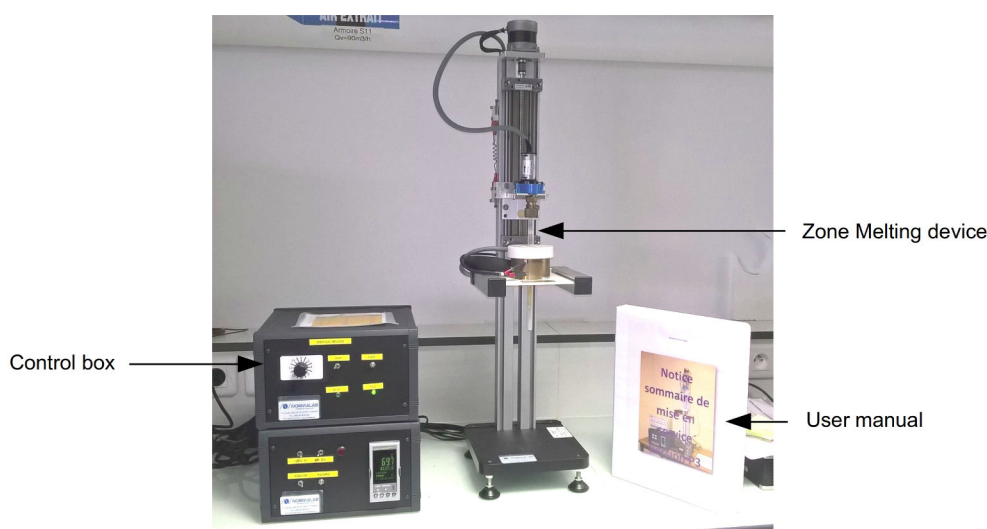


FIG. 10: Global view of the Zone Melting device developed in the SMS laboratory

This prototype allows to deal with ingots disposed as glass tubes whose length and internal diameter are 25 cm and 11 mm, respectively. The molten zone is generated by means of an annular heater made of an electrical resistance (error on zone temperature: ± 0.1 °C). The position of the zone is constant, and the ingot is displaced on a bench by means of a step-by-step motor. Besides, another motor allows the ingot to be rotated along its cylindrical axis with a rate of $0.21 \text{ rad}\cdot\text{s}^{-1}$ and an auto-reversal of the rotation direction every 180° . The aim of that motor is to facilitate molten zone homogenization to improve impurity segregation during zone solidification.

The power supplied by the annular heater can be regulated by means of the control box. By the same way, the ingot translation rate can be adapted.

The different parts of the apparatus are shown and labeled into more details in fig. 11.

Before use for purification purposes, the efficiency of this new prototype had to be assessed. Thanks to its chemical stability upon melting, Phenanthrene was a good candidate for such experiment. Consequently, this molecule was chosen as model compound to test and validate the prototype.

In order to perform qualitative prediction on Zone Melting efficiency at displacing impurities in Phenanthrene ingots (extraction of impurity k_0 values), phase equilibria between the molecule and some of its major impurities were first investigated.

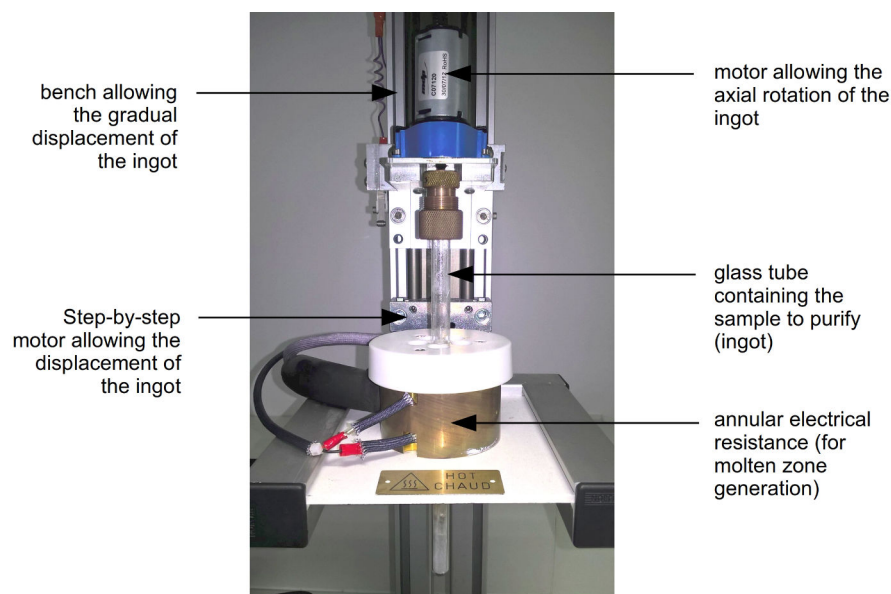


FIG. 11: Detailed view on the Zone Melting device developed in the SMS laboratory

4) Phase equilibria between Phenanthrene and some of its impurities

a) Introduction

As mentioned in part II.2)b, phase equilibria between the molecule to purify and its impurities are of major importance during optimization of Zone Melting experiments: they can be used to assess the potential efficiency of the method by extraction of impurity segregation coefficients (k_0 values).

In the case of Phenanthrene, various impurities can be encountered with different abundances, according to the supplier, the batch and the purity grade (see chapter II). In most of the commercial Phenanthrene samples supplied with a ≥ 98 % indicative purity, Fluorene, 9,10-dihydroanthracene, Dibenzothiophene, Anthracene and Carbazole are generally the main impurities. Up to now, binary solid-liquid phase equilibria between Phenanthrene and every of these impurities were already investigated [18–24], except for the Phenanthrene/9,10-dihydroanthracene system.

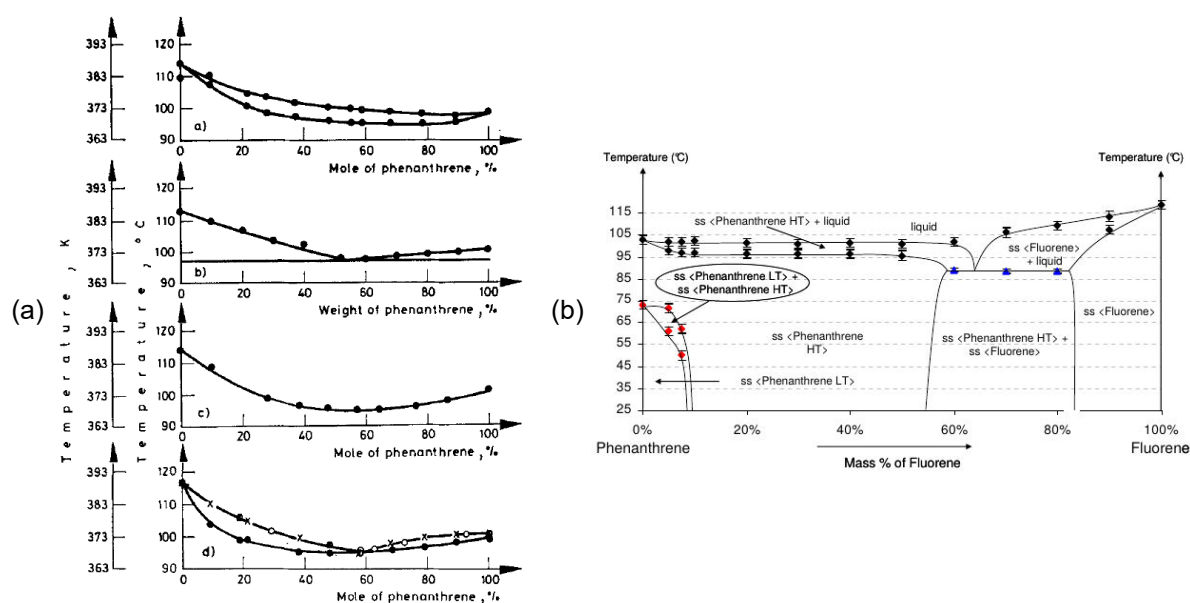


FIG. 12: **Published phase diagrams for the Phenanthrene/Fluorene binary system**
(a) from Kotula and Rabczuk [18], (b) from Couvrat [24].

However, it is worth noting that the proposals cited above show incomplete and/or contradictory data, according to the studies. Moreover, some of them did not comply with thermodynamic rules applicable to binary phase diagrams.

- 5 contradictory proposals were made for the Phenanthrene/Fluorene system (fig. 12) by analysis of samples obtained by melt crystallization [18] or from solvent evaporation [24], which justifies its re-investigation using another sample preparation procedure.
- The authors of the study related to the Phenanthrene/Dibenzothiophene [19] system noted that metastable equilibria were observed during their experimental work on binary

mixtures prepared from solvent evaporation, and that further investigations would be suitable to validate their proposal shown in fig. 13.

- 2 incomplete and contradictory proposals, shown in fig. 14, were made for the Phenanthrene/Anthracene system [20,25]. Moreover, a recent study conducted by Rice *et al.*, proposed another phase diagram without description of the phases in equilibrium in the solid and liquid states [26]. Besides, another study made by Ding *et al.* and related to the study of ternary equilibria between these two species and various solvents highlighted the existence intermediate phase that was previously unknown [27]. However, polythermic phase equilibria between solids obtained from these ternary mixtures were not investigated. Consequently, they have to be assessed after preparation of samples according to their procedure.

- Phenanthrene/Carbazole system was described only once [21], but incomplete data observed on the related proposal justify a re-investigation.

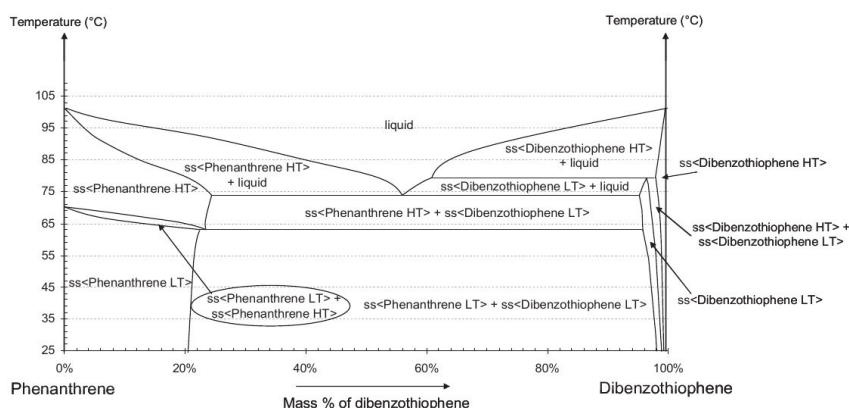


FIG. 13: **Published phase diagram for the Phenanthrene/Dibenzothiophene binary system** from Couvrat *et al.* [19].

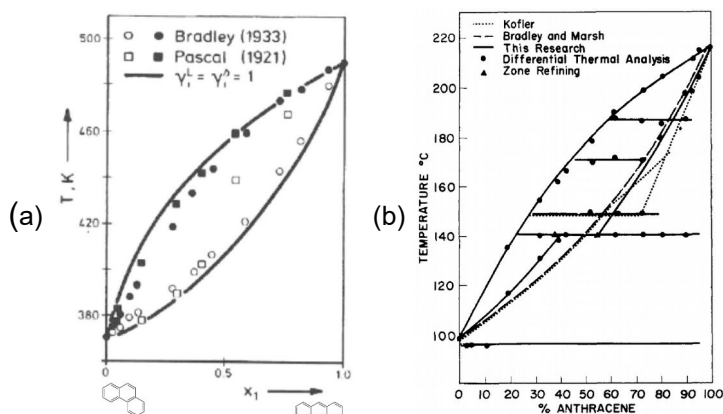


FIG. 14: **Published phase diagram for the Phenanthrene/Anthracene binary system** (a) from Ulrich and Glade [20]; (b) from Joncich and Bailey [25].

Consequently, a systematic re-investigation of all these systems was performed by combining calorimetric and structural studies. Moreover, an assessment of Phenanthrene/9,10-

dihydroanthracene binary equilibria was attempted. Sample preparation was adapted according to the issues observed in the different systems:

- Phenanthrene/9,10-dihydroanthracene and Phenanthrene/Carbazole binary mixtures were prepared by solvent evaporation, after pre-purification of the starting products.
- Phenanthrene/Fluorene and Phenanthrene/Dibenzothiophene binary equilibria were assessed by study of the related ternary systems with Acetone at room temperature. Binary mixtures were obtained after crystallization in this solvent and isolation of solids in equilibrium with saturated liquids.
- Phenanthrene/Anthracene phase equilibria were investigated by study of the ternary phase diagram with Toluene at room temperature.

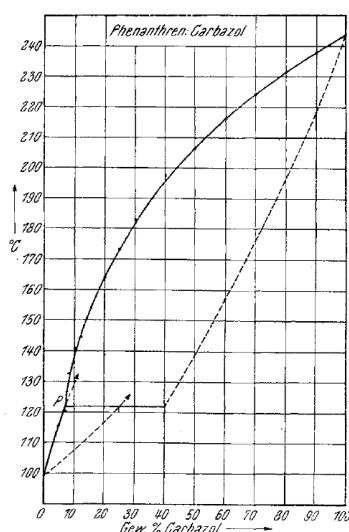


FIG. 15: **Published phase diagram for the Phenanthrene/Carbazole binary system** from Brandstätter-Kuhnert [21]

The solids obtained thanks to these procedures were then characterized by: (i) Differential Scanning Calorimetry (DSC), to evidence phase transformations on heating, (ii) and X-Ray Powder Diffraction (XRPD), to identify the solid phases in the prepared samples. Binary phase diagrams were then established after interpretation of experimental data. The proposals were discussed with reference to the following points:

- the presence of solid solutions of Phenanthrene with its impurities,
- the effect of the different impurities on Phenanthrene melting point (*e. g.*, extraction of impurity k_0 value) and on its solid-solid transition temperature.

b) Experimental procedures

For the study of Phenanthrene/9,10-dihydroanthracene and Phenanthrene/Carbazole binary systems, starting commercial products were first pre-purified by means of recrystallization in Acetone, according to the procedure described in appendix 3 (p. 270). As shown in the appendix, this method led to the decrease of impurity levels in the three products. Various physical mixtures made of the pre-purified products were prepared, dissolved in HPLC grade Acetone (VWR Chemicals) before recrystallization by solvent full evaporation to air. The powders were ground and analyzed by XRPD (apparatus and method are described in appendix 2a (p. 268)) and DSC (appendix 2b, p. 268). During DSC experiments, the following temperature program was set: 5 K min⁻¹ heating ramp from 20 °C to the melt, then 2-minutes isothermal step, then 5 K min⁻¹ cooling ramp to 20 °C, then 2-minutes isothermal step, then 5 K min⁻¹ heating ramp from 20 °C to the melt. The aim of the 2nd heating step was to check the reversibility of thermal events observed during the 1st one.

Phenanthrene/Fluorene/Acetone, Phenanthrene/Dibenzothiophene/Acetone and Phenanthrene/Anthracene/Toluene ternary systems were investigated by preparation of physical ternary mixtures made of commercial products (Phenanthrene: Alfa Aesar, 98 %; Fluorene: Alfa Aesar, 98 + %; Dibenzothiophene: Alfa Aesar, 98 %; Acetone: VWR Chemicals, HPLC grade; Toluene: VWR Chemicals, HPLC grade). The mixtures were equilibrated at room temperature under magnetic stirring for 24 h. After equilibration, ~ 0.3 mL of every mixture was filtered over 0.2 µm PTFE syringe filter. One drop of saturated liquid was dissolved in ~ 2 mL of Toluene (for the 2 1st systems) or Acetone (for the 3rd one). The resulting solutions were analyzed by Gas Chromatography (GC) to determine the compositions of the liquid phases (the analytical methods are described in appendix 2c, p. 268). The compositions of the solids was determined using Schreinemaker's method of wet residues. For every mixture, the solids were recovered by vacuum filtration over 1-porosity glass filters. The wet powders were dried overnight at 20 °C and 200 mbar absolute pressure. Dried solids were analyzed by XRPD (appendix 2a, p. 268) and DSC (appendix 2b, p. 268). During DSC, one single 5 K min⁻¹ heating ramp was applied from 20 °C to the melt.

c) Study of the Phenanthrene/9,10-dihydroanthracene binary system

Purifying effects of recrystallization procedures applied to the starting commercial are reported in appendix 3 (p. 270). Chromatographic measurements revealed that 9,10-dihydroanthracene and Phenanthrene were impurities of each other in the commercial products. Their purification by recrystallization led to the reduction of impurity levels, but not to their complete elimination. One can deduce that Phenanthrene Low Temperature and 9,10-dihydroanthracene phases both form partial solid solutions (<ss PHEN LT> and <ss DHA>, respectively).

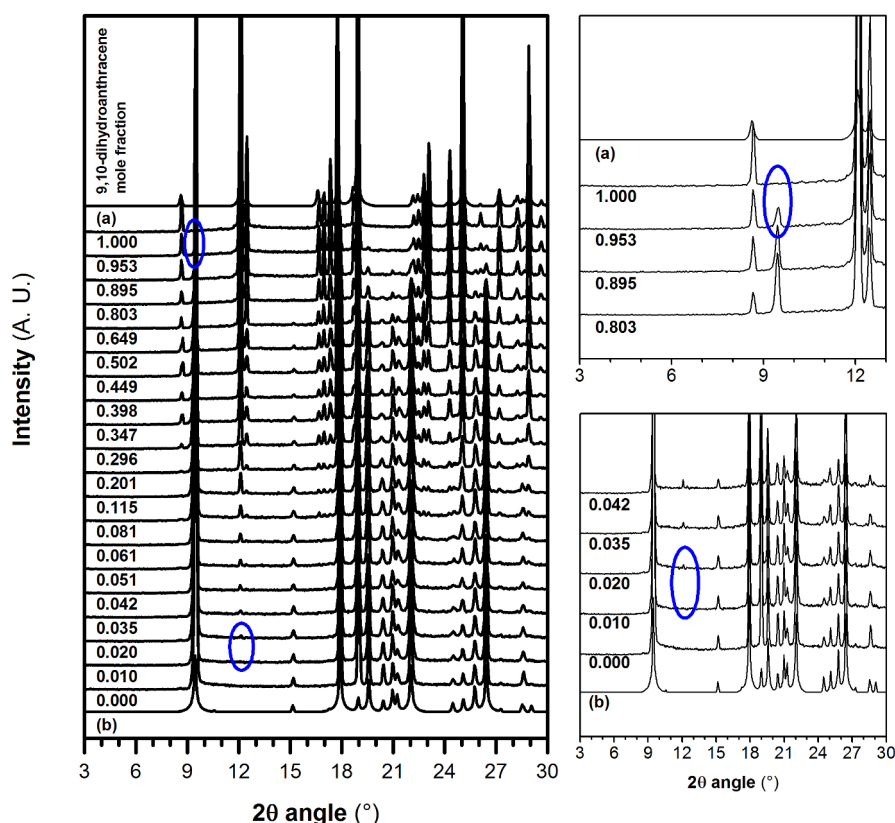


FIG. 16: XRPD patterns of Phenanthrene/9,10-dihydroanthracene mixtures at 20 °C and 1 atm – (a) and (b) are the XRPD patterns of the <PHEN LT> and <DHA> phases predicted from their structures (see refs. [28] and [29]). The main evidences of phase domain changes are highlighted with blue ellipses.

The XRPD patterns of Phenanthrene/9,10-dihydroanthracene binary mixtures are presented in fig. 16. They indicate that mixtures containing less than 2.0 % 9,10-dihydroanthracene in mole fraction (X_{DHA}) crystallized in the <ss PHEN LT> phase. Solids of intermediate compositions ($0.020 \leq X_{\text{DHA}} \leq 0.953$) were mixtures of the <ss PHEN LT> and <ss DHA> phases. Only pure 9,10-dihydroanthracene crystallized in the <ss DHA> phase.

The DSC thermograms (1st heating ramp) related to these mixtures are presented in fig. 17. Note that the thermal events observed during the second heating are consistent with that

observed in this figure, which indicates that the transformations observed in the thermograms were reversible.

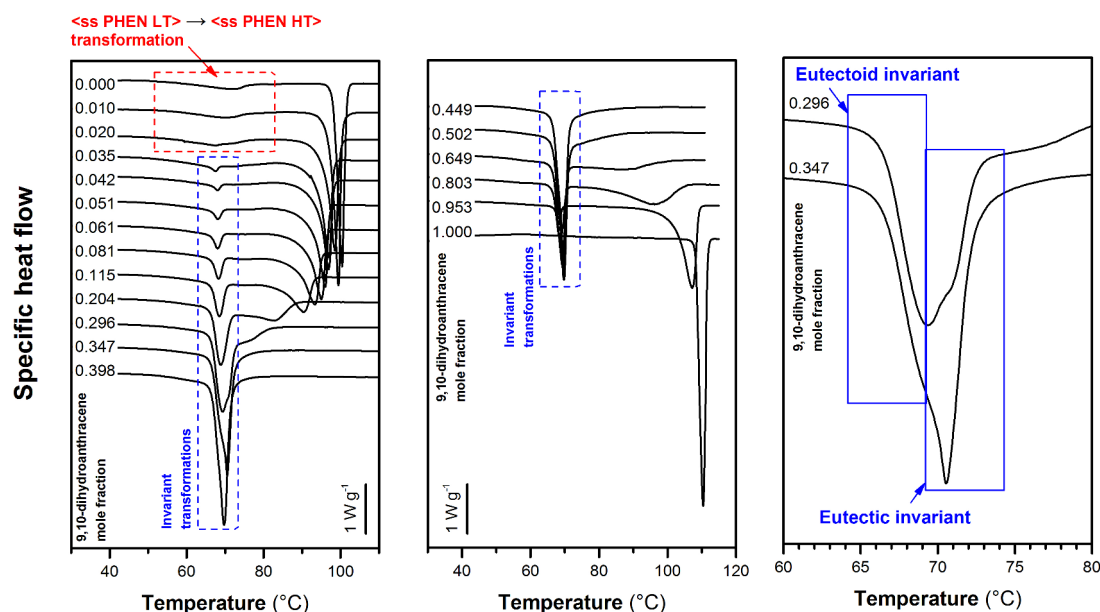


FIG. 17: DSC figures of Phenanthrene/9,10-dihydroanthracene binary mixtures (endo ↓)

Phenanthrene-rich mixture ($X_{\text{DHA}} < 0.020$) thermograms show that the temperature of transition from the <ss PHEN LT> to the <ss PHEN HT> phases was slightly decreased as 9,10-dihydroanthracene contents was increased to 2 mole %. The thermograms of mixtures containing <ss PHEN LT> and <ss DHA> as starting phases all presented an endothermic thermal event at ~ 65 - 66 °C. This was attributed to the eutectoid transformation $\text{<ss PHEN LT>} + \text{<ss DHA>} \rightleftharpoons \text{<ss PHEN HT>}$. However, the thermograms of the mixtures containing 29.6 and 34.7 % 9,10-dihydroanthracene clearly indicate the dual contribution of two successive transformations, which suggests that two invariant transformations occurred in a narrow temperature range. The second one was interpreted as being the eutectic reaction $\text{<ss PHEN HT>} + \text{<ss DHA>} \rightleftharpoons \text{L}$. For every mixture, at higher temperatures, only the thermal events associated with *liquidus* points were observed.

TAB. 2: Data on the invariant transformations observed in the Phenanthrene/9,10-dihydroanthracene binary system

Temperature	Nature	Phases involved in the equilibrium		
65-66 °C	eutectoid	<ss PHEN LT> $X_{\text{DHA}} \sim 0.02$	<ss DHA> $X_{\text{DHA}} \sim 0.96$	<ss PHEN HT> $X_{\text{DHA}} \sim 0.12$
66-67 °C	eutectic	<ss PHEN HT> $X_{\text{DHA}} \sim 0.12$	<ss DHA> $X_{\text{DHA}} \sim 0.96$	L $X_{\text{DHA}} \sim 0.40$

The treatment of the data extracted from DSC and XRPD measurements led to the proposal of the binary phase diagram presented in fig. 18. For the sake of clarity, data on the two invariant transformations observed in this system are summarized in tab. 2. Note that, due to the poor resolution between the thermal events associated with the two invariant transformations, their

calorimetry could not be studied. Consequently, no quantitative data on their enthalpies could be extracted from recorded data.

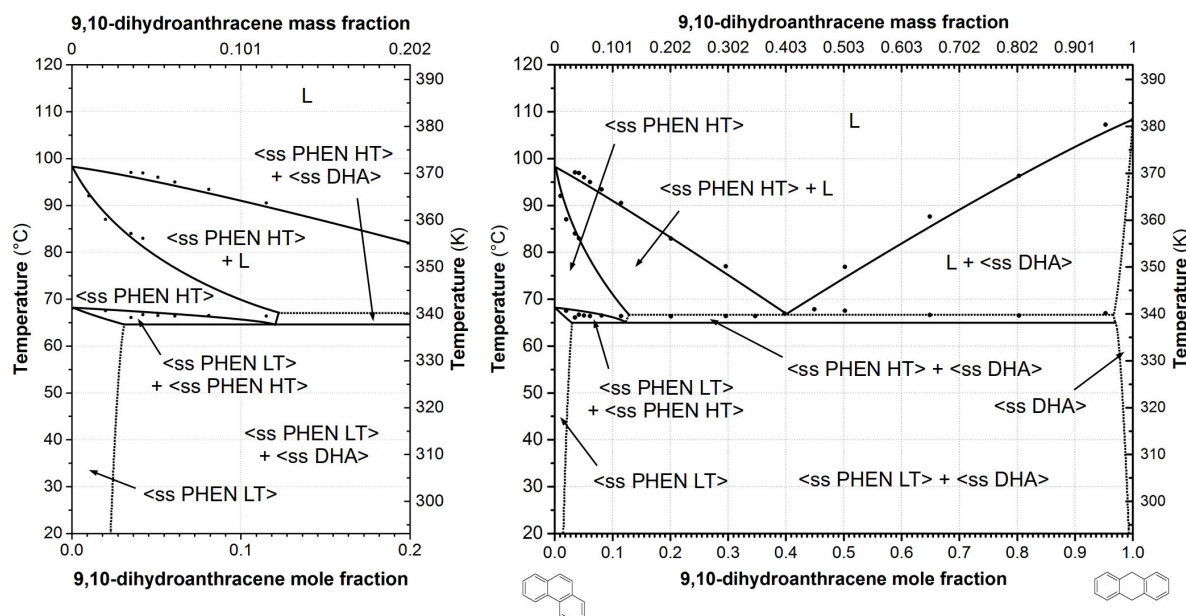


FIG. 18: **Proposal for Phenanthrene/9,10-dihydroanthracene binary phase diagram at atmospheric pressure** – • DSC thermal events, --- equilibrium curves not experimentally observed, and deduced by experimental data cross-checking

The proposed phase diagram reveals that:

- (i) both components make partial solid solutions with each other. However, the extent of these solid solutions on the temperature vs. composition chart is very limited.
- (ii) as impurity, 9,10-dihydroanthracene significantly decreases Phenanthrene melting point (see fig. 18 in the Phenanthrene-rich region). Moreover, its segregation coefficient between the <ss PHEN HT> and L phases seems to be far from unity due to the large extent of the corresponding two-phase domain.
- (iii) 9,10-dihydroanthracene slightly decreases Phenanthrene solid-solid transition temperature. However, this effect is moderate.

d) Re-investigation of the Phenanthrene-Carbazole binary system

As reported in appendix 3 (p. 270), Carbazole and Phenanthrene were impurities of each other in the commercial products. Purification of both products by recrystallization allowed for the partial elimination of the impurities, which indicates that Phenanthrene Low Temperature and Carbazole phases both form partial solid solutions (<ss PHEN LT> and <ss CARB>).

During preliminary analyses on the mixtures prepared according to the procedure described in part b (p. 192), some DSC thermal events observed during the first and second heating steps were not consistent. Consequently, the preparation method was adapted as follows:

- (i) every binary mixture prepared from Acetone evaporation was put into a closed Al DSC pan (~ 15 mg sample) and was heated up to the melt before applying a 5 K/min cooling ramp to 20 °C.
- (ii) the samples recrystallized from the melt during this “preparative DSC” step were then recovered, ground and analyzed by XRPD to identify the phases in equilibrium.
- (iii) the powders were then re-analyzed by DSC by applying a single 5 K/min heating ramp up to the melt to evidence phase transformations between the starting phase(s) observed by XRPD.

XRPD patterns of Phenanthrene/Carbazole binary mixtures recrystallized from the melt during preparative DSC are presented in fig. 19.

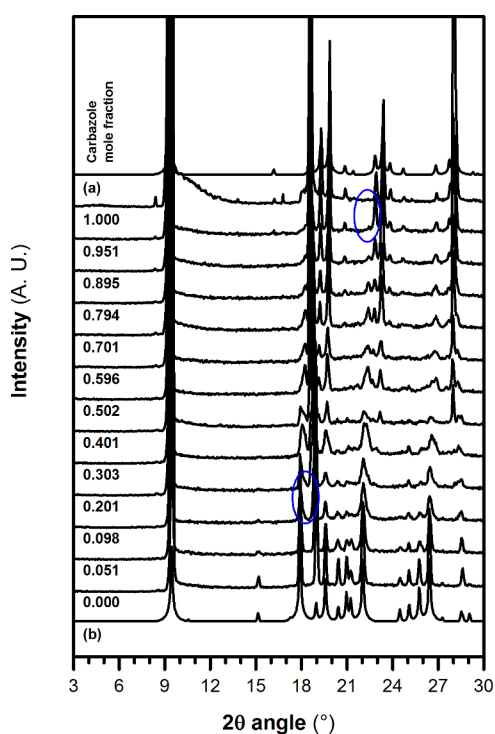


FIG. 19: **XRPD patterns of Phenanthrene/Carbazole mixtures at 20 °C and 1 atm** – (a) and (b) are the XRPD patterns of the <PHEN LT> [28] and <CARB> (Cambridge Structural Database refcode: CRBZOL03) phases predicted from their structures. The main evidences of phase domain changes are highlighted with blue ellipses.

As revealed by this figure, mixtures exhibiting Carbazole mole fraction (X_{CARB}) values lower than 0.098 crystallized as solid solutions of the Phenanthrene Low Temperature phase (<ss PHEN LT>). Only pure Carbazole ($X_{\text{CARB}} = 1.000$) recrystallized in the <ss CARB> phase. Eventually, samples of intermediate compositions ($0.098 \leq X_{\text{CARB}} \leq 0.951$) crystallized as mixtures of these two phases.

The thermograms of the binary mixtures obtained by preparative DSC are shown in fig. 20.

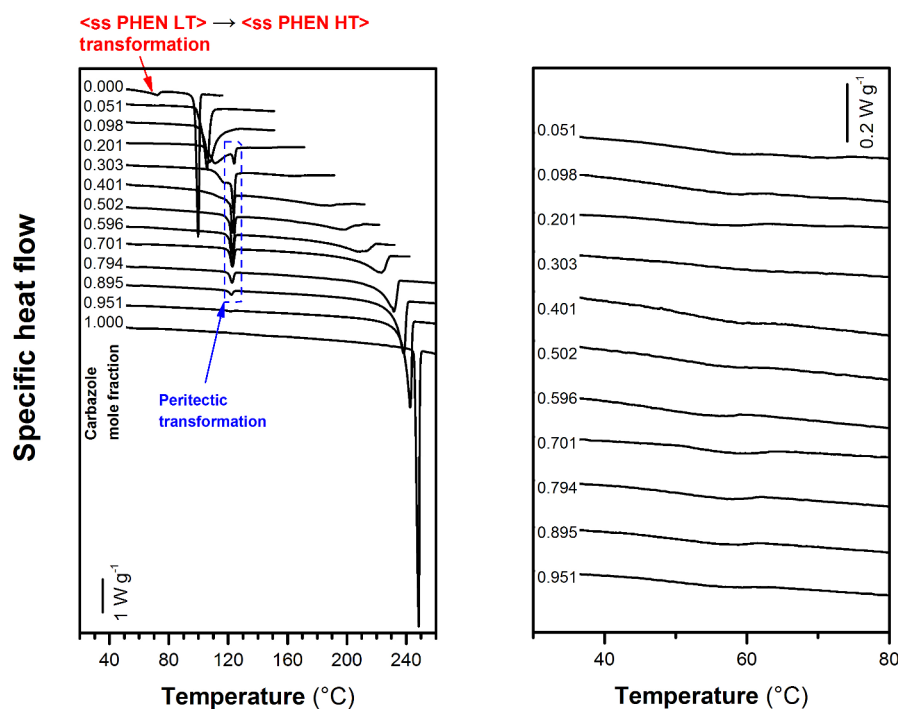


FIG. 20: DSC figures of Phenanthrene/Carbazole mixtures (endo ↓)

For every mixture, a low-enthalpy endothermic thermal event was observed at $\sim 55\text{--}60\text{ }^{\circ}\text{C}$ (see the right part of fig. 20), which indicates the probable occurrence of a eutectoid transformation ($\text{<ss PHEN LT> + <ss CARB>} \rightleftharpoons \text{<ss PHEN HT>}$). However, due to their low intensity, the corresponding signals could not be integrated to characterize the calorimetry of this invariant.

At higher temperatures, *solidus*-related thermal events could be observed. The *solidus* temperature was increased from 98 to $120\text{ }^{\circ}\text{C}$ by increasing X_{CARB} from 0.000 to 0.401. Every mixture of X_{CARB} ranging from 0.201 to 0.895 was found to undergo endothermic transformations at $120\text{ }^{\circ}\text{C}$, which was attributed to the peritectic reaction $\text{<ss PHEN HT> + <ss CARB>} \rightleftharpoons \text{L}$. On heating, these transformations were followed by the melting of the remaining <ss CARB> solid phases, which allowed for the assessment of *liquidus* points.

For mixtures exhibiting $X_{\text{CARB}} < 0.502$, the different thermal events associated with transformations involving simultaneously solid and liquid phases were not sufficiently resolved. Consequently, the peaks associated with the peritectic transformation at $120\text{ }^{\circ}\text{C}$ could not be integrated, which prevented from estimating the invariant point location by plotting the corresponding Tammann graph. Nevertheless, the *solidus* temperature reaches the peritectic temperature when $X_{\text{CARB}} = 0.501$, which gives a good indication of the invariant point composition. The corresponding enthalpy was $33.4\text{ J}\cdot\text{g}^{-1}$ ($2.7\text{ kJ}\cdot\text{mol}^{-1}$).

Besides, these invariant peaks were integrable when $0.502 \leq X_{\text{CARB}} \leq 0.895$, which allowed to plot a partial Tammann graph and to deduce the composition of the <ss CARB> phase involved in the transformation. The latter was estimated at 0.93 ± 0.05 (95 % confidence interval).

Extended data on the different invariant transformations observed in this system are provided in tab. 3. These data are compared with those extracted from the already published phase diagram [21].

TABLE 3: **Data on the invariant transformations observed in the Phenanthrene/Carbazole binary system**

Temperature	Nature	Phases involved in the equilibrium			Enthalpy
This work					
~ 55-60 °C	eutectoid	<ss PHEN LT> $X_{\text{CARB}} \sim 0.07$	<ss CARB> $X_{\text{CARB}} \sim 0.97$	<ss PHEN HT> $X_{\text{CARB}} \sim 0.45\text{-}0.50$	Not measurable
~ 120 °C	peritectic	<ss PHEN HT> $X_{\text{CARB}} \sim 0.50$	<ss CARB> $X_{\text{CARB}} \sim 0.96$	L $X_{\text{CARB}} \sim 0.15$	33 J·g ⁻¹
Data from Brandstätter-Kuhnert and Weiß [21]					
~ 122 °C	peritectic	<ss PHEN HT> $X_{\text{CARB}} \sim 0.25$	<ss CARB> $X_{\text{CARB}} \sim 0.40$	L $X_{\text{CARB}} \sim 0.07$	No data

All the experimental observations allowed to propose the binary phase diagram presented in fig. 21. This proposal gives several indications:

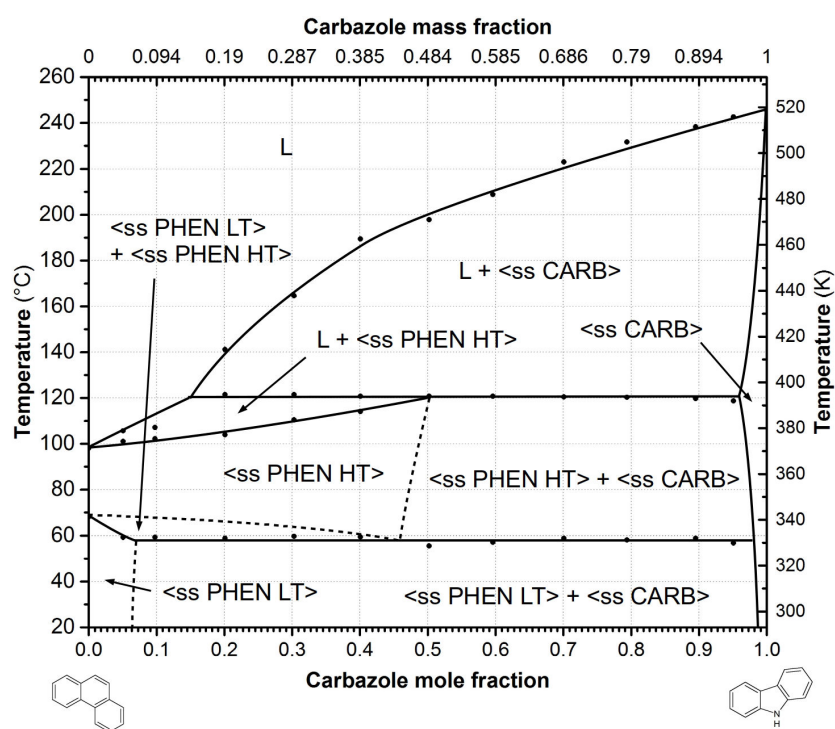


FIG. 21: **Proposal for Phenanthrene/Carbazole binary phase diagram at atmospheric pressure** –
 • DSC thermal events, --- equilibrium curves not experimentally observed, and deduced by experimental data cross-checking

- (i) Both components make partial solid solutions with each other.
- (ii) Carbazole increases the melting point of Phenanthrene, which means that it behaves as a $k_0 > 1$ impurity. This conforms to the previous proposal [21].

(iii) Carbazole slightly decreases the temperature of solid-solid transition of Phenanthrene, but the <ss PHEN HT> phase is not stable at room temperature, which contradicts Glostein data [30].

e) Re-investigation of the Phenanthrene/Fluorene binary system

The compositions of Phenanthrene/Fluorene/Acetone ternary mixtures, and those of its different phases after equilibration, are summarized in tab. S1 (appendix 4, p. 271).

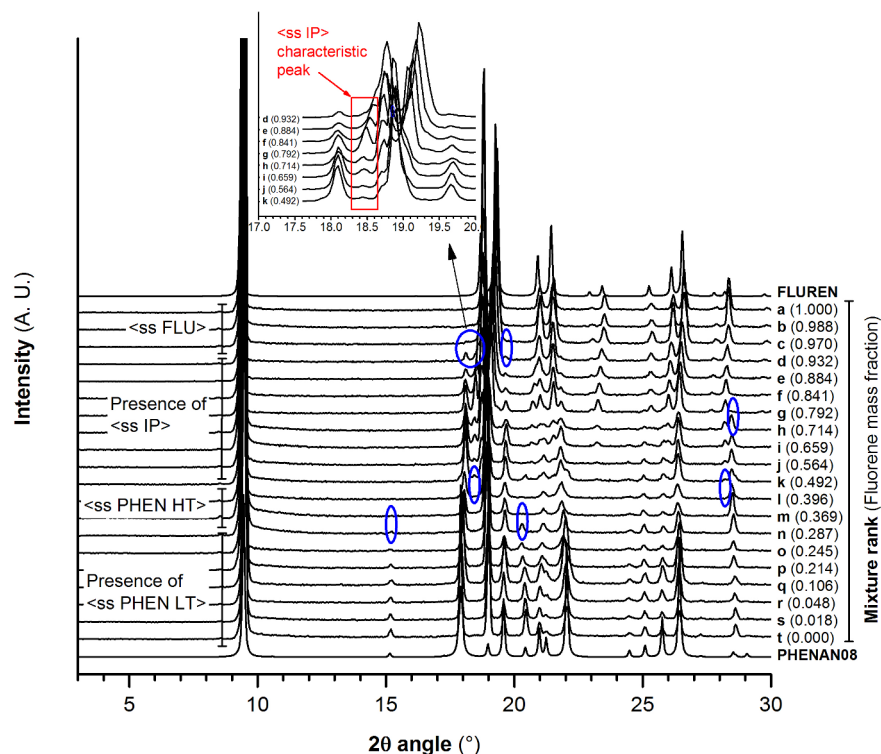


FIG. 22: XRPD patterns of Phenanthrene/Fluorene binary mixtures at 20 °C and 1 atm – PHENAN08 [28] and FLUREN [31] are the patterns predicted from Phenanthrene (low temperature) and Fluorene crystal structures.

XRPD patterns of solid phases isolated by filtration are presented in fig. 22. A solid solution of Phenanthrene Low Temperature phase (<ss PHEN LT>) was evidenced in Phenanthrene-rich mixtures (n–t). Mixtures l–m crystallized as a solid solution of the Phenanthrene high temperature phase (<ss PHEN HT>), as revealed by the disappearance of diffraction peaks at ~ 15 and 20.5 ° with reference to <ss PHEN LT> diffraction patterns. Besides, the patterns of mixtures d–k revealed the presence of a unknown intermediate phase (<ss IP>), as shown by the appearance of new peaks at ~ 18.5 °. Eventually, mixtures a–c crystallized as solid solutions of Fluorene phase (<ss FLU>).

However, the boundaries of one- and two-phase domains in this system at room temperature was not easy to determine by solely use of XRPD patterns, due to their similarity. Consequently, they were determined using the compositions of the solid and liquid phases and the rules applicable to ternary systems. A proposal of phase domain boundaries, compatible with the experimental data, is presented in fig. 23. However, the <ss FLU> + <ss IP> + Liquid

(L) three-phase domain was not evidenced with the recorded data, and some complementary experimental points should be tested to confirm the hypothesis presented in this figure.

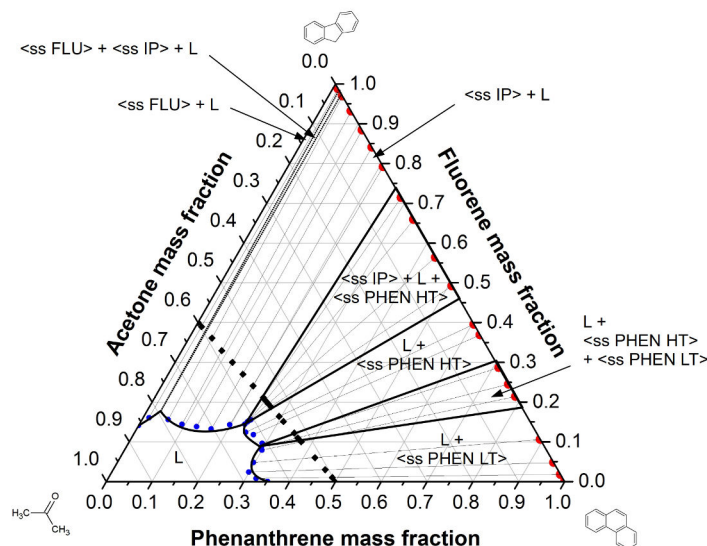


FIG. 23: **Proposal for the Phenanthrene/Fluorene/Acetone ternary phase diagram at room temperature and atmospheric pressure** – • composition of liquids ♦ composition of physical mixtures • composition of solids

DSC thermograms of the solid phases are presented in fig. 24.

They evidenced that, by increasing Fluorene mole fraction from 0 to 0.287 (mixtures **n–t**) led to a decrease of the temperature of the thermal event associated with Phenanthrene solid-solid transition. At around 96-98 °C, thin melting peaks were observed for mixtures containing from 0 to 0.396 Fluorene in mole fraction (mixtures **l–t**). Their onset (chosen as *solidus* point) and peak (*liquidus*) temperatures were very close. Mixtures **e–k**, containing from 49.2 to 88.4 mole % of Fluorene) and in which the <ss IP> phase was detected by XRPD, all underwent an endothermic phenomenon at ~ 93 °C. This was attributed to of this phase during a peritectoid transformation (<ss IP> → <ss FLU> + <ss PHEN HT> on heating). These mixtures underwent another endothermic invariant transformation at ~ 97 °C, which was associated with the eutectic transformation <ss PHEN HT> + <ss FLU> → L. Due to insufficient resolution between the corresponding thermal events, no accurate calorimetric studies could be performed to determine the invariant point coordinates from Tammann plots. Approximate data on these invariant transformations are provided in tab. 4. Fluorene-rich mixtures (**a–d**) shown only *solidus* and *liquidus* related points.

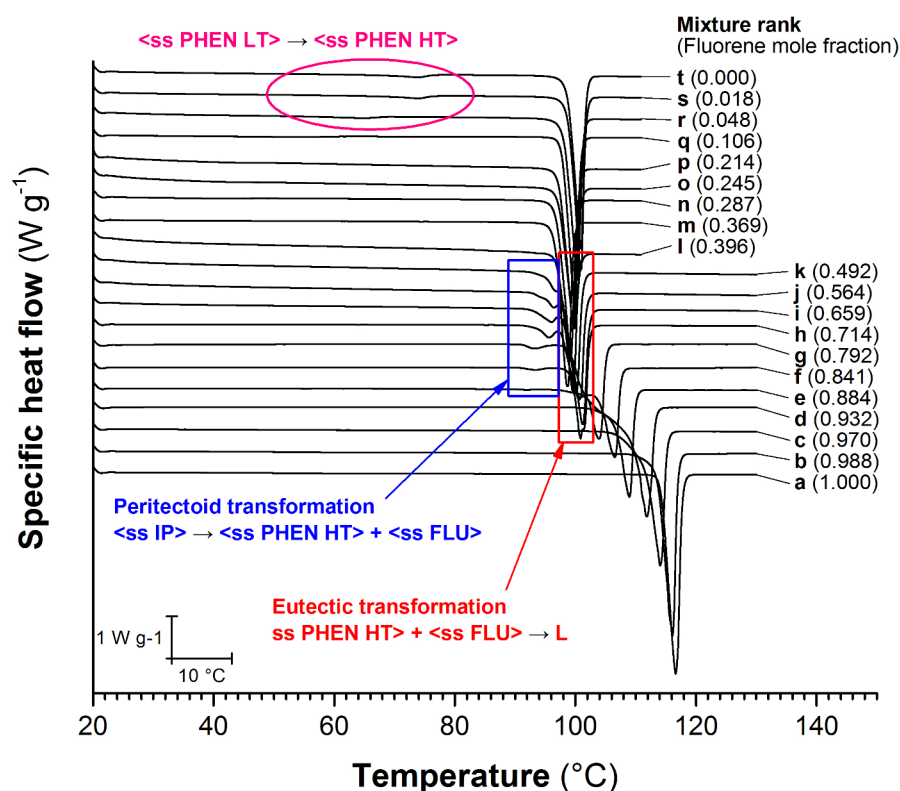


FIG. 24: Thermograms of Phenanthrene/Fluorene binary mixtures recovered by filtration (endo ↓)

A compilation of DSC thermal event points and the cross-checking of all the recorded data led to propose the binary phase diagram shown in fig. 25. As some uncertainties remained about the stability domains of the $\langle ss\ IP \rangle$ and $\langle ss\ IP \rangle + \langle ss\ FLU \rangle$ phase domains, their boundaries were drawn with dotted lines.

TAB. 4: Data on the invariant transformations observed in the Phenanthrene/Fluorene binary system

Temperature	Nature	Phases involved in the equilibrium		
This work				
93 ± 2 °C	peritectoid	<ss IP> $X_{\text{FLU}} \sim 0.75$	<ss PHEN HT> $X_{\text{FLU}} \sim 0.45$	<ss FLU> $X_{\text{FLU}} \sim 0.90$
97 ± 2 °C	eutectic	<ss PHEN HT> $X_{\text{FLU}} \sim 0.45$	<ss FLU> $X_{\text{FLU}} \sim 0.90$	L $X_{\text{FLU}} \sim 0.65$
Data from Couvrat [24]				
~ 89 °C	eutectic	<ss PHEN HT> $X_{\text{FLU}} \sim 0.55$	<ss FLU> $X_{\text{FLU}} \sim 0.85$	L $X_{\text{FLU}} \sim 0.65$

X_{FLU} = Fluorene mole fraction

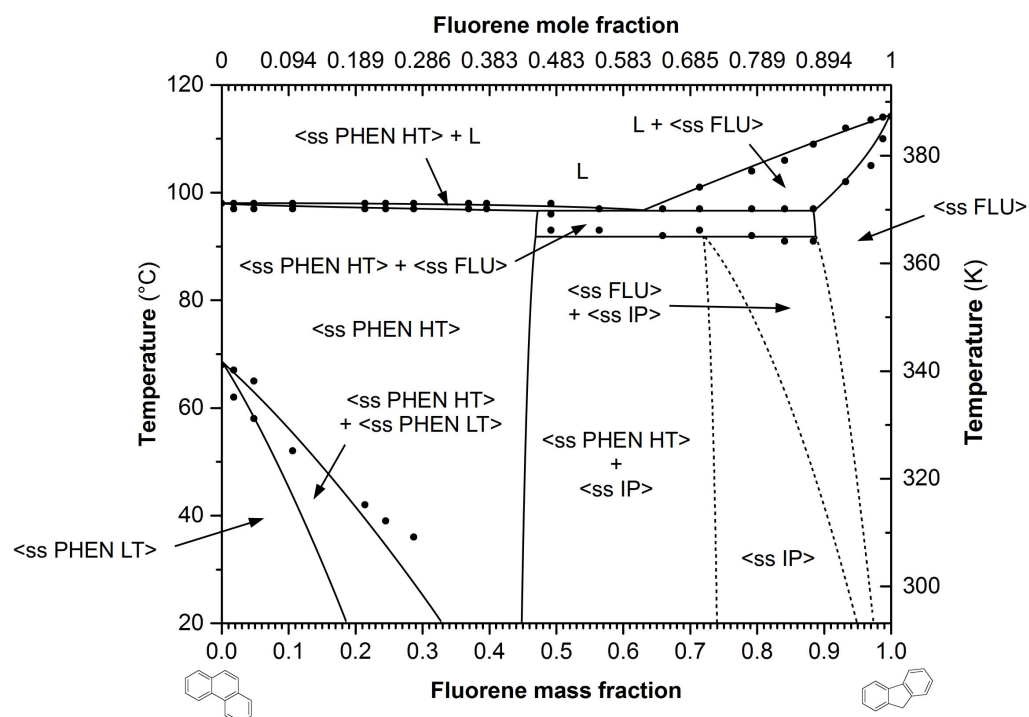


FIG. 25: **Proposal for the Phenanthrene/Fluorene binary phase diagram at 1 atm –**
 • DSC thermal events, --- equilibrium curves not experimentally observed, and deduced by experimental data cross-checking

This proposal brings new elements with reference to the previous ones. Among them, the existence of an intermediate phase, previously unknown, was evidenced. In addition, the following important data can be extracted from this diagram:

- (i) A large domain of <PHEN LT> solid solution was evidenced.
- (ii) as impurity, Fluorene decreases the melting point of Phenanthrene ($k_0 < 1$). Nevertheless, this effect is not very pronounced. However, in the Phenanthrene-rich region, the *solidus* and *liquidus* lines are very close, which indicates that the segregation coefficient of Fluorene is close to unity. This observation is consistent with the existing data on that point [32].
- (iii) Fluorene also decreases the temperature of Phenanthrene solid-solid transition below room temperature when Fluorene mass fraction is increased up to 0.3.

f) Re-investigation of the Phenanthrene/Dibenzothiophene binary system

Compositions of the starting ternary mixtures, the liquids and the solids are summarized in tab. S2 (appendix 4, p. 271).

These data permitted to plot the isothermal section at 20 °C of the Phenanthrene/Dibenzothiophene/Acetone ternary diagram (see fig. 26). As revealed by this figure, *liquidus* points are not very clear and the tested compositions did not generate Phenanthrene/Dibenzothiophene solid binary mixtures exhibiting Dibenzothiophene mass fractions ranging from 0.3 to 0.7.

The XRPD patterns of the solid phases recovered after equilibration are shown in fig. 27. They indicate that solids recovered from mixtures 1–6 crystallized in the <ss PHEN LT> phase. Pure Dibenzothiophene crystallized in the <ss DBT>³ phase. Those recovered from mixtures 7–12 crystallized as mixtures of <ss PHEN LT> and <ss DBT> phases.

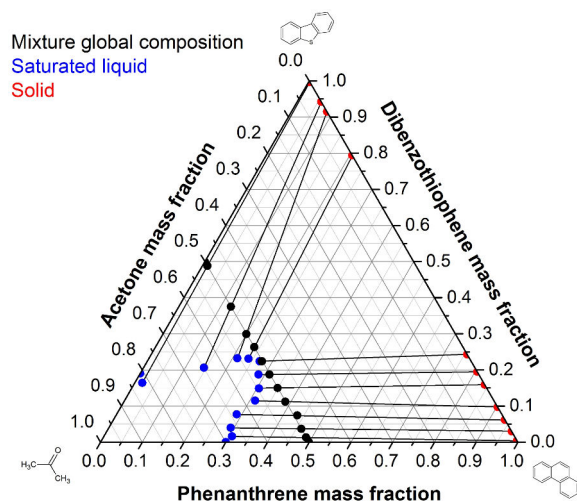


FIG. 26: Points of the Phenanthrene/Dibenzothiophene/Acetone ternary diagram (20 °C, 1 atm)

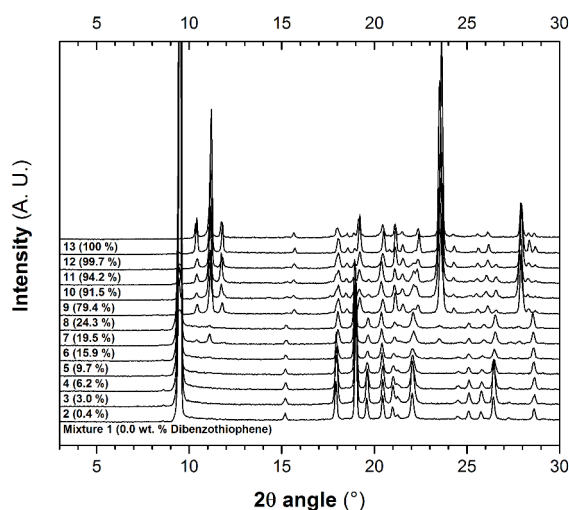


FIG. 27: XRPD patterns of Phenanthrene/Dibenzothiophene solid phases recovered by filtration

The presence of two phases in the recovered solids (mixtures 7–12) necessarily means that the corresponding mixture global composition values lie on a <ss PHEN LT> + <ss DBT> + L three-phase domain. Consequently, the compositions of the corresponding saturated liquids should have the same values, which is not the case here. Therefore, one can deduce that the states of equilibrium were not reached, as the experimental measurements did not comply with the rules applicable on ternary systems (see chapter I).

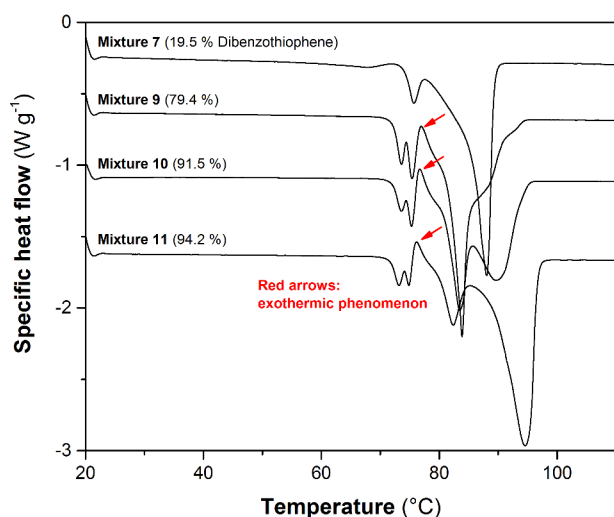


FIG. 28: Thermograms of some Phenanthrene/Dibenzothiophene mixtures recovered by filtration

3. <ss DBT>: solid solution of Dibenzothiophene

This hypothesis was then confirmed during DSC analysis of these mixtures (fig. 28), on which exothermic thermal events could be observed at $\sim 75\text{ }^{\circ}\text{C}$, indicating that the corresponding samples were metastable, and that the increase of temperature enhanced the crystallization of a more stable phase that did not appear during the equilibration procedure.

As it, the recorded data did not allow to assess the Phenanthrene/Dibenzothiophene binary phase diagram. In order to attempt to equilibrate Phenanthrene/Dibenzothiophene mixtures, several tests were carried out:

- (i) A few Phenanthrene/Dibenzothiophene/Acetone ternary mixtures were prepared by full dissolution of the solids on heating, and recrystallization by cooling down to room temperature. After 24 h equilibration under magnetic stirring, the solids generated by this procedure were metastable and exhibited the same behavior as observed in fig. 28 during DSC experiments.
- (ii) The starting procedure was applied by replacing Acetone by Toluene (VWR Chemicals, HPLC grade). The solids recovered were still metastable.

During the study of this system, no procedure could be developed in order to equilibrate Phenanthrene/Dibenzothiophene mixtures. Consequently, no re-investigation of the binary phase diagram was made. In future works, other preparation methods such as melt crystallization should be tested in order to obtain binary samples in the state of equilibrium, in order to assess stable phase equilibria by DSC and XRPD.

g) Re-investigation of the Phenanthrene-Anthracene binary system

The compositions of the starting mixtures, the saturated liquids and the solid phases are summarized in tab. S3 (appendix 4, p. 271).

XRPD patterns (presented in fig. 29) indicate that Anthracene-rich mixtures crystallized as solid solution of Anthracene (<ss ANT>). Phenanthrene-rich mixtures (containing Anthracene fraction (X_{ANT}) below 0.102) crystallized as <ss PHEN LT> phase. Patterns of mixtures of intermediate compositions ranging from $X_{\text{ANT}} = 0.249$ to $X_{\text{ANT}} = 0.698$ clearly indicate that a solid solution of an intermediate phase (<ss IP>) appeared during the equilibration. The characteristic peaks of this phase can be observed at 15.3, 15.8, 19.8, 22.3 and 26.8 $^{\circ}$, and conform to previous remarks made by Ding *et al.* [27].

The pattern of the mixture of $X_{\text{ANT}} = 0.156$ corresponds to that of the <ss PHEN HT> phase, which indicates the existence of a <ss PHEN LT> + <ss PHEN HT> two-phase domain for mixtures exhibiting lower Anthracene contents. Due to the similarity of these two phase patterns, the extent of their domains could not be assessed by solely use of data provided in fig. 29.

The pattern of the $X_{\text{ANT}} = 0.348$ mixture highlights the disappearance of the characteristic peak of <ss PHEN HT> phase at 17.9 $^{\circ}$, which indicates that this mixture was made of pure <ss IP> phase. The $X_{\text{ANT}} = 0.375$ mixture exhibited a peak characteristic of the <ss ANT> phase at 19.4 $^{\circ}$. The characteristic peaks of <ss IP> phase were not observed for mixtures of $X_{\text{ANT}} > 0.976$. This indicates that the <ss IP> + <ss ANT> two-phase domain stability range was $0.375 \leq X_{\text{ANT}} \leq 0.976$; and that of the <ss PHEN HT> + <ss IP> was $0.249 \leq X_{\text{ANT}} \leq 0.315$.

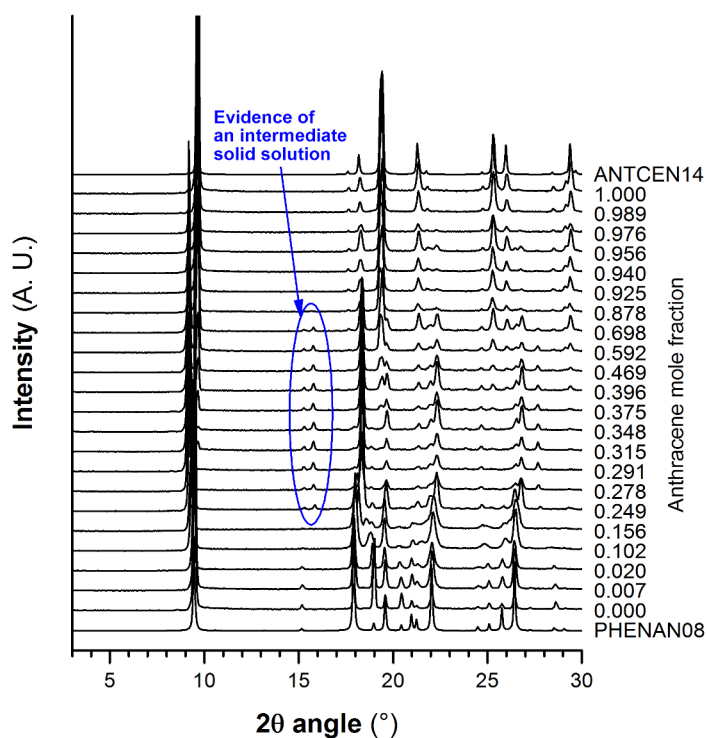


FIG. 29: XRPD patterns of Phenanthrene/Anthracene binary mixtures at 20 °C and 1 atm – ANTCEN14 [33] and PHENAN08 [28] are the predicted patterns calculated from Anthracene and Phenanthrene (LT) crystal structures, respectively.

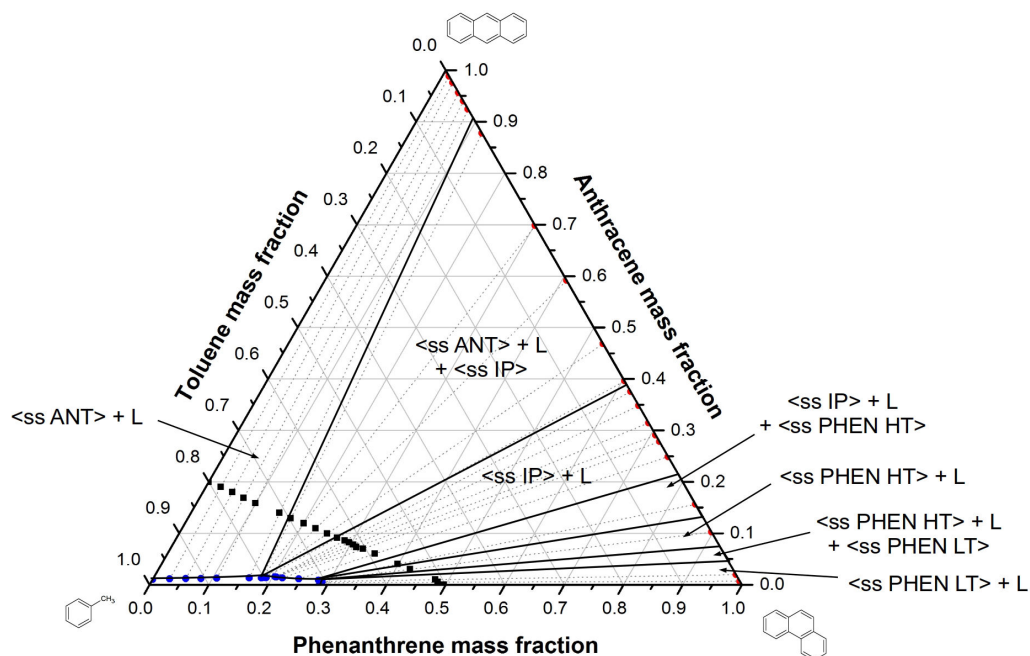


FIG. 30: Proposal for Phenanthrene/Anthracene/Toluene ternary phase diagram at room temperature and atmospheric pressure – ● liquidus points ■ tested compositions (*i. e.*, overall synthetic mixture) ● solid phase compositions

Using these data and those of tab. S3, the stability of the different phase domains at room temperature could be refined. A graphical representation of tab. S3 data on a ternary plot led to propose the ternary phase diagram presented in fig. 30. It is worth noting that *liquidus* points (*e. g.*, the solubility values) indicated that the stability domain of the <ss IP> was more extended than previously assessed using XRPD patterns. The same observation can be made for that of the <ss ANT> one. This was maybe caused by limitations related to the characterization methods and sample preparation.

DSC thermograms of the solid phases recovered by filtration are presented in fig. 31. They show that mixtures presenting the <ss IP> phase underwent endothermic invariant phenomena at ~ 85 - 90 °C, which was attributed to the decomposition of the <ss IP> phase in a peritectoid transformation (<ss IP> \rightarrow <ss PHEN HT> + <ss ANT> on heating). A Tammann plot applied to this transformation allowed for assessing the invariant composition at $X_{\text{ANT}} \approx 0.33$ (see fig. 32).

For $0.249 \leq X_{\text{ANT}} \leq 0.396$ mixtures, another endothermic invariant phenomenon at ~ 110 °C was observed. The latter was attributed to the decomposition of the <ss PHEN HT> phase in a peritectic transformation (<ss PHEN HT> \rightarrow L + <ss ANT> on heating). Note that the occurrence of two successive invariant transformations in a narrow temperature range was suspected due to the shape of the related DSC peaks. However, analyses at lower heating rate did not allow for a clarification on that point.

At higher temperatures, typical *liquidus*-related thermal events were observed.

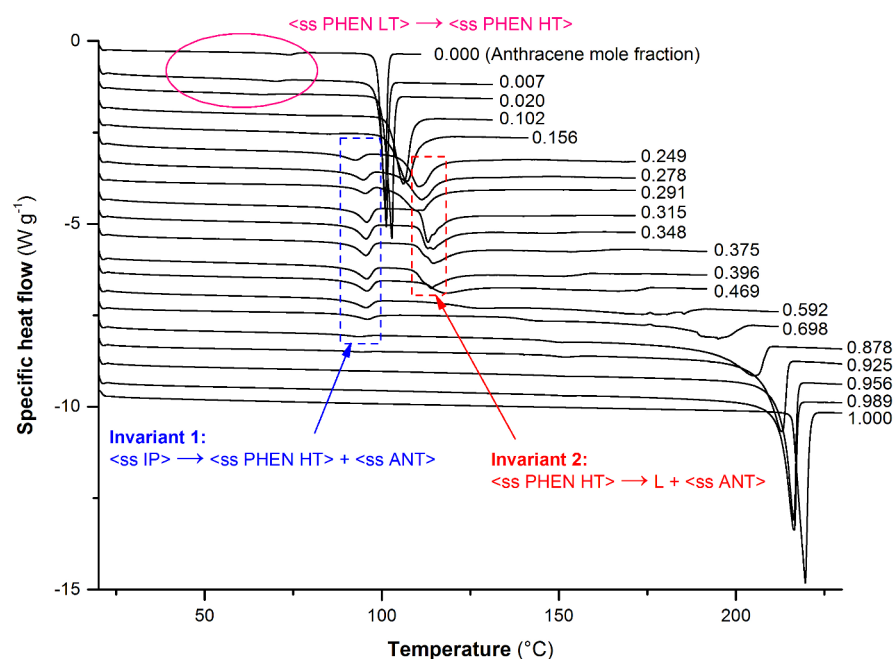
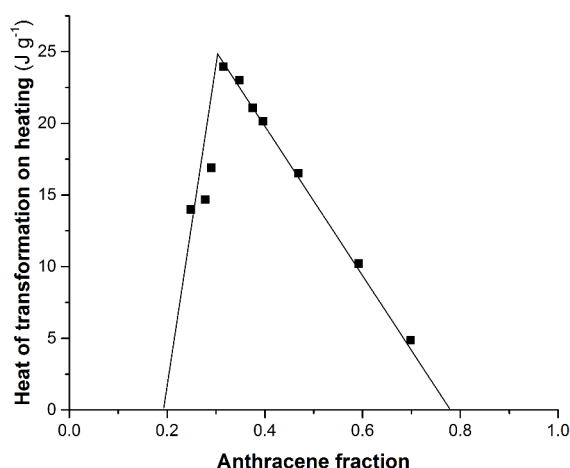


FIG. 31: DSC thermograms of Phenanthrene/Anthracene binary mixtures recrystallized in Toluene (endo down)

FIG. 32: Tammann plot for the invariant transformation occurring at $\sim 90^\circ\text{C}$

TAB. 5: Data on the invariant transformations observed in the Phenanthrene/Anthracene binary system

Temperature	Nature	Phases involved in the equilibrium		
$\sim 90^\circ\text{C}$	peritectoid	$\langle\text{ss IP}\rangle$ $X_{\text{ANT}} \sim 0.20$	$\langle\text{ss PHEN HT}\rangle$ $X_{\text{ANT}} \sim 0.33$	$\langle\text{ss ANT}\rangle$ $X_{\text{ANT}} \sim 0.75$
$\sim 110^\circ\text{C}$	peritectic	$\langle\text{ss PHEN HT}\rangle$ $X_{\text{ANT}} \sim 0.35$	$\langle\text{ss ANT}\rangle$ $X_{\text{ANT}} \sim 0.50$	L $X_{\text{ANT}} \sim 0.20$

A compilation of DSC thermal events on a temperature vs. composition chart led us to propose the binary phase diagram shown in fig. 33. Note that, due to intense signal noise, large errors ($\pm 5^\circ\text{C}$) arose on *liquidus* points. Data on invariant transformation are provided in tab. 5.

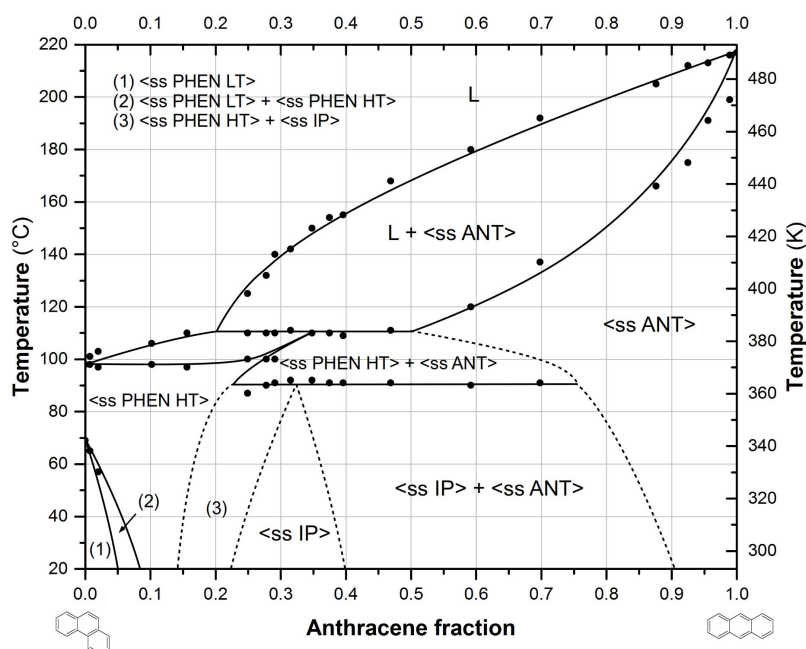


FIG. 33: Proposal for Phenanthrene/Anthracene binary phase diagram at 1 atm – • DSC thermal events, --- equilibrium curves not experimentally observed, and deduced by experimental data cross-checking

To conclude, a new proposal for this binary system was made. The following remarks can be addressed:

- (i) Both components form partial solid solutions with each other.
- (ii) As impurity, Anthracene increases Phenanthrene melting point ($k_0 > 1$ impurity).
- (iii) Anthracene has a strong impact on Phenanthrene solid-solid transition, as an increase of its contents to less than 10 % led to a complete reversal of Phenanthrene LT and HT phase stabilities.
- (iv) At least two invariant transformations were evidenced, which contradicts Bradley and Marsh proposal [22]. However, the potential occurrence of several invariant reactions near 110 °C will have to be clarified in order to validate this proposal.
- (v) The existence of an intermediate solid solution, suggested by Ding *et al.* [27], was confirmed.

h) Summary

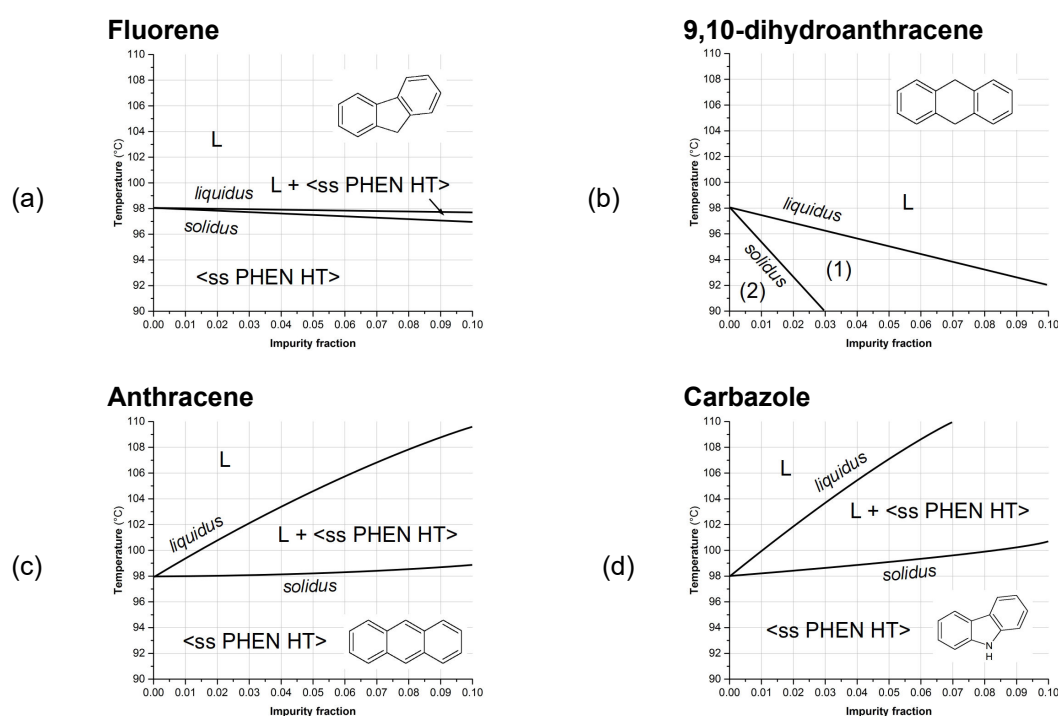


FIG. 34: **Extraction of impurity segregation coefficients from binary phase diagrams determined in this work** – (a) Phenanthrene-Fluorene system, (b) Phenanthrene/9,10-dihydroanthracene system, (c) Phenanthrene-Anthracene system, (d) Phenanthrene/Carbazole system. Compositions are expressed in mass fractions.

In this study, 4 phase diagrams between Phenanthrene and some of its impurities were established. Unfortunately, phase equilibria between Phenanthrene and Dibenzothiophene could not be assessed. The proposals made in this work allowed to complete and/or correct the existing ones. Data on impurity segregation coefficients could be extracted from our proposals (see fig. 34), as summarized in tab. 6.

TAB. 6: Values of Phenanthrene impurity segregation coefficients extracted from binary phase diagrams

Impurity	Fluorene	9,10-dihydroanthracene	Carbazole	Dibenzothiophene	Anthracene
Previous studies	< 1 [18,24]	–	> 1 [21]	< 1 [24]	> 1 [22,25]
This study	< 1, but close to unity	< 1	> 1	–	> 1

These data indicate that, during Zone Melting:

- Phase equilibria are not favorable for Fluorene removal, due to its segregation coefficient that is close to unity.
- 9,10-dihydroanthracene decreases Phenanthrene melting point, which means that this impurity should travel towards the same direction as that of the zone. The same remark can be made for Dibenzothiophene, according to [24].
- Conversely to the two previously mentioned impurities, Carbazole and Anthracene increase Phenanthrene melting point and should be displaced towards the opposite direction with reference to that of the zone.

All the phase diagrams established in this chapter highlighted that Phenanthrene and its impurities form partial solid solutions with each other. This indicates that, due to their similar chemical structures, discrimination between them in the solid state is limited. Consequently, this is consistent with the detection of these impurities in Phenanthrene purified by recrystallization (fig. 1 and tab. 1, p. 177).

Zone Melting could be an interesting alternative to amplify impurity removal in Phenanthrene samples, with reference to solvent-assisted recrystallization. However, the phase diagrams proposed in this chapter confirm that Phenanthrene impurities exhibit antagonist behaviors, which might limit the purifying effect of the method. Consequently, the technique should be tested in order to: (i) check the consistency of impurity displacements with the corresponding phase diagrams, (ii) assess the ability of the method at generating ultrapure Phenanthrene samples.

The next part of this chapter presents the procedure applied to validate our Zone Melting prototype using Phenanthrene as candidate molecule, before attempting its ultrapurification.

Two phase diagrams established in this work (Phenanthrene/9,10-dihydroanthracene and Phenanthrene/Carbazole) were published in the European Physical Journal: Special Topics [34].

5) Zone Refinement of Phenanthrene samples

According to the phase diagrams previously determined, and to the thermodynamic data available in the literature, Phenanthrene impurities exhibit various behaviors during solidification of impure samples. Hence, some impurities are expected to travel in the same direction as that of the molten zone, whereas the others should behave oppositely.

In this part of the study, the purification of Phenanthrene samples by means of the Zone Melting device developed in our lab was attempted.

In a first time, the proper functioning of the prototype was checked by treating two identical samples in different operating conditions. The aim of this part was to check the consistency of impurity distributions in zone-refined Phenanthrene samples with: (i) impurity segregation coefficient values extracted from their binary phase diagrams with Phenanthrene; (ii) Burton, Prim and Slichter relationship (eq. 6, p. 185), that relates zone displacement rate with effective values of impurity segregation coefficients.

In a second time, a Phenanthrene purification experiment by zone refining was attempted using operating conditions chosen according to the observations made in the first part of the work.

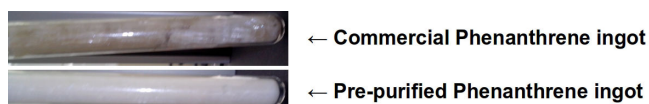
During these experiments, impurity levels were monitored by means of GC-FID, using the method developed in chapter III.

The ability of Zone Melting at purifying Phenanthrene samples was discussed using impurity level measurements in treated ingots.

a) Validation of the SMS laboratory Zone Melting device efficiency

To assess the efficiency of our Zone Melting prototype, commercial Phenanthrene (98 % indicative purity, supplied by Aldrich) was zone refined after application of a pre-purification procedure. This pre-treatment aimed at removing inorganic impurities from the starting material and is described below:

For both validation experiments, 10 g of Phenanthrene was dissolved in 50 mL of Dichloromethane (VWR Chemicals, HPLC grade). Three successive liquid-liquid extractions were performed using 3×50 mL of a 1 mol·L⁻¹ HCl aqueous solution. The same procedure was then applied with the same amounts of: (i) a 1 mol·L⁻¹ NaOH aqueous solution; (ii) milli-Q® water. Then, the organic phase was recovered; the solvent was evaporated and the recrystallized powder was dried overnight at 50 °C. Eventually, it was molten in glass tubes dedicated to our prototype to form ~ 9-cm length ingots. The effect of this pre-treatment was qualitatively evidenced by the color of the Phenanthrene ingots before refinement: a clear brightening of the material was observed after the washing procedure (fig. 35).



← Commercial Phenanthrene ingot

← Pre-purified Phenanthrene ingot

FIG. 35: Pictures of Phenanthrene ingots without and with application of the pre-purification procedure

The two ingots were separately treated in the following operating conditions:

- the first sample was zone refined 15 times using a $5 \text{ mm} \cdot \text{h}^{-1}$ zone displacement rate (270 h effective duration experiment),
- the second one was zone refined 5 times using a $1 \text{ mm} \cdot \text{h}^{-1}$ displacement rate (450 h).

After zone refinement, both ingots were segmented into 1–1.5 cm parts, which were manually ground to obtain powders homogeneous in composition. The latter were then analyzed by GC-FID to determine impurity levels. The impurity distribution profiles were then assessed using the recorded analytical data.

The impurities identified by means of GC-MSD in the pre-purified product are listed in tabs. 7 and 8, as well as impurity levels in the different parts of the two treated ingots. In these tables, 0 and 9 cm correspond to the starting and final positions of the zone during refinement, respectively.

As revealed by their entries, all the impurities were displaced during the two experiments, which means that our prototype works correctly. The main information that can be extracted from these data are:

- (i) an impurity (phenanthrenequinone), absent from the starting samples, was detected in the upper parts of the treated ingots. This indicates that Phenanthrene was probably slightly oxidized when the molten zone reached the end of the sample, as the molecule was exposed to air's oxygen at a high temperature. However, the generated amount of this new impurity was low, as the quantification data revealed that the maximum corresponding levels were 0.12 wt. % in the upper parts.
- (ii) Most of the impurities (*e. g.*, Fluorene, Methylbiphenyl, Dihydroanthracenes, Dihydrophenanthrenes, Tetrahydro-anthracene or -phenanthrene, Dibenzothiophene, Naphthothiophene 1, Anthracene, Methyl-dibenzothiophene or -naphthothiophene and Methylcarbazole) were displaced towards the same direction as that of the zone, which means that they exhibited a $k_0 < 1$ behavior. This observation is in accordance with the binary phase diagrams between Phenanthrene and the following impurities: Fluorene, 9,10-dihydroanthracene and Dibenzothiophene.
- (iii) Conversely, Naphthothiophene 2 and Carbazole were displaced towards the opposite direction with reference to that of the zone, which means that they behaved as $k_0 > 1$ impurities. This is consistent with the binary phase diagram between Phenanthrene and Carbazole (fig. 21).

Besides, the following remarks can be made:

- (i) The efficiency of the prototype at displacing Fluorene was moderate, as the levels of this impurity were of the same order of magnitude in the lower and upper parts of both treated ingots. This is consistent with the binary phase diagram between Phenanthrene and Fluorene, in which the *liquidus* and *solidus* lines in the Phenanthrene-rich region were close and denoted that Fluorene k_0 value is close to unity. Unfortunately, this limitation is due to unfavorable phase equilibria – and not to the method itself – and Zone Melting appears as being irrelevant for Fluorene removal.

TAB. 7: Impurity levels (in wt. %) in the different parts of the Phenanthrene ingot zone refined 15 times at 5 mm·h⁻¹ – impurities are sorted by ascending elution order.

Impurity	Starting sample	0–1 cm	1–2 cm	2–3 cm	3–4 cm	4–5 cm	5–6 cm	6–7.5 cm	7.5–9 cm
Fluorene	0.41 ± 0.02	0.35 ± 0.02	0.373 ± 0.007	0.389 ± 0.003	0.39 ± 0.01	0.43 ± 0.02	0.43 ± 0.03	0.45 ± 0.02	0.46 ± 0.02
Methylbiphenyl*	0.009 ± 0.001	0.0031 ± 0.0003	0.0036 ± 0.0007	0.0047 ± 0.0003	0.0056 ± 0.0003	0.008 ± 0.002	0.011 ± 0.002	0.0143 ± 0.0002	0.019 ± 0.001
9,10-dihydroanthracene	0.025 ± 0.001	ND	0.004 ± 0.002	0.0037 ± 0.0007	0.0029 ± 0.0007	0.0063 ± 0.0007	0.019 ± .002	0.0416 ± 0.0008	0.0853 ± 0.0003
9,10-dihydrophenanthrene	0.017 ± 0.001	0.0091 ± 0.0007	0.010 ± 0.002	0.0129 ± 0.0001	0.0135 ± 0.0004	0.0165 ± 0.0002	0.020 ± 0.002	0.023 ± 0.002	0.0261 ± 0.0006
Tetrahydro-phenanthrene or -anthracene*	0.007 ± 0.001	ND	ND	ND	ND	0.0032 ± 0.0002	0.007 ± 0.002	0.013 ± 0.002	0.0217 ± 0.0001
Dihydro-phenanthrene or -anthracene*	0.015 ± 0.001	0.0064 ± 0.0004	0.0077 ± 0.0002	0.0108 ± 0.0001	0.0114 ± 0.0004	0.0150 ± 0.0009	0.017 8+9 ± 0.002	0.0198 ± 0.0005	0.0241 ± 0.0006
Dibenzothiophene	0.46 ± 0.02	0.124 ± 0.005	0.135 ± 0.005	0.214 ± 0.004	0.270 ± 0.007	0.39 ± 0.03	0.52 ± 0.07	0.69 ± 0.02	0.97 ± 0.03
Naphthothiophene 1*	0.002 ± 0.001	ND	ND	ND	ND	ND	ND	0.0050 ± 0.0002	0.010 ± 0.002
Anthracene	0.43 ± 0.02	0.33 ± 0.02	0.356 ± 0.007	0.37 ± 0.02	0.385 ± 0.001	0.441 ± 0.006	0.46 ± 0.03	0.49 ± 0.02	0.53 ± 0.02
Naphthothiophene 2*	0.065 ± 0.003	0.093 ± 0.005	0.099 ± 0.004	0.074 ± 0.003	0.065 ± 0.005	0.0620 ± 0.0002	0.055 ± 0.001	0.049 ± 0.002	0.042 ± 0.003
Methyl-dibenzothiophene or -naphthothiophene*	0.003 ± 0.001	ND	ND	ND	0.0025 ± 0.0001	0.0039 ± 0.0002	0.0042 ± 0.0007	0.006 ± 0.002	0.007 ± 0.001
Carbazole	0.047 ± 0.003	0.089 ± 0.008	0.094 ± 0.007	0.053 ± 0.004	0.044 ± 0.005	0.040 ± 0.002	0.033 ± 0.003	0.0274 ± 0.0001	0.018 ± 0.001
Methylcarbazole*	0.006 ± 0.001	ND	ND	ND	ND	ND	0.007 ± 0.003	0.012 ± 0.002	0.017 ± 0.001
Phenanthrenequinone	ND	ND	ND	ND	ND	ND	0.012 ± 0.002	0.028 ± 0.001	0.068 ± 0.001
Total	1.50 ± 0.06	1.00 ± 0.05	1.08 ± 0.03	1.14 ± 0.02	1.19 ± 0.03	1.41 ± 0.05	1.60 ± 0.13	1.86 ± 0.06	2.29 ± 0.06

ND: not detected (impurity level below 0.0001 wt. %). *undetermined isomer

TAB. 8: Impurity levels (in wt. %) in the different parts of the Phenanthrene ingot zone refined 5 times at 1 mm·h⁻¹ – impurities are sorted by ascending elution order.

Impurity	Starting sample	0–1 cm	1–2 cm	2–3 cm	3–4 cm	4–5 cm	5–6 cm	6–7.5 cm	7.5–9 cm
Fluorene	0.41 ± 0.02	0.359 ± 0.006	0.34 ± 0.02	0.359 ± 0.009	0.381 ± 0.002	0.379 ± 0.004	0.399 ± 0.002	0.426 ± 0.004	0.514 ± 0.006
Methylbiphenyl*	0.009 ± 0.001	0.0042 ± 0.0004	0.0025 ± 0.0004	0.0035 ± 0.0005	0.0040 ± 0.0004	0.0046 ± 0.0004	0.0064 ± 0.0002	0.0088 ± 0.0003	0.0352 ± 0.0002
9,10-dihydroanthracene	0.025 ± 0.001	0.0054 ± 0.0001	0.0054 ± 0.0001	0.0026 ± 0.0001	0.0031 ± 0.0006	0.0044 ± 0.0008	0.0076 ± 0.0001	0.0148 ± 0.0007	0.264 ± 0.009
9,10-dihydrophenanthrene	0.017 ± 0.001	0.0113 ± 0.0006	0.0086 ± 0.0006	0.0090 ± 0.0001	0.0115 ± 0.0004	0.0120 ± 0.0003	0.0143 ± 0.0002	0.0181 ± 0.0004	0.041 ± 0.002
Tetrahydro-phenanthrene or -anthracene*	0.007 ± 0.001	ND	ND	ND	ND	ND	0.0025 ± 0.0001	0.0038 ± 0.0003	0.048 ± 0.002
Dihydro-phenanthrene or -anthracene*	0.015 ± 0.001	0.0087 ± 0.0001	0.0067 ± 0.0009	0.008 ± 0.002	0.0088 ± 0.0002	0.0101 ± 0.0004	0.012 ± 0.002	0.0153 ± 0.0001	0.041 ± 0.002
Dibenzothiophene	0.46 ± 0.02	0.187 ± 0.004	0.113 ± 0.004	0.149 ± 0.004	0.190 ± 0.004	0.229 ± 0.001	0.312 ± 0.002	0.43 ± 0.03	1.92 ± 0.02
Naphthothiophene 1*	0.002 ± 0.001	ND	ND	ND	ND	ND	ND	ND	0.018 ± 0.002
Anthracene	0.43 ± 0.02	0.351 ± 0.001	0.33 ± 0.01	0.342 ± 0.009	0.365 ± 0.007	0.381 ± 0.001	0.416 ± 0.004	0.455 ± 0.002	0.71 ± 0.02
Naphthothiophene 2*	0.065 ± 0.003	0.084 ± 0.001	0.105 ± 0.002	0.0833 ± 0.0001	0.073 ± 0.004	0.0650 ± 0.0007	0.055 ± 0.002	0.045 ± 0.002	0.020 ± 0.004
Methyl-dibenzothiophene or -naphthothiophene*	0.003 ± 0.001	ND	ND	ND	ND	ND	0.0036 ± 0.0004	0.0041 ± 0.0003	0.0139 ± 0.0005
Carbazole	0.047 ± 0.003	0.0751 ± 0.0001	0.1147 ± 0.0009	0.0645 ± 0.0002	0.049 ± 0.005	0.043 ± 0.002	0.030 ± 0.002	0.018 ± 0.003	0.0232 ± 0.0008
Methylcarbazole*	0.006 ± 0.001	ND	ND	ND	ND	ND	ND	ND	0.009 ± 0.002
Phenanthrenequinone	ND	ND	ND	ND	ND	ND	ND	ND	0.113 ± 0.009
Total	1.50 ± 0.07	1.09 ± 0.02	1.02 ± 0.04	1.02 ± 0.03	1.09 ± 0.03	1.13 ± 0.02	1.26 ± 0.02	1.44 ± 0.04	3.75 ± 0.07

ND: not detected (impurity level below 0.0001 wt. %). *undetermined isomer

(ii) Anthracene was displaced towards the same direction as that of the molten zone, which is not consistent with its phase diagram with Phenanthrene established in part II.4)g (p. 204). Two hypotheses could justify such results: (i) the existence of a congruent point in the Phenanthrene/Anthracene binary phase diagram, in the Phenanthrene-rich region (see fig. 36). Such point can reverse the segregation coefficient of Anthracene during solidification, according to the composition of the zone. If this hypothesis is true, Anthracene should behave as a $k_0 < 1$ impurity when its level is low in the Phenanthrene sample to treat, and as a $k_0 > 1$ impurity if the sample to treat contains large traces of this solute. (ii) The presence of other impurities in Phenanthrene changes the apparent order of the system. Hence, during solidification, binary phase diagrams are irrelevant to predict the segregation coefficient of this impurity.

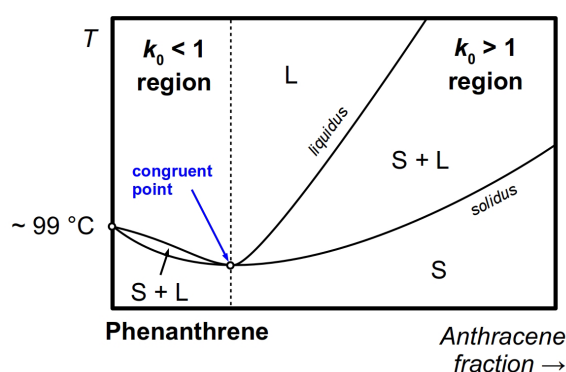


FIG. 36: **Hypothetical binary phase diagram between Phenanthrene and Anthracene** – zoom on the Phenanthrene-rich region, with existence of a congruent melting point.

During the DSC analysis of the bottom and top parts of the treated ingots at $5 \text{ K} \cdot \text{min}^{-1}$, the thermograms shown in fig. 37 were obtained. They revealed that Phenanthrene melting point was slightly decreased by the Zone Melting treatment in the top parts – with reference to the starting sample (see tab. 9) – which is consistent with the fact that the $k_0 < 1$ impurities were concentrated at this end of the ingot. Conversely, the melting point was slightly increased in the bottom parts that were richer in $k_0 > 1$ impurities. According to the experiments, the effect of Zone Melting on Phenanthrene solid-solid transition was more or less moderate.

TAB. 9: **DSC data on Phenanthrene samples before and after Zone Melting**

		Onset temperature (°C)		Heat of transformation (on heating, J g ⁻¹)	
		Solid-solid transition	Melting	Solid-solid transition	Melting
Before Zone Melting		68.8	98.6	4.97	100
5 passes at 1 mm h ⁻¹	Bottom part (0-1 cm)	69.5	99.3	5.05	101
	Top part (7.5-9 cm)	65.9	97.1	4.20	99.8
15 passes at 5 mm h ⁻¹	Bottom part (0-1 cm)	69.5	99.4	5.36	102
	Top part (7.5-9 cm)	68.6	98.0	4.99	100

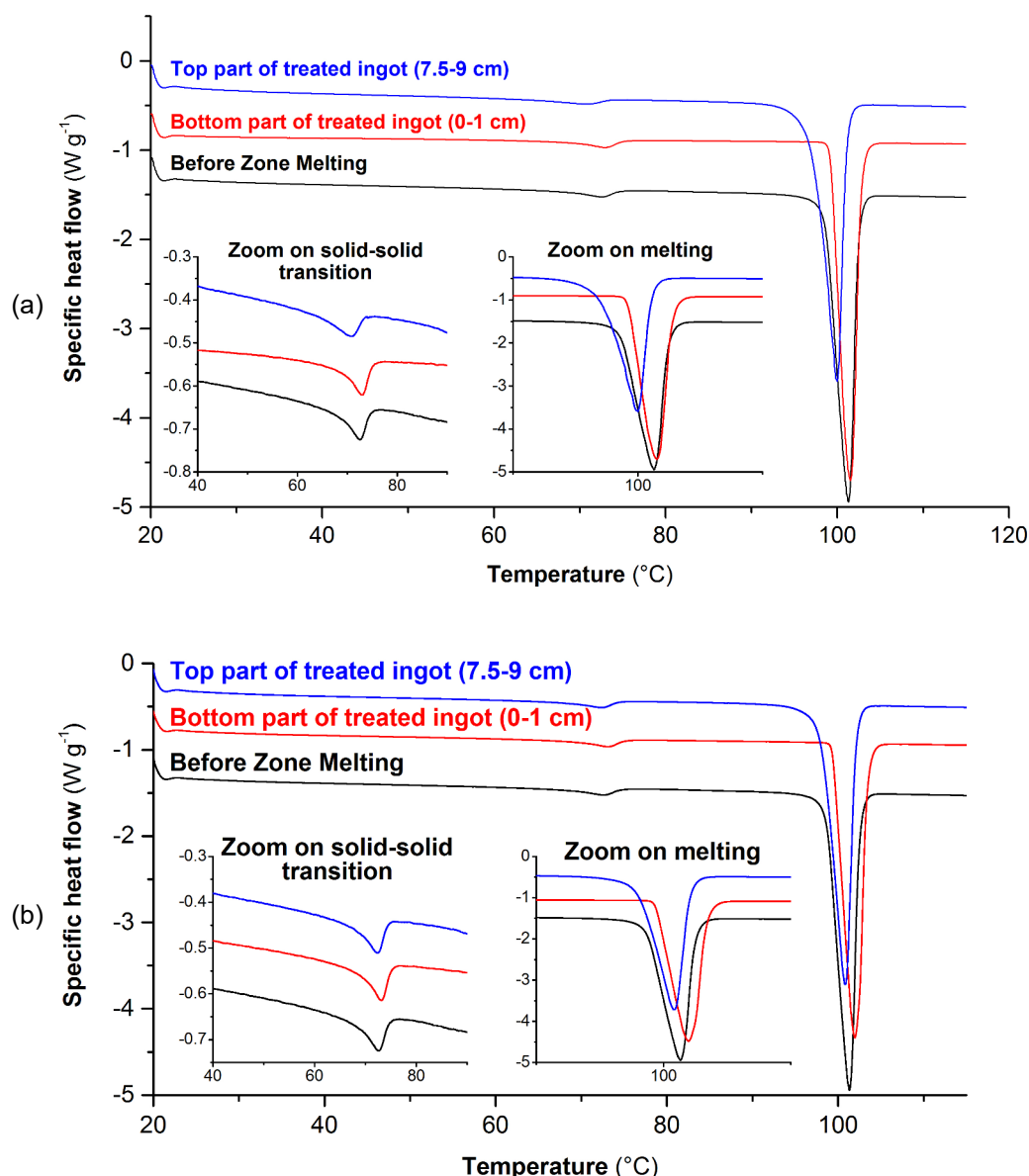


FIG. 37: DSC figures of Phenanthrene samples before and after Zone Melting (endo down) – (a) 5 passes at 1 mm h⁻¹; (b) 15 passes at 5 mm h⁻¹.

In addition, a comparison of impurity distribution profiles in the two treated ingots (fig. 38) highlights that similar impurity displacements were obtained while the operating conditions were different. It is also worth noting that the displacement of $k_0 < 1$ impurities (in fig. 38: Fluorene, 9,10-dihydroanthracene, Dibenzothiophene and Anthracene) was a little bit more efficient by applying the conditions of the second experiment. This indicates that, even if the number of passes was divided by three, the lower zone displacement rate used for this experiment led to impurity effective segregation coefficient values more favorable to their displacement. Consequently, these observations are in accordance with Burton, Prim and Slichter relationship (eq. 6, p. 185). However, this observation was less pronounced for $k_0 > 1$ impurities (here: the Naphthothiophene 2 and Carbazole).

A graphical representation of the sum of impurity levels in the different parts of the two treated ingots highlights that the best purity values measured were similar for the two experiments. However, during the 2nd experiment, a purer material was obtained in a more extended range of the sample.

To conclude, this part allowed to validate the efficiency of the new prototype designed in our laboratory. Measured distribution profiles indicated major information:

- (i) Phenanthrene impurities exhibited various and antagonist k_0 values, which can limit the purifying effect of the method according to the composition of the feed product.
- (ii) Zone Melting is not efficient at displacing some impurities of Phenanthrene – especially Fluorene – due to unfavorable phase equilibria. Conversely, it exhibited a high efficiency at displacing 9,10-dihydroanthracene.
- (iii) The use of lower zone displacement rates allowed for an improvement of the efficiency of the method at displacing impurities, especially those decreasing the melting point of Phenanthrene.
- (iv) In the tested conditions, Phenanthrene ultrapurity was far from being reached. Indeed, the impurity levels were decreased from 1.50 to, at best, 1.00 wt. %. For upcoming purification experiments, the operating conditions should be modified in order to improve the purifying effect of the method.

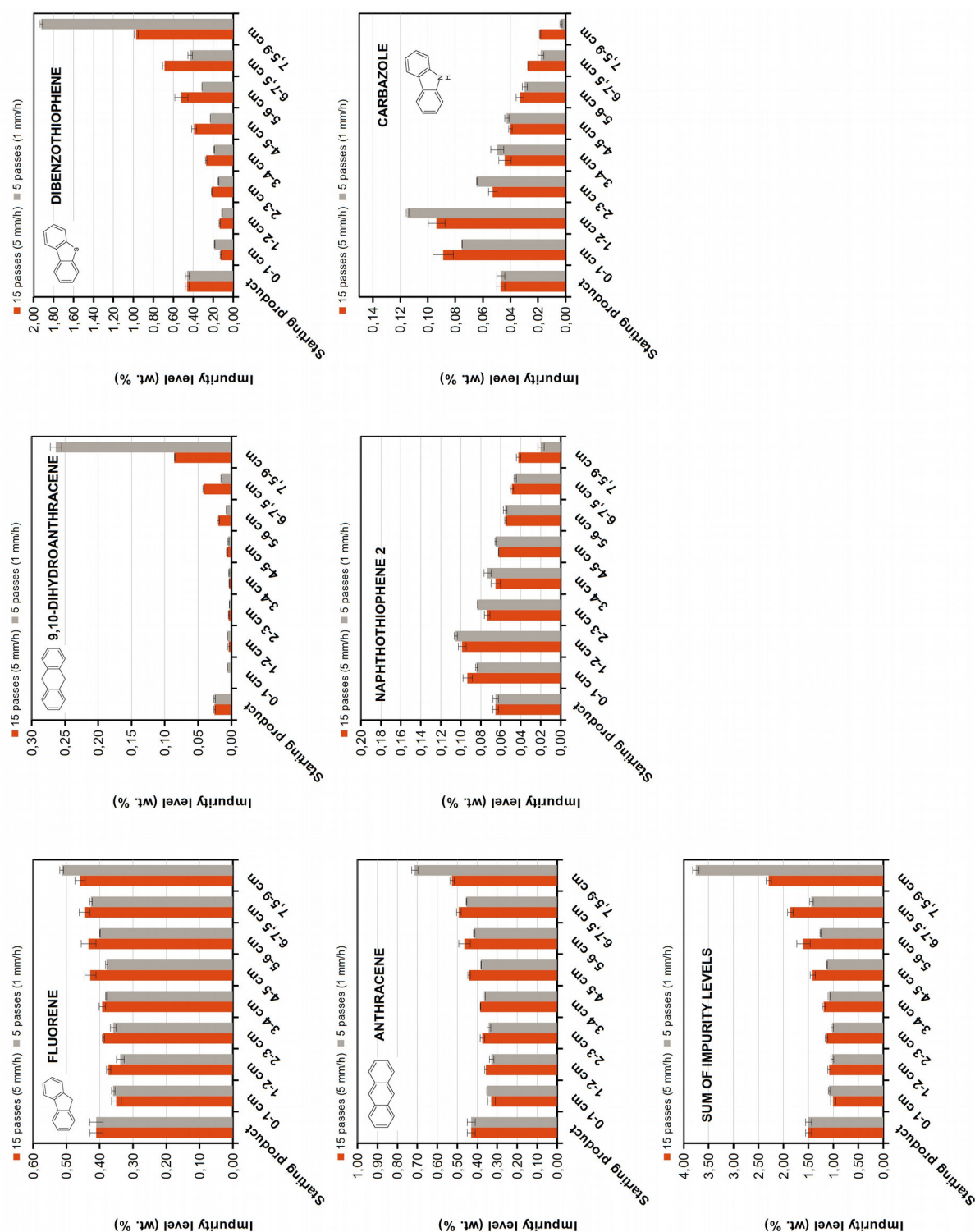


FIG. 38: **Impurity distribution profiles after zone refining experiments** – on the x axes, 0 corresponds to the starting position of the zone, and 9 cm to the final position.

b) Attempt of Phenanthrene ultrapurification by Zone Melting

In the second part of this work, Phenanthrene ultrapurification has been attempted by means of Zone Melting. As no matter of the Phenanthrene batch used for the previous validation experiments was available anymore, another batch from the same supplier was used for this part. This product was found to contain almost the same impurities as that previously used, except Methylbiphenyl and Methylcarbazole. However, two impurities that were not found in the previous starting batch were detected: Phenanthrenequinone and Anthracene-Maleic Anhydride Diels Alder adduct.

Before refining this product by Zone Melting, it was first pre-purified by solvent-assisted recrystallization in order to facilitate the removal of impurity traces during Zone Melting. The two following successive steps were applied:

- (i) 20 g of Phenanthrene was recrystallized in 50 mL of absolute Ethanol (> 99 %, VWR Chemicals). The mixture was heated to reflux, was cooled to room temperature under magnetic stirring and was then let equilibrating for 2 hours. The suspension was recovered by filtration under vacuum over a 2-porosity glass filter. The crystals were washed with 10 mL of 0 °C absolute Ethanol and were dried overnight at 50 °C. 16 g of dried product was recovered.
- (ii) The 16 g of recrystallized product were dissolved in 100 mL of HPLC grade Acetone (VWR Chemicals). The solution was filtered over 0.2 µm PTFE syringe filters to remove the insoluble inorganic impurities. The filtrate was recovered and Acetone was evaporated. The recrystallized powder was dried overnight at 50 °C.

The impurity levels before and after application of this two-step treatment was monitored by means of GC. The quantification results are given in tab. 10. They indicate that the procedure allowed the decrease of the levels of every impurity, except Fluorene and Naphthothiophene 2. Moreover, Phenanthrenequinone and the Anthracene/Maleic Anhydride Diels Alder adduct were completely eliminated by this treatment.

TAB. 10: Impurity levels (in wt. %) in Phenanthrene before and after the pre-purification treatments – impurities are sorted by ascending elution order

Impurity	Commercial product	After pre-purification
Fluorene	0.0051 ± 0.0005	0.005 ± 0.002
9,10-dihydroanthracene	0.31 ± 0.03	0.046 ± 0.002
9,10-dihydrophenanthrene	0.0085 ± 0.0001	0.0039 ± 0.0006
Tetrahydro-phenanthrene or -anthracene*	0.023 ± 0.003	0.0079 ± 0.0007
Dihydro-phenanthrene or -anthracene*	0.012 ± 0.002	0.0097 ± 0.0005
Dibenzothiophene	0.87 ± 0.04	0.46 ± 0.02
Naphthothiophene 1*	0.029 ± 0.002	0.0066 ± 0.0007
Anthracene	0.409 ± 0.003	0.32 ± 0.02
Naphthothiophene 2*	0.0081 ± 0.0004	0.008 ± 0.001
Methyl-dibenzothiophene or -naphthothiophene*	0.0061 ± 0.0004	0.0034 ± 0.0002
Carbazole	0.023 ± 0.002	0.0035 ± 0.0007
Phenanthrenequinone	0.023 ± 0.005	ND
Anthracene/Maleic Anhydride Diels Alder Adduct	0.019 ± 0.004	ND
Total	1.75 ± 0.08	0.88 ± 0.04

ND: not detected (impurity level below 0.0001 wt. %). *undetermined isomer

Fortunately, the level of Fluorene in this product is very low (~ 0.005 wt. %), which is suitable because this impurity is not efficiently displaced and removed from Phenanthrene by zone refining.

After pre-purification, a 7-cm length ingot was made to refine the sample by Zone Melting.

As shown in the part dedicated to the validation of the SMS laboratory Zone Melting device efficiency, the ability of the method at displacing the different impurity depends on many parameters (number of zone passes, zone displacement rate, etc). The latter should be compromised in order to optimize the efficiency of the process. Consequently, it was chosen to perform a large number of zone passes (here, 50) at moderate zone displacement rate (3 mm h^{-1}) to obtain a desirable efficiency without loosing too much time.

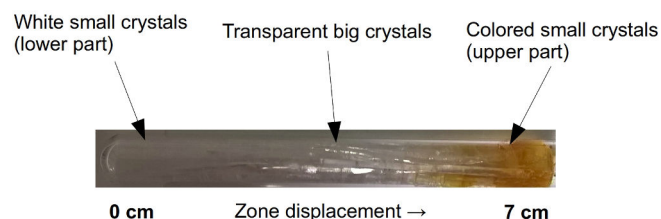


FIG. 39: **Picture of the Phenanthrene ingot treated by Zone Melting**

At the end of the refining (1333 h effective duration, that means ~ 56 days), the ingot was segmented into 7 equivalent 1-cm parts, which were each ground and analyzed by GC-FID to determine impurity levels at the different parts of the sample. A picture of the treated ingot is shown in fig. 39. The quantification results are given in tab. 11.

TAB. 11: **Impurity levels (in wt. %) in the different parts of the Phenanthrene ingot treated for ultrapurification purposes** – impurities are sorted by ascending elution order

Impurity	Starting sample	0–1 cm	1–2 cm	2–3 cm	3–4 cm	4–5 cm	5–6 cm	6–7 cm
Fluorene	0.005 ± 0.002	0.0038 ± 0.0001	0.0039 ± 0.0004	0.0037 ± 0.0005	0.0039 ± 0.0002	0.0044 ± 0.0003	0.005 ± 0.001	0.0048 ± 0.0006
9,10-dihydroanthracene	0.046 ± 0.002	ND	ND	ND	0.0030 ± 0.0007	0.0047 ± 0.0003	0.0138 ± 0.0005	0.113 ± 0.002
9,10-dihydrophenanthrene	0.0039 ± 0.0006	0.0026 ± 0.0003	0.004 ± 0.002	0.004 ± 0.002	0.0046 ± 0.0005	0.0038 ± 0.0008	0.0052 ± 0.0009	0.006 ± 0.002
Tetrahydro-phenanthrene or -anthracene*	0.0079 ± 0.0007	ND	ND	ND	ND	0.0040 ± 0.0001	0.0076 ± 0.0005	0.0144 ± 0.0005
Dihydro-phenanthrene or -anthracene*	0.0097 ± 0.0005	0.0046 ± 0.0002	0.0037 ± 0.0003	0.0054 ± 0.0002	0.0065 ± 0.0001	0.0088 ± 0.0003	0.012 ± 0.002	0.0154 ± 0.0009
Dibenzothiophene	0.46 ± 0.02	0.118 ± 0.004	0.115 ± 0.004	0.143 ± 0.002	0.241 ± 0.005	0.412 ± 0.004	0.636 ± 0.004	0.952 ± 0.001
Naphthothiophene 1*	0.0066 ± 0.0007	ND	ND	ND	ND	0.004 ± 0.001	0.007 ± 0.002	0.013 ± 0.002
Anthracene	0.32 ± 0.02	0.26 ± 0.02	0.256 ± 0.005	0.268 ± 0.004	0.297 ± 0.003	0.338 ± 0.003	0.374 ± 0.006	0.420 ± 0.006
Naphthothiophene 2*	0.008 ± 0.001	0.0121 ± 0.0005	0.0100 ± 0.0005	0.0106 ± 0.0002	0.0081 ± 0.0007	0.0065 ± 0.0005	0.0067 ± 0.0005	0.0053 ± 0.0002
Methyl-dibenzothiophene or -naphthothiophene*	0.0034 ± 0.0002	ND	ND	ND	0.0027 ± 0.0008	0.0038 ± 0.0005	0.0048 ± 0.0003	0.007 ± 0.002
Carbazole	0.0035 ± 0.0007	0.0054 ± 0.0006	0.0051 ± 0.0006	0.0045 ± 0.0004	0.0033 ± 0.0004	0.0028 ± 0.0001	ND	ND
Phenanthrenequinone	ND	ND	ND	ND	ND	ND	0.008 ± 0.002	0.0420 ± 0.0007
Total	0.88 ± 0.04	0.41 ± 0.03	0.40 ± 0.02	0.44 ± 0.02	0.57 ± 0.02	0.79 ± 0.02	1.08 ± 0.03	1.59 ± 0.02

ND: not detected (impurity level below 0.0001 wt. %). *undetermined isomer

As shown by tab. 11 entries, the main information that can be extracted from these quantification results are the following ones:

- (i) ultrapurity was not reached in the tested conditions, as the purest fraction of the treated ingot contained 0.40 wt. % of impurities.
- (ii) the main contributions to the impurity levels in the different parts of the treated ingots are due to Dibenzothiophene and Anthracene, the major impurities of the starting product. Even after 50 molten zone passes, their levels could not be decreased below 0.1 mole %.

Consequently, this ultrapurification experiment was not successful. Many options can be envisaged to reach ultrapure Phenanthrene by Zone melting: (i) increasing the number of zone passes, in order to amplify impurity concentration at ingot ends; (ii) decreasing the zone displacement rate to improve impurity segregation during zone solidification; (iii) changing the dimensions of the sample and/or the zone to adapt the conditions. However, optimizing these conditions by a trial-and-error approach would be time consuming. Moreover, it does not guaranty the reaching of targeted results.

6) Conclusions

In this study, a new Zone Melting prototype was developed, tested and validated using Phenanthrene as model molecule.

The results highlighted that our device was operative. Moreover, the influence of two experimental parameters (*e. g.*, the number of zone passes, the zone displacement rate) was assessed and the results were consistent with the different theoretical elements on Zone Melting previously introduced (II.2, p. 180): using low displacement rates was found to significantly improve the efficiency of the method at displacing the different impurities at sample ends.

Applying this method to Phenanthrene did not lead to ultrapure material. This was mainly due to the presence, with a somewhat “large” abundance, of two impurities in the starting material (*e. g.*, Dibenzothiophene and Anthracene). Repeating the number of passes did not allow to amplify these two impurity concentrations at ingot ends in the tested conditions. Consequently, other purification methods should be envisaged to remove the maximal amount of impurities before applying Zone Melting to remove the last traces. In this view, vacuum sublimation could be an interesting alternative, and was applied to Phenanthrene samples, as reported in the next part.

III. PURIFICATION BY VACUUM SUBLIMATION

1) Introduction

Vacuum sublimation is a crystal growth technique particularly appropriate for chemicals that exhibit moderate or high vapor pressures. Many experimental devices were previously developed for different applications. A few papers reported examples of purification experiments applied to organic chemicals using gradient sublimation apparatuses [35,36].

Gradient sublimers are made of a glass tube containing a sample holder, into which the substance to purify is placed. The tube is connected to a vacuum pump in order to reduce the pressure inside the system. Moreover, it is exposed to a controlled temperature gradient, that leads to sublimation of the sample and recondensation of its species at different parts of the tube corresponding to their condensation temperature (T_{cond}).

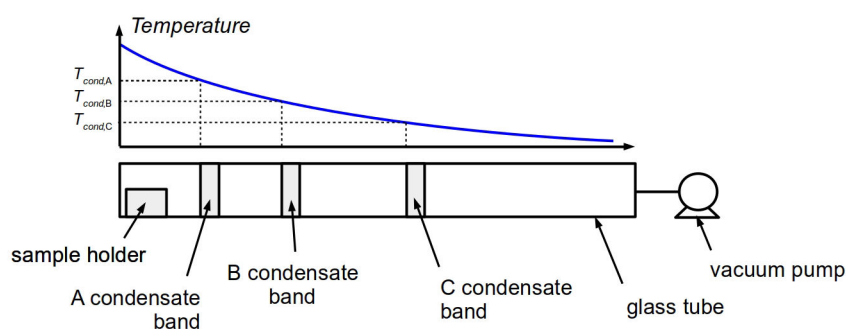


FIG. 40: **Schematic representation of an ordinary gradient sublimer**

This technique has been mainly applied to the purification of chemicals dedicated to electronics [35,36]: organic semiconductors, organic light emitting devices, etc. However, its optimization requires to adapt many parameters: (i) the temperature profile, (ii) the tube length, (iii) the operating pressure. Such a task is not that obvious and generally requires trial-and-error approaches. Nevertheless, when the species to separate are known, the use of thermodynamic data related to their vapor pressures can help at predicting their condensation temperature. Consequently, the operator can adapt more easily the temperature profile along the glass tube.

In the case of Phenanthrene, the molecule and its impurities present vapor pressures that permit their sublimation in experimental conditions that are easy to impose. Moreover, these vapor pressures (fig. 41) are different enough to make impurity recondensate at temperatures whose values are significantly different at low operating pressures (tab. 12), which theoretically paves the way to their separation by gradient sublimation.

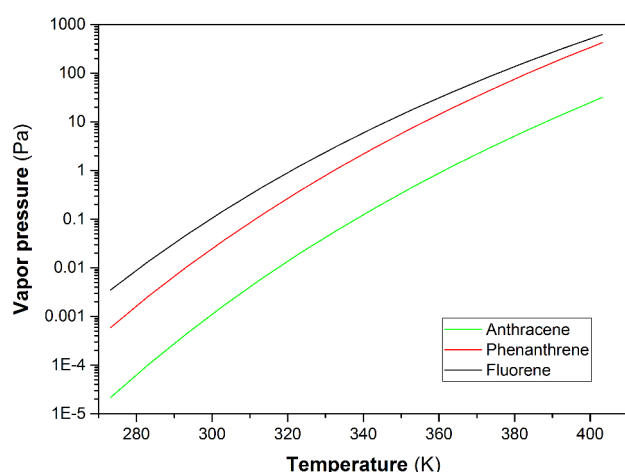


FIG. 41: **Vapor pressures of Phenanthrene and two of its impurities** – calculated from [37,38].

TAB. 12: **Calculated condensation temperatures (in °C) of Phenanthrene and two of its impurities**

Pressure (Pa)	Fluorene [37]	Phenanthrene [38]	Anthracene [38]
10	72.83	82.88	114.99
1	47.83	59.04	88.14
0.1	26.36	38.19	64.76
0.01	7.70	19.81	44.22
0.001	- 8.67	3.47	26.04

Consequently, this technique was tested on the molecule, in order to assess its ability at separating Phenanthrene from its impurities – especially those that could not be removed by Zone Melting or co-crystallization (*e. g.*, Fluorene, Dibenzothiophene, Anthracene and Carbazole).

As shown in upcoming paragraph 2, two gradient sublimers was designed and built in our laboratory. The devices were tested on synthesis-grade Phenanthrene. Impurity levels in the different condensate fractions were monitored by GC to assess the purifying effect of the method (paragraph 3).

2) Development of a new gradient sublimator

In order to purify Phenanthrene by vacuum sublimation, a new gradient sublimator was designed in our laboratory. This part of the work has been made with the thorough support of James COOPER, a student who made its internship of master (2nd year, material science, Université de Rouen-Normandie) in our laboratory.

Two gradient sublimators were developed in this work. The first prototype, presented in part a, exhibited critical inconveniences and was modified to bypass them, which gave a second prototype (presented in part b).

a) Presentation of the first gradient sublimation prototype

The first gradient sublimator developed in our laboratory consisted in a glass tube connected to a vacuum turbomolecular pump (10^{-10} bar regulated pressure). The end of the tube was connected to a cylindrical oven of adjustable power (see fig. 42).

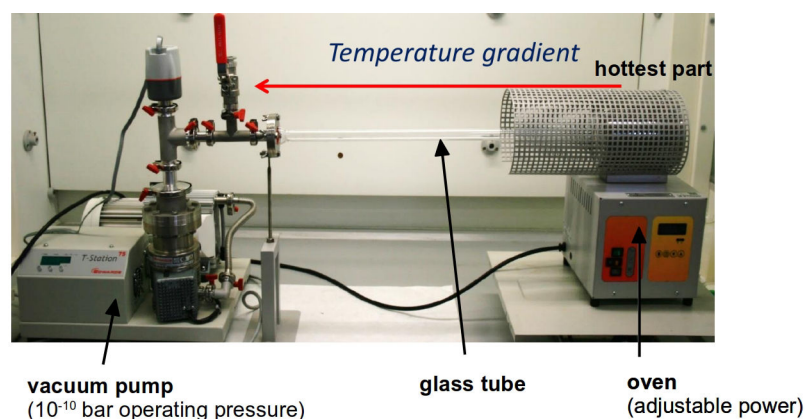


FIG. 42: **Presentation of the first gradient sublimator developed in the laboratory**

This prototype did not allow a complete control of the temperature gradient along the tube. Only the adjustable oven power could be adapted. Preliminary sublimation tests using this configuration led to immediate recondensation of Phenanthrene crystals in the first part of the tube that was not in contact with the oven (see fig. 43a). In order to smooth the temperature gradient, the tube was lined with conductive Al sheets (fig. 43a), in which the sample was put. However, no significant improvement was observed – the crystals immediately recondensated at the end of the oven.

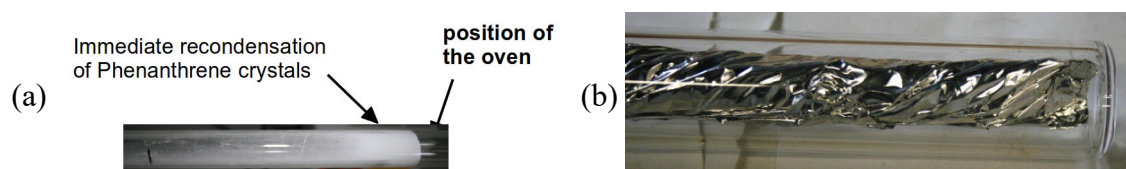


FIG. 43: **Picture of the tube after sublimation of a Phenanthrene sample – without (a) of with (b) Al sheet in the tube**

The major drawbacks of this device were:

- (i) the impossibility to adjust the temperature gradient along the glass tube, which prevented from optimizing the separation of the different species of the feed sample;
- (ii) the embarrassment caused by the difficulty at recovering the recondensated crystals.

Consequently, the device was modified in order to bypass these two drawbacks.

b) Presentation of the new gradient sublimer designed in our laboratory

The new gradient sublimer developed in our laboratory is shown in fig. 44a. The previous oven was replaced by a cascade of ovens of adjustable powers. Besides, a system of cascade of glass blocks fitted with each others (fig. 44b) was inserted inside the glass tube (fig. 44c) in order to facilitate the recovery of recondensated crystals.

During every experiment, the sample to sublime is placed in a glass sample holder that is screwed with several open glass blocks of ~ 5 cm length. This permits the formation of a collapsible glass tube. The latter is then is placed in the sublimation glass tube that is submitted to the temperature gradient. At the end of the sublimation experiment, the different blocks of the internal tube can be disassembled to recover the recondensated crystals at different positions, without breaking the external tube. Every fraction can then be analyzed to determine its purity.

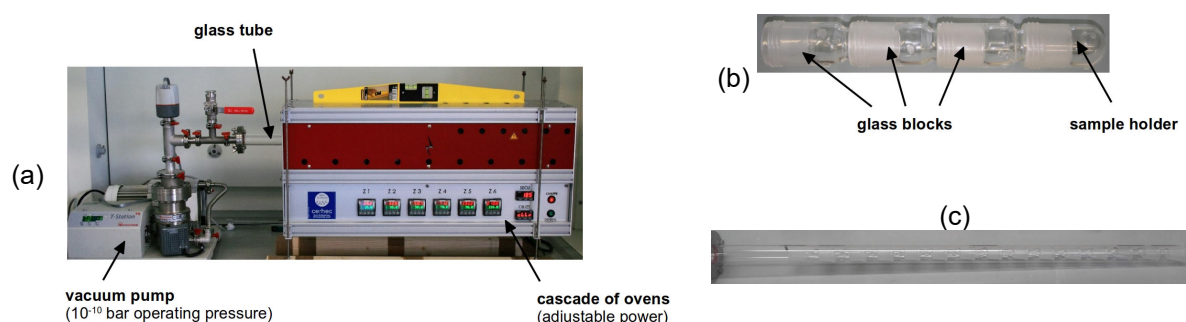


FIG. 44: **Presentation of the new gradient sublimer developed in the laboratory**

(a) global view, (b) cascade of glass blocks, (c) sublimation tube filled with glass block cascade

The oven cascade contains 6 different ovens: Z1, Z2, ..., Z6. The sample holder is placed in Z6 that is programmed to allow for sample sublimation. The other ovens are dedicated to the adjustment of the temperature gradient.

In the next parts of this paragraph, the different fractions collected after sublimation experiments are numbered according to their distance from Z6. The feed (sample holder), placed in Z6, corresponds to fraction 0. The fractions collected starting from the first glass block are numbered 1, 2, ..., 14.

3) Phenanthrene purification experiments

Phenanthrene (Alfa Aesar, 98 %) was purified by vacuum sublimation using the second device described previously. The starting composition of the product is provided in tab. 13⁴, in which the impurities are sorted by GC elution order – in other words, by descending order of vapor pressures. The temperature gradient set during the sublimation experiments is given in tab. 14.

Note that, in these conditions, the feed sample was liquid. Consequently, the term “sublimation” is not really appropriate, as the sample was vaporized. However, this does not change the fact that the different species should recondensate at different parts of the tube.

For the purification experiment, approximately 2 g of Phenanthrene was let sublimating for 2 hours. At the end of the procedure, several condensate fractions could be collected from block 6 to block 10 (30-55 cm away from the sample holder). There was no distinct condensate bands, but only one whose extend was large. The sample holder contained a brown powder mainly made of inorganic impurities (fig. 45). The impurity levels in the different fractions were determined by GC. The quantification results are given in tab. 15.

TAB. 13: **Composition of Phenanthrene samples used for purification experiments**

Impurity	Level (wt. %)
Fluorene	0.260
9,10-dihydroanthracene	0.011
9,10-dihydrophenanthrene	0.029
1-methylfluorene	0.051
Dibenzothiophene	0.490
Anthracene	0.448
Carbazole	0.221
Total	1.510

TAB. 14: **Temperature gradient imposed during sublimation experiments**

Oven	Z1	Z2	Z3	Z4	Z5	Z6
Set temperature (°C)	OFF	30	50	70	90	110
Actual temperature in steady state ⁵ (°C)	OFF	31.1	50.0	70.1	90.3	110.2



FIG. 45: **Pictures of the sample holder before (left) and after (right) the sublimation experiment**

4. Note that, during chromatographic measurements, only one replicate was made per sample. Consequently, confidence intervals are not provided in this part.

5. The time required to reach the steady state was approximately 20 minutes.

TAB. 15: Impurity levels in the different recondensated fractions of Phenanthrene

Impurity	Level (wt. %)					
	Commercial	Condensate fraction				
		6	7	8	9	10
Fluorene	0.260	0.074	0.120	0.419	0.984	1.802
9,10-dihydroanthracene	0.011	ND	ND	ND	0.018	0.044
9,10-dihydrophenanthrene	0.029	ND	ND	0.010	0.035	0.071
1-methylfluorene	0.051	0.024	0.034	0.087	0.165	0.275
Dibenzothiophene	0.490	0.286	0.421	1.092	2.060	3.247
Anthracene	0.448	0.740	0.552	0.403	0.393	0.416
Carbazole	0.221	0.757	0.165	0.015	0.036	0.068
Total	1.510	1.882	1.292	2.027	3.692	5.923

ND: Not detected (< 0.0001 wt. %). Fraction 6 position began 30 cm away from sample holder, fraction 10 ended 55 cm away.

As revealed by tab. 15 data, all the collected fractions mainly contained Phenanthrene. However, the impurity levels depended on the block. Indeed, the impurities more volatile than Phenanthrene (*e. g.*, Fluorene, 9,10-dihydroanthracene, 9,10-dihydrophenanthrene, 1-methylfluorene and Dibenzothiophene) were more concentrated in the blocks farthest away from the sample holder, which means that they preferentially recondensated in the coldest parts of the tube. Conversely, Anthracene and Carbazole – the heaviest impurities – were more concentrated in the blocks closest to the sample holder; they recondensated at the hottest parts of the tube. These results are qualitatively consistent with the relative vapor pressures of these impurities, but not with the predicted condensation temperatures indicated in tab. 12. The purest fraction was fraction 7, that contained 1.292 wt. % of impurity. This corresponds to a limited gain of purity with reference to the starting product.

However, it is worth noting that all the impurities were distributed over a large range in the tube. For example, Fluorene preferentially recondensated in fraction 10, but the impurity is present in all the other fractions at lower levels. This indicates that the temperature gradient was probably too rough to generate thin impurity condensate bands, which might explain the absence of impurity separation.

According to the temperature gradient applied along the sublimation tube, the different condensate fractions corresponded to the 46-55 °C region. Consequently, in order to amplify the separation, fraction 7 (the purest one) was put in the sample holder and was sublimated for 2 hours after smoothing the gradient linearly: Z1 oven was set at 55 °C and Z5 at 46 °C. The impurity levels in the different condensate fractions are given in tab. 16.

Regarding tab. 16 entries, the impurity distribution profiles along the sublimation tube were similar to that observed during the previous experiment. However, the impurity levels were lower. The purity of Phenanthrene could be increased from 98.7 to 99.2 wt. % in the purest fraction (# 7, again). Nevertheless, no remarkable improvement of impurity separation was obtained.

TAB. 16: Impurity levels in the different recondensated fractions of Phenanthrene after resublimation of fraction 7

Impurity	Level (wt. %)					
	Starting product	Condensate fraction				
		6	7	8	9	10
Fluorene	0.120	0.034	0.050	0.111	0.167	0.207
9,10-dihydroanthracene	ND	ND	ND	ND	ND	ND
9,10-dihydrophenanthrene	ND	ND	ND	ND	ND	ND
1-methylfluorene	0.034	0.017	0.023	0.042	0.059	0.068
Dibenzothiophene	0.421	0.200	0.275	0.525	0.751	0.895
Anthracene	0.552	0.483	0.409	0.339	0.340	0.331
Carbazole	0.165	0.160	0.032	0.012	0.012	0.009
Total	1.292	0.895	0.789	1.029	1.329	1.510

ND: Not detected (< 0.0001 wt. %). Fraction 6 position began 30 cm away from sample holder, fraction 10 ended 55 cm away.

4) Discussion, conclusion and outlooks

As revealed by the experiments performed in this work, vacuum sublimation was unable at separating Phenanthrene and its organic impurities in the tested conditions. Moderate purifying effects were observed. However, **the main advantage observed was the separation of Phenanthrene from its inorganic impurities** that did not sublime/vaporize. Moreover, another benefit of this method is that it does not requires the addition of third species (solvent, ...) to perform purification, which prevent from potential further impurity addition in the product to purify.

To achieve a separation of Phenanthrene and its impurities, the effect of the temperature gradient was investigated. However, no improvement was obtained, which indicates that the disappointing results came from other issues. In particular, the effect of operating pressure could not be assessed, as the vacuum pump used in these experiments only operates at 10^{-10} bar.

In future works, the device should be improved by using another vacuum pump, of adjustable regulated pressure. In addition, other technical aspects, such as block filling using small particles to enhance crystallization from gas phase, should be investigated.

IV. PURIFICATION BY CO-CRYSTALLIZATION

1) Introduction

As revealed by previous experiments, no complete elimination of Phenanthrene impurities could be achieved using the methods tested on native product (*e. g.*, solvent-assisted recrystallization, Zone Melting and vacuum sublimation). Indeed, due to unfavorable phase equilibria or technical limitations, these techniques only led to partial decreases of impurity levels. Consequently, other approaches can be chosen to attempt their removal:

- (i) performing successive crystallization steps to amplify the purifying effect until the purity requirements are reached. While this approach seems to be the most simple one, it implies a large loss of matter due to the limited crystallization yield associated with every step. Consequently, this pathway is not the most suitable one.
- (ii) changing the nature of the phase that crystallizes during the purification procedure.

Many procedures can be envisaged to perform the second approach: salt formation, crystallization of a new polymorph, etc. However, due to Phenanthrene characteristics, such pathways cannot be envisaged: the molecule does not present any acidic or basic group, which prevents from salt formation; and no method was reported to stabilize a polymorph other than the LT one in normal conditions.

However, another method to deal with that is co-crystallization. During the process, the molecule to purify is placed in a vessel with another species (*e. g.*, the co-former) able at making a defined compound (*e. g.*, the co-crystal, fig. 46) with it, and a solvent to allow for co-crystal formation⁶. After equilibration, the co-crystal can be isolated by filtration, and treated to remove the co-former and recover the target species.

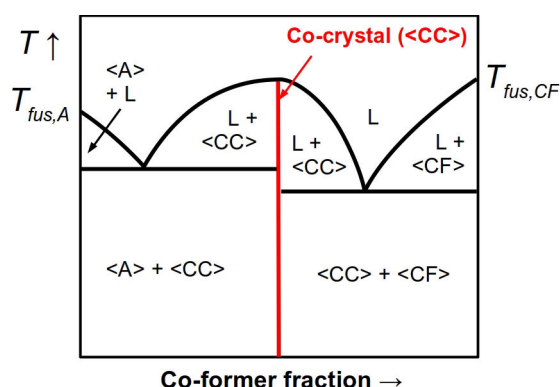


FIG. 46: Example of binary phase diagram between a compound to purify (A) and a co-former (CF) with existence of a co-crystal (CC).

Recently, a few examples of applications of co-crystallization to the separation of chemical species have been reported. Among them, several studies conducted by Springuel and

6. The proportions of the three species should be adapted in order to obtain a two-phase equilibrium between the co-crystal and the saturated liquid.

Leyssens focused on the separation of different couples of enantiomers [39,40]. Their works highlighted that the use of co-crystallization was a promising alternative to enantiomer separation by diastereomeric salt formation, especially when the target molecules are not able to form salts [39].

During crystallization and co-crystallization, phase equilibria drive the purifying effect of the methods. Indeed, the crystallized species (*e. g.*, the compound to purify in case of crystallization, or the co-crystal during co-crystallization) can or cannot incorporate impurities of the starting product in their lattice, which influences the purifying effect of the corresponding method. When impurity incorporation is not permitted by the crystal structure of the species crystallized, they remain in solution and the crystals are impurity-free. Thus, co-crystallization appeared as a potential interesting alternative to remove impurities from Phenanthrene. Consequently, this method was investigated in order to assess its purifying effect. Of course, the latter should depend on the tested co-crystal, and they are as many possibilities as there exists co-crystals.

During preliminary researches, many co-formers were identified, which paved the way to Phenanthrene purification tests using this method. The co-crystals and some of their characteristics (including stoichiometry and chemical properties of the co-formers) are presented in part 2 of this paragraph.

To offer more possibilities in terms of purifying effects, a search for new Phenanthrene co-formers was also attempted. This screening led to the discovery of new co-crystals, which is reported in part 3.

Then, purification experiments by means of co-crystallization with selected known or discovered co-crystals were performed on technical-grade Phenanthrene. After co-former removal, impurity levels were monitored by GC-FID to assess the purifying effect of every co-crystallization procedure. This work is reported in part 4.

Eventually, the purifying effects of this method were compared with that of solvent assisted recrystallization. A discussion is attempted in part 5, with a particular attention paid to phase equilibria and discrimination in the solid state, before concluding this sub-chapter.

2) Phenanthrene known co-crystals

Thanks to a research in the Cambridge Structural Database (CSD, 2016), many Phenanthrene co-crystals could be found. The latter are described in tab. 17 entries, in which the names, formulas and stoichiometry of the different co-formers are given.

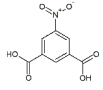
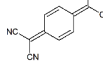
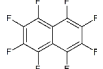
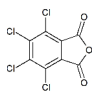
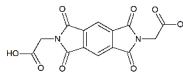
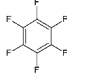
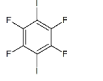
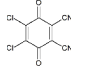
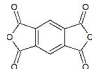
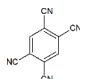
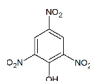
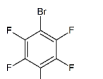
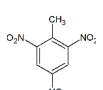
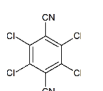
As revealed by the different entries, all the known Phenanthrene co-formers are made of at least one aromatic ring, substituted by several polar groups (nitro, chloro, etc). Many of them appear as being interesting due to the presence of carboxylic acids or other groups than can be converted to acids (cyano, anhydride...). As Phenanthrene is insoluble in water, the presence of such groups on the different co-formers paves the way to their removal from co-crystals by simple extraction treatment with basic water.

However, some other co-formers are not suitable for co-crystallization due to the absence of such aqueous-phase-soluble groups. Among them, OFN, HFB, TFDIB, DCDCBQ, DBTFB and TNT can be cited. Besides, some of them also present hazardous character (NBDCA, PCA, TNT...) so they were not used in this study.

Due to their affordable price and favorable properties, the following co-formers were selected to test their ability at eliminating impurities from Phenanthrene during co-crystallization: TCPA, PMDA and TCTN. Purification experiments are reported in part 4.

As revealed by tab. 17, Phenanthrene co-formers present aromatic cycles substituted by polar groups. Consequently, a search for new co-formers exhibiting similar properties was attempted using the products available at the laboratory. The aim of this procedure was to complete the list of co-formers used for Phenanthrene purification experiments.

TAB. 17: Data on Phenanthrene known co-crystals

#	Co-former	Abbreviation	Formula	Co-former mole fraction in the co-crystal	CSD entry	Reference
a	5-nitrobenzene-1,3-dicarboxylic acid	NBDCA		0.500	ABUPES	[41]
b	2,2'-cyclohexa-2,5-diene-1,4-diylidenedimalononitrile	CHDDYDMN		0.500	BITCIS	[42]
c	Octafluoronaphthalene	OFN		0.500	ECUVED01	[43]
d	Tetrachlorophthalic anhydride	TCPA		0.500	FOZHAD	[44]
e	N,N'-bis(Glyciny)pyromellitic diimide	GPMDI		0.500	GENMIW	[45]
f	Hexafluorobenzene	HFB		0.500	IVOCAX	[46]
g	1,2,4,5-tetrafluoro-3,6-diiodobenzene	TFDIB		0.667	NICSUP	[47]
h	2,3-dichloro-5,6-dicyano-p-benzoquinone	DCDCBQ		0.500	PANCYQ	[48]
i	Pyromellitic dianhydride	PMDA		0.500	PENPYM	[49]
j	1,2,4,5-tetracyanobenzene	TCB		0.500	PHTCBZ01	[50]
k	Picric acid	PCA		0.500	PVVBGS01	[51]
l	1,4-dibromo-2,3,5,6-tetrafluorobenzene	DBTFB		0.400	REVQAM	[52]
m	2,4,6-trinitrotoluene	TNT		0.500	URIJOV	[53]
n	2,3,5,6-tetrachloroterephthalonitrile	TCTN		0.500	WAWPEQ	[54]

3) Screening of Phenanthrene new co-formers

In this part, search for new Phenanthrene co-crystals was attempted in two steps: (i) the identification of new co-formers by testing compounds exhibiting the criteria previously enounced, (ii) the determination of their stoichiometry.

This work was achieved with the great help of Sander BRUGMAN (2nd year Msc trainee from Radboud University (Nijmegen, The Netherlands), present at the laboratory during the first 6 months of 2015). May he be thanked for it.

a) Discovery of new Phenanthrene co-formers

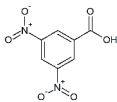
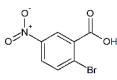
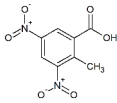
The existence of co-crystals between Phenanthrene and the tested compounds was checked by two ways:

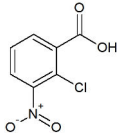
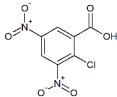
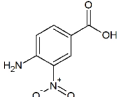
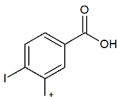
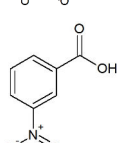
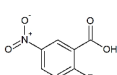
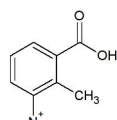
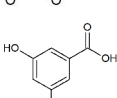
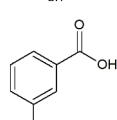
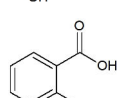
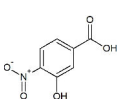
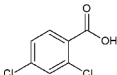
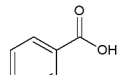
- Mechanochemistry [55–57]: Physical binary mixtures (200 mg Phenanthrene, Alfa Aesar, 98 % + 200 mg of tested compound) were prepared and ground using a Retsch MM 400 ball miller. 11 mm diameter ZrO₂ balls were used for the grinding. The frequency was adjusted to 30 Hz. The grinding duration was 30 minutes.
- Crystallization from solvent evaporation: Equimolar binary mixtures were prepared and dissolved in Ethanol or Acetone (both HPLC grade, purchased from VWR Chemicals). The solvent was let evaporating to air to let the components recrystallize. The crystals obtained were manually ground.

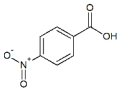
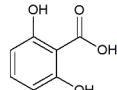
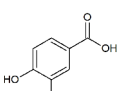
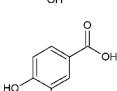
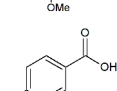
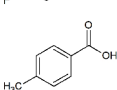
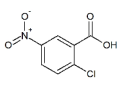
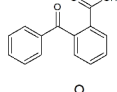
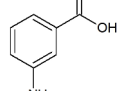
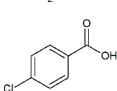
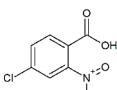
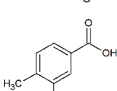
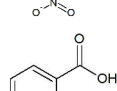
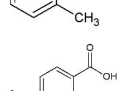
For every test, the mixtures prepared by grinding or solvent evaporation were analyzed by XRPD to evidence potential formation of new phases (co-crystals). The XRPD patterns were compared to those of the starting products, and to those calculated from the different compound polymorph and solvate known crystal structures.

The results are summarized in tab. 18. Tested compounds that were found to form co-crystals with Phenanthrene are written in strong characters. During this screening, 15 new co-crystals of Phenanthrene were discovered. The co-formers that led to positive tests are: 35DNBA, 2Br5NBA, 2M35DNBA, 2Cl35DNBA, 3NBA, 2F5NBA, 4Cl2NBA, 35DNBA, 26DCIBA, 4H3NBA, 25DNBA, 4M35DNBA, 35DNSA, 4F3NBA and 4Cl35DNBA (XRPD patterns related to positive tests are shown in appendix 5, p 273).

TAB. 18: Results of Phenanthrene new co-former screening

Tested compound	Abbreviation	Formula	Supplier	Indicative purity	New phase observed by XRPD (+ yes, – no)	
					Co-grinding	Solvent evaporation
3,5-dinitrobenzoic acid	35DNBA		Alfa Aesar	98 + %	+	+(2)
2-bromo-5-nitrobenzoic acid	2Br5NBA		Alfa Aesar	98 %	+	Not tested
2-methyl-3,5-dinitrobenzoic acid	2M35DNBA		Alfa Aesar	98 %	+	+(2)

Tested compound	Abbreviation	Formula	Supplier	Indicative purity	New phase observed by XRPD (+ yes, – no)	
					Co-grinding	Solvent evaporation
2-chloro-3-nitrobenzoic acid	2Cl3NBA		Alfa Aesar	98 %	–	– (2)
2-chloro-3,5-dinitrobenzoic acid	2Cl35DNBA		Alfa Aesar	97 %	+	+(2)
4-amino-3-nitrobenzoic acid	4A3NBA		Alfa Aesar	97 %	–	– (2)
4-iodo-3-nitrobenzoic acid	4I3NBA		Alfa Aesar	97 %	–	– (2)
3-nitrobenzoic acid	3NBA		Alfa Aesar	99 %	+	+(2)
2-fluoro-5-nitrobenzoic acid	2F5NBA		Acros Organics	98 %	+	+(1)
2-methyl-3-nitrobenzoic acid	2M3NBA		Acros Organics	99 %	–	– (2)
3,5-dihydroxybenzoic acid	35DHBA		Acros Organics	97 %	–	– (2)
3-hydroxybenzoic acid	3HBA		Acros Organics	99 %	–	– (2)
2-chlorobenzoic acid	2ClBA		Acros Organics	98 %	–	– (2)
3-hydroxy-4-nitrobenzoic acid	3H4NBA		Acros Organics	98 %	–	– (1)
2,4-dichlorobenzoic acid	24DCIBA		Acros Organics	98 %	–	– (2)
Benzoic acid	BA		Acros Organics	98 %	–	Not tested

Tested compound	Abbreviation	Formula	Supplier	Indicative purity	New phase observed by XRPD (+ yes, – no)	
					Co-grinding	Solvent evaporation
4-nitrobenzoic acid	4NBA		Acros Organics	99 + %	–	– (2)
2,6-dihydroxybenzoic acid	26DHBA		Acros Organics	97 %	–	– (2)
3,4-dihydroxybenzoic acid	34DHBA		Acros Organics	97 %	–	– (2)
4-hydroxy-3-methoxybenzoic acid	4H3MyBA		Acros Organics	98.5 %	–	– (2)
4-fluorobenzoic acid	4FBA		Acros Organics	99 %	–	– (2)
<i>p</i> -toluic acid	PTA		Acros Organics	98 %	–	– (2)
2-chloro-5-nitrobenzoic acid	2Cl5NBA		Acros Organics	99 + %	–	– (2)
2-benzoylbenzoic acid	2BBA		Acros Organics	98 + %	–	– (2)
3-aminobenzoic acid	3ABA		Acros Organics	99 + %	–	– (2)
4-chlorobenzoic acid	4ClBA		Acros Organics	99 %	–	– (2)
4-chloro-2-nitrobenzoic acid	4Cl2NBA		Acros Organics	97 %	+	+
4-methyl-3-nitrobenzoic acid	4M3NBA		Acros Organics	99 %	–	– (2)
<i>o</i> -toluic acid	OTA		Acros Organics	98 + %	–	– (2)
3,4-dinitrobenzoic acid	34DNBA		Acros Organics	99 %	+	+

Tested compound	Abbreviation	Formula	Supplier	Indicative purity	New phase observed by XRPD (+ yes, – no)	
					Co-grinding	Solvent evaporation
4-chloro-3-nitrobenzoic acid	4Cl3NBA		Acros Organics	99.5 %	–	– (2)
2,6-dichlorobenzoic acid	26DCIBA		Acros Organics	98 + %	+	+
4-hydroxy-3-nitrobenzoic acid	4H3NBA		Aldrich	98 %	+	+
2-amino-3-nitrobenzoic acid	2A3NBA		Aldrich	96 %	–	– (2)
2,5-dinitrobenzoic acid	25DNBA		Aldrich	95 %	+	+
4-methyl-3,5-dinitrobenzoic acid	4M35DNBA		Aldrich	98 %	+	+
3,5-dinitrosalicylic acid	35DNSA		Aldrich	98 %	+	+
4-fluoro-3-nitrobenzoic acid	4F3NBA		Aldrich	98 %	+	+
4-chloro-3,5-dinitrobenzoic acid	4Cl35DNBA		Aldrich	97 %	+	+

(1) recrystallized from Ethanol; (2) recrystallized from Acetone

It is particularly worth noting that almost all the discovered co-formers are Nitrobenzoic acid derivatives, which indicates that this class of compounds shows a significant tendency to make co-crystals with Phenanthrene. Moreover, due to their large solubilities in basic water, they can be easily removed from co-crystals by liquid-liquid extraction.

Due to their unavailability in the laboratory and in commercial supplier stores, some co-formers were excluded from the upcoming parts of the study (*e. g.*, the determination of the discovered co-crystal stoichiometry values; and their use for Phenanthrene purification by co-crystallization). Only the following co-formers were selected: 35DNBA, 3NBA, 2M35DNBA, 4M35DNBA, 4Cl2NBA, 4F3NBA and 4H3NBA.

Before using them for purification experiments, knowledge on their stoichiometry is required. This work was attempted by XRPD measurements and is reported thereafter.

b) Determination of the stoichiometry of new Phenanthrene co-crystals

The stoichiometry of the different co-crystals discovered and selected during the previous part was determined according to the following procedure: binary physical mixtures made of Phenanthrene (Alfa Aesar, 98 %) and the tested co-former were prepared and dissolved in Acetone (HPLC grade, VWR Chemicals). The solvent was evaporated to air for 24 h. Recrystallized powders were manually ground and were analyzed by means of XRPD. The comparison of the XRPD patterns of the mixtures of different compositions allowed to evidence co-crystal stoichiometry.

The stoichiometry values associated with the different discovered co-crystals are summarized in tab. 19. The corresponding XRPD patterns are provided in appendix 6, p. 277.

TAB. 19: **Stoichiometry values of the discovered co-crystals of Phenanthrene**

Co-former	Co-crystal stoichiometry (Phenanthrene:co-former)	XRPD patterns
35DNBA	1:1	fig. S18 / p. 277
3NBA	1:2	fig. S19 / p. 277
4CI2NBA	1:2	fig. S20 / p. 278
2M35DNBA	1:1	fig. S21 / p. 278
4M35DNBA	1:1	fig. S22 / p. 279
4F3NBA	1:2	fig. S23 / p. 279
4H3NBA	1:2	fig. S24 / p. 280

c) Summary

In this study, 15 co-formers of Phenanthrene were discovered. 7 of them were selected thanks to their sufficient availability at the laboratory, and to the *a priori* ease of their removal from Phenanthrene co-crystals. Their stoichiometry was determined by XRPD.

Up to now, the characterization of the co-crystals discovered in this work is incomplete: their crystal structures should be determined in future works. In this view, co-sublimation could be a general method to obtain single crystals of these new solid phases.

4) Phenanthrene purification experiments

To assess the selectivity of Phenanthrene co-crystals with respect to the different impurities of the target compound, technical grade Phenanthrene (Alfa Aesar, 90 %) was purified by co-crystallization using the following co-formers: PMDA, TCPA, 35DNBA, 2M35DNBA, 4CI2NBA, 4H3NBA, 4M35DNBA and 4F3NBA⁷.

For every co-crystal, the following procedure was applied:

Co-crystal formation⁸: 3 g of a physical mixture made of technical grade Phenanthrene and the selected co-former, in the proportions of co-crystal stoichiometry, was prepared. A certain amount of HPLC grade Acetone (VWR Chemicals) was added to the mixture (the amount was adjusted to recover ~ 1.5 g of co-crystal at the end of the co-crystal formation procedure). The system was placed under magnetic stirring for 24 h to let it equilibrate. The amounts of materials engaged in the different purification experiments are provided in tab. 20.

Co-crystal recovery: Then, the co-crystal was recovered by filtration over 3-porosity glass filter. The crystals were washed with a few mL of cold (0 °C) Acetone (HPLC grade, VWR Chemicals).

Phenanthrene recovery: ~ 500-600 mg of wet co-crystal was placed in a vial containing 6 mL of Dichloromethane (reagent grade, VWR Chemicals) and 9 mL of a 10 wt. % NaOH aqueous solution. The mixture was rigorously stirred to form the co-former sodium salt that was extracted towards the aqueous phase. The latter was removed and renewed 2 times. The same procedure was then repeated with 2×6 mL of milliQ[®] water. Then, the organic layer was recovered, dried over anhydrous MgSO₄ (Fisher) and filtered over 0.2 µm PTFE syringe filter. The solvent was let evaporating to air for 24 h to let purified Phenanthrene recrystallize.

At the end of the purification procedure, purified Phenanthrene was analyzed by GC-FID to determine impurity levels in the material. The measured values were then compared: (i) with those of the commercial product, (ii) with those of the commercial product purified by solvent assisted recrystallization (see tab. 1). The impurity levels in Phenanthrene samples (commercial, recrystallized and co-crystallization purified) are provided in tab. 21.

TAB. 20: Amounts of chemicals used for Phenanthrene purification by co-crystallization

Tested co-former	Mass of Phenanthrene (g)	Mass of co-former (g)	Mass of Acetone (g)
PMDA	0.901	1.110	4.014
TCPA	0.770	1.238	3.485
35DNBA	0.911	1.084	5.452
2M35DNBA	0.882	1.117	2.411
4M35DNBA	0.882	1.118	7.729
4CI2NBA	0.456	1.544	1.453
4F3NBA	0.650	1.351	1.515
4H3NBA	0.654	1.346	2.847

7. Preliminary tests on Phenanthrene/TCTN co-crystal highlighted that the co-former could not be removed by treatment with 10 wt. % NaOH or 20 wt. % HCl aqueous solutions. Consequently, no further investigation was performed on this co-crystal. Moreover, crystallization of Phenanthrene/3NBA co-crystal in Acetone led to a viscous solution that could not be stirred. Investigations on this co-crystals were consequently aborted.

8. During this step, the solubility of the co-crystal was assumed to be congruent, which means that the solid in equilibrium with the liquid was the co-crystal, only.

As indicated by tab. 21 entries, Phenanthrene purification by means of co-crystallization led to various impurity removal rates, according to the selected co-former and to the nature of the impurity.

Two impurities (*e. g.*, Biphenyl and the Anthracene/Maleic Anhydride Diels Alder adduct) were completely eliminated whatever the co-former selected, whereas a simple recrystallization did not lead to such results for the second impurity.

Besides, the levels of several impurities could be reduced below the detection threshold of the analytical method (*e. g.*, 0.0001 wt. %) by purification with almost all the tested co-crystals. This is the case of Butenedioic acid, dibutyl ester, Xanthene and Tetrahydro-anthracene or -phenanthrene.

However, many impurities were still detected in the purified samples. This mainly concerns the most abundant in the starting product: Fluorene, Dibenzothiophene, Anthracene and Carbazole, for which no co-crystal was able at completely eliminating them from Phenanthrene.

The most interesting co-former was probably 35DNBA, as indicated by the quantification results. Indeed, the purification procedure allowed for a decrease of the total impurity level from 9.2 to 1.51 wt. %, which corresponds to the best purifying effect observed amongst the tested co-formers. Moreover, the formation of this co-crystal led to the complete elimination of many impurities – especially, the hydrogenated derivatives of Phenanthrene and Anthracene, and the Anthracene/Maleic Anhydride Diels Alder adduct, whereas the recrystallization did not (see fig. 47).

In addition, many other impurity levels were significantly decreased using this co-former. The two main advantages of this co-crystal are: (i) 35DNBA is a low-cost chemical, which makes the purification procedure affordable; (ii) the co-crystal stoichiometry is 1:1, which guarantees an interesting rate of recovering of Phenanthrene with respect to other co-crystals in which the proportion of co-former is larger.

TAB. 21: **Impurity levels in purified Phenanthrene samples** – impurities are sorted by ascending elution order. ND: Not detected (< 0.0001 wt. %). * Undetermined isomer

Impurity	Recovered from co-crystals with									
	Com- mercial	Recrystal- lized in Acetone	PMDA	TCPA	35DNBA	2M35- DNBA	4M35- DNBA	4CI2NBA	4H3NBA	4F3NBA
Biphenyl	0.0071 ± 0.0004	ND	ND	ND	ND	ND	ND	ND	ND	ND
Methylnaphthalene*	0.0068 ± 0.0002	0.0047 ± 0.0003	ND	ND	ND	ND	ND	0.0037 ± 0.0001	0.0033 ± 0.0008	0.0036 ± 0.0006
Butenedioic acid, dibutyl ester*	0.158 ± 0.008	ND	ND	ND	ND	ND	ND	ND	ND	0.0303 ± 0.0009
Dibenzofuran	0.0451 ± 0.0002	0.0083 ± 0.0002	0.0093 ± 0.0006	0.0055 ± 0.0002	ND	0.0087 ± 0.0003	0.0042 ± 0.0001	0.0174 ± 0.0007	0.0088 ± 0.0007	0.0180 ± 0.0006
Fluorene	1.692 ± 0.0002	1.21 ± 0.02	0.362 ± 0.006	0.532 ± 0.002	0.0803 ± 0.0009	0.698 ± 0.005	0.574 ± 0.003	0.91 ± 0.04	0.528 ± 0.008	1.31 ± 0.05
Methylbiphenyl*	0.054 ± 0.002	0.0227 ± 0.0004	0.0035 ± 0.0003	ND	0.0032 ± 0.0005	0.0072 ± 0.0003	0.009 ± 0.002	0.034 ± 0.002	0.0173 ± 0.0007	0.026 ± 0.002
Xanthene	0.017 ± 0.005	ND	ND	ND	ND	ND	ND	ND	ND	0.0048 ± 0.0001
Fluorene isomer*	0.018 ± 0.002	0.0134 ± 0.0003	0.0044 ± 0.0004	0.0053 ± 0.0001	0.0026 ± 0.0005	0.0060 ± 0.0003	0.0056 ± 0.0001	0.0124 ± 0.0009	0.0068 ± 0.0005	0.0111 ± 0.0008
9,10-dihydroanthracene	0.099 ± 0.005	0.0154 ± 0.0005	0.0054 ± 0.0001	0.0044 ± 0.0001	ND	ND	ND	0.0118 ± 0.0001	0.0151 ± 0.0009	0.034 ± 0.002
Dihydro-anthracene or -phenanthrene*	0.0365 ± 0.0003	0.0099 ± 0.0003	0.0065 ± 0.0004	0.0035 ± 0.0005	ND	0.0061 ± 0.0001	0.0043 ± 0.0001	0.0106 ± 0.0001	0.0083 ± 0.0004	0.020 ± 0.002
Dihydro-anthracene or -phenanthrene*	0.087 ± 0.002	0.0143 ± 0.0004	0.0054 ± 0.0008	ND	ND	0.0073 ± 0.0001	0.0044 ± 0.0002	0.0125 ± 0.0002	0.0133 ± 0.0008	0.038 ± 0.002
1-methylfluorene	0.209 ± 0.003	0.104 ± 0.002	0.0165 ± 0.0001	0.020 ± 0.002	ND	0.082 ± 0.007	0.045 ± 0.002	0.059 ± 0.003	0.0591 ± 0.0003	0.150 ± 0.007
Tetrahydro-anthracene or -phenanthrene*	0.017 ± 0.002	ND	0.0031 ± 0.0001	0.0038 ± 0.0001	ND	0.0041 ± 0.0001	0.0035 ± 0.0009	ND	ND	0.0059 ± 0.0005
Tetrahydro-anthracene or -phenanthrene*	0.012 ± 0.001	0.0034 ± 0.0001	ND	ND	ND	ND	ND	0.0039 ± 0.0009	0.003 ± 0.001	0.006 ± 0.001
Dibenzothiophene	1.78 ± 0.04	0.91 ± 0.02	0.86 ± 0.02	1.453 ± 0.005	0.610 ± 0.007	1.71 ± 0.02	0.9359 ± 0.0002	1.10 ± 0.05	0.94 ± 0.02	1.50 ± 0.07
Naphthothiophene 1*	0.114 ± 0.003	0.023 ± 0.002	0.062 ± 0.002	0.094 ± 0.004	0.076 ± 0.004	0.0775 ± 0.0003	0.075 ± 0.004	0.055 ± 0.002	0.048 ± 0.002	0.078 ± 0.004
Anthracene	0.554 ± 0.005	0.37 ± 0.02	0.2132 ± 0.0007	0.377 ± 0.002	0.310 ± 0.009	0.3356 ± 0.0007	0.375 ± 0.007	0.175 ± 0.008	0.2184 ± 0.0001	0.38 ± 0.03
Unknown impurity	0.0446 ± 0.0002	0.022 ± 0.007	0.023 ± 0.005	ND	0.014 ± 0.002	ND	ND	ND	ND	ND
Benzoquinoline*	0.0639 ± 0.0004	0.0101 ± 0.0002	0.040 ± 0.004	0.0071 ± 0.0003	ND	ND	ND	0.008 ± 0.002	0.074 ± 0.003	0.024 ± 0.002
Naphthothiophene 2*	0.297 ± 0.004	0.365 ± 0.008	0.14 ± 0.01	0.174 ± 0.004	0.0381 ± 0.0007	0.155 ± 0.005	0.098 ± 0.003	0.21 ± 0.01	0.1137 ± 0.0003	0.282 ± 0.007
Methyl-dibenzothiophene or -naphthothiophene*	0.17 ± 0.02	0.072 ± 0.004	0.0330 ± 0.0002	0.043 ± 0.003	0.0137 ± 0.0001	0.1113 ± 0.0009	0.0534 ± 0.0009	0.0523 ± 0.0002	0.050 ± 0.005	0.160 ± 0.008
Carbazole	2.8 ± 0.2	1.61 ± 0.03	1.16 ± 0.05	0.80 ± 0.03	0.300 ± 0.004	0.29 ± 0.02	0.36 ± 0.02	1.23 ± 0.04	0.748 ± 0.002	1.49 ± 0.02
Methyl-phenanthrene or -anthracene 1*	0.0831 ± 0.0008	0.0145 ± 0.0007	0.036 ± 0.002	0.0226 ± 0.0001	0.020 ± 0.002	0.042 ± 0.002	0.012 ± 0.004	0.025 ± 0.002	0.0311 ± 0.0007	0.051 ± 0.004
Methyl-phenanthrene or -anthracene 2*	0.036 ± 0.004	0.0056 ± 0.0005	0.0075 ± 0.0007	0.0049 ± 0.0004	0.0088 ± 0.0004	0.0075 ± 0.0006	0.011 ± 0.002	0.0064 ± 0.0002	0.0085 ± 0.0004	0.0178 ± 0.0006
Methyl-phenanthrene or -anthracene 3*	0.157 ± 0.009	0.111 ± 0.003	0.0068 ± 0.0008	0.0117 ± 0.0004	0.033 ± 0.003	0.082 ± 0.003	0.056 ± 0.002	0.0489 ± 0.0005	0.058 ± 0.002	0.186 ± 0.006
Methylcarbazole*	0.012 ± 0.002	0.005 ± 0.001	ND	ND	ND	ND	ND	0.0042 ± 0.0001	ND	0.0055 ± 0.0001
9,10-phenanthrenequinone	0.04 ± 0.02	0.0121 ± 0.0002	ND	ND	ND	0.0086 ± 0.0005	ND	0.0100 ± 0.0007	0.0119 ± 0.0002	0.025 ± 0.005
Anthracene/Maleic Anhydride Diels Alder adduct	0.55 ± 0.09	0.18 ± 0.02	ND	ND	ND	ND	ND	ND	ND	ND
Total	9.2 ± 0.4	5.1 ± 0.2	3.0 ± 0.1	3.56 ± 0.06	1.51 ± 0.03	3.64 ± 0.06	2.63 ± 0.04	4.0 ± 0.2	2.96 ± 0.04	5.9 ± 0.2

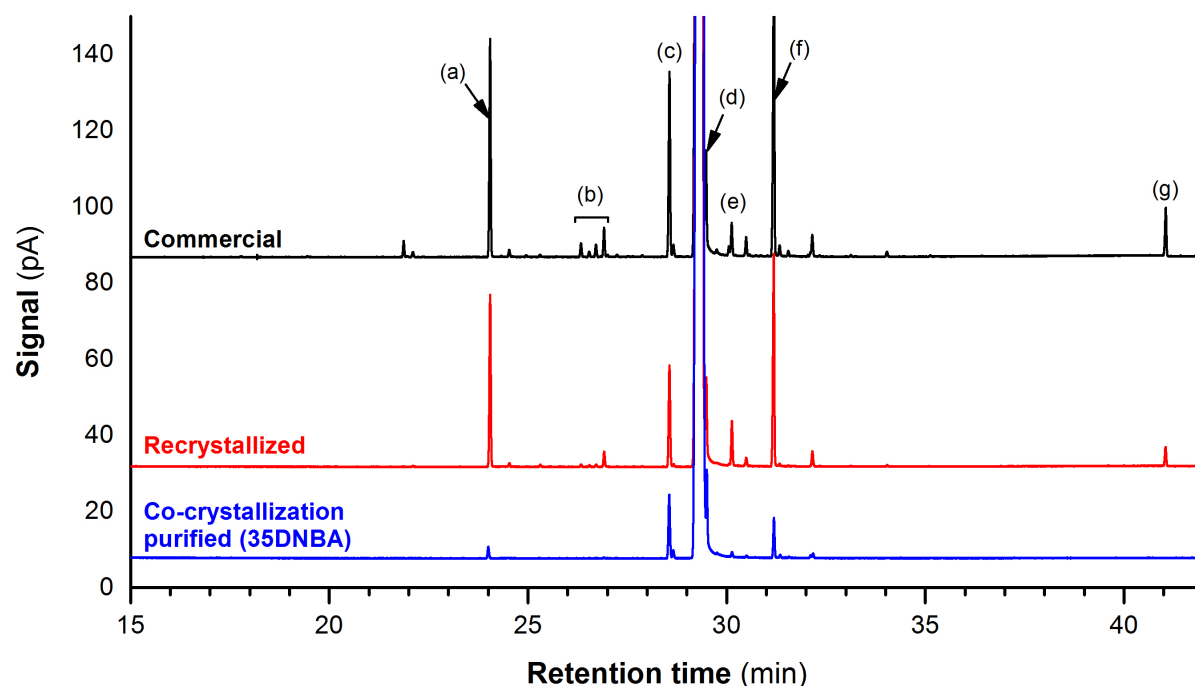


FIG. 47: **Normalized GC-FID chromatograms of commercial (black), recrystallized (red) and co-crystallization purified (blue) technical-grade Phenanthrene** – Major impurities: (a) Fluorene; (b) Hydro-anthracenes and -phenanthrenes; (c) Dibenzothiophene; (d) Anthracene; (e) Naphthothiophene 2; (f) Carbazole; (g) Anthracene/Maleic Anhydride Diels Alder adduct

To optimize upcoming purification experiments on Phenanthrene samples by means of co-crystallization with 35DNBA, the ternary phase diagram between these two compounds and Acetone (*e. g.*, the co-crystallization solvent) was investigated. The following procedure was applied:

Physical ternary mixtures of various compositions made of synthesis-grade Phenanthrene (Alfa Aesar, 98 %), 35DNBA (Alfa Aesar, 98 + %) and Acetone (HPLC grade, VWR Chemicals) were prepared and were equilibrated under magnetic stirring for 24 hours. For every mixture, one drop of saturated liquid was diluted in ~ 2 mL of Toluene (HPLC grade, VWR Chemicals) after filtration over 0.2 μm PTFE syringe filter. The solution was analyzed by GC-FID to determine the composition of the liquid (see appendix 2c, p. 268). That of the solid was assessed using Schreinemaker's method of wet residues. The solid was recovered by filtration over 1-porosity glass filter, and was analyzed by XRPD to determine the phases present.

Experimental data on composition values are summarized in tab. 22.

XRPD analyses (fig. 48) revealed that mixture **a** led to the crystallization of <PHEN LT> phase. Mixture **b** led to the crystallization of <PHEN LT> and co-crystal <CC> phases. Mixtures **c**, **d**, **e**, **f** and **g** led to the formation of <CC> phase. In mixture **h**, the solid was made of <CC> and <35DNBA> phases. Eventually, mixture **i** crystallized as <35DNBA>.

Using these data, the ternary phase diagram shown in fig. 49 could be proposed. This diagram indicates that: (i) the <CC> + L two-phase domain has a large composition range of stability; (ii) the solubility of the <CC> phase is congruent. This proposal was used to optimize system composition during purification procedures by co-crystallization with 35DNBA.

Tab. 22: **Data on ternary Phenanthrene/35DNBA/Acetone mixture compositions** – compositions are expressed in mass fractions. PHEN: Phenanthrene, ACT: Acetone.

#	Composition of mixtures			Composition of liquids			Composition of solids	
	PHEN	35DNBA	ACT	PHEN	35DNBA	ACT	PHEN	35DNBA
a	0.471	0.000	0.529	0.301	0.000	0.699	1.000	0.000
b	0.437	0.046	0.517	0.327	0.007	0.666	0.816	0.184
c	0.347	0.113	0.539	0.338	0.006	0.656	0.459	0.541
d	0.180	0.137	0.683	0.124	0.012	0.864	0.453	0.547
e	0.152	0.150	0.698	0.089	0.021	0.890	0.458	0.542
f	0.123	0.215	0.662	0.037	0.067	0.896	0.454	0.546
g	0.097	0.231	0.672	0.032	0.117	0.851	0.457	0.543
h	0.044	0.429	0.526	0.019	0.252	0.728	0.110	0.890
i	0.000	0.499	0.501	0.000	0.277	0.723	0.000	1.000

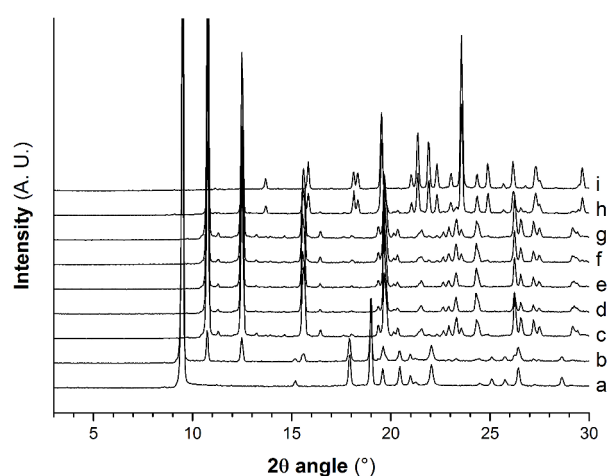


FIG. 48: XRPD patterns of Phenanthrene/35DNBA mixtures at 20 °C and 1 atm

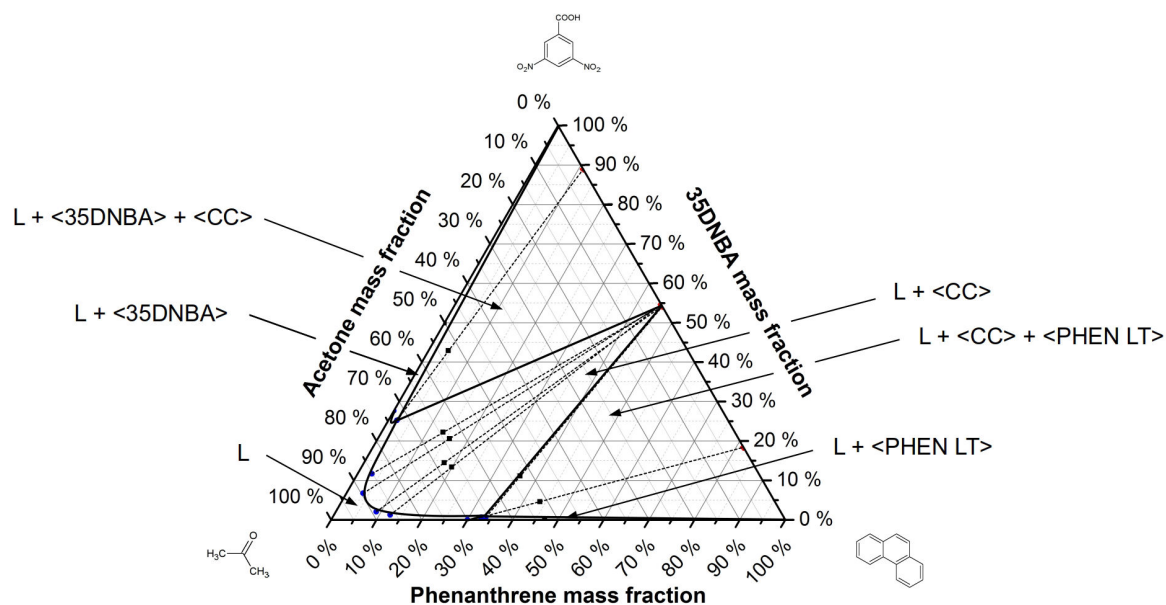


FIG. 49: **Proposal for Phenanthrene/35DNBA/Acetone ternary phase diagram at 20 °C and 1 atm**
 ■ tested ternary mixtures, ● liquidus (solubility) points, ◆ composition of solids, --- straight lines used for solid phase composition assessment.

5) Discussion

As shown in this work, solvent assisted recrystallization and co-crystallization applied to Phenanthrene samples exhibit various selectivity with respect to the different impurities of the product:

- (i) During solvent-assisted recrystallization of raw Phenanthrene, a few impurities (*e. g.*, Biphenyl, Butenedioic acid dibutyl ester and Tetrahydro-phenanthrene or -anthracene) were completely eliminated from the product, whereas the others were still present in the purified sample. This indicates that these three compounds exhibit chemical structures sufficiently different from that of Phenanthrene to avoid their inclusion in the crystal lattice of the interest product during the process. However, the other impurities are structurally too similar to Phenanthrene, which prevented from sufficient discrimination in the solid state to allow for their complete elimination. This hypothesis is validated by the phase diagrams between Phenanthrene and its major impurities established in this work, in which solid solutions of Phenanthrene were evidenced.
- (ii) During co-crystallization with 35DNBA, more impurities, especially those whose molecular volume is significantly larger than that of Phenanthrene (*e. g.*, hydrogenated impurities, Anthracene/Maleic Anhydride Diels Alder adduct...) were completely eliminated from the product. This suggests that the co-crystal was too dense to accept impurities without high energetical penalty. Consequently, the discrimination in the solid state was larger during co-crystallization than during recrystallization.

These observations can be explained by rational use of phase diagrams between the species involved in both purification processes (fig. 50): Phenanthrene, a considered impurity and the recrystallization solvent (in case of solvent-assisted recrystallization), or the co-crystal, the impurity and the solvent (in case of purification by co-crystallization).

Indeed, during these procedures, the starting mixtures (*e. g.*, raw impure Phenanthrene in case of solvent-assisted recrystallization, or raw impure Phenanthrene + co-former in case of co-crystallization) can be represented by points M_0 on the corresponding ternary phase diagrams. Addition of solvent leads to a change in system composition that is now represented by points M_1 . After equilibration, the saturated liquids (M_2) are in equilibrium with the solid phase recrystallized (M_3). From there, two cases should be distinguished: (i) the solid phase recrystallized makes a partial solid solution with the impurity (cases a and c). Consequently, a certain amount of the latter is still present in the solid, while a partial elimination occurs with reference to the starting mixture. (ii) or it does not form any solid solution (cases b and d), and the solid phase recrystallized is impurity free.

According to tab. 21 entries, during solvent-assisted recrystallization, all the impurities of Phenanthrene (except Biphenyl, Butenedioic acid, dibutyl ester and Tetrahydro-phenanthrene or -anthracene) behaved according to the first case. Consequently, this method was not appropriate to eliminate them from Phenanthrene. However, during co-crystallization with 35DNBA, more impurities – especially the hydro-anthracenes and -phenanthrenes, as well as the Anthracene/Maleic Anhydride adduct) behaved according to the second case, which was more favorable to Phenanthrene purification.

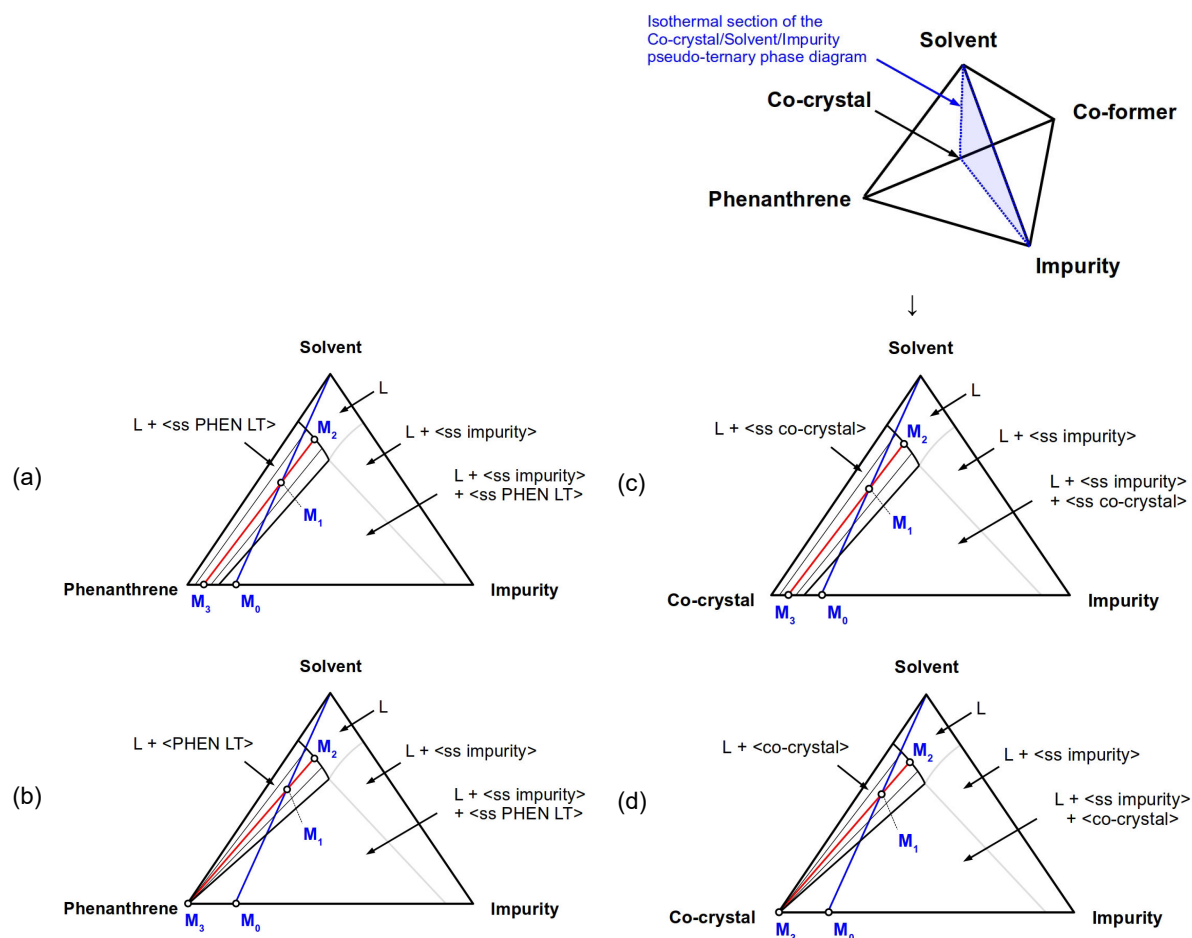


FIG. 50: **Phase diagrams for rational discussion of purification results** – a, b. ternary diagrams between Phenanthrene, an impurity and the solvent with (a) or without (b) existence of a Phenanthrene solid solution. c, d. pseudo ternary diagrams between Phenanthrene co-crystal, an impurity and the solvent with (a) or without (b) existence of a co-crystal solid solution.

It is worth noting that impurities that were completely eliminated during co-crystallization with 35DNBA are those whose molecular volumes are significantly higher than that of Phenanthrene. This indicates that they were too big to substitute Phenanthrene molecules during co-crystal formation. Conversely, during simple recrystallization of the product, the levels of these impurities were decreased but not below the detection thresholds of the analytical method. This means that they were able at substituting Phenanthrene molecules during the process. Consequently, this work highlight that during co-crystallization with 35DNBA, discrimination between Phenanthrene and its impurities was larger than during recrystallization.

6) Conclusions and outlooks

In this study, 15 new co-formers of Phenanthrene were discovered. Purification experiments were performed on technical-grade material by formation of 8 different co-crystals in solution. Measurements of impurity levels in Phenanthrene recovered from co-crystals shown that co-crystallization exhibited various efficiencies with respect to the different impurities, according to the selected co-former.

Co-crystallization of Phenanthrene with 35DNBA shown the best purifying effect observed in this work. Indeed, it gives complete removal of Hydrophenanthrenes, Hydroanthracenes and Anthracene/Maleic Anhydride adduct, and substantial decreases of the levels of other impurities. The purity of the material was increased from 90.8 to 98.49 wt. % in one single shot, against 90.8 to 94.9 wt. % during recrystallization.

Even if a better discrimination between Phenanthrene and its impurities was observed during co-crystallization than during recrystallization, this method was unable at eliminating the 4 major impurities of the starting product: Fluorene, Dibenzothiophene, Anthracene and Carbazole. Indeed, due to their structural similarity with Phenanthrene, discrimination was insufficient to avoid their inclusion in co-crystals during their formation.

In order to develop the discussion attempted on the relationship between chemical structures of Phenanthrene, its impurities and discrimination in the solid state during co-crystallization, further investigation is required to perform structural characterization of the co-crystals discovered. Their structures will have to be determined in future work.

To summarize, co-crystallization allowed for the complete removal of some impurities of Phenanthrene. The grade of the material could be increased from “technical” to “synthesis”. However, the presence of remaining traces of Fluorene, Dibenzothiophene, Anthracene and Carbazole in the purified material justifies the search for other purification methods. In the next part of this chapter, combinatorial approaches are introduced.

Works on Phenanthrene purification by Zone Melting and co-crystallization served for the publication of a paper in Chemical Engineering & Technology [58].

V. COMBINATORIAL APPROACHES

1) Introduction

The studies reported in the previous parts shown that solvent assisted recrystallization, Zone Melting, co-crystallization and vacuum sublimation were not appropriate to remove all the impurities from Phenanthrene samples in one single step. Consequently, this paves the way to the combination of several purification methods in order to benefit from their selectivity and efficiency with respect to the different impurities. Of course, a combination in the right order is required to reach ultrapurity.

Previous experiments shown that, due to unfavorable phase equilibria, the major impurities of Phenanthrene (*e. g.*, Fluorene, Dibenzothiophene, Anthracene and Carbazole) could not be eliminated from the target compound using the techniques previously employed. Consequently, other approaches should be attempted to achieve their removal.

In this part, the following approaches were investigated to access to ultrapure Phenanthrene:

- (i) the combination of co-crystallization and Zone Melting. Indeed, previous work highlighted that co-crystallization of Phenanthrene with 35DNBA had a purifying effect larger than that of recrystallization. Consequently, this method can be a promising pre-purification technique before the removal of last impurity traces by zone refining. Investigations using this approach were attempted and are reported in paragraph 2.
- (ii) impurity modification by chemical treatments, followed by their removal using appropriate procedures: liquid-liquid extraction or co-crystallization. This second approach aims at modifying the identity of Phenanthrene impurities in order to benefit from potentially more favorable phase equilibria during their removal. Paragraph 3 presents the different procedures applied to investigate that point, as well as their results.

2) Purification by co-crystallization and Zone Melting

a) Introduction

As revealed by Phenanthrene purification experiments by co-crystallization with 35DNBA, this method was able at completely eliminating impurities exhibiting large molecular volumes. Nevertheless, major impurities structurally similar to Phenanthrene (*e. g.*, Fluorene, Dibenzothiophene, Anthracene and Carbazole) could not be fully removed from the product. Hence, a combinatorial approach was envisaged to reach ultrapurity:

- (i) the removal of hydrogenated impurities by means of co-crystallization with 35DNBA, in order to increase the purity of the compound and to reduce the levels of Fluorene, Dibenzothiophene, Anthracene and Carbazole.
- (ii) the removal of remaining impurity traces by means of Zone Melting.

Of course, applying this procedure to technical-grade Phenanthrene would be irrelevant due to the large number of impurities and to their high levels. Consequently, the procedure was applied to synthesis-grade (~ 98 % purity) Phenanthrene exhibiting more favorable composition. During preliminary tests, a batch provided by Sigma-Aldrich was found to exhibit low Fluorene and Carbazole levels, which could simplify its purification by this pathway. Consequently, it was chosen as starting material to assess the relevance of this combinatorial approach.

b) Experimental part

i. Phenanthrene pre-purification by co-crystallization

In the first part of this work, commercial Phenanthrene (Sigma Aldrich, 98 %) was purified by means of co-crystallization with 35DNBA (Alfa Aesar, 98 + %) according to the following procedure:

30 g of an equimolar binary mixture (13.7 g of Phenanthrene, 16.3 g of 35DNBA) was placed in a round-bottom flask in which 100 mL of HPLC grade Acetone (VWR Chemicals) was added. The system was placed under magnetic stirring for 24 h to form the co-crystal. The suspension was filtered and washed with 10 mL of HPLC grade cold methanol (VWR Chemicals, 0 °C). The co-crystal was dried overnight at 50 °C. The co-former was removed by placing the co-crystal in 150 mL of Dichloromethane (HPLC grade, VWR Chemicals) and 150 mL of a 10 wt. % aqueous NaOH solution. The extraction was performed 3 times with the same volume of extracting phase. It was then repeated 3 times with milli-Q® water. The organic layer was recovered and dried over 5 g of anhydrous MgSO₄ (Fisher Scientific). The suspension was filtered over 0.2 µm PTFE syringe filters. The solvent was then evaporated under vacuum. The recrystallized powder was eventually dried overnight at 50 °C. ~ 9 g of purified Phenanthrene were recovered at the end of the procedure.

ii. Purification by Zone Melting

The pre-purified Phenanthrene was molten to form a 9-cm length ingot. The ingot was zone refined by applying 10 zone passes at 1 mm·h⁻¹ displacement rate, in order to obtain the best possible efficiency. At the end of the experiment, the tube was segmented into 1-cm length

equivalent parts which were manually ground and analyzed by GC-FID to determine their purity.

c) Results and discussion

The impurity levels in Phenanthrene, before/after pre-purification and purification by co-crystallization and Zone Melting are given in tab. 23.

Tab. 23: **Impurity levels** (in wt. %, unless specified) **in Phenanthrene samples before and after purification by co-crystallization and zone refining** – impurities are sorted by ascending elution order.

Impurity	Commercial	After co-crystallization	Zone refined								
			0–1 cm	1–2 cm	2–3 cm	3–4 cm	4–5 cm	5–6 cm	6–7 cm	7–8 cm	8–9 cm
Fluorene	0.0051 ± 0.0005	ND	ND	ND	ND	ND	ND	ND	ND	ND	ND
9,10-dihydroanthracene	0.31 ± 0.03	ND	ND	ND	ND	ND	ND	ND	ND	ND	ND
9,10-dihydrophenanthrene	0.0085 ± 0.0002	ND	ND	ND	ND	ND	ND	ND	ND	ND	ND
Tetrahydro-anthracene or -phenanthrene*	0.023 ± 0.003	ND	ND	ND	ND	ND	ND	ND	ND	ND	ND
Dihydro-anthracene or -phenanthrene*	0.012 ± 0.002	ND	ND	ND	ND	ND	ND	ND	ND	ND	ND
Dibenzothiophene	0.87 ± 0.04	0.25 ± 0.02	0.015 ± 0.002	0.0148 ± 0.0006	0.021 ± 0.002	0.031 ± 0.002	0.054 ± 0.004	0.0977 ± 0.0005	0.1985 ± 0.0001	0.48 ± 0.02	1.3 ± 0.2
Naphthothiophene 1*	0.029 ± 0.002	0.021 ± 0.002	ND	ND	ND	ND	ND	0.003 ± 0.001	0.0064 ± 0.0005	0.018 ± 0.003	0.058 ± 0.003
Anthracene	0.409 ± 0.003	0.212 ± 0.004	0.09 ± 0.02	0.101 ± 0.003	0.118 ± 0.006	0.139 ± 0.005	0.170 ± 0.002	0.200 ± 0.008	0.2555 ± 0.0002	0.35 ± 0.02	0.483 ± 0.002
Naphthothiophene 2*	0.0081 ± 0.0004	0.004 ± 0.001	0.0041 ± 0.0006	0.0039 ± 0.0005	0.0039 ± 0.0005	0.003 ± 0.001	ND	ND	ND	ND	ND
Methyl-dibenzothiophene or -naphthothiophene*	0.0061 ± 0.0004	ND	ND	ND	ND	ND	ND	ND	ND	ND	ND
Carbazole	0.023 ± 0.002	0.013 ± 0.002	0.0199 ± 0.0003	0.014 ± 0.002	0.0046 ± 0.0008	ND	ND	ND	ND	ND	ND
9,10-phenanthrenequinone	0.023 ± 0.004	ND	ND	ND	ND	ND	ND	ND	ND	0.009 ± 0.002	0.054 ± 0.008
Anthracene/Maleic Anhydride Diels Alder adduct	0.019 ± 0.004	ND	ND	ND	ND	ND	ND	ND	ND	ND	ND
Total	1.75 ± 0.08	0.53 ± 0.03	0.13 ± 0.02	0.13 ± 0.02	0.15 ± 0.02	0.17 ± 0.02	0.22 ± 0.02	0.30 ± 0.02	0.46 ± 0.01	0.85 ± 0.05	1.9 ± 0.2
Global molar purity (mole %)	98.30	99.49	99.87	99.87	99.85	99.83	99.78	99.70	99.54	99.16	98.16

ND: Not detected (< 0.0001 wt. %); * undetermined isomer

As shown in tab. 23, the starting product was found to contain 13 impurities, among which 9,10-dihydroanthracene, Dibenzothiophene, and Anthracene were the most abundant – they represented ~ 91 wt. % of the total impurity amount. The other impurities were detected at significantly lower levels.

Comparison of impurity levels before and after purification by co-crystallization highlight that traces of 8 impurities (*e. g.*, all the Hydro-phenanthrenes and -anthracenes, the traces of Fluorene, Methylbenzothiophene/naphthothiophene, 9,10-phenanthrenequinone and Anthracene/Maleic Anhydride Diels Alder adduct) were reduced below the detection thresholds of the analytical method (*e. g.*, 0.0001 wt. %). Such results led to the increase of Phenanthrene chemical purity from 98.30 to 99.49 mole %. Consequently, before Zone Melting experiment, only 5 impurities (Dibenzothiophene, the two Naphthothiophenes, Anthracene and Carbazole) were present in the sample to purify.

During zone refinement of the pre-purified product, Carbazole and Naphthothiophene 2 were displaced towards the opposite direction with respect to that of the zone. All the other impurities followed the opposite behavior, which conforms to observations made during the validation of our apparatus (see part II.5)a, p. 210). The impurity Phenanthrenequinone, which was removed by co-crystallization, has been re-generated during Zone Melting by Phenanthrene oxidation when the zone reached the end of the ingot. This impurity was detected only in the two upper parts of the ingot.

The purest parts of the ingot were the two closest to the starting position of the zone. They contained only 0.13 wt. % of impurities (Dibenzothiophene, Anthracene, the 2nd isomer of Naphthothiophene and Carbazole), which corresponds to 99.87 mole % purity. These values are very close to ultrapurity while they remain lower than 99.9 %.

Even if ultrapurity was not reached, the purest fraction of the treated ingot (*e. g.*, 0-1 cm) was analyzed by DSC at 5 K min⁻¹. The thermogram was compared with those of the commercial Phenanthrene and co-crystallization pre-purified samples (fig. 51). Quantitative data on solid-solid transition and melting peak onset temperatures and enthalpies are provided in tab. 24.

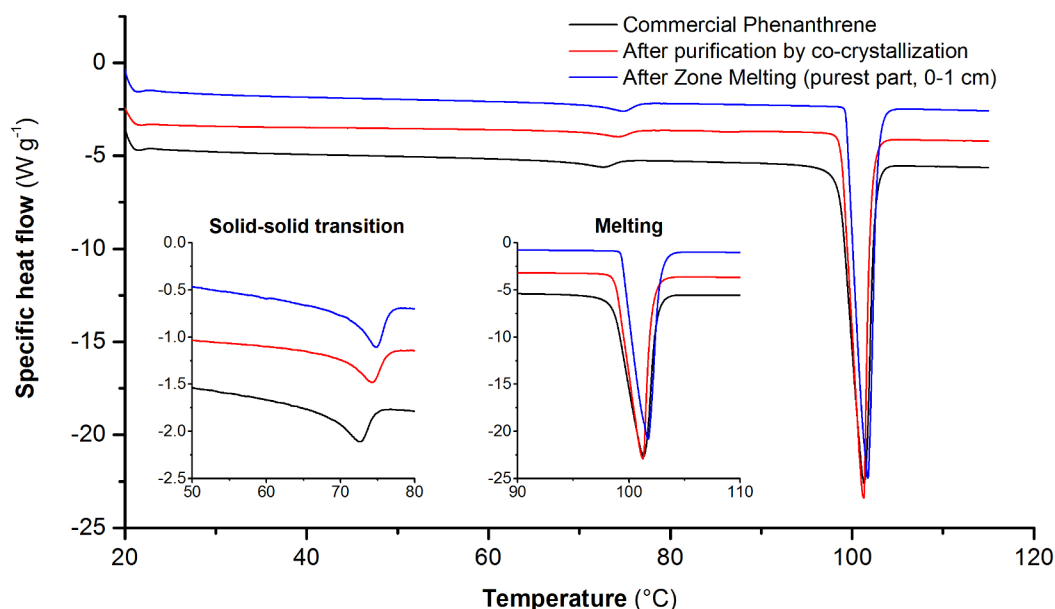


FIG. 51: DSC thermograms of Phenanthrene samples before and after purification by co-crystallization and Zone Melting (endo down)

TAB. 24: Quantitative data on Phenanthrene sample thermograms

	Solid-solid transition		Melting	
	Onset temperature (°C)	Enthalpy (J g ⁻¹)	Onset temperature (°C)	Enthalpy (J g ⁻¹)
Commercial Phenanthrene	68.7	5.02	98.6	99.7
After purification by co-crystallization	69.8	5.10	98.8	100
After purification by Zone Melting (purest part, 0-1 cm)	71.8	5.49	99.3	102

The DSC curves indicate that the purification of Phenanthrene by co-crystallization led to the increase of solid-solid transition and melting onset temperatures. The further purification by Zone Melting did not significantly change the transition signal. However, the melting peak was well defined for the purest sample (sharp drop from baseline at onset temperature, which is consistent with an increase of chemical molar purity).

d) Conclusion

During this first attempt of Phenanthrene purification by combinatorial approach, ultrapurity was almost reached (~ 2 g of 99.87 mole % Phenanthrene were obtained). Unfortunately, only one or two supplementary zone passes would have probably led to a > 99.9 mole % purity.

The results shown the relevance of this approach in view of reaching ultrapurity. However, the Zone Melting experiment was time-consuming (~ 38 days), which makes the combination of co-crystallization and zone refining not that productive.

In this context, new approaches were attempted in order to change phase equilibria between Phenanthrene and its impurities and to benefit from new – potentially more favorable – purifying effects. Their relevance and productivity was then compared with that of the present one.

3) Purification by chemical modification and crystallization

a) Introduction

Besides the combination of crystallization techniques (co-crystallization and Zone Melting) previously attempted, another approach was explored: the modification of Phenanthrene impurities by chemical treatments on the raw material, followed by their removal using liquid-liquid extraction or co-crystallization.

Before introducing experimental procedures and results, an overview of the chemical reactivities of Phenanthrene impurities is first provided.

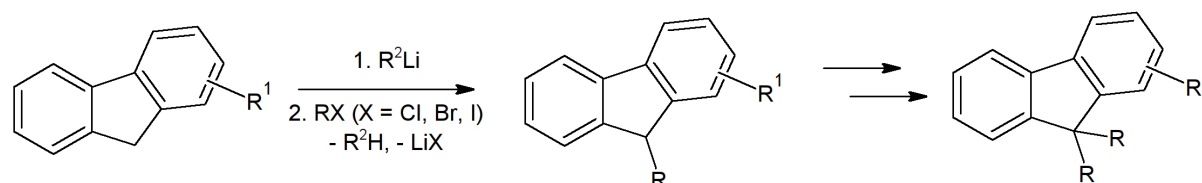
b) Chemical reactivity of Phenanthrene impurities

Phenanthrene and its impurities present various chemical reactivities that opens up many pathways for their modification.

In this section, a brief review of the literature is made in order to summarize possible reactions of these impurities.

i. Fluorene and its derivatives

Due to favorable pK_a values (around ~ 22 [59]), Fluorenes can be converted to their conjugated bases in basic medium. As fluorenyl anions exhibit strong nucleophilic character, they easily react with alkyl halides to form the corresponding *9H*-alkylfluorene derivatives [60,61] (see sch. 1).



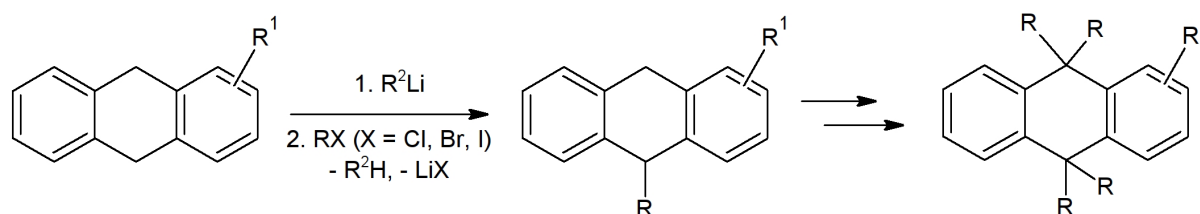
SCH. 1: **9H alkylation of Fluorenes**

Besides, Fluorenes can also undergo many other reactions, such as catalytic hydrogenation [62], oxidation [61], etc. The corresponding products are Hydrofluorenes and 9-fluorenes, respectively.

ii. Dihydroanthracenes and dihydrophenanthrenes

Dihydroanthracenes and Dihydrophenanthrenes present various chemical reactivities. Indeed, these compounds can be oxidized in order to form Anthracenes and Phenanthrenes in a first time, and Anthraquinones and Phenanthrenequinones, in a second time [63].

However, these compounds also exhibit acidic characters. Like Fluorene, they can be converted to their conjugated bases in order to perform alkylations of the products [64] (see sch. 2).

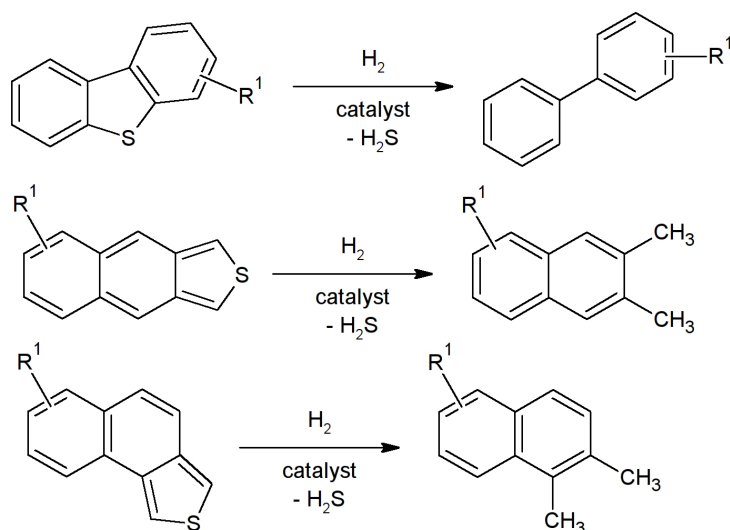


SCH. 2: Alkylation of Dihydroanthracenes

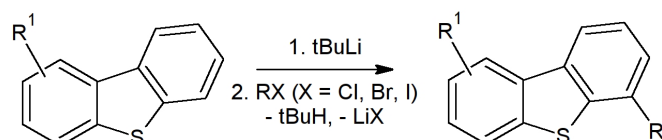
iii. Dibenzothiophene and its derivatives

The reactivity of Dibenzothiophene and its derivatives and isomers has been widely studied for crude oil desulfurization purposes. Many reductions with hydrogen, using various catalysts, were previously reported in the literature. The hydrogenation and desulfurization of Dibenzothiophenes and Naphthothiophenes was found to lead to Biphenyls or Dimethylnaphthalenes [65] (sch. 3).

Dibenzothiophenes can also undergo various oxidation processes but can also be converted to their conjugated bases. However, due to their high pK_a value, this operation requires extremely strong bases such as tert-butyl lithium (tBuLi) [66]. The conjugated bases of Dibenzothiophenes can react as nucleophiles for alkylation purposes, for example (sch. 4).



SCH. 3: Desulfurization of Dibenzothiophenes and Naphthothiophenes

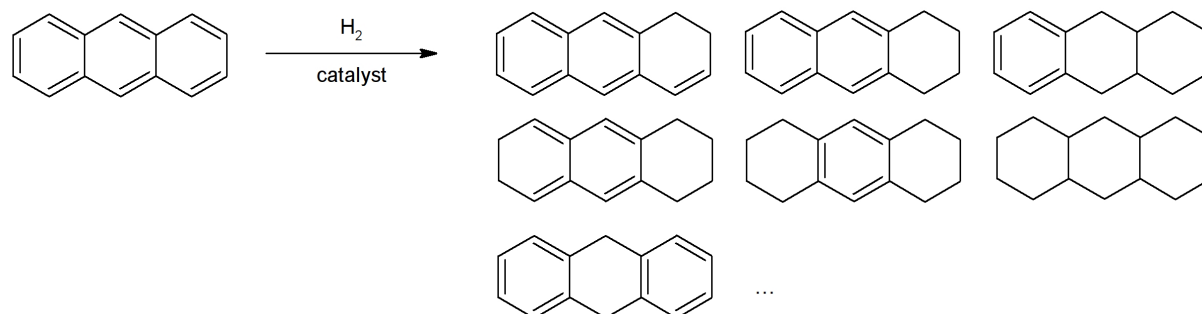


SCH. 4: Alkylation of Dibenzothiophenes

iv. Anthracene and its derivatives

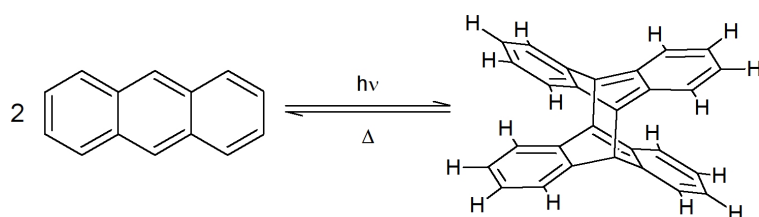
Anthracene and its derivatives can react with hydrogen under catalytic conditions to form many hydrogenated products, whose nature and proportions depend on the selected operating

conditions [67] (sch. 5). Note that Phenanthrene can also react in such conditions, but Anthracene is more reactive due to its lower aromaticity [68].



SCH. 5: **Hydrogenation of Anthracene**

Moreover, Anthracene is well known to form dimers under UV radiations [69,70] (sch. 6). The dimer can be converted to its monomers by heating the product. However, this reversible reaction is impossible with Phenanthrene [71].

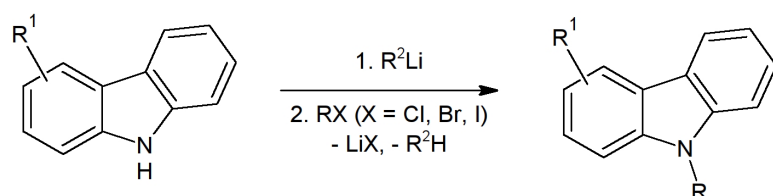


SCH. 6: **Dimerization of Anthracene**

Anthracene can also react with dienophiles in Diels Alder reactions. The most known example is that of Maleic Anhydride that is used for the separation of Phenanthrene from Anthracene [32] during their manufacturing. This product can be easily extracted using an aqueous phase due to the reactivity of anhydrides with water.

v. Carbazole and its derivatives

Thanks to favorable pK_a values, Carbazole conjugated bases can be easily formed in basic medium. This reaction permits *N*-alkylation of the products by means of alkyl halides [72] (sch. 7).



SCH. 7: ***N*-alkylation of Carbazole derivatives**

In addition, Carbazole can be hydrogenated using catalysts such as Raney Nickel. However, the hydrogenation process requires to operate at high temperature to convert the reactant [73].

Eventually, Carbazole can also be denitrogenated using specific catalysts. The product is then converted to Bicyclohexyl [74].

vi. Summary

As shown in this part, the impurities of Phenanthrene present various chemical reactivities. Most of them are able to be alkylated using alkyl halides, or hydrogenated under catalytic conditions. Hydrogenation process can lead to hydrogenated and/or desulfurized/denitrogenated products, according to the impurity. Consequently, these reactivities offer many possibilities for impurity chemical modification, especially for alkylation.

c) Purification of Phenanthrene by chemical treatments

As revealed by the previous part, Phenanthrene impurities exhibit various chemical reactivities. In this part, several chemical treatments were applied:

- (i) treatment with Maleic Anhydride, in order to transform impurities exhibiting the reactivity of dienes to their corresponding Diels Alder adduct;
- (ii) treatments with *n*-butyllithium and alkyl halides to perform impurity alkylations;
- (iii) treatments with Hydrogen and Raney Nickel, to perform impurity hydrogenations.

The effect of these treatments on Phenanthrene impurity identities was assessed by means of GC-MSD. In case of successful impurity conversion, treated products were purified by means of co-crystallization with 35DNBA. The ability of the procedure at removing the daughter impurities was assessed by GC-FID.

i. Purification of Phenanthrene by treatment with Maleic Anhydride

Detection of Anthracene/Maleic Anhydride Diels Alder adduct in commercial Phenanthrene samples (see chapter III) indicates that, during manufacturing, the product is treated with Maleic Anhydride to attempt Anthracene removal by adduct formation and extraction of the latter with a basic-pH aqueous phase. This treatment was also performed by McArdle *et al.* [32] and Feldman *et al.* [75], which led to Anthracene complete elimination. However, in commercial products, the simultaneous detection of Anthracene and the adduct highlights that the conversion of Anthracene was incomplete, which requires to re-apply the treatment with Maleic Anhydride to improve the conversion rate. In this part, treatment of commercial technical-grade Phenanthrene with Maleic Anhydride was performed. Its effect was assessed by means of GC-FID measurements.

Experimental procedure

A mixture of 4 g (22.4 mmol) of technical-grade Phenanthrene (Alfa Aesar, 90 %) and 2.20 g (22.4 mmol) of Maleic Anhydride (Acros Organics, 99 %) was refluxed for 9 h in 25 mL of Toluene (HPLC grade, VWR Chemicals). After reflux, Toluene was evaporated under vacuum. 300 mg of wet powder was put into 6 mL of Dichloromethane (Reagent grade, VWR Chemicals). Anhydrides were extracted using 3 × 6 mL of 10 wt. % aqueous NaOH solution and 3 × 6 mL of milli-Q® water. The organic layer was recovered, dried over MgSO₄ (Fischer), and filtered over 0.2 µm PTFE syringe filter. The solvent was let evaporating to air for 10 h, and the recrystallized powder was dried overnight at 50 °C.

Results

GC-FID chromatograms of the starting and treated products are shown in fig. 52.

No difference between both chromatograms could be evidenced, which shows that the treatment had no effect on Anthracene conversion. This indicates that the kinetics of the Diels Alder transformation was too low in the tested conditions.

Moreover, the presence of Anthracene/Maleic Anhydride adduct in the treated product indicates that the adduct extraction procedure was unable at eliminating this impurity, which might be caused by low sodium salt formation kinetics and unfavorable partition coefficient during extraction.

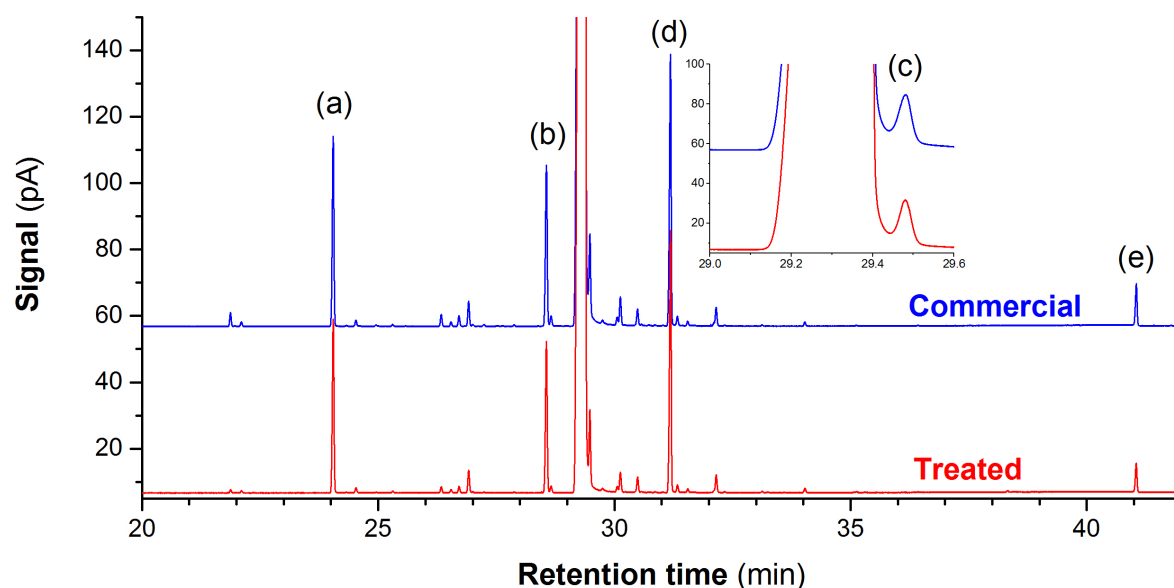


FIG. 52: **Normalized GC-FID chromatograms of commercial and Maleic Anhydride-treated technical-grade Phenanthrene samples** – (a) Fluorene, (b) Dibenzothiophene, (c) Anthracene, (d) Carbazole, (e) Anthracene/Maleic Anhydride Diels Alder adduct

Conclusion

In the tested conditions, treatment of Phenanthrene with Maleic Anhydride was unable at converting Anthracene to its adduct. Consequently, no removal of this impurity was obtained, and other chemical treatments should be envisaged.

In future works, high pressure conditions (200-300 bars) should be tested. For now, this could not be achieved in our laboratory due to lack of dedicated equipment.

ii. *Purification of Phenanthrene by impurity alkylation and co-crystallization of treated product*

As shown by literature review (part V.3)b, p. 249), many Phenanthrene impurities can be alkylated in strongly basic medium in presence of alkyde halides. In this part, alkylation treatments using Iodomethane and *n*-bromopentane were attempted in order to modify the impurities. Treated products were analyzed by GC-MSD to identify the impurities generated. Then, their removal was attempted by co-crystallization of the treated products with 35DNBA. Impurity level variations were qualitatively monitored by GC-FID.

Experimental part

The following procedures were successively applied:

Alkylation treatments: 2 g (11.2 mmol) of technical-grade Phenanthrene (Alfa Aesar, 90 %) was placed in a 50 mL round bottom flask. 12 mL of anhydrous Tetrahydrofuran (Acros Organics, 99.9 + %, stabilized with BHT) was added, as well as a magnet olive. The flask was sealed by septum, flushed with Argon and put into Acetone/solid CO₂ bath to let temperature decrease to – 78 °C. 6 mL of *n*-butyllithium (Sigma-Aldrich, 2 M in hexanes, 12 mmol) was added dropwise to the flask under magnetic stirring. The mixture was let stirring for 1 h at – 78 °C. Then, 22 mmol of Iodomethane (Acros Organics, 99 %, stabilized with Cu, ~ 3.2 g) or *n*-bromopentane (Acros Organics, 98 %, ~ 3.4 g) was added dropwise. The mixture was let

stirring for 18 h by letting the Acetone/solid CO₂ bath warm up to room temperature. Eventually, the potential excess of *n*-butyllithium was neutralized by slow addition of 5 mL of Isopropanol (HPLC grade, VWR Chemicals).

Recovery of treated Phenanthrene: First, the solvents were evaporated under vacuum. Then, the recrystallized powder was dissolved in 100 mL of Dichloromethane (reagent grade, VWR Chemicals). Lithium salts were extracted with 3 × 50 mL of milli-Q® water. The organic layer was recovered, dried over MgSO₄, and filtered over 0.2 µm PTFE syringe filter. Dichloromethane was evaporated under vacuum and recrystallized Phenanthrene was dried overnight at 50 °C.

Purification of treated Phenanthrene: For every treated product, 2 g of an equimolar binary mixture of treated Phenanthrene and 35DNBA (Alfa Aesar, 98 + %) was co-crystallized for 24 h in 6.5 g of Acetone (HPLC grade, VWR Chemicals), under magnetic stirring and at room temperature. The suspension was filtered over 3-porosity glass filter. Wet crystals were washed with 1 mL of 0 °C Acetone. They were then put in 6 mL of Dichloromethane (reagent grade, VWR Chemicals). 35DNBA was extracted with 3 × 6 mL of 10 wt. % aqueous NaOH solution and 3 × 6 mL of milli-Q® water. The organic layer was recovered, dried over MgSO₄ and filtered over 0.2 µm PTFE syringe filters. The solvent was evaporated to air for 24 h. ~ 0.6 g of purified Phenanthrene was obtained.

To identify impurities generated by the treatments, Phenanthrene samples were analyzed by GC-MSD.

Results

Alkylation using Iodomethane

GC-FID chromatograms of commercial, treated and co-crystallization purified Phenanthrene samples are shown in fig. 53.

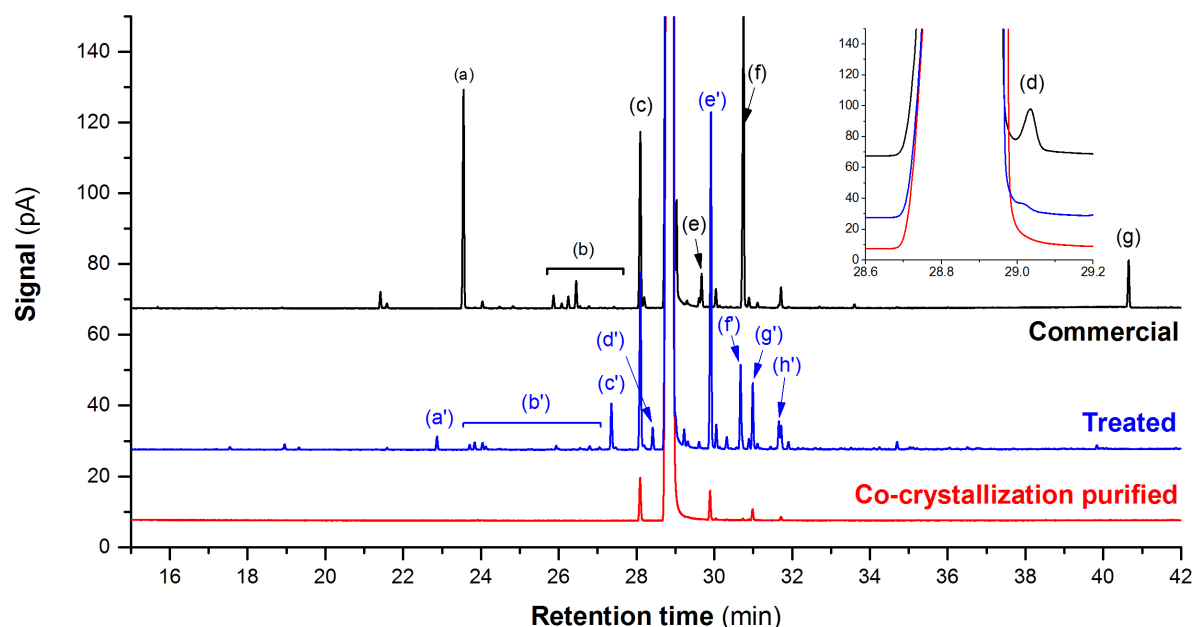


FIG. 53: **Normalized GC-FID chromatograms of commercial technical-grade Phenanthrene (black), Phenanthrene treated with iodomethane and *n*-butyllithium (blue) and co-crystallization purified Phenanthrene (red)** – (a) Fluorene, (b) Hydroanthracenes, Hydrophenanthrenes, (c) Dibenzothiophene, (d) Anthracene, (e) Naphtothiophene 2, (f) Carbazole, (g) Anthracene/Maleic Anhydride Diels Alder adduct – (a') Dimethylfluorene, (b') Hydrophenanthrene and Hydroanthracene (poly)methyl derivatives, (c') Butylmethylfluorene, (d') Dimethylfluorene, (e') Methylcarbazole, (f') Dibutylfluorene, (g', h') Methylnaphthothiophenes.

Comparison of commercial and treated product chromatograms highlights that, during the treatment, Fluorene (a) hydroanthracenes/phenanthrenes (b), Naphthothiophene (the 2nd isomer, e), Carbazole (f) and the Anthracene/Maleic Anhydride adduct (g) were completely converted. Anthracene (d) was partially converted. However, no evidence of Dibenzothiophene (c) conversion was observed.

New peaks on treated product chromatogram show that many daughter impurities were generated. However, their identity was hard to determine by GC-MSD. Mass spectra of labeled peaks allowed for the following attributions: (a') Dimethylfluorene, (b') Hydrophenanthrene and Hydroanthracene (poly)methyl derivatives, (c') Butylmethylfluorene, (d') another Dimethylfluorene, (e') Methylcarbazole, (f') Dibutylfluorene, (g', h') Methylnaphthothiophenes.

The identity of the impurities generated by the treatment are consistent with alkylation of the converted impurities. It also reveals that exchanges between iodide and lithium occurred during the transformation ($\text{CH}_3\text{I} + n\text{-BuLi} \rightarrow n\text{-BuI} + \text{CH}_3\text{Li}$), as butyl groups were detected on Fluorene derivatives. Note that, during the treatment, Fluorene was alkylated twice, and 4 daughter impurities were generated (a', c', d', f').

Comparison of treated and co-crystallization purified product chromatograms indicates that the purification procedure led to the complete elimination of Fluorene (a', c', d', f') and Hydrophenanthrene/Hydroanthracene (b') daughter impurities. Anthracene (d) remaining traces in the treated product were reduced below the detection thresholds. Dibenzothiophene, that was not converted during the treatment, was partially eliminated during co-crystallization. The daughter impurity of Carbazole (e') was only partially removed, as well as Methylnaphthothiophenes (g', h').

Consequently, this method was able at completely eliminating Fluorene, Hydrophenanthrenes and Hydroanthracenes from Phenanthrene by modification of the impurities and elimination of their daughter ones by co-crystallization. Similarly, a complete elimination of Anthracene could be achieved. However, even if the chemical treatment allowed for a complete conversion of the major impurity Carbazole, its daughter impurity was not eliminable co-crystallization.

Hence, the interest of this method was evidenced, while further optimization is required to obtain the complete conversion of all the impurities and the removal of their daughter products.

Alkylation using n-bromopentane

The chromatograms of the commercial, treated and co-crystallization purified products are shown in fig. 54.

Comparison of commercial and treated product chromatograms highlights that many impurities were completely converted during the treatment: Butenedioic acid, dibutyl ester (b), Fluorene (c), Hydro-anthracenes and -phenanthrenes (d), Phenanthrenequinone (i) and the Anthracene/Maleic Anhydride adduct (p). A large number of new impurities was generated by the treatment. GC-MSD measurements allowed for the identification of some of them: Dimethylnaphthalene (a), Pentylfluorene (h), Dipentylidihydro-anthracene(s) and/or

-phenanthrene(s) (k, l), Pentylcarbazole (m), Butylpentylidihydro-anthracene or -phenanthrene (n) and Dipentylidihydro-anthracene or -phenanthrene (o).

Detection of dimethylnaphthalene (a) in the treated product indicates that one of the Naphthothiophenes present in the starting products was maybe (and surprisingly) desulfurized during the treatment. The other generated impurity identities are consistent with mono- or poly-alkylation of Fluorene (c), Hydro-anthracenes and -phenanthrenes (d). Detection of Butylpentylidihydro-anthracene or -phenanthrene (n) suggests the occurrence of lithium-halide exchange during the treatment (n -butyllithium + n -bromopentane \leftrightarrow n -bromobutane + n -pentyllithium). Simultaneous detection of Carbazole (g) and Pentylcarbazole (m) indicates that Carbazole conjugated base was not reactive enough with n -bromopentane to allow for its complete conversion.

The chromatogram of the treated product purified by co-crystallization highlights that the impurities generated during the treatment were not completely eliminated from the product, as they were still detected.

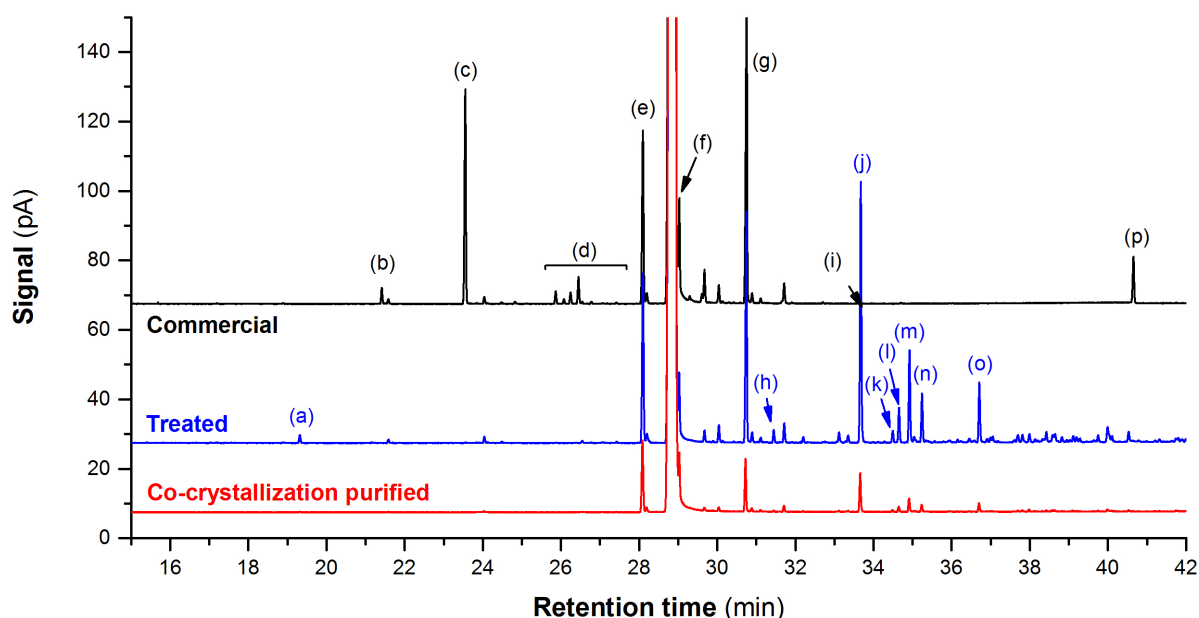


FIG. 54: **Normalized GC-FID chromatograms of commercial technical-grade Phenanthrene (black), Phenanthrene treated with n -bromopentane and n -butyllithium (blue) and co-crystallization purified Phenanthrene (red)** – (a) Dimethylnaphthalene, (b) Butenedioic acid, dibutyl ester, (c) Fluorene, (d) Hydro-anthracenes and -phenanthrenes, (e) Dibenzothiophene, (f) Anthracene, (g) Carbazole, (h) Pentylfluorene, (i) Phenanthrenequinone, (j) Dipentylfluorene, (k, l) Dipentylidihydro-anthracene(s) and/or -phenanthrene(s), (m) Pentylcarbazole, (n) Butylpentylidihydro-anthracene or -phenanthrene, (o) Dipentylidihydro-anthracene or -phenanthrene, (p) Anthracene/Maleic Anhydride adduct

Discussion and conclusion

During application of alkylation treatments on Phenanthrene, many impurities of the starting product could be chemically modified. However, for each impurity converted during both experiments (except Carbazole), several daughter impurities were generated. This was due to two reasons: (i) the fact that Fluorene and Hydro-anthracenes or -phenanthrenes can undergo

several successive alkylation transformations, (ii) the occurrence of lithium-halide exchanges between *n*-butyllithium and alkyl halides during the treatment.

In the tested conditions, Iodomethane was the most reactive alkyl halide, which allowed for the complete conversion of two major impurities of Phenanthrene (Fluorene and Carbazole), and the partial one of Anthracene. However, during both experiments, no conversion of Dibenzothiophene was observed.

Purification of the product treated with Iodomethane permitted the complete elimination of all the Fluorene daughter impurities. As the latter exhibited large molecular volumes, their removal during co-crystallization can be explained by the fact that they were too big to substitute Phenanthrene molecules in the co-crystal. However, the other daughter impurities of Carbazole and Naphthothiophene generated by the treatment were only partially removed, which indicates that they could be included in partial solid solution of the co-crystal.

Consequently, this approach is promising for impurity elimination purposes, even if all of them could not be completely eliminated. The results introduced in this study should serve as a base for future optimization works on the following points:

- (i) a stronger base, such as *tert*-butyllithium, should be employed in order to generate the conjugated base of Dibenzothiophene, which would allow for its reaction with alkyl halides, and, thus, for its conversion.
- (ii) other alkyl halides should be tested to tune the chemical group grafted on the impurities. Among them, *iso*-propyl iodide and *sec*-butyl iodide could have an interesting reactivity and would generate daughter impurities with large molecular volumes. This would maybe increase the probability of their removal from Phenanthrene during co-crystallization.

Besides alkylation, Phenanthrene impurity reactivities permits to test other treatments, amongst which hydrogenation under catalytic conditions. This pathway was experimentally investigated and is reported in the next paragraph.

iii. Purification of Phenanthrene by hydrogenation treatment and co-crystallization

As revealed by purification attempts on technical-grade Phenanthrene (part IV, p. 227), co-crystallization with 35DNBA permitted the complete elimination of hydrogenated impurities due to their molecular volumes larger than that of Phenanthrene – and, probably, to their lack of planeity. Consequently, in this part, a study of hydrogenation treatments on Phenanthrene impurities was performed before attempted their removal by co-crystallization.

In a first time, technical-grade Phenanthrene was treated in order to identify the different impurities sensitive to the treatment. Then, the procedure was applied to a purer synthesis-grade Phenanthrene to achieve a complete conversion of its starting major impurities. The treated product was purified first, by co-crystallization with 35DNBA, and then, by Zone Melting.

Chromatographic measurements were performed to:

- (i) identify the impurities generated by the treatment (GC-MSD),
- (ii) assess their levels in the treated and purified products (GC-FID).

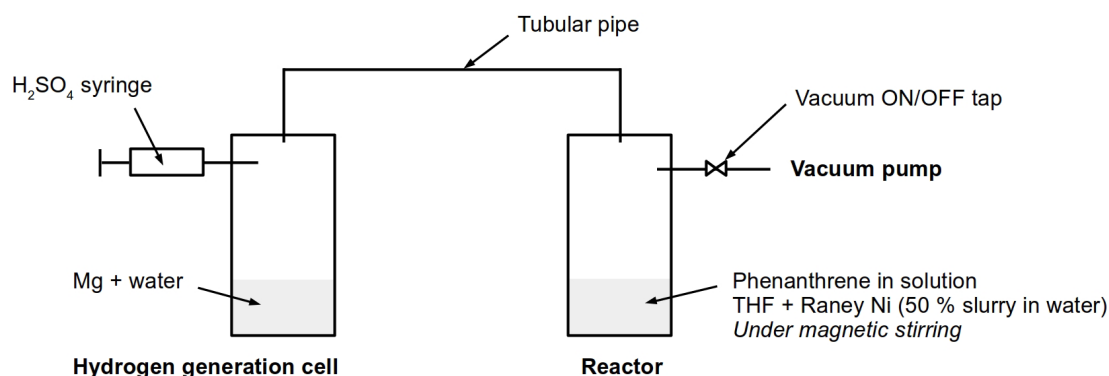
Experimental procedure

FIG. 55: **Experimental set-up for Phenanthrene hydrogenation treatment**

Hydrogenation treatments were attempted using the set-up described in fig. 55. The set-up was made of two separate cells connected by an open tubular pipe – pressure was thus homogeneous inside both cells. The hydrogen generation cell was loaded with a certain amount of Magnesium (Acros Organics, 99 + %) in suspension in water. The reactor was loaded with a solution containing 8 g of Phenanthrene in 50 mL of Tetrahydrofuran (THF, Acros Organics, 99.9 + %, stabilized with BHT), and 12 mL of Raney Nickel suspension (50 % slurry in water, Acros Organics). Both cells were also loaded with bar magnets to ensure a good stirring. Once loaded, the system was put under reduced pressure by means of a basic laboratory vacuum pump. The reduced pressure was maintained by switching off the vacuum tap. At this time, an excess of 25 % H₂SO₄ aqueous solution was added dropwise in the hydrogen generation cell through a septum in order to produce H₂ in the system ($\text{Mg} + \text{H}_2\text{SO}_4 \rightarrow \text{MgSO}_4 + \text{H}_2$). The latter was let under magnetic stirring for 48 hours.

At the end of the procedure, pressure was restored to 1 atm by switching the vacuum tap. The liquid of the reactor was recovered and filtered over 0.2 μm PTFE syringe filter. Water was removed by drying the liquid over MgSO_4 . A second filtration was performed and the solvent was evaporated under vacuum. Recrystallized Phenanthrene was then dried overnight at 50 $^\circ\text{C}$.

The following amounts of reactants were engaged during the treatments:

- (i) technical-grade Phenanthrene (Alfa Aesar, 90 %) was treated with ~ 40 mmol of H_2 generated by oxidation of ~ 950 mg of Mg.
- (ii) synthesis-grade Phenanthrene (Alfa Aesar, 98 %) was treated with ~ 10 mmol of H_2 generated from ~ 240 mg of Mg.

After treatment, synthesis-grade Phenanthrene was purified by co-crystallization with 35DNBA according to the following procedure:

3.7 g of treated Phenanthrene and 4.3 g of 35DNBA (Alfa Aesar, 98 +%) was placed in 25 mL of HPLC grade Acetone (VWR Chemicals). The mixture was equilibrated under magnetic stirring for 24 hours. The suspension was recovered by filtration over 4-porosity glass filter. The wet co-crystal was placed in 50 mL of Dichloromethane (HPLC grade, Alfa Aesar) and 35DNBA was extracted with 3×50 mL of a 10 wt. % aqueous NaOH solution and 3×50 mL of milli-Q® water. The organic layer was recovered, dried over MgSO_4 , and filtered over 0.2 μm PTFE syringe filter. The solvent was evaporated to air for 24 h to let purified Phenanthrene recrystallize. ~ 2.3 g of purified Phenanthrene was obtained.

The purified product was eventually treated by Zone Melting:

A 2-cm length ingot was made in a glass tube sealed under Argon (to avoid Phenanthrene oxidation and generation of Phenanthrenequinone). 10 zone passes were applied at 1 mm h^{-1} displacement rate. After refining, the ingot was segmented into 2 parts that were analyzed by GC to determine their purity.

Results

GC-FID chromatograms of the commercial and treated technical-grade Phenanthrene are shown in fig. 56.

As revealed by the chromatograms, five impurities (*e. g.*, Butenedioic acid, dibutyl ester (c), the two Naphthothiophenes (d) and (f), Phenanthrenequinone (g) and the Anthracene/Maleic Anhydride adduct (h)) were completely converted during the treatment. Moreover, the remarkable decrease of Anthracene (e) level was evidenced, which indicates that the impurity was almost completely converted.

Besides, new chromatographic peaks (a) and (b) on treated product chromatogram indicate that new impurities were generated by the treatment. Complementary GC-MSD measurements permitted to identify these impurities as being Ethyl- and Dimethyl-naphthalenes, respectively. The identity of these impurities is consistent with the desulfurization products of the two Naphthothiophenes (d) and (f). However, no new impurity could be affiliated to one of the others that were converted. Moreover, no change was observed in Hydroanthracene levels (26-28 min elution range), while Anthracene was converted. In the literature, some papers reported that Anthracene can undergo hydrogenolysis transformations under catalytic conditions, with breaking of C=C bonds [67,76,77]. Consequently, it is possible that the impurity was converted to many daughter volatile

impurities that exited the reactor as gases, which would explain why they were not detected by GC.

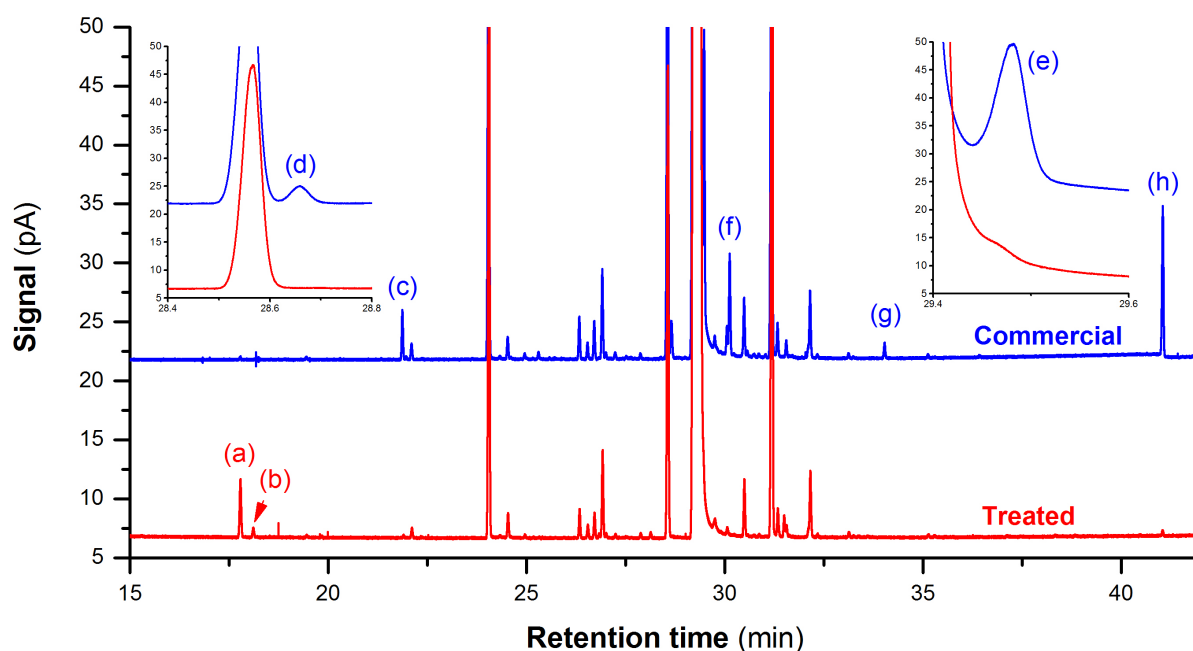


FIG. 56: **Normalized GC-FID chromatograms of commercial technical-grade Phenanthrene (blue) and Phenanthrene treated with Hydrogen and Raney Nickel (red)** – (a) Ethylnaphthalene, (b) Dimethylnaphthalene, (c) Butenedioic acid, dibutyl ester, (d) Naphthothiophene (1st isomer), (e) Anthracene, (f) Naphthothiophene 2, (g) Phenanthrenequinone, (h) Anthracene/Maleic Anhydride Diels Alder adduct.

Note that, during this treatment, no hydrogenation product of some major impurities (Fluorene, Dibenzothiophene and Carbazole) was detected, which raises two hypotheses: (i) the amount of hydrogen was not sufficient enough to allow for their hydrogenation, (ii) the kinetics of hydrogenation of these impurities was too low to observe their conversion.

This treatment was also applied to a synthesis-grade Phenanthrene lot that exhibits low Fluorene and Carbazole contents. Sample chromatograms before and after hydrogenation and after purification of the treated product by co-crystallization are shown in fig. 57. Impurity levels in the different samples are listed in tab. 25.

As revealed by sample chromatograms and impurity level values, hydrogenation treatment led to the complete conversion of 7 impurities of the starting material: the Hydro-anthracene or -pneanthrene (j), Dibenzothiophene (k), the two Naphthothiophenes (l) and (n), Anthracene (m), Phenanthrenequinone (q) and the Anthracene/Maleic Anhydride adduct (r). In this experiment, Dibenzothiophene was completely converted, whereas it was not the case during the previous one carried out on technical-grade Phenanthrene. This indicates that the amount of Hydrogen was maybe insufficient during this previous test. The variation of Hydrophenanthrene and Hydroanthracene (e, f, h) levels suggests that potential interconversions or hydrogenolyses occurred during the treatment. This phenomenon was previously observed during hydrogenation of Phenanthrene under catalytic conditions [67,76,77].

TAB. 25: Impurity levels (in wt. %) in Phenanthrene before/after hydrogenation treatment and purification by co-crystallization

Impurity	Starting product	After hydrogenation treatment	After purification by co-crystallization
(a) Biphenyl (+ ethylnaphthalene?*)	ND	0.35 ± 0.02	ND
(b) Dimethylnaphthalene**	ND	0.0285 ± 0.0008	ND
(c) Butylhydroxytoluene***	ND	0.0049 ± 0.0005	ND
(d) Fluorene	0.0052 ± 0.0003	0.0054 ± 0.0003	ND
(e) 9,10-dihydroanthracene	0.285 ± 0.007	0.189 ± 0.003	ND
(f) 9,10-dihydrophenanthrene	0.0077 ± 0.0001	0.0569 ± 0.0003	ND
(g) 1-methylfluorene	0.0039 ± 0.0001	0.0039 ± 0.0002	ND
(h) Tetrahydro-phenanthrene or -anthracene**	0.022 ± 0.001	0.030 ± 0.001	ND
(i) Tetrahydro-phenanthrene or -anthracene**	ND	0.023 ± 0.001	ND
(j) Dihydro-anthracene or phenanthrene**	0.012 ± 0.001	ND	ND
(k) Dibenzothiophene	0.809 ± 0.007	ND	ND
(l) Naphthothiophene	0.025 ± 0.001	ND	ND
(m) Anthracene	0.393 ± 0.008	ND	ND
(n) Naphthothiophene**	0.008 ± 0.001	ND	ND
(o) Methyl-naphthothiophene or -dibenzothiophene**	0.006 ± 0.002	0.0037 ± 0.0002	ND
(p) Carbazole	0.0229 ± 0.0005	0.0226 ± 0.0007	0.010 ± 0.001
(q) 9,10-phenanthrenequinone	0.021 ± 0.002	ND	ND
(r) Anthracene/Maleic Anhydride Diels Alder adduct	0.015 ± 0.004	ND	ND
Total	1.64 ± 0.04	0.72 ± 0.03	0.010 ± 0.001

* During GC-MSD measurements, a co-elution of Biphenyl and Ethylnaphthalene was suspected, **undetermined isomer, *** stabilizer of the solvent of hydrogenation treatment, (impurities generated by hydrogenation treatment)

At least 4 impurities were generated by the treatment: Biphenyl (a), Dimethylnaphthalene (b), Butylhydroxytoluene (c) and a tetrahydroanthracene/phenanthrene (i). Butylhydroxytoluene comes from Tetrahydrofuran – it is the stabilizer of the solvent used for the hydrogenation treatment. Co-elution of Biphenyl with Ethylnaphthalene was suspected, which might indicate the generation of a fifth impurity. Their identity is consistent with the conversion products of Dibenzothiophene, Naphthothiophenes, Anthracene. However, no filiation could be established for Phenanthrenequinone (q) and Anthracene/Maleic Anhydride adduct (r), which suggests that they were hydrogenolyzed during the treatment.

The purification by co-crystallization led to the complete elimination of all the impurities of the treated product, except Carbazole (p). The latter was still detected in the purified sample at a very low level (*e. g.*, 0.01 wt. or mole %). Consequently, this procedure allowed for reaching Phenanthrene ultrapurity. However, a further purification step by Zone Melting was attempted in order to remove the remaining traces of Carbazole. Impurity distribution in the treated ingot is indicated in tab. 26.

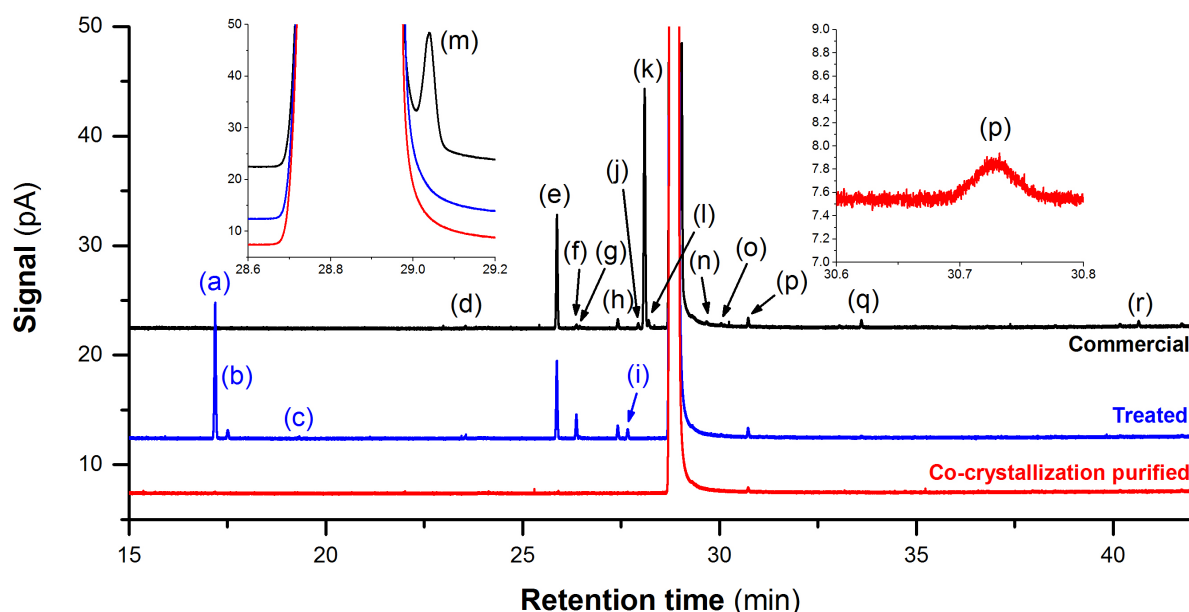


FIG. 57: **Normalized GC-FID chromatograms of synthesis-grade Phenanthrene samples before (black) and after (blue) hydrogenation treatment and after (red) purification of the treated product by co-crystallization** – (a) Biphenyl (+ ethylnaphthalene?), (b) Dimethylnaphthalene, (c) Butylhydroxytoluene, (d) Fluorene, (e) 9,10-dihydroanthracene, (f) 9,10-dihydrophenanthrene, (g) 1-methylfluorene, (h, i) Tetrahydro-anthracenes and/or -phenanthrenes, (j) Dihydro-anthracene or -phenanthrene, (k) Dibenzothiophene, (l) Naphthothiophene (1st isomer), (m) Anthracene, (n) Naphthothiophene (2nd isomer), (o) Methyl-naphthothiophene or -dibenzothiophene, (p) Carbazole, (q) 9,10-phenanthrenequinone, (r) Anthracene/Maleic Anhydride Diels Alder adduct.

TAB. 26: **Carbazole levels and chemical purity of Phenanthrene purified by Zone Melting after hydrogenation treatment and purification by co-crystallization**

Impurity	0-1 cm	1-2 cm
Carbazole (wt. %)	0.019 ± 0.002	ND (< 0.0001 wt. %)
Purity (wt. %)	99.981	> 99.999(9)
Purity (mole %)	99.980	> 99.999(9)

As revealed by tab. 26 entries, the purity of half part of the sample could be increased above 99.999 wt. and mole %. Conversely, the other part was enriched by two in Carbazole.

Summary

After application of the treatment on synthesis-grade Phenanthrene, the daughter impurities generated were completely eliminated from the product by co-crystallization. Carbazole traces were still detected in the purified product. They could be reduced below the detection thresholds (0.0001 wt. %) by means of zone refining. Consequently, this procedure allowed for reaching ultrapure Phenanthrene.

d) Conclusion

Chemical treatments attempted in this work exhibited various selectivity with respect to the different impurities of Phenanthrene.

- (i) Treatment with Maleic Anhydride did not change the identity of Phenanthrene impurities and was therefore unsuccessful.
- (ii) Alkylation treatments were able at substituting Fluorene, Anthracene and Carbazole. However, many impurities were generated by the tested treatments, and only Fluorene daughter impurities could be eliminated by co-crystallization.
- (iii) Hydrogenation treatments allowed for the conversion of Anthracene, Dibenzothiophene, and Naphthothiophenes. Their products were completely eliminated by co-crystallization.

The application of hydrogenation and co-crystallization procedures on synthesis-grade Phenanthrene led to ultrapure material, exhibiting low Carbazole contents. The duration of the procedure was ~ 4 days, against ~ 40 days for the first combinatorial approach attempted in this work (*e. g.*, pre-purification by co-crystallization and impurity removal by Zone Melting).

After treatment and impurity removal by co-crystallization, the remaining traces of Carbazole were reduced below 0.0001 wt. % by Zone Melting. DSC analyses of the starting and ultrapure products (fig. 58) highlight that the substantial increase of purity had a significant impact on Phenanthrene solid-solid transition temperature (increased by 3 °C), as well as on its melting point (increased by 1 °C). Moreover, a sharper signal was observed for melting peak after purification, as well as a rough drop from baseline, which is consistent with an increase of purity. Extended data on DSC figures are provided in tab. 27.

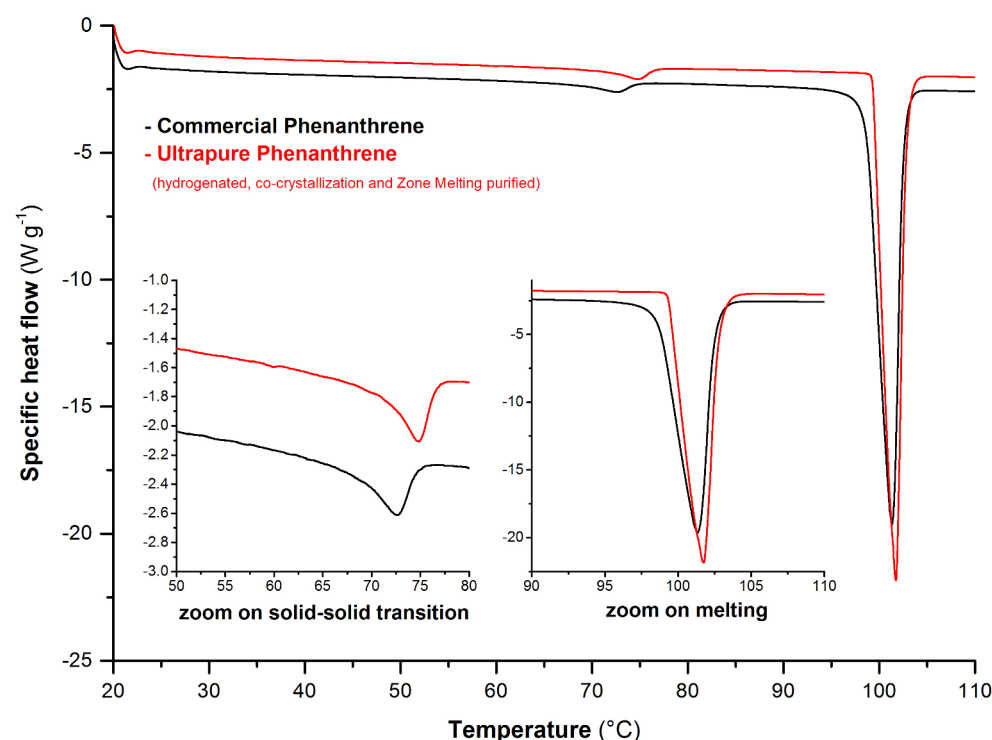


FIG. 58: DSC thermograms of commercial starting Phenanthrene (black) and ultrapure sample prepared by hydrogenation treatment and purification by co-crystallization and Zone Melting (red). Endo down.

TAB. 27: DSC data on commercial and ultrapure Phenanthrene

	Solid-solid transition		Melting	
	Onset temperature (°C)	Enthalpy (J g ⁻¹ , on heating)	Onset temperature (°C)	Enthalpy (J g ⁻¹ , on heating)
Commercial Phenanthrene	68.0	4.99	98.3	99.8
Ultrapure Phenanthrene	71.0	5.45	99.3	102

VI. CONCLUSION

In this chapter, purification experiments performed on Phenanthrene by solvent assisted recrystallization and Zone Melting shown that unfavorable phase equilibria prevented from impurity removal using these methods. In particular, they did not exhibit interesting purifying effects with respect to the major impurities of starting materials (Fluorene, Dibenzothiophene, Anthracene and Carbazole). Similar results were obtained using vacuum sublimation, probably due to technical limitations.

Alternative co-crystallization method shown better ability at eliminating impurities from Phenanthrene, especially those whose molecular volumes were larger than that of the target compound. The complete removal of Hydrophenanthrenes, Hydroanthracenes, and Anthracene/Maleic Anhydride adduct was achieved using this technique. Partial removals of the main impurities were observed, but their rate of removal was higher than observed during recrystallization.

Besides, sublimation tests were unable at separating Phenanthrene from its organic impurities. However, the method was successful at eliminating inorganic impurities from the product.

As: (i) all these methods exhibited different efficiencies with respect to the different impurities, (ii) none of them was able at removing all the impurities by a single shot; combinatorial approaches were investigated to reach ultrapure Phenanthrene. On the one hand, combination of co-crystallization and Zone Melting on synthesis-grade product almost allowed for reaching 99.9 mole % purity. On the other hand, chemical treatments followed by purification using co-crystallization with 35DNBA allowed to benefit from favorable phase equilibria for the entire removal of Fluorene (treatment of technical-grade Phenanthrene with *n*-butyllithium and Iodomethane), Dibenzothiophene, Naphthothiophenes and Anthracene (hydrogenation treatment).

Hydrogenation treatment of synthesis-grade Phenanthrene, followed by co-crystallization and Zone Melting, allowed for the preparation of 99.999 mole % product. Consequently, an ultrapurification procedure was successfully developed thanks to this combinatorial approach. This paves the way for future studies on Phenanthrene solid-solid transition mechanism.

However, the procedure developed to achieve ultrapurification was applied to synthesis-grade Phenanthrene. In future works, methods for the ultrapurification of technical-grade Phenanthrene will have to be developed by optimization of chemical treatments to convert impurities as to allow for their complete elimination during co-crystallization.

A summary of the advantages and drawbacks of the different methods and procedures applied to Phenanthrene and tested in this work is provided in tab. 28.

TAB. 28: Summary of Phenanthrene purification method advantages and drawbacks

Method	Advantages	Drawbacks
Solvent-assisted recrystallization	<ul style="list-style-type: none"> Applicable with basic laboratory equipment. 	<ul style="list-style-type: none"> Leads to partial removal of impurities from Phenanthrene.
Zone Melting	<ul style="list-style-type: none"> Amplifies impurity displacement at ingot ends. 	<ul style="list-style-type: none"> Not appropriate to remove Fluorene from Phenanthrene. Requires pre-purification procedures before application. Generates Phenanthrenequinone when the tube is not sealed under protective atmosphere.
Vacuum sublimation	<ul style="list-style-type: none"> Separates Phenanthrene from its inorganic impurities. Does not require the use of solvent, which prevents from sample pollution. 	<ul style="list-style-type: none"> Does not separate Phenanthrene from its organic impurities (using our prototype)
Co-crystallization with 35DNBA	<ul style="list-style-type: none"> Completely eliminates Hydroanthracenes, Hydrophenanthrenes and Anthracene/Maleic Anhydride adduct from Phenanthrene. Significantly decreases Fluorene, Dibenzothiophene, Anthracene and Carbazole levels in Phenanthrene. 	<ul style="list-style-type: none"> Requires the use of 35DNBA and a procedure to separate it from Phenanthrene.
Co-crystallization with 35DNBA followed by Zone Melting	<ul style="list-style-type: none"> Facilitates impurity removal by Zone Melting. 	<ul style="list-style-type: none"> Time-costing procedure.
Impurity alkylation followed by co-crystallization of treated Phenanthrene with 35DNBA	<ul style="list-style-type: none"> Converts Fluorene and eliminates its daughter impurities. 	<ul style="list-style-type: none"> Converts most of the other impurities, whose daughter ones are not systematically completely eliminated. Does not convert Dibenzothiophene in the tested conditions.
Impurity hydrogenation followed by co-crystallization of treated Phenanthrene with 35DNBA	<ul style="list-style-type: none"> Desulfurizes Dibenzothiophene and Naphthothiophenes. Converts Anthracene. Eliminates the impurities generated by the treatment. 	<ul style="list-style-type: none"> Does not convert Fluorene and Carbazole (in this case, further application of a supplementary method is required).

VII. APPENDICES

1) Supplementary bibliographic item

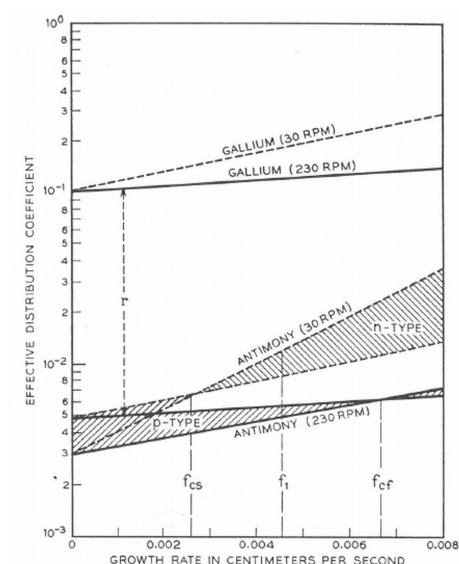


FIG. S1: **Effect of ingot rotation on impurity effective segregation coefficient (y axis) at variable zone displacement rate (x axis) during Zone Melting of Germanium** – adapted from Pfann [3].

2) Methods

a) X-Ray Powder Diffraction

XRPD measurements were carried out on a Bruker D8 Discover apparatus, using the Cu K α radiation (1.54 Å). The samples were scanned from 3 to 30 ° 2 θ angles, with a 0.04 ° step (0.3 s duration). The sample was let rotating at 20 RPM with the phi-spinner. The detector slit was set at 2 mm.

b) Differential Scanning Calorimetry

DSC experiments were performed on a Netzsch DSC214 Polyma apparatus. The samples were put into closed Al pans (25 μ L). The oven was continuously supplied with 40 mL \cdot min⁻¹ N₂. The temperature programs were adjusted according to the nature of the samples analyzed.

c) Analytical Gas Chromatography for ternary phase diagram investigations

Analyses of liquid phases of ternary systems were performed on an Agilent 7890B Series GC apparatus equipped with a Split/Splitless injector (300 °C) and a Flame Ionization Detector (300 °C, 200 Hz acquisition frequency, supplied with 30 mL min⁻¹ H₂ and 300 mL min⁻¹ air). Separations were achieved on an Agilent DB-35ms column (30 m \times 0.25 mm \times 0.25 μ m).

H₂ was used as carrier gas (2.0 mL min⁻¹). For every sample, 0.2 µL of solution was injected. According to the ternary system, the following temperature programs were applied:

- Phenanthrene/Fluorene/Acetone: 40 °C for 2 min, then 10 °C/min to 280 °C, then 280 °C for 2 min
- Phenanthrene/Anthracene/Toluene: 40 °C for 5 min, then 20 °C/min to 100 °C, then 100 °C for 8 min, then 5 °C/min to 280 °C.
- Phenanthrene/Dibenzothiophene/Acetone: 100 °C for 10 min, then 5 °C/min to 280 °C.
- Phenanthrene/35DNBA/Acetone: 100 °C for 10 min, then 5 °C/min to 280 °C.

For each method, the following retention times were observed:

- Phenanthrene/Fluorene/Acetone: Acetone: 1.42 min, Fluorene: 17.01 min, Phenanthrene: 19.54 min.
- Phenanthrene/Anthracene/Toluene: Toluene: 4.63 min, Phenanthrene: 35.26 min, Anthracene: 35.43 min.
- Phenanthrene/Dibenzothiophene/Acetone: Acetone: 1.10 min, Dibenzothiophene: 28.15 min, Phenanthrene: 28.81 min.
- Phenanthrene/35DNBA/Acetone: Acetone: 1.10 min, Phenanthrene: 28.78 min, 35DNBA: 32.12 min.

The mass fractions of every component i , \bar{X}_i , was calculated as follows:

$$\bar{X}_i = \frac{A_i / RF_i}{\sum_i A_i / RF_i} \quad (7)$$

where A_i and RF_i are component peak area and FID response factor.

Relative RF_i values determined by external standard calibration are entered below:

- Phenanthrene/Fluorene/Acetone: Acetone: 1.00, Fluorene: 2.06, Phenanthrene: 2.24.
- Phenanthrene/Anthracene/Toluene: Toluene: 1.00, Phenanthrene: 1.08 min, Anthracene: 1.08.
- Phenanthrene/Dibenzothiophene/Acetone: Acetone: 1.00, Dibenzothiophene: 1.84, Phenanthrene: 2.21.
- Phenanthrene/35DNBA/Acetone: Acetone: 1.00, Phenanthrene: 2.21 min, 35DNBA: 0.377.

3) Pre-purification of products for phase equilibria investigation

For the investigation of the Phenanthrene/9,10-dihydroanthracene and Phenanthrene/Carbazole binary systems, the starting products were purified by means of solvent assisted recrystallization in Acetone (HPLC grade, VWR Chemicals).

For every compound, ~ 20 g of material was placed in 20 mL (Phenanthrene, 9,10-dihydroanthracene) or 50 mL (Carbazole) of Acetone. The mixture was let equilibrating for 24 h under magnetic stirring. The suspension was recovered by vacuum filtration over glass filters. The crystals were washed with 10 mL of cold (0 °C) Acetone and were eventually dried overnight at 60 °C. The three recrystallized samples were then analyzed by GC-FID using the same method as that used for Phenanthrene purity determination. The chromatograms are shown in fig. S2.

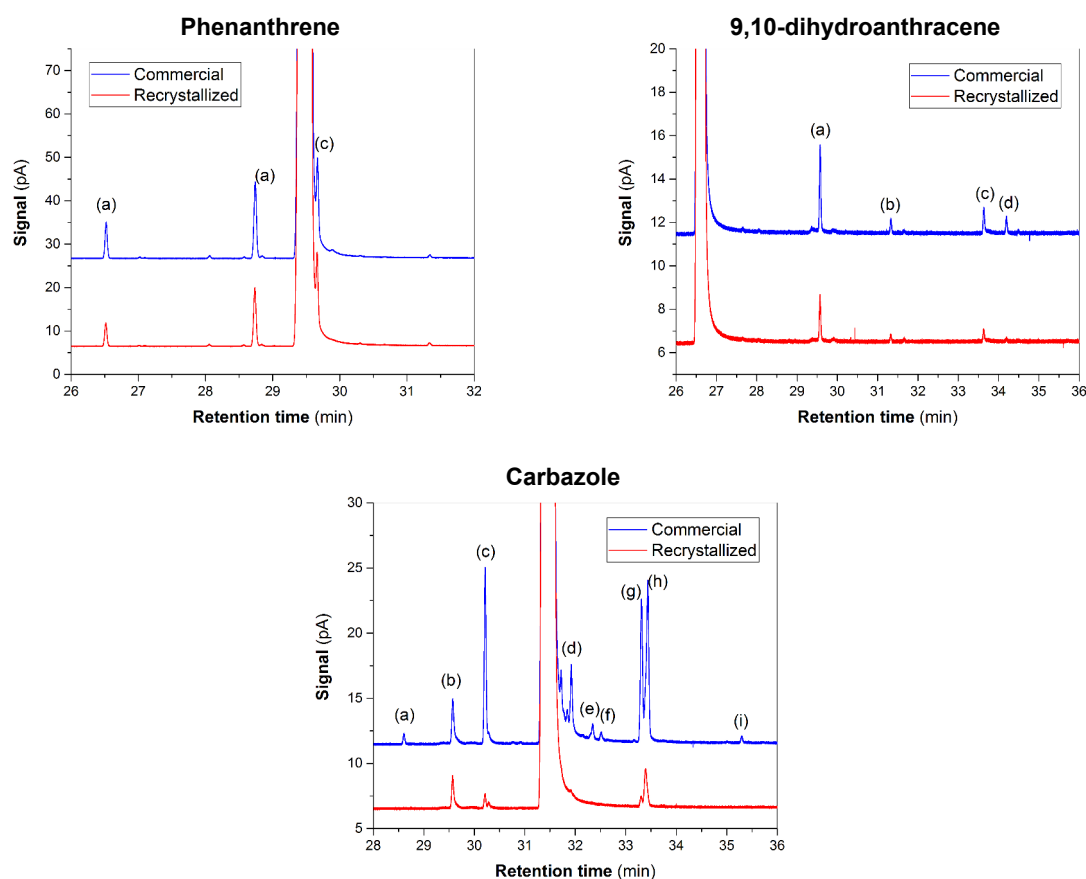


FIG. S2: GC-FID chromatograms of commercial and recrystallized Phenanthrene, 9,10-dihydroanthracene and Carbazole

A rough estimate of impurity level variations was made by peak integration. The rates of removal (in wt. %) are listed below:

Phenanthrene: impurity (a) (9,10-dihydroanthracene): 35 %, impurity (b) (Dibenzothiophene): 24 %, impurity (c) (Anthracene): 14 %.

9,10-dihydroanthracene: impurity (a) (Phenanthrene): 47 %, impurity (b): 49 %, impurity (c): 67 %, impurity (d): 100 %*.

Carbazole: impurity (a): 100 %*, impurity (b) (Phenanthrene): 32 %, impurity (c): 89 %, impurity (d): 100 %*, impurity (e): 100 %*, impurity (f): 100 %*, impurity (g): 94 %, impurity (h): 74 %, impurity (i): 100 %*.

* The corresponding impurities were not detectable in the recrystallized products.

4) Composition data on ternary systems investigated in this work

TAB. S1: **Data on Phenanthrene/Fluorene/Acetone ternary mixture compositions** (in mass fractions) – PHEN: Phenanthrene, FLU: Fluorene, ACT: Acetone.

	Composition of the physical ternary mixtures			Composition of the liquids measured by GC			Composition of the solids deduced using Schreinemaker's method of wet residues	
	PHEN	FLU	ACT	PHEN	FLU	ACT	PHEN	FLU
a	0.000	0.400	0.600	0.000	0.141	0.859	0.000	1.000
b	0.013	0.390	0.598	0.013	0.161	0.827	0.012	0.988
c	0.050	0.361	0.589	0.057	0.156	0.787	0.030	0.970
d	0.087	0.329	0.583	0.093	0.144	0.763	0.068	0.932
e	0.125	0.300	0.575	0.128	0.138	0.735	0.116	0.884
f	0.163	0.270	0.567	0.163	0.132	0.705	0.159	0.841
g	0.200	0.241	0.560	0.198	0.143	0.659	0.208	0.792
h	0.237	0.211	0.552	0.230	0.144	0.626	0.286	0.714
i	0.245	0.204	0.551	0.234	0.152	0.613	0.341	0.659
j	0.255	0.196	0.549	0.233	0.150	0.617	0.436	0.564
k	0.265	0.188	0.547	0.238	0.155	0.607	0.508	0.492
l	0.295	0.164	0.541	0.242	0.124	0.633	0.604	0.396
m	0.311	0.151	0.538	0.262	0.118	0.620	0.631	0.369
n	0.349	0.122	0.529	0.292	0.096	0.612	0.713	0.287
o	0.363	0.110	0.528	0.295	0.087	0.618	0.755	0.245
p	0.375	0.100	0.525	0.300	0.079	0.620	0.786	0.214
q	0.425	0.060	0.515	0.297	0.048	0.655	0.894	0.106
r	0.463	0.030	0.508	0.299	0.024	0.677	0.952	0.048
s	0.488	0.010	0.502	0.323	0.008	0.669	0.982	0.018
t	0.498	0.000	0.502	0.352	0.000	0.648	1.000	0.000

TAB. S2: **Data on Phenanthrene/Dibenzothiophene/Acetone ternary mixture compositions** (in mass fractions) – PHEN: Phenanthrene, DBT: Dibenzothiophene, ACT: Acetone.

Mixture	Composition of the physical ternary mixtures			Composition of the liquids measured by GC			Composition of the solids deduced using Schreinemaker's method of wet residues	
	PHEN	DBT	ACT	PHEN	DBT	ACT	PHEN	DBT
1	0.499	0.000	0.501	0.300	0.000	0.700	1.000	0.000
2	0.486	0.013	0.501	0.307	0.016	0.677	0.996	0.004
3	0.462	0.037	0.500	0.392	0.040	0.669	0.970	0.030
4	0.435	0.074	0.492	0.288	0.077	0.635	0.938	0.062
5	0.386	0.112	0.501	0.313	0.115	0.573	0.903	0.097
6	0.349	0.150	0.500	0.305	0.149	0.546	0.841	0.159
7	0.311	0.187	0.501	0.285	0.187	0.528	0.805	0.195
8	0.275	0.224	0.501	0.269	0.224	0.507	0.757	0.243
9	0.237	0.263	0.500	0.239	0.231	0.530	0.206	0.794
10	0.200	0.299	0.501	0.212	0.232	0.556	0.085	0.915
11	0.125	0.375	0.500	0.145	0.206	0.649	0.058	0.942
12	0.012	0.488	0.500	0.018	0.164	0.818	0.003	0.997
13	0.000	0.500	0.500	0.000	0.190	0.810	0.000	1.000

TAB. S3: **Data on Phenanthrene/Anthracene/Toluene ternary mixture compositions** (in mass fractions) – PHEN: Phenanthrene, ANT: Anthracene, TOL: Toluene.

Composition of the physical ternary mixtures			Composition of the liquids measured by GC			Composition of the solids deduced using Schreinemaker's method of wet residues	
PHEN	ANT	TOL	PHEN	ANT	TOL	PHEN	ANT
0.497	0.000	0.503	0.287	0.000	0.713	1.000	0.000
0.484	0.005	0.511	0.287	0.004	0.709	0.993	0.007
0.477	0.010	0.513	0.288	0.006	0.705	0.980	0.020
0.425	0.030	0.545	0.283	0.008	0.709	0.898	0.102
0.399	0.040	0.561	0.281	0.009	0.710	0.844	0.156
0.350	0.060	0.589	0.246	0.011	0.742	0.751	0.249
0.325	0.070	0.605	0.218	0.013	0.769	0.722	0.278
0.313	0.073	0.614	0.206	0.015	0.779	0.709	0.291
0.305	0.078	0.617	0.204	0.015	0.780	0.685	0.315
0.296	0.082	0.622	0.206	0.015	0.779	0.652	0.348
0.287	0.086	0.628	0.204	0.015	0.780	0.625	0.375
0.271	0.091	0.638	0.187	0.014	0.799	0.604	0.396
0.250	0.099	0.650	0.185	0.014	0.801	0.531	0.469
0.226	0.109	0.665	0.190	0.014	0.796	0.408	0.592
0.201	0.119	0.680	0.183	0.013	0.804	0.302	0.698
0.174	0.129	0.697	0.182	0.013	0.805	0.122	0.878
0.150	0.140	0.711	0.162	0.013	0.825	0.075	0.925
0.100	0.158	0.742	0.107	0.012	0.880	0.060	0.940
0.075	0.168	0.757	0.081	0.012	0.907	0.044	0.956
0.050	0.180	0.770	0.055	0.012	0.933	0.024	0.976
0.025	0.190	0.785	0.028	0.011	0.960	0.011	0.989
0.000	0.200	0.800	0.000	0.010	0.990	0.000	1.000

5) Screening of Phenanthrene new co-formers

The present appendix contains XRPD patterns of the different mixtures prepared to evidence the existence of co-crystals between the tested compounds and Phenanthrene.

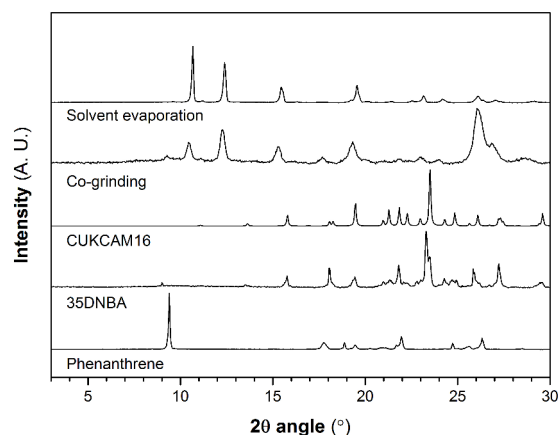


FIG. S3: XRPD patterns of Phenanthrene/35DNBA samples – CUKCAM16 corresponds to 35DNBA XRPD pattern predicted from its crystal structure [78].

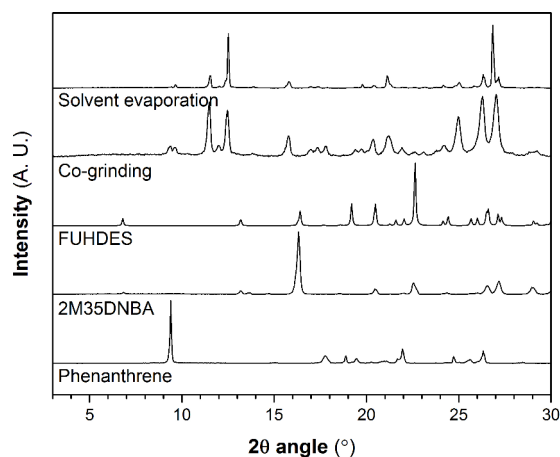


FIG. S5: XRPD patterns of Phenanthrene/2M35DNBA samples – FUHDES corresponds to 2M35DNBA XRPD pattern predicted from its crystal structure [79].

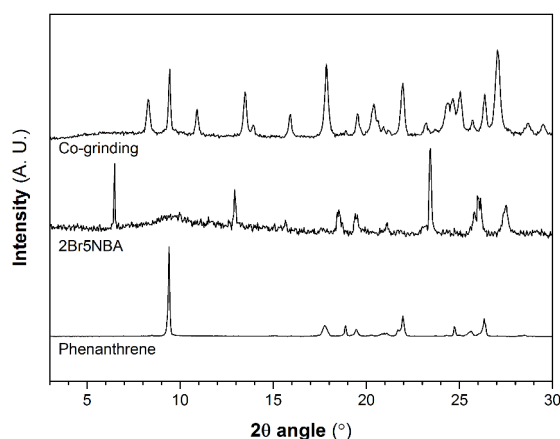


FIG. S4: XRPD patterns of Phenanthrene/2Br5NBA samples

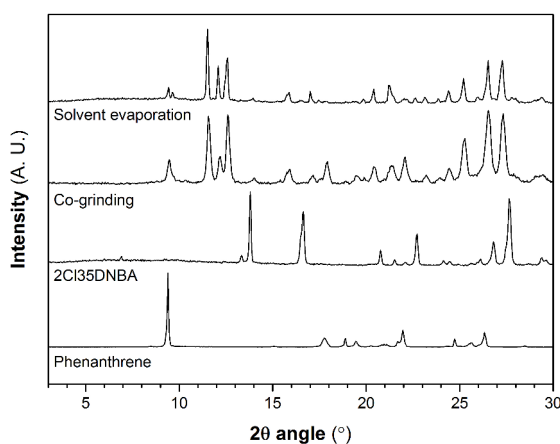


FIG. S6: XRPD patterns of Phenanthrene/2Cl35DNBA samples

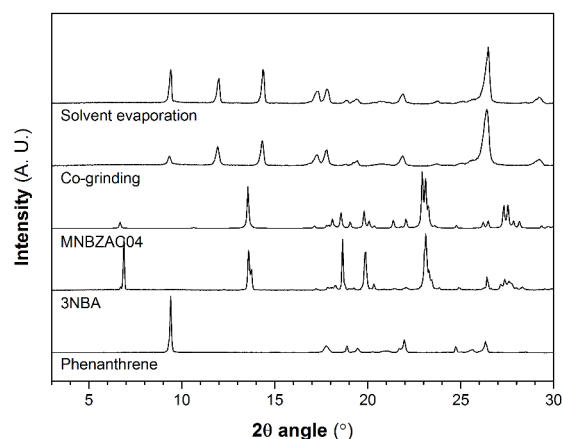


FIG. S7: XRPD patterns of Phenanthrene/3NBA samples – MNBZAC04 corresponds to 3NBA XRPD pattern predicted from its crystal structure [80].

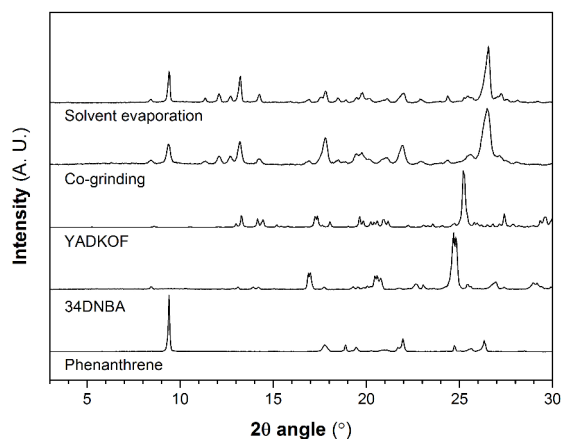


FIG. S10: XRPD patterns of Phenanthrene/34DNBA samples – YADKOF corresponds to 34DNBA XRPD pattern predicted from its crystal structure [81].

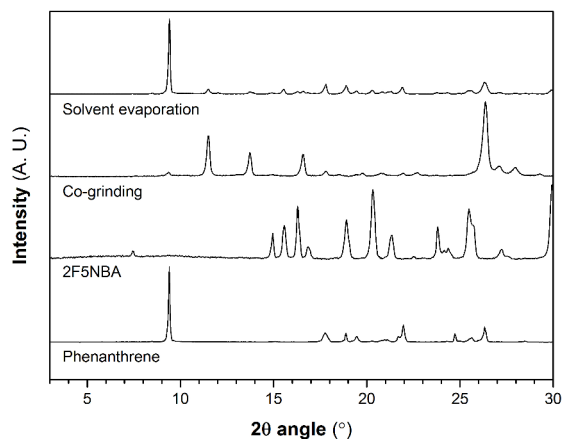


FIG. S8: XRPD patterns of Phenanthrene/2F5NBA samples

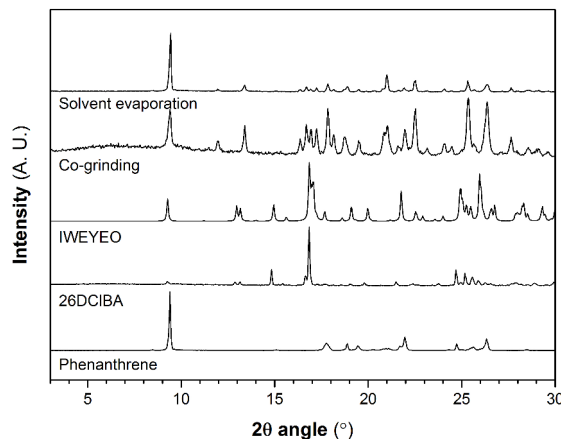


FIG. S11: XRPD patterns of Phenanthrene/26DCIBA samples – IWEYEO corresponds to 26DCIBA XRPD pattern predicted from its crystal structure [82].

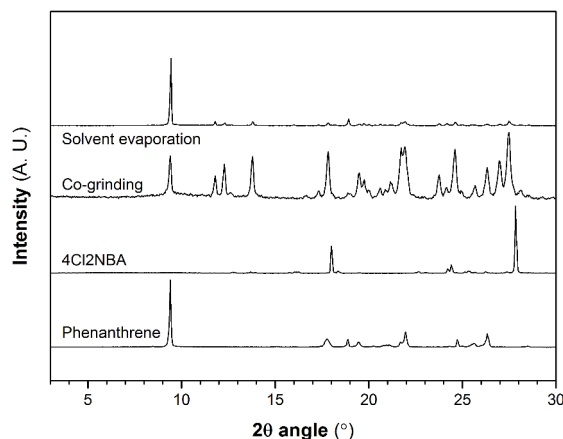


FIG. S9: XRPD patterns of Phenanthrene/4Cl2NBA samples

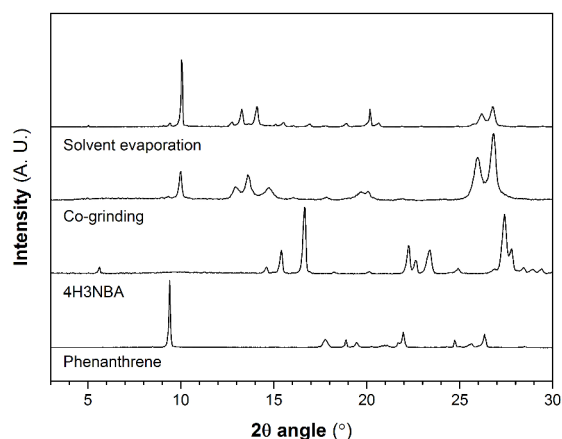


FIG. S12: XRPD patterns of Phenanthrene/4H3NBA samples

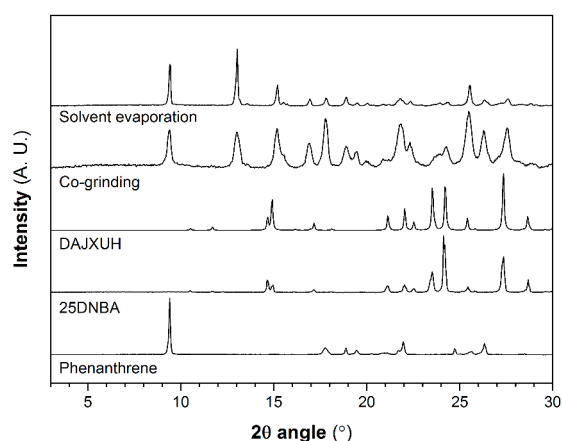


FIG. S13: XRPD patterns of Phenanthrene/25DNBA samples – DAJXUH corresponds to 25DNBA XRPD pattern predicted from its crystal structure [83].

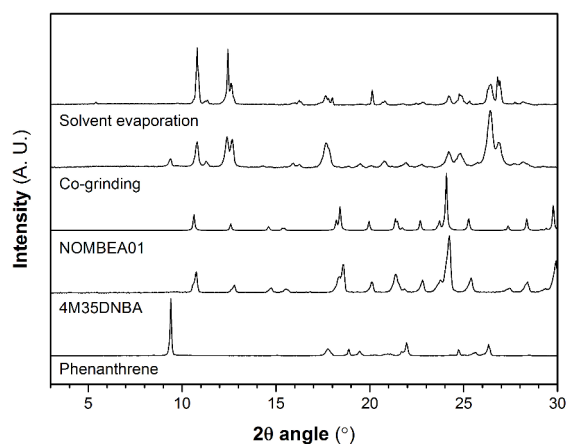


FIG. S14: XRPD patterns of Phenanthrene/4M35DNBA samples – NOMBEA01 corresponds to 4M35DNBA XRPD pattern predicted from its crystal structure [84].

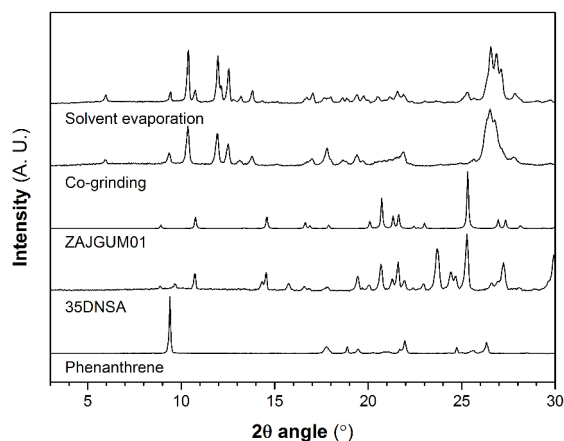


FIG. S15: XRPD patterns of Phenanthrene/35DNSA samples – ZAJGUM01 corresponds to 35DNSA monohydrate XRPD pattern predicted from its crystal structure [85].

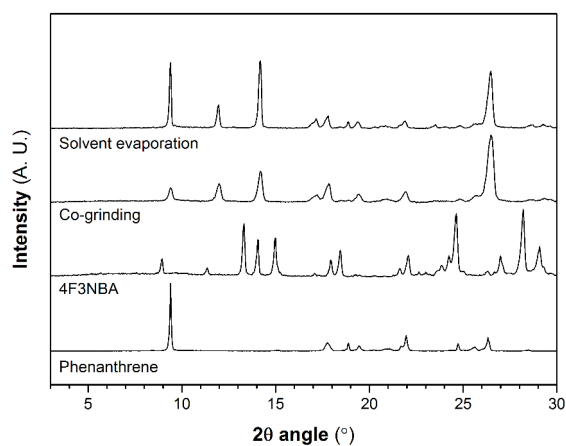


FIG. S16: XRPD patterns of Phenanthrene/4F3NBA samples

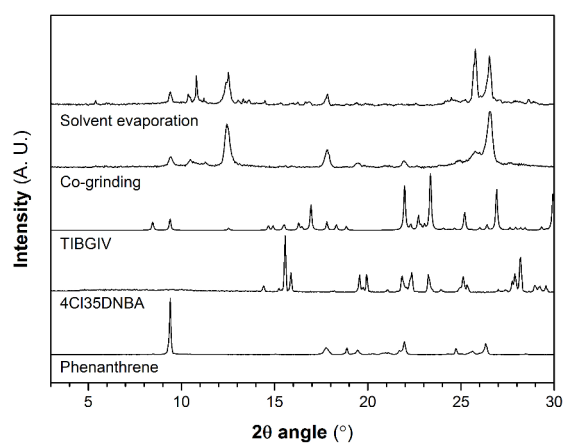


FIG. S17: XRPD patterns of Phenanthrene/4CI35DNBA samples – TIBGIV corresponds to 4CI35DNBA XRPD pattern predicted from its crystal structure [86].

6) Determination of the stoichiometry of the discovered co-crystals

This appendix presents the XRPD patterns of the different Phenanthrene/co-former systems, at various compositions. The comparison of the patterns allowed to determine the stoichiometry of the different co-crystals of Phenanthrene discovered in this work.

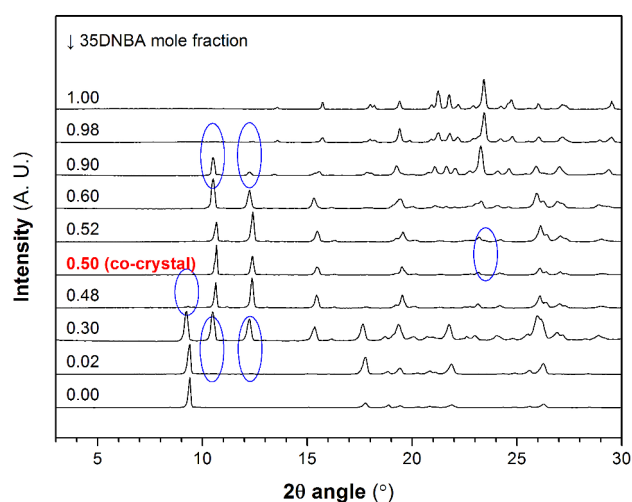


FIG. S18: **XRPD patterns of Phenanthrene/35DNBA binary mixtures (room temperature)** – a 1:1 co-crystal is evidenced. Mixtures exhibiting 35DNBA molar fraction values less than 0.50 crystallized as mixtures of <PHEN LT> and <CC> phases. Those exhibiting molar fraction values above 0.50 crystallized as mixtures of the <CC> and <35DNBA> phases.

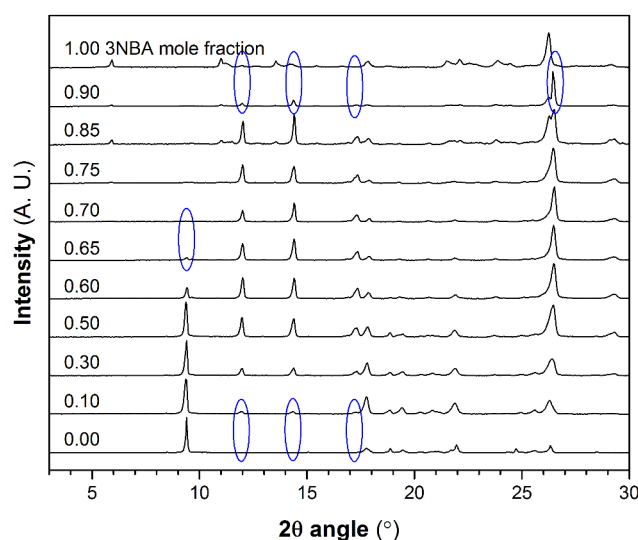


FIG. S19: **XRPD patterns of Phenanthrene/3NBA binary mixtures (room temperature)** – a 1:2 co-crystal is evidenced. Mixtures exhibiting 3NBA molar fraction values less than 0.67 crystallized as mixtures of <PHEN LT> and <CC> phases. Those exhibiting molar fraction values above 0.67 crystallized as mixtures of the <CC> and <3NBA> phases.

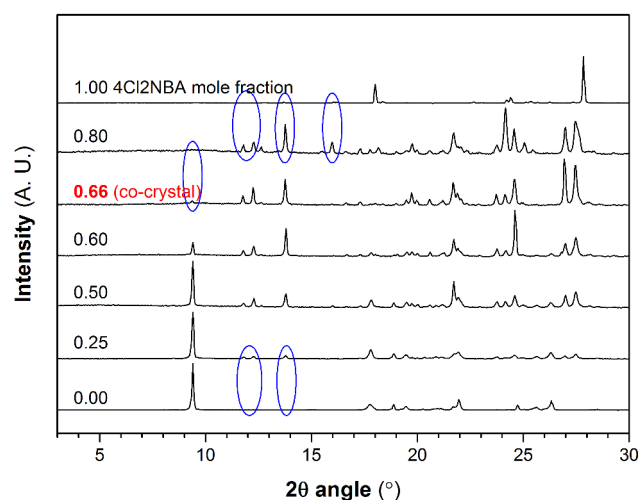


FIG. S20: **XRPD patterns of Phenanthrene/4CI2NBA binary mixtures (room temperature)** – a 1:2 co-crystal is evidenced. Mixtures exhibiting 4CI2NBA molar fraction values less than 0.67 crystallized as mixtures of <PHEN LT> and <CC> phases. Those exhibiting molar fraction values above 0.67 crystallized as mixtures of the <CC> and <4CI2NBA> phases.

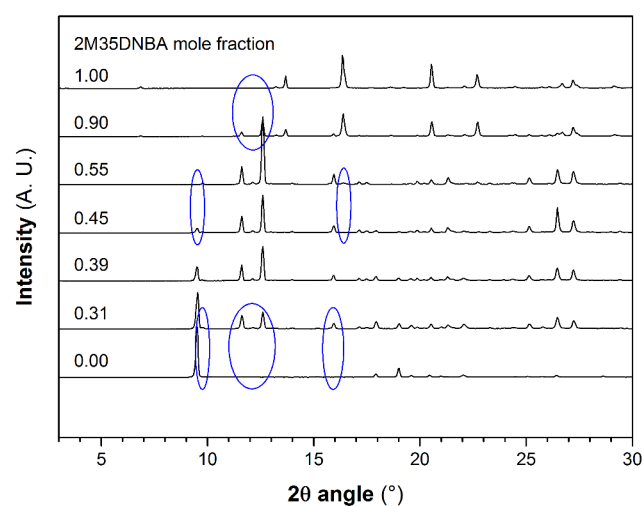


FIG. S21: **XRPD patterns of Phenanthrene/2M35DNBA binary mixtures (room temperature)** – a 1:1 co-crystal is evidenced. Mixtures containing between 0⁺ and 50⁻ mole % 2M35DNBA crystallized as mixtures of <PHEN LT> and <CC> phases. Those containing between 50⁺ and 100⁻ % 2M35DNBA crystallized as mixtures of the <CC> and <2M35DNBA> phases.

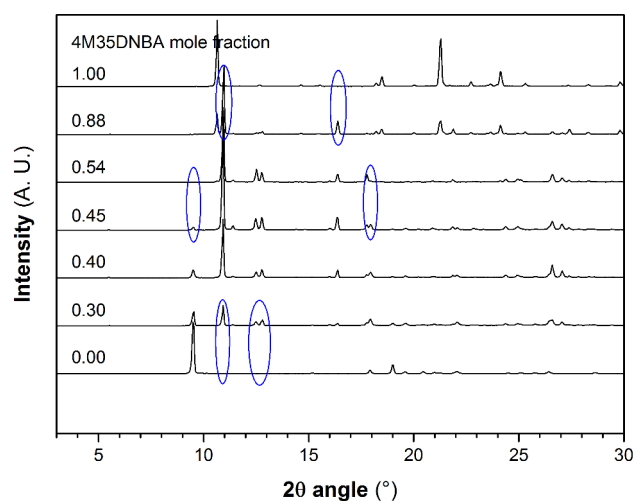


FIG. S22: **XRPD patterns of Phenanthrene/4M35DNBA binary mixtures (room temperature)** – a 1:1 co-crystal is evidenced. Mixtures containing between 0⁺ and 50⁻ mole % 4M35DNBA crystallized as mixtures of <PHEN LT> and <CC> phases. Those containing between 50⁺ and 100⁻ % 4M35DNBA crystallized as mixtures of the <CC> and <4M35DNBA> phases.

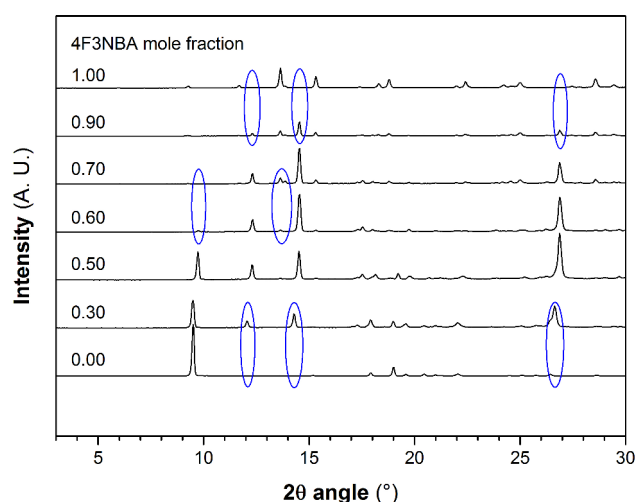


FIG. S23: **XRPD patterns of Phenanthrene/4F3NBA binary mixtures (room temperature)** – a 1:2 co-crystal is evidenced. Mixtures containing between 0⁺ and 66.7⁻ mole % 4F3NBA crystallized as mixtures of <PHEN LT> and <CC> phases. Those containing between 66.7⁺ and 100⁻ % 4F3NBA crystallized as mixtures of the <CC> and <4F3NBA> phases.

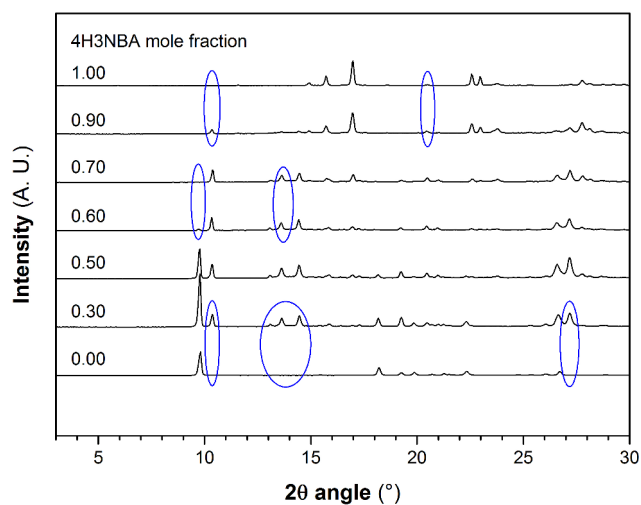


FIG. S24: **XRPD patterns of Phenanthrene/4H3NBA binary mixtures (room temperature)** – a 1:2 co-crystal is evidenced. Mixtures containing between 0⁺ and 66.7⁻ mole % 4H3NBA crystallized as mixtures of <PHEN LT> and <CC> phases. Those containing between 66.7⁺ and 100⁻ % 4H3NBA crystallized as mixtures of the <CC> and <4H3NBA> phases.

VIII. REFERENCES

- [1] W.G. Pfann, Process for controlling solute segregation by zone-melting, US2739088 A, 1956. <http://www.google.com/patents/US2739088> (accessed May 20, 2017).
- [2] W.G. Pfann, Temperature gradient zone-melting, US2813048 A, 1957. <http://www.google.com/patents/US2813048> (accessed May 20, 2017).
- [3] W.G. Pfann, Zone Melting, John Wiley & Sons, Inc., New York, 1958.
- [4] 1 part in 10,000,000,000, Radio Telev. News. 52 (1954) 6.
- [5] M. Ross, Zone Refining—William G. Pfann, MRS Bull. 12 (1987) 15. doi:10.1557/S0883769400068688.
- [6] The Michigan Technic, UM Libraries, 1959.
- [7] G.J. Sloan, Studies on the Purification of Anthracene; Determination and Use of Segregation Coefficients, Mol. Cryst. 1 (1966) 161–194. doi:10.1080/15421406608083267.
- [8] J.L. Solà Cervera, P. Keil, A. König, Determination of Distribution Coefficients in 1-Ethyl-3-Methyl Imidazolium Chloride-Methylimidazole Mixtures by Zone Melting, Chem. Eng. Technol. 33 (2010) 821–826. doi:10.1002/ceat.200900555.
- [9] T. Cheung, N. Cheung, C.M.T. Tobar, P.R. Mei, A. Garcia, Zone Refining of Tin: Optimization of Zone Length by a Genetic Algorithm, Mater. Manuf. Process. 28 (2013) 746–752. doi:10.1080/10426914.2012.736651.
- [10] Y. REN, J. LI, X. DUAN, Determination of Equilibrium Distribution Coefficients of Impurities in Phosphorus by Vertical Zone-melting Technique, Chin. J. Chem. Eng. 19 (2011) 223–226. doi:10.1016/S1004-9541(11)60158-4.
- [11] M. Ezheiyani, H. Sadeghi, Simulation for purification process of high pure germanium by zone refining method, J. Cryst. Growth. 462 (2017) 1–5. doi:10.1016/j.jcrysgro.2017.01.012.
- [12] J.A. Spim, M.J.S. Bernadou, A. Garcia, Numerical modeling and optimization of zone refining, J. Alloys Compd. 298 (2000) 299–305. doi:10.1016/S0925-8388(99)00655-6.
- [13] S. Wang, H.S. Fang, Z.L. Jin, C.J. Zhao, L.L. Zheng, Integrated analysis and design optimization of germanium purification process using zone-refining technique, J. Cryst. Growth. 408 (2014) 42–48. doi:10.1016/j.jcrysgro.2014.09.019.
- [14] J. Yang, H. Wang, B. Wang, R. Hu, Y. Liu, X. Luo, Numerical and experimental study of electron beam floating zone melting of Iridium single crystals, J. Mater. Process. Technol. (n.d.). doi:10.1016/j.jmatprotec.2017.07.016.
- [15] Z. Zhang, X. Zhang, X. He, X. Wang, Y. Mi, Purification of phosphorus by a zero pollution zone melting technique, Sep. Purif. Technol. 98 (2012) 249–254. doi:10.1016/j.seppur.2012.07.023.
- [16] J.A. Burton, R.C. Prim, W.P. Slichter, The Distribution of Solute in Crystals Grown from the Melt. Part I. Theoretical, J. Chem. Phys. 21 (1953) 1987–1991. doi:10.1063/1.1698728.
- [17] W.G. Pfann, Techniques of Zone Melting and Crystal Growing, Solid State Phys. 4 (1957) 423–521. doi:10.1016/S0081-1947(08)60158-7.
- [18] I. Kotula, A. Rabczuk, Solid-liquid equilibrium of the phenanthrene-fluorene system, J. Therm. Anal. 15 (1979) 343–346. doi:10.1007/BF01903658.
- [19] N. Couvrat, Y. Cartigny, S. Tisse, M.-N. Petit, G. Coquerel, Binary phase diagram between phenanthrene and its main impurity: dibenzothiophene, in: EDP Sciences, 2011: p. 00006. doi:10.1051/jeep/201100006.
- [20] J. Ulrich, H. Glade, eds., Melt crystallization: fundamentals, equipment and applications, Shaker, Aachen, 2003.
- [21] M. Brandstätter-Kuhnert, H. Weiß, Zur Mischkristallbildung in der isomorphen Gruppe: Anthracen, Phenanthren, Carbazol und Fluoren, Monatshefte Für Chem. Verwandte Teile Anderer Wiss. 88 (1957) 1007–1016. doi:10.1007/BF00906079.
- [22] G. Bradley, J.K. Marsh, 166. The system anthracene–phenanthrene, J. Chem. Soc. Resumed. (1933) 650–652. doi:10.1039/JR9330000650.
- [23] J.W. Rice, J. Fu, E. Sandström, J.C. Ditto, E.M. Suuberg, Thermodynamic study of (anthracene + phenanthrene) solid state mixtures, J. Chem. Thermodyn. 90 (2015) 79–86. doi:10.1016/j.jct.2015.06.021.
- [24] N. Couvrat, Four case studies on the impact of the heterogeneous equilibria on physicochemical behaviours of organic solids, European PhD thesis, Université de Rouen, 2011. <http://www.theses.fr/s149502>.
- [25] M.J. Joncich, D.R. Bailey, Zone Melting and Differential Thermal Analysis of Some Organic Compounds, Anal. Chem. 32 (1960) 1578–1581. doi:10.1021/ac60168a010.
- [26] J.W. Rice, J. Fu, E. Sandström, J.C. Ditto, E.M. Suuberg, Thermodynamic study of (anthracene + phenanthrene) solid state mixtures, J. Chem. Thermodyn. 90 (2015) 79–86. doi:10.1016/j.jct.2015.06.021.

- [27] S. Ding, Q. Yin, W. Du, X. Sun, B. Hou, M. Zhang, Z. Wang, Formation of Solid Solution and Ternary Phase Diagrams of Anthracene and Phenanthrene in Different Organic Solvents, *J. Chem. Eng. Data*. 60 (2015) 1401–1407. doi:10.1021/je501121v.
- [28] V. Petříček, I. Císařová, L. Hummel, J. Kroupa, B. Březina, Orientational disorder in phenanthrene. Structure determination at 248, 295, 339 and 344 K, *Acta Crystallogr. B*. 46 (1990) 830–832. doi:10.1107/S0108768190007510.
- [29] J.P. Reboul, Y. Odden, C. Caranoni, J.C. Soyfer, J. Barbe, G. Pèpe, Structure du dihydro-9,10 anthracène. Support tricyclique de médicaments psychotropes, *Acta Crystallogr. C*. 43 (1987) 537–539. doi:10.1107/S010827018709512X.
- [30] U. Glostein, M. Epple, H.K. Cammenga, Influencing the Solid-Solid Phase Transition in Phenanthrene by Suitable Doping, *Z. Für Phys. Chem.* 214 (2009) 379. doi:10.1524/zpch.2000.214.3.379.
- [31] D.M. Burns, J. Iball, The Crystal and Molecular Structure of Fluorene, *Proc. R. Soc. Lond. Math. Phys. Eng. Sci.* 227 (1955) 200–214. doi:10.1098/rspa.1955.0004.
- [32] B.J. McArdle, J.N. Sherwood, A.C. Damask, The growth and perfection of phenanthrene single crystals, *J. Cryst. Growth*. 22 (1974) 193–200. doi:10.1016/0022-0248(74)90094-3.
- [33] C.P. Brock, J.D. Dunitz, Temperature dependence of thermal motion in crystalline anthracene, *Acta Crystallogr. B*. 46 (1990) 795–806. doi:10.1107/S0108768190008382.
- [34] A. Burel, N. Couvrat, S. Tisse, Y. Cartigny, P. Cardinael, G. Coquerel, Binary phase diagrams between phenanthrene and two of its impurities: 9,10-dihydroanthracene and carbazole, *Eur. Phys. J. Spec. Top.* 226 (2017) 869–880. doi:10.1140/epjst/e2016-60270-0.
- [35] A.R. McGhie, A.F. Garito, A.J. Heeger, A gradient sublimator for purification and crystal growth of organic donor and acceptor molecules, *J. Cryst. Growth*. 22 (1974) 295–297. doi:10.1016/0022-0248(74)90173-0.
- [36] J. Drechsel, A. Petrich, M. Koch, S. Pfützner, R. Meerheim, S. Scholz, J. Drechsel, K. Walzer, M. Pfeiffer, K. Leo, 53.3: Influence of Material Purification by Vacuum Sublimation on Organic Optoelectronic Device Performance, *SID Symp. Dig. Tech. Pap.* 37 (2006) 1692–1695. doi:10.1889/1.2433332.
- [37] S.P. Verevkin, Vapor pressure measurements on fluorene and methyl-fluorenes, *Fluid Phase Equilibria*. 225 (2004) 145–152. doi:10.1016/j.fluid.2004.08.037.
- [38] V. Oja, E.M. Suuberg, Vapor Pressures and Enthalpies of Sublimation of Polycyclic Aromatic Hydrocarbons and Their Derivatives, *J. Chem. Eng. Data*. 43 (1998) 486–492. doi:10.1021/je970222l.
- [39] G. Springuel, T. Leyssens, Innovative Chiral Resolution Using Enantiospecific Co-Crystallization in Solution, *Cryst. Growth Des.* 12 (2012) 3374–3378. doi:10.1021/cg300307z.
- [40] G. Springuel, K. Robeyns, B. Norberg, J. Wouters, T. Leyssens, Cocrystal Formation between Chiral Compounds: How Cocrystals Differ from Salts, *Cryst. Growth Des.* 14 (2014) 3996–4004. doi:10.1021/cg500588t.
- [41] O. Ermer, J. Neudörfl, Comparative Supramolecular Chemistry of Coronene and Hexahelicene: Helix Alignment in Crystalline Complexes with Trimesic Acid (=Benzene-1,3,5-tricarboxylic Acid) and π -Acceptor Compounds, *Helv. Chim. Acta*. 84 (2001) 1268–1313. doi:10.1002/1522-2675(20010613)84:6<1268::AID-HLCA1268>3.0.CO;2-Z.
- [42] M.A. Dobrowolski, G. Garbarino, M. Mezouar, A. Ciesielski, M.K. Cyrański, Structural diversities of charge transfer organic complexes. Focus on benzenoid hydrocarbons and 7,7,8,8-tetracyanoquinodimethane, *CrystEngComm*. 16 (2013) 415–429. doi:10.1039/C3CE41703D.
- [43] J.C. Collings, K.P. Roscoe, R.L. Thomas, A.S. Batsanov, L.M. Stimson, J.A.K. Howard, T.B. Marder, Arene-perfluoroarene interactions in crystal engineering. Part 3. Single-crystal structures of 1 : 1 complexes of octafluoronaphthalene with fused-ring polyaromatic hydrocarbons, *New J. Chem.* 25 (2001) 1410–1417. doi:10.1039/B105502J.
- [44] J. Krzystek, J.U. von Schütz, H.C. Wolf, R.-D. Stigler, J.J. Stezowski, Characterization of the Phenanthrene-Tetrachlorophthalic Anhydride (P/TCPA) 1:1 Charge-Transfer Crystal: Spectroscopic and Structural Investigations, *Z. Für Naturforschung A*. 42 (1987). doi:10.1515/zna-1987-0618.
- [45] N. Barooah, R.J. Sarma, J.B. Baruah, Solid-state hydrogen bonded assembly of N,N'-bis(glyciny)-pyromellitic diimide with aromatic guests, *CrystEngComm*. 8 (2006) 608–615. doi:10.1039/B607323A.
- [46] J.C. Collings, K.P. Roscoe, E.G. Robins, A.S. Batsanov, L.M. Stimson, J.A.K. Howard, S.J. Clark, T.B. Marder, Arene-perfluoroarene interactions in crystal engineering 8: structures of 1 : 1 complexes of hexafluorobenzene with fused-ring polyaromatic hydrocarbons, *New J. Chem.* 26 (2002) 1740–1746. doi:10.1039/B207102A.
- [47] Q.J. Shen, X. Pang, X.R. Zhao, H.Y. Gao, H.-L. Sun, W.J. Jin, Phosphorescent cocrystals constructed by 1,4-diiodotetrafluorobenzene and polyaromatic hydrocarbons based on C–I $\cdots\pi$ halogen bonding and other assisting weak interactions, *CrystEngComm*. 14 (2012) 5027–5034. doi:10.1039/C2CE25338K.
- [48] F.H. Herbstein, M. Kapon, G. Rzonzew, D. Rabinovich, Molecular compounds and complexes. XI. The crystal structure of the π -molecular compound phenanthrene-2,3-dichloro-5,6-dicyano-p-benzoquinone, *Acta Crystallogr. B*. 34 (1978) 476–481. doi:10.1107/S0567740878003386.

- [49] D.L. Evans, W.T. Robinson, The charge-transfer complex phenanthrene–pyromellitic acid dianhydride (PMDA), *Acta Crystallogr. B* 33 (1977) 2891–2893. doi:10.1107/S0567740877009704.
- [50] S. Varughese, M.S.R.N. Kiran, U. Ramamurty, G.R. Desiraju, Nanoindentation as a Probe for Mechanically-Induced Molecular Migration in Layered Organic Donor–Acceptor Complexes, *Chem. – Asian J.* 7 (2012) 2118–2125. doi:10.1002/asia.201200224.
- [51] S. Yamaguchi, M. Goto, H. Takayanagi, H. Ogura, The Crystal Structure of Phenanthrene: Picric Acid Molecular Complex, *Bull. Chem. Soc. Jpn.* 61 (1988) 1026–1028. doi:10.1246/bcsj.61.1026.
- [52] X. Pang, H. Wang, X.R. Zhao, W.J. Jin, Co-crystallization turned on the phosphorescence of phenanthrene by C–Br... π halogen bonding, π –hole... π bonding and other assisting interactions, *CrystEngComm* 15 (2013) 2722–2730. doi:10.1039/C3CE26661C.
- [53] K.B. Landenberger, A.J. Matzger, Cocystal Engineering of a Prototype Energetic Material: Supramolecular Chemistry of 2,4,6-Trinitrotoluene, *Cryst. Growth Des.* 10 (2010) 5341–5347. doi:10.1021/cg101300n.
- [54] D. Britton, 1:1 Complexes of 2,3,5,6-tetrachlorobenzene-1,4-dicarbonitrile with pyrene and phenanthrene: pseudo-isomorphs, *Acta Crystallogr. C* 61 (2005) o662–o664. doi:10.1107/S0108270105032002.
- [55] T. Friščić, New opportunities for materials synthesis using mechanochemistry, *J. Mater. Chem.* 20 (2010) 7599–7605. doi:10.1039/C0JM00872A.
- [56] V. Nemec, N. Škvorc, D. Cinčić, Mechanochemical and solution-based cocrystallization of 9,10-phenanthrenequinone and thiourea, *CrystEngComm* 17 (2015) 6274–6277. doi:10.1039/C5CE01291K.
- [57] M. Zaworotko, J. Wouters, A. Bond, L. Quéré, T.N.G. Row, D.E. Thurston, N. Rodriguez-Hornedo, G. Coquerel, R. Hilfiker, T. Rager, Pharmaceutical Salts and Co-crystals, Royal Society of Chemistry, 2011. <https://books.google.fr/books?id=3HIoDwAAQBAJ>.
- [58] A. Burel, S.J.T. Brugman, M. Mignot, Y. Cartigny, S. Tisse, N. Couvrat, V. Peulon-Agasse, P. Cardinael, G. Coquerel, Phenanthrene Purification: Comparison of Zone Melting and Co-Crystallization, *Chem. Eng. Technol.* 39 (2016) 1317–1325. doi:10.1002/ceat.201600033.
- [59] F.G. Bordwell, Equilibrium acidities in dimethyl sulfoxide solution, *Acc. Chem. Res.* 21 (1988) 456–463. doi:10.1021/ar00156a004.
- [60] G. Saikia, P.K. Iyer, Facile C–H Alkylation in Water: Enabling Defect-Free Materials for Optoelectronic Devices, *J. Org. Chem.* 75 (2010) 2714–2717. doi:10.1021/jo100028d.
- [61] G. Rieveschl, F.E. Ray, The Chemistry of Fluorene and its Derivatives., *Chem. Rev.* 23 (1938) 287–389. doi:10.1021/cr60075a002.
- [62] A.T. Lapinas, M.T. Klein, B.C. Gates, A. Macris, J.E. Lyons, Catalytic hydrogenation and hydrocracking of fluorene: reaction pathways, kinetics, and mechanisms, *Ind. Eng. Chem. Res.* 30 (1991) 42–50. doi:10.1021/ie00049a007.
- [63] K. Hashimoto, H. Tanaka, T. Ikeno, T. Yamada, Selective Nitrous Oxide Oxidation for C–H Oxidation and Aromatization of 9,10-Dihydroanthracene Derivatives, *Chem. Lett.* 31 (2002) 582–583. doi:10.1246/cl.2002.582.
- [64] M. Daney, R. Lapouyade, Reactivite des carbanions benzyliques, *J. Organomet. Chem.* 172 (1979) 385–390. doi:10.1016/S0022-328X(00)92310-6.
- [65] G.R. Pettit, E.E. van Tamelen, Desulfurization with Raney Nickel, in: *Org. React.*, John Wiley & Sons, Inc., 2004. doi:10.1002/0471264180.or012.05.
- [66] J. Ashby, C.C. Cook, Recent Advances in the Chemistry of Dibenzothiophenes, *Adv. Heterocycl. Chem.* 16 (1974) 181–288. doi:10.1016/S0065-2725(08)60462-6.
- [67] M. Yalpani, R. Köster, Partial Hydrogenation: From Anthracene to Coronene, *Chem. Ber.* 123 (1990) 719–724. doi:10.1002/cber.19901230412.
- [68] A. Stanislaus, B.H. Cooper, Aromatic Hydrogenation Catalysis: A Review, *Catal. Rev.* 36 (1994) 75–123. doi:10.1080/01614949408013921.
- [69] S. Grimme, C. Diedrich, M. Korth, The Importance of Inter- and Intramolecular van der Waals Interactions in Organic Reactions: the Dimerization of Anthracene Revisited, *Angew. Chem. Int. Ed.* 45 (2006) 625–629. doi:10.1002/anie.200502440.
- [70] G.W. Breton, X. Vang, Photodimerization of Anthracene, *J. Chem. Educ.* 75 (1998) 81. doi:10.1021/ed075p81.
- [71] A.A. Politov, A.P. Chupakhin, V.M. Tapilin, N.N. Bulgakov, A.G. Druganov, To mechanochemical dimerization of anthracene. Crystalline phenanthrene under high pressure and shear conditions, *J. Struct. Chem.* 51 (2010) 1064–1069. doi:10.1007/s10947-010-0163-3.
- [72] D. Bogdal, J. Pielichowski, K. Jaskot, New Synthesis Method of N-Alkylation of Carbazole Under Microwave Irradiation in Dry Media., *Synth. Commun.* 27 (1997) 1553–1560. doi:10.1080/00397919708006093.
- [73] H. Adkins, H.L. Coonradt, The Selective Hydrogenation of Derivatives of Pyrrole, Indole, Carbazole and Acridine, *J. Am. Chem. Soc.* 63 (1941) 1563–1570. doi:10.1021/ja01851a020.

- [74] M. Nagai, T. Masunaga, N. Hanaoka, Hydrodenitrogenation of carbazole on a molybdenum/alumina catalyst. Effects of sulfiding and sulfur compounds, *Energy Fuels*. 2 (1988) 645–651. doi:10.1021/ef00011a007.
- [75] J. Feldman, P. Pantages, M. Orchin, Purification and Freezing Point of Phenanthrene, *J. Am. Chem. Soc.* 73 (1951) 4341–4343. doi:10.1021/ja01153a091.
- [76] Z.-G. Zhang, K. Okada, M. Yamamoto, T. Yoshida, Hydrogenation of anthracene over active carbon-supported nickel catalyst, *Catal. Today*. 45 (1998) 361–366. doi:10.1016/S0920-5861(98)00264-8.
- [77] M.G. Meiramov, Angular–linear isomerization on the hydrogenation of phenanthrene in the presence of iron-containing catalysts, *Solid Fuel Chem.* 51 (2017) 107–110. doi:10.3103/S0361521917020070.
- [78] A.O.F. Jones, N. Blagden, G.J. McIntyre, A. Parkin, C.C. Seaton, L.H. Thomas, C.C. Wilson, Tuning Proton Disorder in 3,5-Dinitrobenzoic Acid Dimers: the Effect of Local Environment, *Cryst. Growth Des.* 13 (2013) 497–509. doi:10.1021/cg300906j.
- [79] M.N. Tahir, A.R. Raza, A. Saddiqa, M. Danish, I. Saleem, 2-Methyl-3,5-dinitrobenzoic acid, *Acta Crystallogr. Sect. E Struct. Rep. Online*. 65 (2009) o2819–o2819. doi:10.1107/S1600536809042627.
- [80] A. Domenicano, G. Schultz, I. Hargittai, M. Colapietro, G. Portalone, P. George, C.W. Bock, Molecular structure of nitrobenzene in the planar and orthogonal conformations, *Struct. Chem.* 1 (1990) 107–122. doi:10.1007/BF00675790.
- [81] M. Zeller, J.L. Stouffer, V.C. Solomon, L.S. Curtin, High- Z' and twinning behavior in 3,4-dinitrobenzoic acid, *Acta Crystallogr. C*. 67 (2011) o397–o404. doi:10.1107/S0108270111035797.
- [82] A.G. Pinkus, J.A. Kautz, P. Ahobila-Vajjala, Crystal structures of 2,6- and 3,5-dichlorobenzoic acids: nonbonded Cl \cdots Cl contacts, *J. Chem. Crystallogr.* 33 (2003) 181–186. doi:10.1023/A:1023597409468.
- [83] S.J. Grabowski, T.M. Krygowski, Crystallographic studies and physicochemical properties of π -electron compounds. IV. Structure of 2,5-dinitrobenzoic acid (2,5-DNBA), *C₇H₄N₂O₆*, *Acta Crystallogr. C*. 41 (1985) 1224–1226. doi:10.1107/S0108270185007211.
- [84] V.R. Pedireddi, W. Jones, A.P. Chorlton, R. Docherty, Design and synthesis of host-guest complexes through non-covalent bonds, *Tetrahedron Lett.* 39 (1998) 5409–5412. doi:10.1016/S0040-4039(98)01015-6.
- [85] V.S.S. Kumar, S.S. Kuduva, G.R. Desiraju, Pseudopolymorphs of 3,5-dinitrosalicylic acid, *J. Chem. Soc. Perkin Trans. 2*. (1999) 1069–1074. doi:10.1039/A902134E.
- [86] Aziz-ur-Rehman, M. Helliwell, S. Ali, S. Shahzadi, 4-Chloro-3,5-dinitrobenzoic acid, *Acta Crystallogr. Sect. E Struct. Rep. Online*. 63 (2007) o1743–o1744. doi:10.1107/S1600536807011221.

Conclusion

CONCLUSION

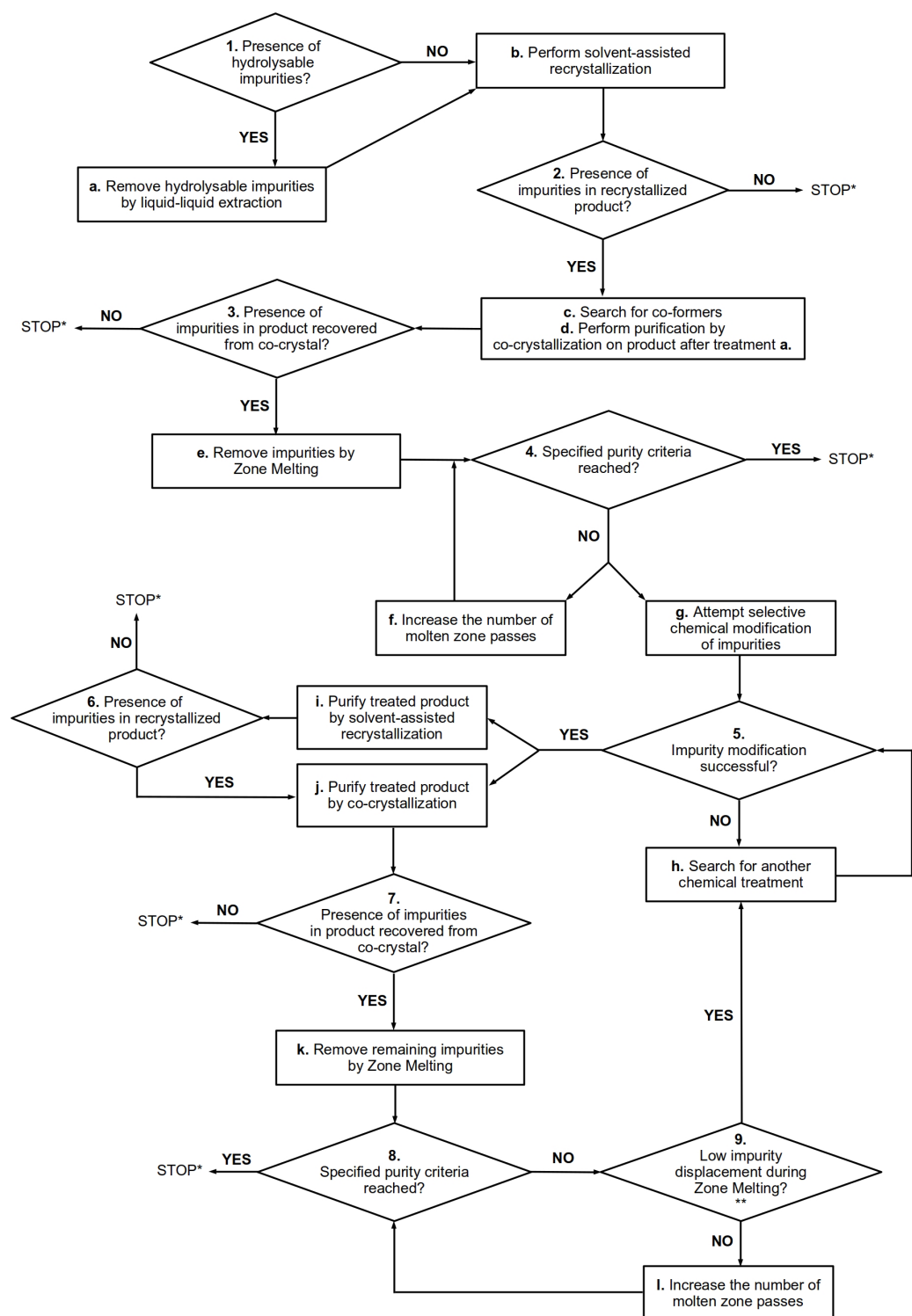
In this thesis, many crystallization methods were employed to attempt Phenanthrene ultrapurification : solvent-assisted recrystallization, zone melting, vacuum sublimation and co-crystallization. Single separated applications of these methods to the commercial product did not achieve the complete elimination of the impurities. Hence, combinatorial approaches were tested. The key learnings of this work highlighted the following points:

- (i) Classical crystallization procedures applied to a product (recrystallization in solution or from the melt) exhibit limited purifying effects when the impurities are structurally similar to the compound to purify. Indeed, the formation of partial solid solutions imposes severe limitations to the discrimination in the solid state.
- (ii) Bypassing these thermodynamic limitations is possible by addition of a third component providing a selective formation of co-crystals. However, this method requires the development of a procedure to recover the purified product with a complete elimination of the co-crystal former.
- (iii) When the impurities are structurally too similar to the solute, the purifying methods mentioned above are not discriminative enough to ensure their complete eliminations. Consequently, a selective chemical modification of them is needed prior the application(s) of the crystallization procedures. Nevertheless, new phase equilibria have to be considered for the design of the selective crystallizations.

In these work these pathways have been explored and a 99.999 % ultimate purity of Phenanthrene has been achieved. The order–disorder transition can now be studied with a sufficiently pure material.

It is also necessary to note that this work would not have been achieved without the development of a validated analytical method permitting the quantification of impurity levels down to hundreds of ppm. This point was the key pre-requisite for monitoring the actual purification methods.

Starting from the observations made in this thesis, a flow chart could be proposed to provide guidelines for the purification of non-polar polycyclic aromatic hydrocarbons that are stable upon melting (fig. 1). Of course, the instructions can be followed with some degrees of freedom, according to the issues faced during purification experiments.



* After organic impurity elimination, a sublimation step is recommended to remove potential solvent traces and inorganic impurities

** Inefficiency of Zone Melting related to unfavorable phase equilibria (impurity segregation coefficient close to 1).

FIG. 1: Flow chart proposing guidelines for the purification of non-polar polycyclic aromatic hydrocarbons stable upon melting

Discrimination à l'état solide durant la cristallisation : application à l'ultrapurification du phénanthrène

La cristallisation est un processus d'auto-assemblage de molécules à partir d'une phase désordonnée (liquide, amorphe ou gazeuse). De façon générale, la miscibilité à l'état solide entre un constituant d'intérêt et son impureté dépendent d'une part, de la structure moléculaire de ces deux espèces, et d'autre part, de la structure cristalline du réseau hôte, c'est-à-dire celui du composé d'intérêt. En cas d'absence de miscibilité, l'optimisation des conditions de cristallisation permet un retrait total de l'impureté du composé visé.

Cette thèse vise à démontrer que, lorsque deux molécules sont semblables et que leur structure cristalline est peu dense, des solutions solides de substitutions peuvent se former et empêcher le retrait de l'impureté de l'espèce cible. Inversement, lorsque les impuretés sont très différentes de l'espèce à purifier, l'absence de solution solide est observée et permet leur élimination totale grâce à une bonne discrimination à l'état solide.

Le système du phénanthrène, un composé servant entre autres de base pour la synthèse de composés morphiniques, a été choisi pour illustrer cette thèse. Diverses méthodes de cristallisation (fusion de zone, co-cristallisation, recristallisation en solution, sublimation-condensation) ont été testées et ont permis, après optimisation et combinaison, l'obtention à l'échelle préparative de phénanthrène pur à plus de 99,999 % en moles, ce qui le place sur l'échelle de l'ultra-pureté (pureté > 99,9 % en moles).

Mots clés : *phénanthrène, discrimination, état solide, cristallisation, co-cristallisation, fusion de zone, sublimation, chromatographie en phase gazeuse.*

Discrimination in the solid state during crystallization: application to phenanthrene ultrapurification

Crystallization is a process during which molecules self assembly from a disordered (liquid, amorphous or gaseous) phase. The miscibility in the solid state between a component of interest and its impurity depends on: (i) their molecular structures, (ii) the crystal structure of the host lattice (namely, that of the component of interest). When no solid solution exists, the impurity can be completely eliminated from the target product after optimization of the crystallization conditions.

The present thesis intends to demonstrate that, when two compounds present similar molecular structures with low-density crystal structures, solid solution formation can occur which prevents from their complete separation. Conversely, in case of sufficient dissimilarity, no solid solution is stable and their separation is possible thanks to a large discrimination in the solid state.

The phenanthrene system – a model compound used as base for the synthesis of morphine derivatives – was chosen to illustrate this thesis. Several crystallization methods (zone melting, co-crystallization, solvent assisted crystallization and sublimation-condensation) were investigated and permitted, after optimization and combination, to obtain 99.999(9) mole % purity phenanthrene (which is above the ultrapure grade of 99.9 mole %).

Keywords: *phenanthrene, discrimination, solid state, crystallization, co-crystallization, zone melting, sublimation, gas chromatography.*